NONLINEAR LONG-TERM BEHAVIOUR OF HIGH-STRENGTH CONCRETE WALL PANELS

By

Yue Huang

A thesis submitted as partial fulfilment of
the requirements for the degree of

DOCTOR OF PHILOSOPHY

School of Civil and Environmental Engineering
The University of New South Wales
Sydney, Australia

April 2015

PLEASE TYPE

THE UNIVERSITY OF NEW SOUTH WALES
Thesis/Dissertation Sheet

Surname or Family name: Huang

First name: Yue

Other name/s:

Abbreviation for degree as given in the University calendar: PhD

School: School of Civil and Environmental Engineering

Faculty: Faculty of Engineering

Title: Nonlinear long-term behaviour of high-strength concrete wall panels

Abstract 350 words maximum: (PLEASE TYPE)

This thesis investigates the time-dependent behaviour of slender reinforced high-strength concrete (HSC) panels, with particular emphasis on the combined effects of creep and shrinkage on the buckling capacity and its degradation with time.

The short-term response of one-way HSC panels is studied first, in order to set the basis for the long-term analysis. A theoretical model is developed, which accounts for the geometric and material nonlinearities including the strain softening and cracking of concrete, tension-stiffening and reinforcement yielding. An experimental study is carried out, including testing to failure of eight one-way full-scale panels under in-plane loads with different load eccentricities, slenderness, and reinforcement ratios. The failure of all panels was a sudden buckling failure. A close correlation between the theoretical model and the experimental results is obtained.

The time-dependent response of one-way HSC panels is then investigated. A nonlinear theoretical model is developed based on a time-stepping analysis to account for the variation of the internal stresses and deformations with time. A rheological generalized Maxwell chain model is used to account for creep of the concrete as well as its shrinkage, cracking, tension-stiffening and aging through strain- and time-dependent springs and dashpots. The incremental governing equations are solved numerically at each time step. An experimental program is conducted, which consists of testing five one-way HSC panels under sustained in-plane loads with various eccentricities and load levels. Two panels failed by creep buckling and the rest exhibited long-term stable behaviour, which were then loaded to failure. Good agreement is achieved between the test and theoretical results.

Finally, the long-term behaviour of two-way HSC panels is examined by developing an incremental nonlinear model that uses the Von Karman plate theory with large displacement kinematics. The rheological generalized Maxwell chain model is used to model the creep of concrete, including the shrinkage and cracking. The numerical and parametric study reveals that the time-dependent behaviour can be significantly weakened by cracking of concrete.

Based on the results presented here, it can be concluded that creep and shrinkage can significantly influence the load-carrying capacity of HSC panels. The theoretical models developed here provide effective tools to predict their time-dependent response.

Declaration relating to disposition of project thesis/dissertation

Yue Huang

Signature

Witness

15/04/2015

Date

FOR OFFICE USE ONLY

Date of completion of requirements for Award:

THIS SHEET IS TO BE GLUED TO THE INSIDE FRONT COVER OF THE THESIS

COPYRIGHT STATEMENT

'I hereby grant the University of New South Wales or its agents the right to archive and to make available my thesis or dissertation in whole or part in the University libraries in all forms of media, now or here after known, subject to the provisions of the Copyright Act 1968. I retain all proprietary rights, such as patent rights. I also retain the right to use in future works (such as articles or books) all or part of this thesis or dissertation.
I also authorise University Microfilms to use the 350 word abstract of my thesis in Dissertation Abstract International (this is applicable to doctoral theses only).
I have either used no substantial portions of copyright material in my thesis or I have obtained permission to use copyright material; where permission has not been granted I have applied/will apply for a partial restriction of the digital copy of my thesis or dissertation.'

Signed ....Yue Huang....

Date ....15/04/2015....

AUTHENTICITY STATEMENT

'I certify that the Library deposit digital copy is a direct equivalent of the final officially approved version of my thesis. No emendation of content has occurred and if there are any minor variations in formatting, they are the result of the conversion to digital format.'

Signed ....Yue Huang....

Date ....15/04/2015....

ORIGINALITY STATEMENT

I hereby declare that this submission is my own work and to the best of my knowledge it contains no materials previously published or written by another person, or substantial proportions of material which have been accepted for the award of any other degree or diploma at UNSW or any other educational institution, except where due acknowledgement is made in the thesis. Any contribution made to the research by others, with whom I have worked at UNSW or elsewhere, is explicitly acknowledged in the thesis. I also declare that the intellectual content of this thesis is the product of my own work, except to the extent that assistance from others in the project's design and conception or in style, presentation and linguistic expression is acknowledged.

Signed ....Yue Huang..

Date ....15/04/2015..

ABSTRACT

This thesis investigates the time-dependent behaviour of slender reinforced high-strength concrete (HSC) panels, with particular emphasis on the combined effects of creep and shrinkage on the buckling capacity and its degradation with time.

The short-term response of one-way HSC panels is studied first, in order to set the basis for the long-term analysis. A theoretical model is developed, which accounts for the geometric and material nonlinearities including the strain softening and cracking of concrete, tension-stiffening and reinforcement yielding. An experimental study is carried out, including testing to failure of eight one-way full-scale panels under in-plane loads with different load eccentricities, slenderness, and reinforcement ratios. The failure of all panels was a sudden buckling failure. A close correlation between the theoretical model and the experimental results is obtained.

The time-dependent response of one-way HSC panels is then investigated. A nonlinear theoretical model is developed based on a time-stepping analysis to account for the variation of the internal stresses and deformations with time. A rheological generalized Maxwell chain model is used to account for creep of the concrete as well as its shrinkage, cracking, tension-stiffening and aging through strain- and time-dependent springs and dashpots. The incremental governing equations are solved numerically at each time step. An experimental program is conducted, which consists of testing five one-way HSC panels under sustained in-plane loads with various eccentricities and load levels. Two panels failed by creep buckling and the rest exhibited long-term stable behaviour, which were then loaded to failure. Good agreement is achieved between the test and theoretical results.

Finally, the long-term behaviour of two-way HSC panels is examined by developing an incremental nonlinear model that uses the Von Karman plate theory with large displacement kinematics. The rheological generalized Maxwell chain model is used to model the creep of concrete, including the shrinkage and cracking. The numerical and parametric study reveals that the time-dependent behaviour can be significantly weakened by cracking of concrete.

Based on the results presented here, it can be concluded that creep and shrinkage can significantly influence the load-carrying capacity of HSC panels. The theoretical models developed here provide effective tools to predict their time-dependent response.

PUBLICATIONS

Journal papers

Huang, Y., and Hamed, E. (2013). "Buckling of one-way high-strength concrete panels: Creep and shrinkage effects." *Journal of Engineering Mechanics*, 139(12), 1856-1867.

Huang, Y., Hamed, E., Chang, Z.-T., and Foster, S. J. "Theoretical and experimental investigation of the failure behaviour of one-way high-strength concrete panels." *Journal of Structural Engineering*. (In press).

Huang, Y., Hamed, E., Chang, Z.-T., and Foster, S. J. "Exeprimental study of the time-dependent behavior of slender one-way high-strength concrete panels." (In prep).

Huang, Y., Hamed, E., and Foster, S. J. "Creep buckling of two-way high-strength concrete panels." (In prep).

Conference papers

Huang, Y., Hamed, E., and Foster, S. J. (2011). "Creep buckling analysis of high-strength concrete panels." *Proc.,9th Int. Symposium on High Performance Concrete*, Rotorua, New Zealand.

Huang, Y., and Hamed, E. (2012a). "Effect of reinforcement ratio on the creep buckling behavior of high-strength concrete panels." *the 7th International Conference on Computational Mechanics for Spatial Structures* Sarajevo, Bosnia-Herzegovina.

Huang, Y., and Hamed, E. (2012b). "Effect of supporting conditions on the long-term load capacity of high strength concrete panels." *Proc.,22nd Australian conference on the mechanics of structures and materials*, Sydney, Australia.

Huang, Y., Hamed, E., and Foster, S.J. (2014). "Creep testing and analysis of high strength concrete panels under eccentric loading – buckling effects." To be presented at the *23rd Australasian Conference on the Mechanics of Structures and Materials*, Byron Bay, Australia, 9-12 December 2014.

ACKNOWLEDGEMENT

First of all, I wish to express my sincere gratitude and appreciation to my main supervisor, Dr. Ehab Hamed, for his boundless assistance, invaluable guidance, encouragement and support during the course of this research study. Without his help, this thesis would not have been possible to complete.

I would also like to thank my co-supervisor Professor Stephen Foster for his insightful suggestions and discussions during the research work, especially on the experimental studies. His inspirational guidance and continuous support is much appreciated.

The Australian Research Council (ARC) is thankfully acknowledged for funding the research reported in this thesis through the Discovery Grant DP120102762 "Nonlinear long-term behaviour and analysis of high-strength concrete panels".

Special thanks go to all the staff at the Randwick Heavy Structures Laboratory, including Mr. Paul Gwynne, Mr. Ron Moncay, Mr. Greg Worthing, Mr. John Gilbert and Mr. Frank Scharfe. Thanks to Mr. Tony Macken in the Structure and Materials laboratories for his assistance in grinding the concrete cylinders and testing steel material.

Finally, I would like to express my deepest gratitude to my wife and parents for all the love, support and encouragement they have been giving me throughout the study. Without their continued support, the completion of this research study would have been impossible.

TABLE OF CONTENTS

LIST OF TABLES

LIST OF FIGURES

CHAPTER 1 INTRODUCTION

1.1 BACKGROUND AND SIGNIFICANCE

The use of high-strength concrete (HSC) in various construction applications has become widely accepted. Applications in columns and walls of high-rise building, long-span box-girder bridges, and structural components of offshore structures have been reported. The popularity of HSC is due to the pronounced advantages of the material, such as the superior strength and stiffness, long durability, and light-weight construction. In comparison to normal-strength concrete (NSC) structures, it is now possible to build slender columns and walls using high-strength concrete without reducing their load-carrying capacity. Thus, its use allows for reduced dimensions of the structural members and consequently, for a reduction in the overall cost of the building. Among the various applications of HSC for structural members, this research focuses on high-strength concrete wall panels.

Vertical high-strength concrete wall panels are subjected to compression forces in general, which apart from leading to axial shortening of the members, increase the susceptibility of the walls to buckling failures. In this sense, HSC panels are more prone to buckling failure than panels made of conventional normal-strength concrete because of their high slenderness ratio. This becomes even more critical when initial imperfection exists or when the axial load is an eccentric one, which is the case in most practical applications. The buckling failure of slender HSC panels is characterized by sudden and explosive manner, which initiates crushing of the concrete and/or yielding of steel reinforcement.

On the other hand, stubby walls with low slenderness may fail by concrete crushing or yielding of the reinforcement before the loss of geometrical stability. Many factors affect the buckling and failure behavior of HSC panels, including the steel reinforcement ratios in the two orthogonal directions, location of the reinforcement, slenderness ratio, aspect ratio, concrete strength, and the boundary conditions. These parameters need to be fully investigated and understood in order to enhance the effective design and safe use of HSC panels.

However, in most cases, the wall panel is subjected to sustained loads that result from its self-weight and loads that are transferred from the structure. When these loads are combined with the normal construction inaccuracies and load eccentricities that cannot be prevented especially in concrete construction, the wall will undergo increasing lateral deflection with time due to creep of the concrete. The time-dependent behavior is likely to cause excessive deflection and cracks, may consequently lead to loss of stability of the member, a phenomenon usually referred to as creep buckling.

In addition to the parameters mentioned above, the time-dependent behavior of HSC panels is characterized by many physical phenomena that introduce a level of complexity into their structural analysis. These include the dependence of the creep strains on the level of stresses that vary with time, their interaction with non-mechanical shrinkage and thermal strains, the aging and nonlinear time-dependent behavior of the concrete material, and the effects of structural imperfections that cannot be avoided in practice. Consideration and characterization of these effects make accurate prediction of the nonlinear behavior of wall panels a challenging and difficult task. Therefore, the problem of creep buckling needs to be thoroughly understood and properly addressed in the course of wall design in order to achieve safely designed structures and to extend their design life.

The short-term behavior of reinforced concrete (RC) wall panels, especially those made of normal-strength concrete has been extensively studied during the past few decades. Both experimental and analytical investigations have been carried on. (Swartz and Rosebraugh 1974; Swartz et al. 1974; Saheb and Desayi 1989, 1990; Gupta and Rangan 1998; Farvashany et al. 2008). Among the existing analytical studies, a number of studies were based on empirical or semi-empirical equations to predict the ultimate strength of concrete panels. Rigorous analytical studies were also undertaken by a few researchers, in which the material and geometric nonlinearities were accounted for. On the other hand, the studies on high-strength concrete panels under eccentric loading, and especially experimental investigations are limited.

Long-term studies on HSC panels cannot be found in the open literature. On the other hand, only a limited number of research works have focused on the time-dependent performance of NSC wall panels under sustained loading, but without addressing their creep buckling response. Numerous research works have been conducted on studying the creep buckling behavior of structures made of metals and polymers, and reinforced concrete structures other than wall panels (Rabotnov and Shesterikov 1957; Hoff 1958; Bažant 1968; Behan and O'Connor 1982; Chang 1986; Hamed et al. 2010a, b; Hamed et al. 2011). These studies shed light on the creep behavior of HSC panels in general and the creep buckling behavior in particular, but the numerical tools developed in these studies cannot be directly applied to concrete panels due to the different geometry and different material behavior. Hence, there is a need for further studies in this field.

This research focuses on investigating the long-term and creep buckling behavior of high-strength concrete wall panels. For this, theoretical models and numerical tools are developed, and a new experimental investigation regarding the buckling and the creep buckling behavior of HSC panels is conducted. The models take into account the effects of creep and shrinkage, the aging, cracking, tension-stiffening and the geometric nonlinearity. Design and analysis recommendations are established in the light of the outcomes of this research study.

1.2 OBJECTIVES AND SCOPE

The primary objective of this research is to enhance the fundamental understanding and to provide an insight into the long-term behavior of high-strength concrete wall panels. This goal will be achieved by developing nonlinear mathematical models for their analysis and by conducting experimental investigations that will reveal further aspects of the structural behavior, and will be used to validate the theoretical models. The following specific tasks are undertaken:

- To develop nonlinear theoretical models that is able to predict the short-term behavior of HSC panels, in order to establish the foundation for the long-term analysis. Experimental study will also be conducted to verify the short-term theoretical model.
- To develop nonlinear theoretical models that are able to characterize, describe and explain quantitatively the long-term physical performance of high-strength reinforced concrete panels under sustained loads, taking into account the geometric and material nonlinearities. Emphasis will be placed on the phenomenon of creep buckling;
- To undertake short-term and long-term experiments on full-scale one-way HSC panels to validate the theoretical models developed in this study and to provide benchmark data for other researchers;

- To parametrically analyze key material and geometric variables, and the boundary conditions that can affect the behavior of HSC panels;
- To review the existing design codes of concrete walls and to provide recommendations for the analysis and design of HSC panels.

1.3 OUTLINE OF THESIS

The thesis includes eight chapters. Chapter 2 present a review of the previous works published in the literature that are relevant to this study. The design codes are reviewed first with focuses on their approaches dealing with the creep and shrinkage effects in the design of wall panels. Then the literature on the short-term behavior of RC panels is addressed. Since there is lack of studies on the time-dependent response of HSC panels, the investigations on the long-term behavior of panels/plates and columns made of other materials are reported. Following that, the works on studying the long-term response of RC columns and shells are summarized. The last part of the chapter describes the material studies of the HSC in the literature and the theoretical models for the prediction of the material properties of HSC that can be employed in this research study are reported.

Chapter 3 describes the theoretical and experimental investigations of the short-term response of slender one-way HSC wall panels. The study focuses on the failure behavior of one-way HSC panels under instantaneous in-plane eccentric loading. The nonlinear model accounts for the geometric and material nonlinearities including the strain softening of concrete in compression, cracking and tension-stiffening as well as yielding of the steel reinforcement. The model describes the entire equilibrium path of HSC panels through the use of the arc-length method. The theoretical model is compared to and verified by the test results of 8 one-way HSC panels, which were tested to failure in this study under short-term in-plane loading. The effects of reinforcement ratio and arrangement, load eccentricity and slenderness ratio are also examined in the experimental study.

The long-term behavior of one-way HSC panels is studied in Chapters 4, 5 and 6 progressively. Chapter 4 conducts a theoretical time-stepping analysis on general slender one-way panel subjected to sustained in-plane loading without the consideration of cracking. A rheological model that is based on the generalized Maxwell chain is adopted to model creep. The model accounts for the geometric nonlinearity through large displacements kinematic relations and accounts for the change of the internal stresses and deformation with time. A numerical example is presented and a parametric study is conducted to highlight the importance of the in-plane load level and eccentricity on the nonlinear time-dependent behavior of one-way general panels.

Chapter 5 develops a more detailed and more specific nonlinear long-term theoretical model to study the time-dependent response of one-way HSC panels based on the time-stepping analysis presented in Chapter 4. Apart from the creep, the model takes into account the shrinkage, aging, cracking and tension-stiffening of the concrete through strain- and time-dependent springs and dashpots in the generalized Maxwell chain. The incremental governing equations are derived and solved using the multiple shooting method. A smeared cracking model is adopted, and an iterative procedure is conducted at each time step for the determination of the unknown rigidities of the cracked section, as well as the length of the cracked region. The capabilities of the model are demonstrated through numerical and parametric studies.

The theoretical model developed in Chapter 5 is validated by the test results reported in Chapter 6, where a long-term experimental study is carried out on one-way HSC panels. Five simply-supported slender one-way HSC panels are tested in this study under sustained eccentric in-plane loads up to a period of four months. A variety of parameters including the in-plane load level, the load eccentricity and age of concrete are investigated in the test. Two panels failed by creep buckling under the sustained loads, whereas the other three panels exhibited stable behavior, and thus, were loaded to failure at some time after initial loading without the release of the sustained loads. Close correlations are achieved between the test and theoretical results.

In Chapter 7, the nonlinear long-term behavior of slender HSC panels in two-way action is investigated. A nonlinear theoretical model that considers the geometric nonlinearity is developed for the two-way panel based on the time-stepping analysis. Von Karman plate theory is used and the plane stress condition is adopted. A rheological material model that is based on the generalized Maxwell chain is adopted to model the creep of concrete. The concrete is assumed to be linear viscoelastic at first in order to highlight the effect of creep on the time-dependent response. Then, the cracking is included in the model using a smeared cracking approach. The incremental governing equations are solved numerically at each time step through the combined use of Fourier series expansions of the deformations and loads in one direction and the multiple shooting method in the other direction. Numerical examples are demonstrated and a parametric study is conducted to investigate the effects of in-plane load level and eccentricity, slenderness ratio, boundary conditions, aspect ratio, reinforcement ratio and shrinkage.

Chapter 8 summarizes the main outcomes and conclusions drawn from this research investigation, and recommendations for the future research are also made.

CHAPTER 2 LITERATURE REVIEW

A summary of the existing research studies published in the open literature pertained to the subject of this thesis is presented in this chapter. It starts with a general review on the design codes of practice including AS3600, ACI318 and Eurocode 2 regarding the design of wall panels. Emphasis is placed on the design approaches that deal with the time-dependent effects of concrete. Next, the findings of the studies on the short-term responses of the NSC and HSC wall panels are reported, in order to set the basis for the long-term investigation of HSC panels. The panels in both one-way and two-way actions are included. It is found that the instantaneous behavior of NSC and HSC panels have been extensively investigated in the literature, but studies that focused on the long-term response of HSC panels cannot be found in the open literature. Therefore, the literature on long-term behavior of the panels and columns made of metals and composite materials are addressed in the next section, followed by a summary of the research works on the long-term behavior of RC columns and shells. The last section describes the prior investigations on the material properties of the high-strength concrete. Typical theoretical material models which can be potentially utilized in the theoretical models to be developed in this thesis are summarized in this section, including the ones for predicting the creep and shrinkage, compressive and tensile strength, elastic modulus, constitutive relations, tension-stiffening effect and crack width of high-strength concrete.

2.1 REVIEW OF CODE PROVISIONS FOR WALL DESIGN

A general overview of three major codes of practice (AS3600, ACI318, Eurocode 2) that provide design guidelines for concrete walls is presented in this section with emphasis on the design methods of wall panels against the time-dependent effects of concrete. A detailed discussion on the codes can be found in the following chapters where they are compared to the short-term and long-term theoretical models developed in this study.

2.1.1 Australian Standards – Concrete Structures (AS3600-2009)

AS3600 (2009) discusses the design of reinforced concrete walls in Section 11 with characteristic concrete compressive strength at 28 days ranging from 20 MPa to 100 MPa, namely from normal-strength to high-strength. The one-way and two-way buckling strengths of walls are both accounted for in the provisions and they are distinguished and characterized by the effective length of the wall. The strength design formulae apply only when walls are subjected to in-plane loading. For walls subjected to combined in-plane and out-of-plane loading, the provisions of designing slabs and columns, wherever appropriate, should be used as recommended in Section 11. The AS3600 (2009), however, provided no specific guidelines for including the long-term effects into the design of the walls for which the effect of creep may substantially influence their performance. Creep might lead to gradual lost in the structural capacity and may eventually lead to creep buckling. Therefore, it should carefully be accounted for in slender structures.

2.1.2 American Concrete Institute code ACI318 (2008)

The ACI318 (2008) presents an empirical method for designing concrete walls in Chapter 14. It focuses on panels generally subjected to a resultant force of all factored loadings located within the middle third of the overall thickness of the wall. Only one-way action of the wall is taken into account in this design procedure. Chapter 14 also includes another method specified for out-of-plane design of slender wall panels. In this approach, the slender wall panel is treated as a simply supported member subjected to combined axial load and out-of-plane uniform lateral load. The empirical methods for general wall design and slender wall design are applicable to both normal and high strength concrete. Yet, similar to AS3600 (2009), the time-dependent characteristics of the HSC are not considered here.

2.1.3 European code (Eurocode 2)

The Eurocode2 (2005) provides design guidelines for walls in Section 5 where they are considered as columns subjected to vertical load and transverse moments at the top and bottom ends. According to Eurocode 2, when the wall is subjected predominately to lateral bending, the design of a wall will be carried out as a slab. In addition, the code provides instructions in Section 12 for designing walls made of plain concrete or reinforced concrete with reinforcement less than the minimum quantity required in the code. A simplified design method is given in this section where the wall is subjected to bending and axial force. One-way and two-way actions are both accounted for in this equation, and it is suitable for the design of both NSC and HSC walls. Nevertheless, the long-term behavior of HSC walls is not discussed.

2.2 SHORT-TERM BEHAVIOR OF CONCRETE WALL PANELS

Many research works have been found in the literature to investigate the behavior of reinforced NSC and HSC panels in one-way/two-way actions. Yet, the majority of these works focused on their short-term performance. To the best of the author’s knowledge, studies on their long-term behaviors of HSC and even NSC panels cannot be found in the open literature. Therefore, the existing experimental and analytical studies pertained to short-term behavior of the RC panels are reported first, followed by review of the literature on the long-term response of plates and columns made from metals and polymers. After that, the findings of existing studies on the time-dependent behaviors of reinforced concrete columns and shells are reported, which will provide some insights into the investigation of the long-term behavior of HSC panels.

2.2.1 Short-term behavior of concrete panels in one-way action

2.2.1.1 NSC wall panels

Oberlender and Everard (1977) presented results of testing 54 concrete walls and compared the test results with the analytical methods for wall design prescribed by ACI318 (1971). Two axial loading schemes, namely, concentric loading and eccentric loading were applied to each wall configuration. The slenderness ratio of the walls ranged from 8 to 28. The strength of concrete was varied between 25 MPa to 46 MPa. It was shown that the empirical equations for wall design provided by Chapter 14 of ACI318 (1971) gave considerably lower predictions of the failure loads for walls with small slenderness ratio (8 to12). The predictions for intermediate slenderness ratios (16 to 20) were compatible with test failure loads. For larger slenderness ratios (24 to 28), the equations overestimated the failure loads. The other comparison was made between the test results and the method appearing in Chapter 10 of ACI318 (1971) which treated walls as columns for design purposes. The ultimate strength method in Chapter 10 actually takes the slenderness effects into account. It was found that this method has correlated well with test data and was recommended as the proper method for designing wall panels.

Saheb and Desayi (1989) reported test results of 24 reinforced concrete wall panels carrying eccentric in-plane vertical loading in one-way action with concrete compressive strength ranging from 20.17 MPa to 25.17 MPa. The experimental study investigated the effects of various parameters that can influence the strength and behavior of wall panels, such as slenderness ratio (height-to-thickness ratio of the wall), aspect ratio (height-to-width ratio of the wall), and amounts of reinforcement in the vertical and horizontal directions. The experimental ultimate loads were compared with the predictions of an empirical equation which was developed by modifying the ACI318 (1977) and Zielinski et al. (1982) equations. It was shown in this study that the ultimate strength of wall panels decreased linearly with an increase in the aspect ratio but decreased nonlinearly with an increase in the slenderness ratio. The vertical reinforcement had significant effect on the wall strength, which grew linearly with the increase of the vertical reinforcement ratio. The effect of horizontal reinforcement on the ultimate strength was found to be negligible. The proposed modified empirical formula gave slightly conservative but safe estimations of the ultimate load of wall panels in one-way actions, and so it was recommended to be used in the design of reinforced concrete wall panels.

2.2.1.2 HSC wall panels

Gupta and Rangan (1998) presented an experimental study on high strength concrete structural walls which were subjected to in-plane axial compressive load and horizontal in plane load. The authors also developed a model that is based on the modified Compression Field Theory proposed by Vecchio and Collins (1986) and the conventional theory of reinforced concrete sections subjected to combined bending moment and axial compression for predicting the shear and flexural strengths. The analytical results showed good correlation with the ones obtained from tests conducted in this study as well as other test results available in the literature.

Fragomeni and Mendis (1998) tested 16 eccentrically loaded normal and high-strength concrete wall specimens and compared the results with theoretical predictions based on ACI318 (1995). The strength of concrete used in the study varied between 32.9 MPa and 67.4 MPa. The high-strength concrete walls exhibited a more brittle bending failure in contrast to normal-strength concrete walls. The failure of HSC walls involved less concrete crushing than normal strength concrete specimens did, which occurred after yielding of reinforcement. The difference was attributed to the higher compressive strength of the high-strength concrete walls, which prevented early occurrence of concrete crushing. The comparison with the ACI318 (1995) code indicated that the code produced reasonable evaluations of the axial load capacity of normal-strength concrete wall panels but overestimated the axial capacity of high-strength concrete walls.

Yun et al. (2004) also compared the predictions of the ACI318 (1999) with experiments performed on high-strength concrete walls. Yet, it was found that the ACI318 (1999) underestimated the load-carrying capacity of high-strength concrete wall panels.

Farvashany et al. (2008) tested seven large-scale HSC shear-wall specimens that were loaded to failure under constant in-plane axial load and horizontal in-plane load. The effect of the ratio of steel reinforcement on the strength of the shear-wall was examined. It was found that increasing the vertical reinforcement ratio led to an increase in the horizontal failure load, while the effect of horizontal reinforcement ratio was less profound, only leading to marginal increase of the shear strength for higher ratio.

Doh (2002) carried out tests on 18 concrete wall panels in both one-way and two-way actions. The panels were subjected to eccentric in-plane loads in the test. Both normal strength concrete panels and high strength concrete panels were tested, with compressive concrete strength varying from 35.7 MPa to 78.2 MPa. The aspect ratio and slenderness ratio were varied in the test to examine their influences on the panel behavior. The test results showed that both NSC and HSC panels in one-way action have developed a single curvature in the vertical direction at failure. The failure cracks were horizontal (perpendicular to the loading direction) and near the center of the panels, signifying bending failure.

Regarding the panels in two-way actions, both NSC and HSC panels developed biaxial curvature crack pattern at failure. Also here sudden and explosive types of failure were observed for HSC panels. The ultimate strength of both NSC and HSC panels were found to decrease gradually with the increase in the slenderness ratio. However, the reduction appeared to be greater for HSC panels. As indicated in this chapter, the HSC panels generally possessed smaller axial strengths than NSC panels, due to their relatively high slenderness ratios (30 to 40 in this study). Furthermore, the test results showed that the strengths of two-way panels were about three times higher than those of one-way panels.

In addition to the experimental works on the NSC and HSC plates/panels, theoretical works were also carried out to analyze the short-term behavior of these structures.

El-Metwally et al. (1990) performed a stability analysis of eccentrically loaded reinforced concrete walls using the finite element (FE) method. The wall was modeled as a beam-column and it was subjected to axial loads and moments at both ends. The results showed that the failure mode of the beam-column was sensitive to the slenderness ratio and eccentricity. For walls with moderate slenderness ratio, material failure rather than instability becomes dominate.

Fragomeni and Mendis (1997) performed a numerical analysis on the stability of normal and high-strength reinforced concrete walls. The model developed in the study took into account the P-Δ effect by implementing iterative analysis that yielded more accurate and generally less conservative results than the ACI318 (1989) design provisions. Based on their theoretical findings, the authors pointed out that there was no significant increase of the strength of the wall as a result of increasing the vertical reinforcement ratio if the reinforcement was only placed centrally in one layer. On the contrary, increasing the reinforcement ratio in the walls with two layers of reinforcement placed in each face would produce substantial increase in the strength of the wall.

Shousha et al. (2007) proposed equations to predict the load-carrying capacity of high-strength concrete wall panels supported on all four edges and subjected to combined axial and transverse loads. The analysis was undertaken based on equilibrium of forces and compatibility of the strains, taking into account nonlinear effects between axial load and lateral deflection. The analytical model was verified by the experimental results.

2.2.1.3 Concrete wall panels with openings

Apart from the studies that focused on solid panels, a few researchers investigated the behavior of concrete panels with openings as well.

Saheb and Desayi (1990b) tested 12 concrete wall panels to failure, which were with openings of various geometries, representing the windows and doors. The wall panels were eccentrically loaded in both one-way and two-way actions. It was found that the failure of the wall panels both in one-way or two-way actions, is characterized by a buckling of the concrete column strips adjacent to the openings. The presence of openings offsets the supporting effect in two-way action, leading to approximately equal ultimate strength of wall panels in both one-way and two-way actions. Empirical equations were developed for assessing the ultimate strength of wall panels with openings in one-way and two-way actions. The equations were formulated by means of multiplying the equations for predicting the ultimate strength of identical concrete wall panels without openings (developed by Saheb and Desayi, 1989), with a reduction parameter that represents the geometry of the openings. The equations appeared to be satisfactory in terms of estimating the ultimate load of panels with openings.

Guan et al. (2010) undertook finite element analysis on concrete panels with openings. The results were verified with experimental data published prior to the study, and consequently, more comprehensive formulae that took into consideration the length, height and location of openings were proposed. The authors pointed out that the ultimate strength of the panel was more susceptible to the combined effects of simultaneous change in both the height and length of the openings rather than a change in one of these parameters separately.

It is shown that many efforts have been made to study the short-term behavior of concrete panels. Yet, only few research studies were devoted to the long-term performance.

2.2.2 Short-term behavior of concrete wall panels in two-way action

Swartz et al. (1974) tested 24 rectangular concrete walls in two-way action which were subjected to uniaxial compression along shorter edges, and simply supported along all edges. They proposed an equation to predict the buckling pressure of the walls based on the test results. The strengths of concrete used in the panels range from 17.2 MPa to 20.7 MPa. The concrete wall panels failed by buckling (biaxial curvature) at stress levels remarkably lower than the concrete compressive strength. The authors pointed out that the collapse mechanism of the tested panels was similar to that for simply-supported panels subjected to uniform transverse loads. It was concluded in the paper that the presence of steel reinforcement was essentially inconsequential to the buckling load, but was important with respect to the panel ductility. The proposed formula as explained in details in Swartz and Rosebraugh (1974) for predicting the buckling pressure, which yielded reasonably conservative and accurate results. However, the simplified formula was based on simply-supported boundary conditions and on the elastic behaviour of concrete before buckling, which significantly limits its applicability in other cases.

Saheb and Desayi (1990a) tested 24 rectangular reinforced concrete wall panels loaded eccentrically in two-way action, with concrete strength ranging from 20.17 MPa to 25.17 MPa. The panels were simply supported along four edges and were subjected to in-plane loading. The influences of the aspect ratio (defined as length-to-width ratio), thinness ratio (defined as width-to-thickness ratio in this paper), slenderness ratio (defined as length-to-thickness ratio), and the ratio of steel reinforcement on the performance of the panels were examined. Based on the experimental results, the authors proposed two equations to predict the ultimate load-bearing capacity of the reinforced concrete panels, in which one is empirical and the other one is semi-empirical. It was found that the ultimate strength of wall panels in two-way action increased linearly with the increase of the aspect ratio as well as the vertical reinforcement. On the other hand, it reduced nonlinearly with the increase in thinness or slenderness ratios. These findings are somehow similar to the ones observed by Saheb and Desayi (1989) for the case of one-way action. Also here, the effect of horizontal reinforcement on ultimate strength was negligible. The proposed design equations were able to produce safe predictions of the ultimate strength of concrete wall panels in two-way action in comparison with the test results and with other nine test results obtained in other studies. Yet, the empirical equation was more accurate than the semi-empirical one.

Aghayere and Macgregor (1990b) reported test results on 9 concrete plates, simply supported along four edges and subjected to combined uniform in-plane compression and uniform transverse loading. No tests had been conducted before this study for RC plates under this combined loading scheme. The parameters examined in the study included the aspect ratio, slenderness ratio, and reinforcement ratio. The aspect ratios of the panels are 1 and 1.5, with slenderness ratio (defined by height/thickness) ranging from 27.3 to 33. The plates were made with concrete strength of 32.2 MPa to 40.3 MPa.

For the square specimen that was subjected to the transverse load only, yield lines formed on the tension face of the specimens at maximum loads. Cracks were observed along the diagonal on the bottom (tension) face near the corners. At failure, crushing of concrete occurred on the top face of the specimen above these cracks. In addition, cracks developed perpendicular to the diagonals on the top surface near the corners. These cracks resulted from the plate corners being held down, which permitted the development of anticlastic corner surfaces. The twisting moment near the corners caused torsional cracks on the edges of the plate near the corners.

In the square specimen tested under combined transverse loads and uniaxial loads, cracks were first observed at the bottom face of the specimen in the direction of the in-plane load. The reinforcement at the center of the plate yielded at this load. Final failure was characterized by an explosive concrete crushing. Cracks were more prevalent in the direction of the in-plane loading.

Based on the test results, it can be concluded that in most axially loaded specimens, buckling of the reinforcement adjacent to the compression face took place at failure and all final failures were compression failures due to crushing of the concrete. For all specimens, the cracks in the tension face tended to propagate in an orthogonal pattern that coincided with the reinforcement layout due to the local stress concentrations caused by the presence of reinforcing steel. The crack patterns for the axially loaded specimens approached that of a similar plate under transverse loads only.

As expected, the results of the investigation revealed that the presence of the axial in-plane load results in a reduction in the transverse load-carrying capacity. It was also found that the degree of reduction depends on the aspect ratio, the concrete strength, the amount of reinforcement, and the width-to-thickness ratio. The square wall plates (aspect ratio equals to 1.0) exhibited an instability failure mode followed by the concrete crushing as a secondary failure, whereas the collapse of rectangular plates (aspect ratio equals to 1.5) was caused by concrete crushing.

Ghoneim and MacGregor (1994a) tested 19 two-way RC plates that were subjected to combined in-plane compressive and transverse loads and simply supported on the four edges. The variables in the test included loading type, plate slenderness and aspect ratio, reinforcement ratios in the two orthogonal directions, in-plane load level and loading sequence. Normal-strength concrete were used with compressive strength varying from 18.7 MPa to 26.1 MPa.

The cracking patterns in Series A which had the largest aspect ratio (length/width) (2.17) is shown in Fig. 2.1. These panels were tested under combined transverse loads and in-plane load with the in-plane loads applied along the shorter edges. It can be seen that the cracks developed in parallel to the long direction, indicating almost a one-way action of the plate strips in the middle region, as indicated in Fig. 2.1. The other specimens which had smaller aspect ratios developed orthogonal patterns of cracks (see Fig. 2.2) that reflected the reinforcing pattern and indicted a two-way action.

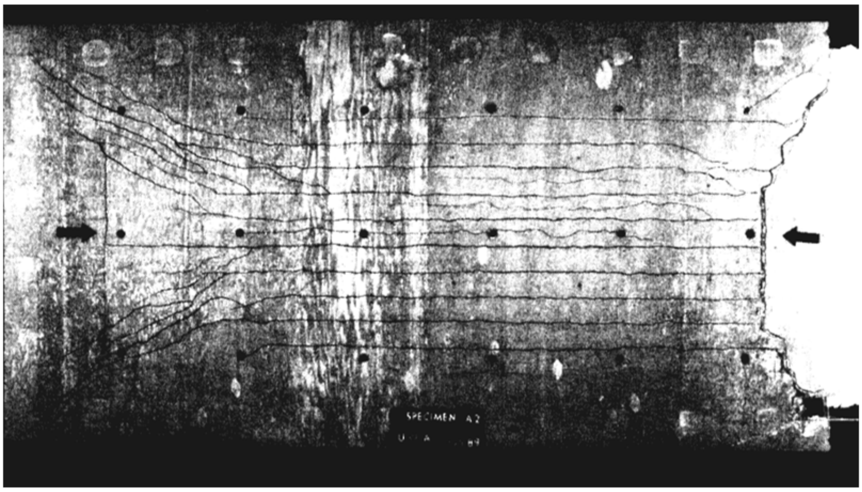

Fig. 2.1 Typical cracking pattern of Series A (aspect ratio=2.17) (Reproduced from Ghoneim and MacGregor (1994a))

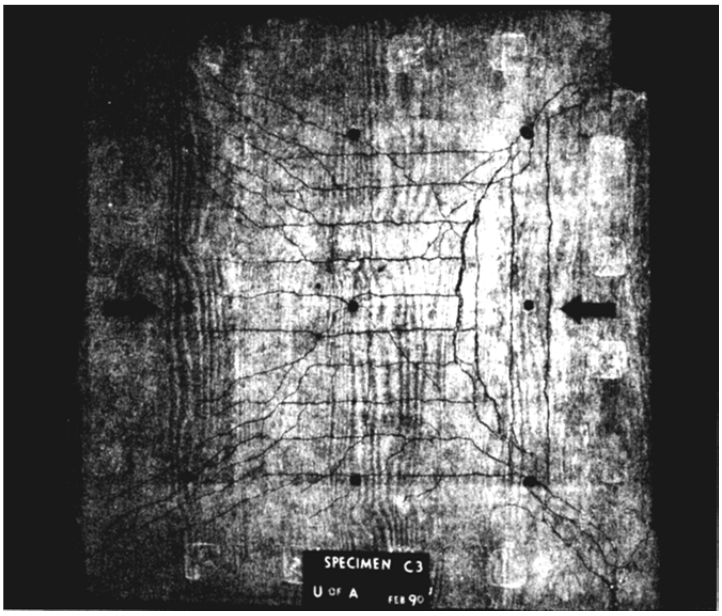

Fig. 2.2 Typical cracking pattern of square specimen (aspect ratio=1) (Reproduced from Ghoneim and MacGregor (1994a))

The failure of the specimens that were tested under transverse load only was very ductile. However, the ones tested under combined transverse and in-plane compressive loads failed explosively. Concrete crushing lines were formed on the top surface accompanied by buckling of the compression reinforcement in the direction of the in-plane load. The test results indicated that the slenderness of the plate and the loading sequence mainly determined the effect of the in-plane load on the lateral load capacity of RC plates. Both material failure including crushing of concrete and yielding of the tension steel and stability failure occurred in the RC plates tested under combined loads.

The effects of different parameters on the behavior of the RC plates were discussed in details in Ghoneim and MacGregor (1994b). It was found that for stocky square plates, the presence of the in-plane load increased the lateral load capacity, as the geometrically nonlinear effect was insignificant. On the other hand, the presence of the in-plane load resulted in substantial reduction in the lateral load capacity of slender plates, since the second-order effect of the in-plane load dominated the behavior. It was also found that the RC plates behaved highly anisotropically under the action of combined uniaxial in-plane and lateral loads because the presence of the in-plane load increased the cracking moment about the axis perpendicular to its direction. As revealed in the paper, the behavior of the RC plates was also significantly influenced by the loading sequence. The proportional loading or prior application of the in-plane load resulted essentially in the same load-deflection response. On the other hand, the prior application of the lateral loads followed by the application of the in-plane loads led to considerably different results from the former two loading cases, which were mainly determined by the state of the cracking and the out-of-plane deflection when the in-plane load was applied.

Sanjayan and Maheswaran (1999) carried out experiments on 8 high-strength concrete walls loaded eccentrically. The walls were simply supported along the side edges only. Different parameters that included the reinforcement ratio, eccentricity, and concrete compressive strength were examined. It was found that the load capacity of the wall was significantly influenced by the eccentricity of in-plane loading, while it was insensitive to the concrete strength. The typical crack patterns on the tension faces are illustrated in Fig. 2.3 and Fig. 2.4 for the eccentrically loaded HSC concrete panels with eccentricity that equals to 8 mm and 25 mm, respectively. Ductile type failures were observed in walls subjected to eccentricity of 25 mm, while more sudden and explosive types of failure were observed in walls with eccentricity of 8 mm. The crack patterns on the tension side of all the walls clearly showed that the specimens developed a two-way action, typical to classical buckling of thin walls.

The test results were compared to three codes of practice, namely ACI318 (1992), AS3600 (1994) and BS8110 (1985), and to three prediction formulae proposed by Swartz et al. (1974), Saheb and Desayi (1990a) and Aghayere and MacGregor (1990a). The comparison led to the conclusions that the three codes of practice severely underestimated the failure loads of eccentrically loaded high-strength concrete panels, while the proposed formulae by Swartz et al. (1974) and Saheb and Desayi (1990a) considerably overestimated the wall strength. The analytical model of Aghayere and MacGregor (1990a) had partial success in predicting the loading capacities, but the estimates were still largely different from the test results.

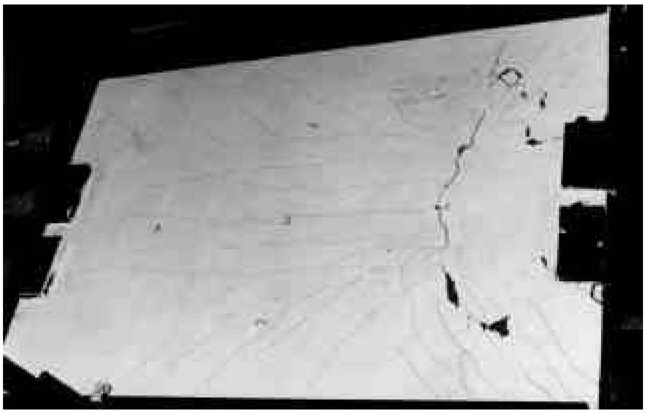

Fig. 2.3 Typical cracking pattern of HSC panels (2000 x 1500 x 50mm) simply supported on two side edges and free on the loading edges (*e* = 8 mm) (Reproduced from Sanjayan and Maheswaran (1999))

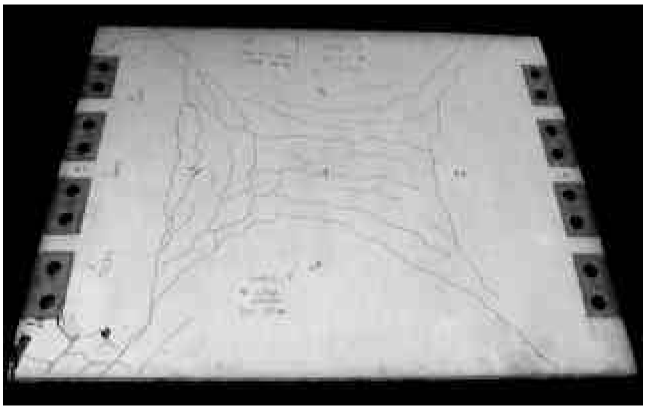

Fig. 2.4 Typical cracking pattern of HSC panels (2000 x 1500 x 50mm) simply supported on two side edges and free on the loading edges (*e* = 25 mm) (Reproduced from Sanjayan and Maheswaran (1999))

In terms of analytical studies, Aghayere and MacGregor (1990a) described the load-deflection response of simply-supported concrete plates in two-way actions based on the assumed deflection method where a deflection function was assumed over the entire load range. The plates were under transverse (lateral) and in-plane compression loads. The material nonlinearities were taken into account in the analysis by utilizing the moment-curvature relationship including the tension-stiffening effect. The predictions agreed well with the experimental results. It was indicated that the presence of axial in-plane load would be favorable for the transverse load-carrying capacity of the plates, provided that the in-plane load is less than the balanced failure load and that the slenderness ratio (height/thickness) is less than 25. However, for a given in-plane load, the transverse capacity decreased with increasing the slenderness ratio. Nevertheless, the model only used uniaxial constitutive relation of concrete, which greatly simplified the problem of two-way panel. It also assumed a deflected shape to solve the governing equation, which may not always be valid once the concrete started to crack.

Massicotte et al. (1990) investigated the behavior of two-way slender RC plates that were simply-supported along four edges and subjected to combined in-plane and lateral loads using a finite element (FE) analysis. The FE analysis was based on the two-dimensional incremental hypoelastic model in which plane stress condition was assumed. The concrete was assumed to be isotropic up to either cracking or crushing, and the model allowed for strain softening after both cracking and crushing. A smeared crack approach was adopted and a three-dimensional plate-shell element that can accommodate large strains and large displacements was used in the model. The comparison of the model results with the experimental results showed that the FE model could adequately predict the behavior of RC plates. A parametric study based on the FE model revealed that the ductility of the plates was strongly affected by the in-plane load magnitude. In addition, it was concluded that for a simply-supported RC plates subjected to uniaxial in-plane and lateral loading, the lateral load-carrying capacity of the plates could be increased more efficiently by increasing the reinforcement ratio in the direction perpendicular to the in-plane load than in the direction parallel to the in-plane load. This is because for RC plates with typically low reinforcement ratios, the strengthening influence of reinforcement in the direction parallel to the in-plane loading on the lateral load-carrying capacity was small in comparison to the deteriorating influence of in-plane loading. Therefore, the combined effect of increasing the lateral capacity by increasing the reinforcement in the parallel direction was insignificant. However, in the transverse direction, as there did not exist in-plane loading, the increase of the reinforcement could directly increase the lateral load-carrying capacity.

Ghoneim and MacGregor (1994c) presented an analytical method that was capable of predicting the ultimate strength of RC plates supported on four edges and subjected to combined uniaxial or biaxial in-plane and out-of-plane loads. Material nonlinearities including yielding of reinforcing steel, cracking of concrete and tension-stiffening effect, strain-hardening and softening of concrete in compression were taken into account in the model by using elastic theory of plates with secant rigidities. The geometrical nonlinearity was incorporated in the governing equations, which were solved by means of expanding the plate deflection and the out-of-plane load into Fourier series. The theoretical results were compared with the test results and good correlations were reached.

Attard et al. (1996) also used the FE model to study the out-of-plane buckling of reinforced concrete walls. The concrete was modeled using nonlinear orthotropic 16 degree-of-freedom plate elements. The cracking and nonlinearity of concrete in compression were taken into account in the model. However, tension-stiffening was not included. The comparison between the theoretical results to available experimental results revealed a good correlation.

2.3 LONG-TERM BEHAVIOR OF PLATES/PANELS AND COLUMNS MADE FROM OTHER MATERIALS

The findings of previous research works with regard to structures made from metals and composite materials are reported first. Then, the literature on concrete structures is investigated including columns and shells that may experience creep buckling.

The phenomenon of creep buckling of structural members has attracted extensive research attentions. Among the first studies, Hoff (1956) studied the creep buckling behavior of structural metal columns with initial crookedness and presented a theory that was able to address the critical time at which the initially imperfect column would collapse due to the effect of creep. Both instantaneous elastic and plastic deformations were taken into account in the development of the theory that accounted for the transient and secondary creep of the material. The rate-of-creep method was applied to model the time-dependent stress-strain relations of the metal.

An alternative method to creep buckling was proposed by Rabotnov and Shesterikov (1957) in their investigation of creep stability problem of columns and plates. Here, a small out-of-plane disturbance was introduced to the initially straight compressed column/plate. Based on the response with time, the column/plate was considered unstable if the lateral deflection caused by the disturbance increased in the subsequent interval of time or stable if it decreased.

Distefano (1965) presented a study on the critical loads of axially loaded metal columns using linear and nonlinear creep law. The metal investigated in the study exhibited bounded creep as time tended to infinity. The author found out using the reduced modulus method that the lateral deflection of imperfect columns may become unbounded in some cases, thus, exhibiting creep buckling failures.

Huang (1976) introduced the large deformation kinematics into the creep buckling analysis of initially imperfect columns. As indicated, the analysis that was based on the small deformation approach might lead to misleading results given that the critical time for creep buckling was determined by the unbounded deflection or deflection rates. It was found that creep buckling could be characterized by upper and lower bounds at a finite time according to the large deformation analysis. If the acting load exceeded the upper bound, instantaneous buckling would occur, while if the load was smaller than the lower bound, creep buckling would not occur.

Tvergaard (1979) investigated the creep buckling behavior of simply-supported rectangular plates made from metals under axial compression. The elastic and plastic behaviors of the material along with creep were accounted for. A perturbation method is used to analyze the creep buckling behavior. An iterative incremental numerical analysis was also carried out to investigate the plate creep buckling by further considering plasticity. It was shown that in addition to the elastic and creep deformations, when plastic yielding also occurred, the imperfection-sensitivity was considerably increased.

Vinogradov (1985) presented a theoretical model for describing the behavior of linear viscoelastic eccentrically loaded columns. The study focused on the geometrically nonlinear effects of viscoelastic structures using the quasi-elastic method. For material exhibiting limited creep, both solutions obtained from geometrically linear and geometrically nonlinear analyses predicted the existence of a safe load limit below which the deflection of the column would approach an asymptotic value as time went to infinity. Moreover, reasonable agreement between the linear and nonlinear results could be found when the lateral deflection of the columns remained below 10% of the length of the column. Beyond this magnitude of deflection, as the deflections developed with time, the difference between the two solutions increased, and becomes more significant for loadings equal or greater than the safe load limit. The linear analysis predicted greater rates of creep deformation and in contrary to the nonlinear theory, infinite increase of the deflection within a finite time was detected. This conclusion implied that the critical time of the structure could not be assessed based on the infinite deformation criterion because critical time corresponding to infinite deflection did not exist in the geometrically nonlinear analysis, which is more accurate.

Chang (1986) examined two basic approaches for studying the creep buckling problem, namely the linearized dynamical approach developed by Rabotnov and Shesterikov (1957) and the quasi-static nonlinear approach proposed by Hoff (1956). The former method was used in the case of perfectly straight nonlinear viscoelastic columns where a small perturbation was applied in analyzing the stability problem. A linear relation of the changes in the stress and strain quantities was characterized in this method during the small excursions from the uniformly compressed state following the lateral disturbance. On the contrary, the quasi-static nonlinear approach was applied for the initially curved or eccentrically loaded columns. Although the former method predicted the critical buckling loads while the latter one yielded critical times, it was found that the two methods were closely related to each other by taking the transient creep (also called primary creep in theory of metal creep) into consideration. The Hoff’s approach could also be used to find the critical creep buckling load.

Minahen and Knauss (1993) analytically and experimentally investigated the creep buckling of viscoelastic polymeric columns. The growth of initial imperfections was estimated by utilizing the hereditary integral formulation. Small deformation kinematics was first used in solving the problem and then the solution was generalized to take the non-linear kinematics into account. The results showed that the small deformation theory represented the deformations of the structure closely to the experiments and conservatively.

Ashour (1994) reported an incremental analysis of the creep buckling problem of geometrically imperfect circular cylindrical metal panels under uniaxial, lateral and multiaxial loading with simply-supported boundary conditions. The analysis was developed based on a non-dimensional form of Donnell-type equations for a slightly imperfect cylindrical panel and Odqvist's constitutive equations for steady creep were employed. The numerical results showed a good agreement with previous experimental and analytical results. As revealed by the parametric study, the creep buckling time (critical time) of the cylindrical plate was significantly affected by the level of loads, the magnitude and direction of initial imperfection and the curvature of the plate.

Birman and Magid (1995) presented a practical method for the analysis of simply-supported columns with an arbitrary symmetric cross-section. This method was applicable as long as the creep of the column material followed Norton's law. Analysis of the numerical results indicated that critical time was sensitive to many parameters, such as the chemical content of the material, the test temperature, and the magnitudes of the imperfections and compressive loads.

Kirsanov (1997) analyzed the creep buckling of a column using singular point theory and suggested a criterion for creep buckling based on singular points of deformation for a perfect system. A singular point was defined as a moment of the history of the deformation process if the initial value of speed, acceleration or some time-derivative of deflection corresponded to infinity of deflection at this moment. The theory of transient creep with power law strain hardening was examined in the analysis. The comparison between theoretical and experimental results indicated good agreement.

Oliveira and Creus (2000) presented a FE study on plates and shells made of polymeric composite materials. The material behavior including thermal, hygroscopic, and viscoelastic effects were modelled using an efficient state variable representation. An incremental approach was adopted, where the damage was determined and used to calculate the modified stiffness matrix. The proposed numerical model was verified by an analytical solution for the case of viscoelastic bending. The presented numerical examples demonstrated the capability of the model in predicting and describing the time-dependent behavior including post-critical behavior of composite shells and plates.

Selim and Akbarov (2003) studied the three-dimensional creep buckling problem of a thick rectangular plate made of viscoelastic composite materials. The plate was clamped at four edges and subjected to in-plane compression forces along two shorter edges. The plate was assumed to have an initial imperfection. A three-dimensional linearized theory of stability was used to derive the boundary-value equations, which were then solved by employing the finite element method and the Laplace transformation. Based on the proposed modelling, the critical time which was defined as the time where the imperfection started to increase indefinitely can be predicted. The numerical study showed that the critical time depended on the parameters used in the creep model of the material.

Amoushahi and Azhari (2013) developed a semi analytical finite strip method to analyze viscoelastic plates with different boundary conditions by using bubble functions. A continuous harmonic function series were used as displacement functions in the longitudinal direction and a piecewise interpolation polynomial was used in the transverse direction. The material was considered to be linear viscoelastic by expressing the relaxation modules into Prony series. Through this method, the change of the deflection of viscoelastic plates with time can be predicted and the buckling loads can be determined.

Jafari et al. (2014) investigated the local buckling behaviour of moderately thick viscoelatic composite plates subjected to in-plane loading using finite strip method. Higher-order shear deformation theory and effective modulus method were used to form the governing equations in the time domain. The critical buckling loads were determined through solving the eigenvalue problem related to the global stiffness and geometry matrices. The model was validated against other methods reported in the literature. A comprehensive parametric study revealed that the local buckling coefficient increased with the increase of the rigidity in the longitudinal edges of the composite plates.

Despite the significant achievement in analyzing the creep behavior of structures, the solutions of all aforementioned studies cannot be directly applied for the creep analysis of concrete structures, since they were carried out based on material models of metals or materials other than concrete. Concrete material possesses a number of distinctive features like cracking, material nonlinearity, shrinkage and aging that metal and other composite materials do not have. This leads to different material model to be considered in modelling the time-dependent behavior of concrete structures.

2.4 LONG-TERM BEHAVIOR OF CONCRETE COLUMNS AND SHELLS

As mentioned above, one of the main characteristics of the viscoelastic response of concrete is the aging effect, which introduces different modeling and computational complexities in the creep analysis of concrete structures, and distinguishes the analysis approaches from those suitable for metals. A number of methods had been developed to predict the material behavior of concrete, in which the ones that are commonly used including the effective modulus method, the age-adjusted effective modulus method, rate of creep method, improved Dischinger method, superposition method, and the solidification theory (Bažant and Prasannan 1989a; b). Each individual method was extensively discussed and well documented in the literature, and therefore will not be the focus of this section. This section, however, will present an overview of the research studies that are related to the investigation of the long-term or time-dependent performance of concrete structures.

Mauch and Holley (1963) undertook an analytical investigation on the instability of reinforced concrete columns with initial curvature under sustained load. Instability was characterized by a finite desired life time. The concrete was considered as a nonlinear material while only linear geometric behavior was considered in the analysis of the columns. The constitutive law of the material was expressed in the form of differential type. Other factors that were likely to influence the column strength including the slenderness of the column, the initial curvature, and the creep coefficient were taken into account. It was found that all these parameters significantly affected the column strength.

Behan and O'Connor (1982) adopted the superposition creep approach for studying the long-term buckling behavior of reinforced concrete columns. The age-hardening and cracking of concrete were considered in the nonlinear analysis. Also the yielding of steel and the inelastic response of the concrete material at all levels of stress were considered. Generally satisfactory analytical estimations were obtained for the design life, compared with results from 16 columns under sustained loads.

Wu (1983) used the integral type law of creep to investigate the creep buckling phenomenon in concrete columns with initial imperfections. The elastic-viscoelastic correspondence principle was used where the concrete was modeled as a linear standard solid. It was shown that the critical load could be significantly reduced due to creep in comparison with the instantaneous buckling load. The critical load was defined as the initial load that leads to unbounded magnitude of the displacement over time. It was recommended to use the step-by-step method along with non-linear creep laws once the linearized solution ceased to be valid. The effects of the reinforcement and aging of concrete were also investigated. It was revealed that the long-term displacement can be decreased considerably (by almost 50% in the examined cases) by introducing additional reinforcement in the concrete structure.

Bažant and Tsubaki (1980) considered the nonlinear creep buckling behavior of concrete columns. In the examined cases, the stress levels exceeded the serviceable limit stress of 50 percent of the concrete strength, where the linear aging creep law of concrete ceased to be valid. The criterion for failure was the critical time defined as a finite time where the deflection of the column tended to infinity rather than the long-time critical load which was calculated from a linearized small-deflection theory. Bažant and Kim (1979) examined both types of creep of concrete and developed their constitutive relations which were then used by Bažant and Tsubaki (1980) in a step-by-step incremental analysis of columns. The deflection of the column was found to rapidly increase after certain period of loading followed by a total collapse of the structure. As expected, it was revealed that the larger the applied load, the sooner the time of collapsing.

Tatsa (1989) presented test results of 7 concrete panels subjected to eccentric sustained loading and developed a numerical method to predict the time-dependent behavior of the panels. It was found that creep might lead to significant reduction of the panel strength, and therefore it was indicated that it is unsafe to design panels based on the immediate load-carrying capacity. The step-by-step numerical analysis provided a tool to predict the long-term load capacity of panels as its estimates showed good correlation with test results.

Bažant and Cedolin (1991) discussed the creep buckling behavior of pin-ended imperfect columns by using the rate-of-creep method to describe the linear aging stress-strain relations, which was firstly introduced by Glanville (1933) and Whitney (1932). The concrete was treated as aging viscoelastic material. It was indicated that the rate-of-creep method yielded inevitable errors and substantially underestimated the creep response compared to the real one. Yet, the deficiency of the method could be overcome by deliberately increasing the initial elastic deformation. Nevertheless, the errors of the solutions were still large in contrast to the age-adjusted effective modulus method which was proposed by Bažant (1972).

Gilbert (1989) carried out a step-by-step time analysis of concrete columns under sustained eccentric loading by assuming a pre-defined deflection function through the height of the column and by ignoring the tension-stiffening effect. The model showed a reasonably good agreement with experimental results. However, the assumed deflection function can actually change after concrete cracking or under different types of boundary restraints; and hence, a more accurate model is needed for a more general analysis of RC columns.

Mickleborough and Gilbert (1991) described test results of 15 slender columns subjected to sustained eccentric loading. The eccentricity and the magnitude of applied loads were varied among the specimens. The concrete strength ranged between 27 MPa to 39 MPa. The columns were loaded over periods of up to 40 days. None of the columns failed due to creep buckling over the test period, but substantial time-dependent lateral deflections were recorded especially for columns with relatively high slenderness ratio, large eccentricities of the applied load and relatively large magnitudes of load. Nonetheless, the slenderness played a small role in the time-dependent deformation of slender columns that were subjected to minimum design eccentricities based on ACI318 (1983).

Claeson and Gylltoft (2000) studied the behavior of eccentrically loaded concrete columns under both short-term and sustained loading experimentally and theoretically. The experimental investigation comprised both normal strength concrete and high strength concrete specimens, with concrete strength of approximately 35 MPa to 100 MPa. The level of the maximum applied sustained axial load ranged between 70 percent and 100 percent of the maximum short-term load. The test results indicated that the normal strength concrete columns exhibited significant nonlinear creep deformation under sustained loading where the high strength concrete columns exhibited relatively small nonlinear creep deformation. Furthermore, from the test results it was shown that the high strength concrete columns undergo less creep deformations compared to the normal strength concrete columns. The numerical analysis used the moment-curvature approach of the column. It adopted the modifications to the CEB-FIP (1990) equations recommended by Han (1996) as the creep function for high strength concrete and took into account the nonlinearity of creep with stress. The results of the analysis had satisfactory agreement with the test results.

Lee et al. (2008) examined the time-dependent behavior of normal strength concrete walls by testing 3 wall specimens and developing a corresponding three dimensional finite element model. Concentrated axial loads were applied on the middle part of the width of wall panels to represent the concentrated loads transferred through the connections between walls and beams, slabs, or columns in reality. The finite element model was verified by the test results and both showed that the stress and strain in wall panels under concentrated loading reached their maximum at the middle zone of the width of the specimens and decreased towards the edges. The longitudinal long-term deflection was therefore expected to reach the maximum at the middle zone of the specimen as well.

Hamed et al. (2010a) and Hamed et al. (2010b) studied the long-term behavior of imperfect thin-walled shallow concrete domes. Nonlinear theoretical models were developed using the variational principle, equilibrium conditions, and integral-type constitutive relations that accounted for the time-dependent effects of creep and shrinkage. The aging of the concrete material and the variation of the internal stresses and geometry in time were both considered in the theoretical models through the use of incremental step-by-step procedure for the solutions of the governing equations in time. Hamed et al. (2010b) indicated that the long-term effects played a critical role in the nonlinear behavior and structural safety of shallow, thin-walled concrete domes, while Hamed et al. (2010a) showed that the structural behavior of imperfect concrete domes and the critical time to cause creep buckling were very sensitive to geometric and material imperfections.

Hamed et al. (2011) theoretically and experimentally investigated both the short-term and long-term failure behaviors of thin-walled shallow concrete domes. Nonlinear long-term theoretical model of domes that accounted for the nonlinear material behavior, creep and shrinkage, and the nonlinear geometric behavior were developed in this paper. The governing equations of the long-term model were formulated using a time incremental approach and the nonlinear material response was characterized by applying the approximate modified principle of superposition method. The experiment included testing of two domes in short-term and long-term loading to failure. The analytical models were verified by the test results to some extent.

These studies provide the basis for this research, however, here, different material, different structural member and boundary conditions, and different material models and mathematical creep models will be investigated.

2.5 TIME-DEPENDENT MATERIAL PROPERTIES OF HIGH-STRENGTH CONCRETE

Ngab et al. (1981) studied the creep and shrinkage properties of high- and normal-strength concrete by testing concrete specimens in uniaxial compression. The test specimens were cured under sealed and dry conditions. The specimens had a compressive strength of over 70 MPa and were loaded uniaxially for up to 90 days. It was found that the creep for high-strength concrete was significantly less than that for normal-strength concrete. This phenomenon was more pronounced for concrete under drying conditions. The creep coefficient for high-strength concrete, defined as the ratio of creep strain over the instantaneous strain upon loading, was 50 to 75 percent of that for normal-strength concrete under drying conditions. In the nondrying concrete, this value varied from 75 to 90 percent. Furthermore, the linearity of the stress creep-strain relation for high-strength concrete went up to 70 percent of the concrete compressive strength f_c, which was considerably greater than that in normal-strength concrete (usually considered as linear under 0.5 f_c). A sustained load in the range of serviceability was to increase the compressive strength of both NSC and HSC, whereas higher load intensity or staged loading had a detrimental effect on the strength. It was also indicated that the ratio of the sustained strength to the short-term strength was greater in HSC than NSC. The drying shrinkage strains were found to be slightly higher in this study for high strength concrete in contrast to normal strength concrete.

Smadi et al. (1987) experimentally investigated and compared the influences of drying and sustained compressive stress on the creep and shrinkage properties of high, medium, and low strength concretes. The test specimens had compressive strength at 28 days varying from 21 MPa to 69 MPa. The results revealed that the creep strain, creep coefficient, and specific creep (creep strain per unit stress), were smaller for high-strength concrete than for medium- and low-strength concrete when they were stressed at the same percentage of strength. The creep coefficients for high-, medium-, and low-strength concrete at 60 days subjected to $0.6f_c$ stress were 0.9, 1.8, and 2.7, respectively. In addition, high-strength concrete had higher linear proportionality limit in the stress-creep strain relation than the other medium- and low-strength concrete. The stress at the limit reached 65% of the ultimate strength for the high-strength concrete and 45% for the other ones. It was also revealed that the long-term drying shrinkage for low-strength concrete was larger than the medium- and high- strength concrete.

Similar findings regarding the low creep characteristics of high-strength concrete were also obtained by Hwee and Vijaya (1990). The authors tested columns made of high-strength concrete with compressive strength of 60 MPa. The creep attained from the experiments for high-strength concrete was substantially smaller than that for normal-strength concrete. The final shrinkage of high strength concrete at 20 years was estimated at 750 μin./in. which was close to the corresponding final shrinkage strain of normal strength concrete that was estimated at 710 μin./in. according to AS3600 (1988). This was also in accordance with Ngab et al. (1981) and ACI363 (1984).

Mokhtarzadeh and French (2000) conducted tests to address a variety of factors affecting the creep and shrinkage characteristics of high-strength concrete, including the curing temperature of the specimens, the compressive strength, and the size of the coarse aggregate. It was concluded that temperature increases the specific creep of high-strength concrete. Moreover, the specific creep was found to decrease with the increase of the compressive strength. Efforts were also made to evaluate the creep coefficient of high-strength concrete using the equations given in ACI209 (1971), which were normally applied for the prediction of creep coefficients of normal-strength concrete. The creep coefficient as predicted in this study varied from 0.92 to 2.46, which is considerably different than the values predicted by ACI209 (1971), i.e., 1.30 to 4.15. Furthermore, the drying shrinkage strain observed in this study ranged between 63 and 83 percent of values predicted by ACI209 (1971).

ACI363 (2010) compares the outcomes of a number of researchers regarding HSC shrinkage. It concludes that no clear census exists among the reported results with regard to the magnitude of drying shrinkage of HSC as compared with normal-strength concrete. The drying shrinkage, arising from diffusion of internal water into the outer environment, is deemed to be a predominate mechanism of volume change for NSC but a less significant one for HSC because HSC has lower water-cement ratio (*w/cm*). On the other hand, the chemical and autogenous shrinkage, which are induced by hydration of cement, become more crucial mechanisms for the volume change of HSC due to its increased binder content than NSC. Tazawa (1999) reported the autogenous shrinkage can be significant for HSC, with values of 200×10^{-6} to 400×10^{-6} for concrete with *w/cm* less than 0.40 and silica fume contents of not less than 10%. Eurocode 2 (1992) indicates the autogenous shrinkage strain is a linear function of the concrete strength.

2.5.1 Models to predict HSC creep and shrinkage

2.5.1.1 Bažant and Panula (1984)

Bažant and Panula (1984) proposed theoretical prediction equation for creep and shrinkage of high-strength concrete based on the models of normal-strength concrete creep as given by (Bažant and Panula 1978a; b; c; d; 1979a; b) but with slight modification. It was shown that the formulae for basic creep and shrinkage needed no change and only a small change in the formula for the concrete strength effect was required for drying creep, as shown in the following.

$$\phi_d' = \left(1 + \frac{t' - t_0}{a_d \tau_{sh}}\right)^{-1/2} \phi_d \tag{2.1}$$

where a_d =10 for $f_c' \le 41\,\text{MPa}$, and a_d =1 for $f_c' \ge 69\,\text{MPa}$

$$S_d\left(t, t'\right) = \left(1 + b_d \frac{\tau_{sh}}{t - t'}\right)^{c_d n} \tag{2.2}$$

where b_d =10 for $f_c' \le 41\,\text{MPa}$, and b_d =100 for $f_c' \ge 69\,\text{MPa}$

Linear interpolation could be used for strength falling between 41 MPa and 69 MPa. In these equations, t_0 is age at start of drying, t' is the age at application of load, $S_d\left(t, t'\right)$ is the time shape function, n is the exponent of double power law, c_d is a correction factor, τ_{sh} is the shrinkage-square half-time, proportional to the square of thickness of concrete and f_c' is the standard cylindrical strength at age of 28 days.

The equation produced acceptable agreement with test measurements available in the literature. Nevertheless, due to the limited test data, the method, as suggested by the authors, needed further verification when more test results were to be reported.

2.5.1.2 AS3600 (2009)

The AS3600 (2009) gives prediction equations for shrinkage strain and creep coefficient of concrete with characteristic compressive strength ranging from 20 MPa to 100 MPa at 28 days, which implies they are applicable for both NSC and HSC.

a) Creep

The creep coefficient following AS3600 (2009) is determined in the following form:

$$\phi_{cc} = k_2 k_3 k_4 k_5 \phi_{cc.b} \tag{2.3}$$

- $\varphi_{cc.b}$ = the basic creep coefficient;
- k_2, k_3 = coefficients accounting for the member size and aging of the concrete;
- k_4 = 0.70 for an arid environment; 0.65 for an interior environment; 0.60 for a temperature inland environment; 0.50 for a tropical or near-coastal environment;
- k_5 = modification factor for high strength concrete; $k_5 = 1.0$ when $f_c^{'} \le 50$ MPa or $k_5 = (2.0 - \alpha_3) - 0.02(1.0 - \alpha_3) f_c^{'}$ when $50 < f_c^{'} \le 100$ MPa;

b) Shrinkage

According to the code, he shrinkage strain should be calculated as the sum of autogenous shrinkage (ε_{cse}) strain and the drying shrinkage strain (ε_{csd}) of concrete as follows:

$$\varepsilon_{cs} = \varepsilon_{cse} + \varepsilon_{csd} \tag{2.4}$$

The autogenous shrinkage strain is taken as

$$\varepsilon_{cse} = \varepsilon_{cse}^{*} \times \left(1.0 - e^{-0.1t}\right) \tag{2.5}$$

where t is the time (in days) after setting and $\varepsilon_{csd.b}^{*}$ is the final autogenous shrinkage strain determined by

$$\varepsilon_{cse}^{*} = \left(0.06 f_c^{'} - 1.0\right) \times 50 \times 10^{-6} \tag{2.6}$$

The drying shrinkage is calculated as

$$\varepsilon_{csd} = k_1 k_4 \varepsilon_{csd.b} \tag{2.7}$$

$$\varepsilon_{csd.b} = (1.0 - 0.008 f_c^{'}) \times \varepsilon_{csd.b}^{*} \tag{2.8}$$

where k_1 and k_4 are factors accounting for influence of member size and environment, $\varepsilon_{csd.b}$ and $\varepsilon_{csd.b}^{*}$ are basic drying shrinkage strain and final drying basic shrinkage strains.

2.5.1.3 CEB-FIP (1990)

The CEB-FIP (1990) model code provides equations for creep and shrinkage prediction of concrete. These equations are suitable for C12-C80 concrete, where the number denotes the specified characteristic compressive strength in MPa.

a) Creep

$$\varphi(t,t_0) = \varphi_0 \beta_c (t - t_0) \tag{2.9}$$

- φ_0 = notional creep coefficient, as given in Eq.(2.10)
- β_c = coefficient to describe the development of creep with time after loading, as defined in Eq.(2.15)
- t = age of concrete (days) at the moment considered
- t_0= age of concrete at loading (days), adjusted by taking into account of effects of type of cement and curing tempature

$$\varphi_0 = \varphi_{RH} \beta(f_{cm}) \beta(t_0) \tag{2.10}$$

with

$$\varphi_{RH} = 1 + \frac{1 - RH/RH_0}{0.46(h/h_0)^{1/3}} \tag{2.11}$$

$$\beta(f_{cm}) = \frac{5.3}{(f_{cm}/f_{cm0})^{0.5}} \tag{2.12}$$

$$\beta(t_0) = \frac{1}{0.1 + (t_0/t_1)^{0.2}} \tag{2.13}$$

where

- $h = 2A_c / u$ (2.14)
- h = notational size of member (mm), where A_c is the cross-sectional area and u is the perimeter of the member in contact with the atmosphere
- f_{cm} = mean compressive strength of concrete at the age of 28 days (MPa)
- f_{cm0} = 10 MPa
- RH = relative humidity of the ambient environment (%)
- RH_0 = 100%
- h_0 = 100 mm
- t_1 = 1 day

$$\beta_c(t - t_0) = \left[\frac{(t - t_0)/t_1}{\beta_H + (t - t_0)/t_1} \right]^{0.3} \tag{2.15}$$

with

$$\beta_H = 150 \left\{ 1 + \left(1.2 \frac{RH}{RH_0} \right)^{18} \right\} \frac{h}{h_0} + 250 \leq 1500 \tag{2.16}$$

where

- t_1 = 1 day
- RH_0 = 100%
- h_0 = 100 mm

b) Shrinkage

The shrinkage or swelling strains can be calculated as

$$\varepsilon_{cs}(t, t_s) = \varepsilon_{cs0} \beta_s (t - t_s) \tag{2.17}$$

where

- ε_{cs0} = notional shrinkage coefficient; (see Eq.(2.18))
- β_s = coefficient to describe the development of shrinkage with time, as given in Eq.(2.23)
- t = age of concrete (days)
- t_s = age of concrete (days) at the beginning of shrinkage or swelling

The notional shrinkage coefficient may be obtained from

$$\varepsilon_{cs0} = \varepsilon_s\left(f_{cm}\right)\beta_{RH} \tag{2.18}$$

with

$$\varepsilon_s\left(f_{cm}\right) = \left[160 + 10\beta_{sc}\left(9 - f_{cm}/f_{cm0}\right)\right]\times 10^{-6} \tag{2.19}$$

where

- f_{cm} = mean compressive strength of concrete at the age of 28 days (MPa)
- f_{cm0} = 10 MPa
- β_{sc} = coefficient which depends on the type of cement: β_{sc} = 4 for slowly hardening cements SL, β_{sc} = 5 for normal or rapid hardening cements N and R, and β_{sc} = 8 for rapid hardening high strength cements RS

$$\beta_{RH} = -1.55\beta_{sRH} \qquad \text{for} \qquad 40\% \le RH < 99\% \tag{2.20}$$

$$\beta_{RH} = +0.25 \qquad \text{for} \qquad RH \ge 99\% \tag{2.21}$$

with

$$\beta_{sRH} = 1 - \left(RH/RH_0\right)^3 \tag{2.22}$$

where

- RH = relative humidity of the ambient atmosphere (%)
- RH_0 = 100%

The development of shrinkage with time can be determined by

$$\beta_s\left(t-t_s\right)=\left[\frac{\left(t-t_s\right)/t_1}{350\left(h/h_0\right)^2+\left(t-t_s\right)/t_1}\right]^{0.5} \tag{2.23}$$

where

- h is defined in Eq.(2.14)
- t_1 = 1 day
- h_0 = 100 mm

2.5.1.4 Eurocode2 (2005)

The Eurocode2 (2005) uses the same equations for prediction of concrete creep and shrinkage as given in CEB-FIP (1990) but with adjustments made to characterize the effect of concrete strength. The adjustments are summarized herein.

a) Creep

Eq.(2.10) is adopted by Eurocode2 (2005) as well to estimate concrete creep. However, the influence of concrete strength is characterized in these equations by modifying ϕ_{RH} and β_H. In Eurocode2 (2005),

$$\varphi_{RH}=1+\frac{1-RH/100}{0.1\left(h\right)^{1/3}} \qquad \text{for} \quad f_{cm}\le 35\text{ MPa} \tag{2.24}$$

$$\varphi_{RH}=\left[1+\frac{1-RH/100}{0.1\left(h\right)^{1/3}}\cdot\alpha_1\right]\cdot\alpha_2 \qquad \text{for} \quad f_{cm}>35\text{ MPa} \tag{2.25}$$

$$\beta_H=1.5\left[1+\left(0.012RH\right)^{18}\right]h+250\le 1500 \qquad \text{for} \quad f_{cm}\le 35\text{ MPa} \tag{2.26}$$

$$\beta_H=1.5\left[1+\left(0.012RH\right)^{18}\right]h+250\alpha_3\le 1500 \qquad \text{for} \quad f_{cm}>35\text{ MPa} \tag{2.27}$$

where

- $h=2A_c/u$
- f_{cm} = mean compressive strength of concrete at the age of 28 days (MPa)
- RH = relative humidity of the ambient environment (%)
- h = notational size of member (mm), where A_c is the cross-sectional area and u is the perimeter of the member in contact with the atmosphere
- α_1 , α_2 , α_3 = coefficients to consider the influence of the concrete strength:

$$\alpha_1 = \left(35/f_{cm}\right)^{0.7} \qquad \alpha_2 = \left(35/f_{cm}\right)^{0.2} \qquad \alpha_3 = \left(35/f_{cm}\right)^{0.5} \tag{2.28}$$

b) Shrinkage

The shrinkage strain as specified in Eurocode 2 (1992) is calculated as the sum of the drying shrinkage strain and autogenous shrinkage strain, as indicated in Eq.(2.29)

$$\varepsilon_{cs} = \varepsilon_{cd} + \varepsilon_{ca} \tag{2.29}$$

- ε_{cs} = total shrinkage strain
- ε_{cd} = drying shrinkage strain
- ε_{ca} = autogenous shrinkage strain

The drying shrinkage strain is given by

$$\varepsilon_{cd}\left(t\right) = \beta_{ds}\left(t,t_s\right) \cdot k_h \cdot \varepsilon_{cd,0} \tag{2.30}$$

with

$$\beta_{ds}\left(t,t_s\right) = \frac{t-t_s}{\left(t-t_s\right)+0.04h^{3/2}} \tag{2.31}$$

$$\varepsilon_{cd,0} = 0.85\left[\left(220+110\alpha_{ds1}\right) \cdot \exp\left(-\alpha_{ds2} \cdot \frac{f_{cm}}{f_{cm0}}\right)\right] \cdot \beta_{RH} \times 10^{-6} \tag{2.32}$$

$$\beta_{RH} = 1.55\left[1-\left(RH/RH_0\right)^3\right] \tag{2.33}$$

where

- t = age of concrete (days)
- t_s = age of concrete (days) at the beginning of shrinkage or swelling
- k_h = coefficient depending on the notional size $h=2A_c/u$
- h = notational size of member (mm), where A_c is the cross-sectional area and u is the perimeter of that part of the cross section which is exposed to drying
- f_{cm} = mean compressive strength of concrete at the age of 28 days (MPa)
- f_{cm0} = 10 MPa
- α_{ds1} = coefficient which depends on the type of cement

  = 3 for cement Class S

  = 4 for cement Class N

  = 6 for cement Class R
- α_{ds2} = coefficient which depends on the type of cement

  = 0.13 for cement Class S

  = 0.12 for cement Class N

  = 0.11 for cement Class R
- RH = relative humidity of the ambient environment (%)
- RH_0 = 100%

The autogenous shrinkage strain is taken as

$$\varepsilon_{ca}(t) = \beta_{as}(t) \cdot \varepsilon_{ca}(\infty) \tag{2.34}$$

with

$$\varepsilon_{ca}(\infty) = 2.5(f_{ck} - 10) \times 10^{-6} \tag{2.35}$$

$$\beta_{as}(t) = 1 - \exp\left(-0.2t^{0.5}\right) \tag{2.36}$$

where

- f_{ck} = characteristic compressive cylinder strength of concrete at 28 days

2.5.1.5 JSCE (2002)

a) Creep

The creep strain per unit stress $\varepsilon'_{cc}\left(t,t'\right)/\sigma'_{cp}$ of high strength concrete is determined from

$$\varepsilon'_{cc}\left(t,t'\right)\Big/\sigma'_{cp} = \frac{4W\left(1-RH/100\right)+350}{12+f'_c(t')}\log_e\left(t-t'+1\right) \tag{2.37}$$

where

- $f'_c(t')$ = compressive strength of concrete at loading age (MPa)
- *t'* and *t* = effective age (days) at the beginning of loading and during loading, respectively;
- W = unit water content (kg/m^3) (130kg/m$^3 \leq W \leq$ 230kg/m^3)
- RH = relative humidity (%) (40% $\leq RH \leq$ 90%)

b) Shrinkage

In JSCE (2002), shrinkage of high-strength concrete is evaluated as the sum of autogenous and drying shrinkages, which are separately predicted.

$$\varepsilon'_{cs}\left(t,t_0\right) = \varepsilon'_{ds}\left(t,t_0\right) + \varepsilon'_{as}\left(t,t_0\right) \tag{2.38}$$

where

- $\varepsilon'_{cs}\left(t,t_0\right)$= shrinkage strain of concrete from age t_0 to t (x10^{-6})
- $\varepsilon'_{ds}\left(t,t_0\right)$= drying shrinkage strain of concrete from age t_0 to t (x10^{-6})
- $\varepsilon'_{as}\left(t,t_0\right)$= autogenous shrinkage strain of concrete from age t_0 to t (x10^{-6})

The drying shrinkage strain is predicted by

$$\varepsilon'_{ds}\left(t,t_0\right) = \frac{\varepsilon_{ds\infty}\cdot\left(t-t_0\right)}{\beta+\left(t-t_0\right)} \tag{2.39}$$

with

$$\beta = \frac{4W\sqrt{V/S}}{100+0.7t_0} \tag{2.40}$$

$$\varepsilon_{ds\infty} = \frac{\varepsilon_{ds\rho}}{1+\eta \cdot t_0} \tag{2.41}$$

$$\varepsilon_{ds\rho} = \frac{\alpha\left(1-RH/100\right)W}{1+150\exp\left\{-\dfrac{500}{f_c^{'}(28)}\right\}} \tag{2.42}$$

$$\eta = 10^{-4}\left\{15\exp\left(0.007 f_c^{'}\left(28\right)\right)+0.25W\right\} \tag{2.43}$$

where

- β = representing the time dependency of drying shrinkage
- $\varepsilon_{ds\infty}$ = final value of drying shrinkage strain (x10^{-6})
- W = unit water content (kg/m^3) (130kg/m$^3 \le W \le$ 230kg/m^3)
- V/S = volume surface ratio (mm) (100mm $\le V/S \le$ 300mm)
- RH = relative humidity (%) (40% $\le RH \le$ 90%)
- $f_c^{'}(28)$ = compressive strength of concrete at age of 28 days (MPa) ($f_c^{'}(28) \le 80$ MPa)
- t_0 and t = effective age (days) at the beginning of drying and during drying, respectively (1 day $\le t_0 \le 98$ days, $t_0 = 98$ days for $t_0 > 98$) ;
- α = coefficient representing the influence of the cement type;

  = 11 for ordinary or low-heat cement

  = 15 for high-early-strength cement

The autogenous shrinkage strain is obtained as

$$\varepsilon_{as}^{'}\left(t,t_0\right) = \varepsilon_{as}^{'}\left(t\right) - \varepsilon_{as}^{'}\left(t_0\right) \tag{2.44}$$

with

$$\varepsilon'_{as}(t) = \gamma \varepsilon'_{as\infty}\left[1-\exp\left\{-a\left(t-t_s\right)^b\right\}\right] \tag{2.45}$$

$$\varepsilon'_{as\infty} = 3070\exp\left\{-7.2\left(W/C\right)\right\} \tag{2.46}$$

- $\varepsilon'_{as}(t)$= autogenous shrinkage strain of concrete from the start of setting to age t ($\times 10^{-6}$)
- γ= coefficient representing the influence of the cement and admixtures type (γ may be 1 when only ordinary Portland cement is used.)
- $\varepsilon'_{as\infty}$= final value of autogenous shrinkage strain ($\times 10^{-6}$)
- W/C = water-cement ratio
- t_s = start of setting (days)
- a, b = coefficient representing the characteristic of progress of autogenous shrinkage

2.5.1.6 Mazloom (2008)

Mazloom (2008) proposed equations which were expressed in hyperbolic-power form for predicting the creep and shrinkage of high-strength concrete. The derivations of the equations were based on the test results conducted for high-strength concrete specimens containing various ratios of silica fume.

a) Creep

$$\varphi(t,t_0) = E_c(t_0)\cdot\frac{(t-t_0)^{0.6}}{(26.5-SF)+(t-t_0)^{0.6}}\cdot C(u)\cdot Y\times 10^{-6} \tag{2.47}$$

with

$$C(u) = 103-3.65SF \tag{2.48}$$

$$Y = 1.08-0.0114t_0 \tag{2.49}$$

where

- $\phi(t,t_0)$ = creep coefficient of concrete at time t in days
- t_0 = age of loading in days
- $C(u)$ = ultimate specific creep (creep per unit stress)
- SF = percentage of silica fume replacing cement in concrete mix
- Y = correction factor accounting for aging of concrete

b) Shrinkage

$$\varepsilon_{sh}(t,t_0) = \frac{(t-t_0)}{(0.3SF+12.6)+(t-t_0)}\varepsilon_{sh}(u) \tag{2.50}$$

with

$$\varepsilon_{sh}(u) = Y \cdot 516 \times 10^{-6} \tag{2.51}$$

$$Y = 0.014SF + 0.39 \qquad \text{for sealed specimen} \tag{2.52}$$

$$Y = 1.14 - 0.007(V/S) \geq 0.014SF + 0.39 \qquad \text{for drying specimen} \tag{2.53}$$

where

- $\varepsilon_{sh}(t,t_0)$ = shrinkage strain of high-strength concrete at time t;
- $\varepsilon_{sh}(u)$ = ultimate shrinkage strain;
- Y = correction factor, accounting for ratio of silica fume and volume-surface ratio of member;
- t_0 = loading age;
- SF = percentage of silica fume replacing cement in concrete mix;
- V/S = volume to surface ratio of concrete specimen;

After comparing the predicted results to a survey of experimental data available in the literature, the equations developed in this study were found to yield more accurate estimations than several common methods, such as ACI209 (1992) and CEB-FIP (1999), which were used to predict creep and shrinkage for normal strength concrete.

2.5.2 Strength and modulus of elasticity

Concrete strength (compressive and tensile) and elasticity develop with the maturation of concrete and vary with regard to environmental temperature and cement type. The predictive formulae are given in many building codes, which account for both normal strength concrete and high strength concrete.

2.5.2.1 CEB-FIP (1990)

a) Compressive Strength

The development of concrete compressive strength with time is given as

$$f_{cm}(t) = \beta_{cc}(t)\, f_{cm} \tag{2.54}$$

with

$$\beta_{cc}(t) = \exp\left\{ s\left[1 - \left(\frac{28}{t/t_1}\right)^{1/2}\right]\right\} \tag{2.55}$$

$$f_{cm} = f_{ck} + \Delta f \tag{2.56}$$

where

- $f_{cm}(t)$ = mean concrete compressive strength (MPa) at an age of t days
- f_{cm} = mean compressive strength (MPa) after 28 days
- $\beta_{cc}(t)$ = coefficient depends on the age of concrete t
- t = age of concrete (days)
- t_1 = 1 day
- s = coefficient depends on the type of cement
- f_{ck} = characteristic compressive strength of concrete (MPa)
- Δf = 8 MPa

The age of concrete t will be adjusted according to Eq.(2.57) to take into account the effect of temperature during curing.

$$t_T = \sum_{i=1}^{n} \Delta t_i \exp\left[13.65 - \frac{4000}{273 + T(\Delta t_i)/T_0}\right] \qquad (2.57)$$

where

- t_T = temperature adjusted concrete age, replacing t (days)
- Δt_i = number of days where a temperature T prevails
- $T(\Delta t_i)$ = temperature (^oC) during the time period Δt_i
- $T_0 = 1\ ^oC$

When subjected to sustained high compressive stresses, the compressive strength of concrete is calculated as

$$f_{cm,sus}(t,t_0) = f_{cm}\beta_{cc}(t)\beta_{c,sus}(t,t_0) \qquad (2.58)$$

$$\beta_{c,sus}(t,t_0) = 0.96 - 0.12\left\{\ln\left[72\left(\frac{t-t_0}{t_1}\right)\right]\right\}^{1/4} \qquad (2.59)$$

where

- $f_{cm,sus}$ (t,t_0) = mean concrete compressive strength (MPa) at an age of t (days) when subjected to a high sustained compressive stress at an age at loading $t_0<t$
- $\beta_{cc}(t)$ = coefficient according to Eq.(2.55)
- $\beta_{c,sus}(t)$ = coefficient which depends on the time under high sustained loads t-t_0 (>20 min)
- f_{cm} = mean compressive strength (MPa) after 28 days
- t_0 = age of concrete at loading (days)
- t = age of concrete (days)
- t_1 = 1 day

b) Tensile Strength

The mean value of tensile strength associated with a specified characteristic compressive strength f_{ck} can be estimated from the follow.

$$f_{ctm} = f_{ctko,m}\left(\frac{f_{ck}}{f_{cko}}\right)^{2/3} \tag{2.60}$$

where

- f_{ctm} = mean concrete tensile strength (MPa)
- f_{ck} = characteristic compressive strength of concrete (MPa)
- $f_{ctko,m}$ = 1.40 MPa
- f_{cko} = 10 MPa

c) Modulus of Elasticity

The modulus of elasticity of concrete according to CEB-FIP (1990) is calculated as follows

$$E_{ci}(t) = \beta_E(t)E_{ci} \tag{2.61}$$

$$\beta_E(t) = \left[\beta_{cc}(t)\right]^{1/2} \tag{2.62}$$

$$E_{ci} = E_{co}\left[\left(f_{ck} + \Delta f\right)/f_{cmo}\right]^{1/3} \tag{2.63}$$

where

- $E_{ci}(t)$ = modulus of elasticity (MPa) at the age of t (days)
- $\beta_E(t)$ = coefficient depends on the age of concrete
- $\beta_{cc}(t)$ = coefficient according to Eq.
- E_{ci} = modulus of elasticity (MPa) at age of 28 days
- f_{ck} = characteristic strength of concrete (MPa)
- Δf = 8 MPa
- f_{cmo} = 10 MPa
- E_{co} = 2.15 x 10^4 MPa

2.5.3 Constitutive relations

2.5.3.1 CEB-FIP (1990)

The compressive and tensile stress-strain relations prescribed in CEB-FIP (1990) are valid for concrete with characteristic compressive strength up to 80 MPa. The compressive stress-strain relation of concrete given in CEB-FIP (1990) is schematically illustrated in Fig. 2.5.

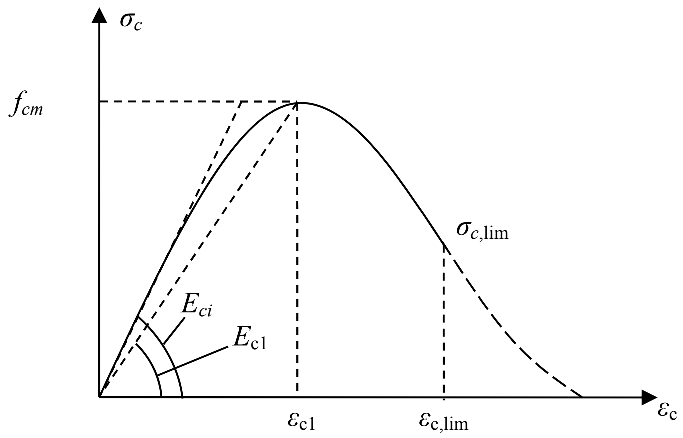

Fig. 2.5 Stress-Strain Diagram for Uniaxial Compression (after CEB-FIP, 1990)

The stress-strain curve can be predicted as

$$\sigma_c = -\frac{\dfrac{E_{ci}}{E_{c1}}\dfrac{\varepsilon_c}{\varepsilon_{c1}} - \left(\dfrac{\varepsilon_c}{\varepsilon_{c1}}\right)^2}{1+\left(\dfrac{E_{ci}}{E_{c1}}-2\right)\dfrac{\varepsilon_c}{\varepsilon_{c1}}} f_{cm} \qquad \text{for} \qquad |\varepsilon_c| < |\varepsilon_{c,\lim}| \tag{2.64}$$

where

- E_{ci} = tangent modulus of concrete according to Eq.(2.61)
- σ_c = compression stress (MPa)
- ε_c = compression strain
- ε_{c1} = -0.0022
- $E_{c1} = f_{cm}/0.0022$ = secant modulus from the origin to the peak compressive stress

f_{cm}

For the descending part of stress-strain curve, Eq.(2.64) can only be used for values of $|\sigma_c|/f_{cm} \geq 0.5$.

The stress-strain diagram for unloading of uncracked concrete can be described by

$$\Delta\sigma_c = E_{ci}\Delta\varepsilon_c \tag{2.65}$$

where

- $\Delta\sigma_c$ = stress reduction
- $\Delta\varepsilon_c$ = strain reduction

2.5.3.2 Constitutive Relations in Tension

The tensile behavior of concrete is described by a bilinear stress-strain relation for uncracked concrete and a stress-crack opening relation for cracked section due to discrete nature of concrete fracture, as shown in Fig. 2.6.

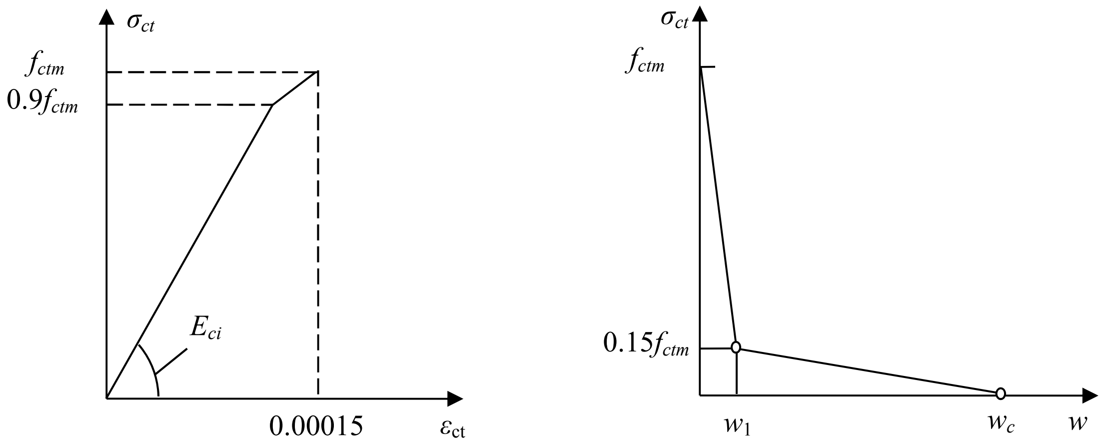

Fig. 2.6 Stress-Strain and Stress-Crack Opening Diagrams for Uniaxial Tension

For uncracked concrete,

$$\sigma_{ct} = E_{ci}\varepsilon_{ct} \qquad \text{for} \qquad \sigma_{ct} \leq 0.9 f_{ctm} \tag{2.66}$$

$$\sigma_{ct} = f_{ctm} - \frac{0.1 f_{ctm}}{0.00015 - 0.9 f_{ctm} / E_{ci}}\left(0.00015 - \varepsilon_{ct}\right) \qquad \text{for} \qquad 0.9 f_{ctm} < \sigma_{ct} \leq f_{ctm} \tag{2.67}$$

where

- E_{ci} = tangent modulus of concrete according to Eq.(2.61)
- σ_{ct} = tensile stress (MPa)
- ε_{ct} = tensile strain
- f_{ctm} = tensile strength in MPa

For cracked concrete,

$$\sigma_{ct} = f_{ctm}\left(1 - 0.85\frac{w}{w_1}\right) \qquad \text{for} \qquad 0.15 f_{ctm} \le \sigma_{ct} \le f_{ctm} \tag{2.68}$$

$$\sigma_{ct} = \frac{0.15 f_{ctm}}{w_c - w_1}\left(w_c - w\right) \qquad \text{for} \qquad 0 \le \sigma_{ct} < 0.15 f_{ctm} \tag{2.69}$$

with

$$w_1 = 2\frac{G_F}{f_{ctm}} - 0.15 w_c \tag{2.70}$$

$$w_c = \alpha_F \frac{G_F}{f_{ctm}} \tag{2.71}$$

where

- w = crack opening (mm)
- w_1 = crack opening (mm) for $\sigma_{ct} = 0.15 f_{ctm}$
- w_c = crack opening (mm) for $\sigma_{ct} = 0$
- G_F = fracture energy (Nmm/mm^2)
- f_{ctm} = tensile strength (MPa)
- α_F = coefficient, depends on maximum aggregate size

2.5.4 Tension stiffening

The tension stiffening refers to the contribution of concrete between cracks to the reinforced concrete member stiffness after cracking takes place. The contribution is a result of the tensile capacity of concrete which will resist the tensile stress transmitted from steel by bond forces. The contribution is to increase the stiffness of the cracked RC member.

Formulae and models that characterize the phenomenon of tension stiffening have been specified in various codes. The ones given in CEB-FIP (1990) and AS3600 (2009) are summarized herein.

2.5.4.1 CEB-FIP (1990)

The tension stiffening effect may be taken into account by a modified stress-strain relation of the embedded reinforcement for practical application as follows:

a) Uncracked

$$\varepsilon_{s,m} = \varepsilon_{s1} \qquad \text{for} \qquad 0 < \sigma_s \le \sigma_{sr1} \tag{2.72}$$

b) Crack Formation Phase

$$\varepsilon_{s,m} = \varepsilon_{s2} - \frac{\beta_t\left(\sigma_s - \sigma_{sr1}\right) + \left(\sigma_{srn} - \sigma_s\right)}{\left(\sigma_{srn} - \sigma_{sr1}\right)}\left(\varepsilon_{sr2} - \varepsilon_{sr1}\right) \qquad \text{for} \qquad \sigma_{sr1} < \sigma_s \le \sigma_{srn} \tag{2.73}$$

c) Stabilized Cracking

$$\varepsilon_{s,m} = \varepsilon_{s2} - \beta_t\left(\varepsilon_{sr2} - \varepsilon_{sr1}\right) \qquad \text{for} \qquad \sigma_{srn} < \sigma_s \le f_{yk} \tag{2.74}$$

d) Post-yielding

$$\varepsilon_{s,m} = \varepsilon_{sy} - \beta_t\left(\varepsilon_{sr2} - \varepsilon_{sr1}\right) + \delta\left(1 - \frac{\sigma_{sr1}}{f_{yk}}\right)\left(\varepsilon_{s2} - \varepsilon_{sy}\right) \qquad \text{for} \qquad f_{yk} < \sigma_s < f_{tk} \tag{2.75}$$

where

- ε_{sy} = strain at the yield strength

- σ_s = steel stress in the crack
- σ_{sr1} = steel stress in the crack, when first crack has formed
- σ_{srn} = steel stress in the crack, when stabilized crack pattern has formed (last crack)
- β_t = 0.40 for short-term loading (pure tension)
- β_t = 0.25 for long-term or repeated loading (pure tension)
- δ = 0.8; coefficient to take into account the ratio f_{tk}/f_{yk} and the yield stress f_{yk}

2.5.4.2 AS3600 (2009)

In calculation of the deflection or crack width of beams, the AS3600 (2009) adopts the effective stiffness method to account for the tension stiffening effect. The effective stiffness after cracking is determined in Eq.(2.76) for estimation of short-term deflection or curvature of beams.

$$I_{ef} = I_{cr} + \left(I - I_{cr}\right)\left(\frac{M_{cr}}{M_s^*}\right)^3 \le I_{ef.\max} \tag{2.76}$$

with

$$M_{cr} = Z\left(f'_{ct.f} - \sigma_{cs} + P/A_g\right) + Pe \ge 0 \tag{2.77}$$

$$\sigma_{cs} = \frac{2.5p_w - 0.8p_{cw}}{1 + 50p_w} E_s \varepsilon_{cs}^* \tag{2.78}$$

where

- I_{ef} = effective second moment of area after first cracking
- $I_{ef.\max}$ = maximum effective second moment of area after first cracking, taken as I for RC sections having $p = A_{st}/bd \ge 0.005$ and prestressed sections and $0.6I$ for RC sections when $p = A_{st}/bd < 0.005$
- M_s^* = maximum bending moment at the section

- M_{cr} = cracking moment
- Z = section modulus of the uncracked section, referred to the extreme fiber at which cracking occurs
- $f'_{ct.f}$ = characteristic flexural tensile strength of concrete
- σ_{cs} = maximum shrinkage-induced tensile stress on the uncracked section at the extreme fiber at which cracking occurs
- p_w = web reinforcement ratio for tensile reinforcement $=\left(A_{st}+A_{pt}\right)/b_w d$
- p_{ew} = web reinforcement ratio for compressive reinforcement $=A_{sc}/b_w d$
- ε^*_{cs} = final design shrinkage strain

For calculation of long-term deflection induced by shrinkage and creep of concrete, AS3600 (2009) specifies a deflection multiplier as in Eq.(2.79) The long-term deflection is then equal to the short-term deflection timed by k_{cs}.

$$k_{cs}=\left[2-1.2\left(A_{sc}/A_{st}\right)\right]\geq 0.8 \tag{2.79}$$

2.5.5 Crack Width

2.5.5.1 CEB-FIP (1990)

For all stages of cracking, the design crack width may be calculated according to

$$w_k=l_{s,\max}\left(\varepsilon_{sm}-\varepsilon_{cm}-\varepsilon_{cs}\right) \tag{2.80}$$

with

$$l_{s,\max}=2\frac{\sigma_{s2}-\sigma_{sE}}{4\tau_{bk}}\varphi_s \tag{2.81}$$

$$l_{s,\max}=\frac{\varphi_s}{3.6\rho_{s,ef}} \qquad \text{for stabilized cracking} \tag{2.82}$$

$$l_{s,\max} = \frac{\sigma_{s2}}{2\tau_{bk}} \varphi_s \frac{1}{1+\alpha_e \rho_{s,ef}} \quad \text{for single crack formation} \tag{2.83}$$

where

- w_k = characteristic crack width
- $l_{s,\max}$ = length over which slip between steel and concrete occurs
- ε_{sm} = average steel strain within $l_{s,\max}$
- ε_{cm} = average concrete strain within $l_{s,\max}$
- ε_{cs} = strain of concrete due to shrinkage
- σ_{s2} = steel stress at the crack
- σ_{sE} = steel stress at the point of zero slip
- τ_{bk} = lower fractile value of the average bond stress
- ϕ_s = diameter of the steel bar
- $\alpha_e = E_s / E_{ci}$
- $\rho_{s,ef}$ = effective reinforcement ratio (= $A_s/A_{c,ef}$)
- $A_{c,ef}$ = effective area of concrete in tension

2.6 SUMMARY

A literature review regarding the long-term behavior of high-strength concrete panels has been presented. Five major topics have been outlined, which included review of the wall design from existing international codes, the short-term behavior of normal and high strength concrete wall panels, the long-term behavior of panels and columns made of materials other than concrete, the long-term behavior of RC columns and shells and the time-dependent material properties of HSC.

A number of research works have been conducted to examined the instantaneous behaviour of concrete panels; however, the studies on high-strength concrete panels under eccentric in-plane loading, and especially the experimental investigations are limited. Therefore, the short-term response of HSC panels is investigated first in this research study both theoretically and experimentally. This is essential in order to provide a benchmark for studying the long-term response of HSC panels.

Based on the literature review, there are currently no studies that have investigated the long-term and creep buckling behaviour of HSC panels. The review on the long-term behavior of structures made from metals and polymers as well as reinforced concrete columns and shells, reveal the need for studying the time-dependent performance of concrete walls. The analytical methods used in the creep buckling analysis of concrete columns provided some insights into the creep buckling phenomenon of HSC walls, but the application of these methods for the analysis of panels and even RC columns is limited, because none of them comprehensively accounts for the combined effects of creep, shrinkage, aging, geometric nonlinearity, cracking and tension-stiffening through a detailed and general model.

The last part of the review only presents the findings on time-dependent properties of high-strength concrete material, which are investigated and applied in this study.

Finally, it can be seen that high-strength concrete panels are being widely used, while their short-term and long-term behavior, especially the effects of creep on the stability characteristics of the wall are yet to be clarified. Therefore, further studies are needed in order to achieve safely designed HSC panels, and in order to enhance their effective design.

CHAPTER 3 THEORETICAL AND EXPERIMENTAL STUDIES OF THE SHORT-TERM BEHAVIOR OF ONE-WAY HSC PANELS

3.1 INTRODUCTION

Based on the literature review, it can be seen that the amount of experimental and theoretical studies regarding the instantaneous and time-dependent behaviors of HSC panels are both limited. Therefore, the short-term and long-term responses of one-way HSC panels will both be investigated in this research study. This chapter focuses on the short-term response of the one-way HSC panels, the results of which will provide the basis for investigating the long-term behavior, as presented in Chapters 4 and 5.

In this chapter, a nonlinear theoretical model is developed, which accounts for concrete cracking, tension-stiffening, strain softening in compression and yielding of the reinforcement, along with the geometric nonlinear effects. The theoretical study is supported by a comprehensive experimental study, aiming to provide further insight into the buckling and failure behavior of one-way HSC panels. The governing equations of the model are developed based on large displacement kinematics and are solved numerically along with the use of the arc-length continuation method (Crisfield 1983; Foster 1992; Sundararajan and Noah 1997). The experimental study includes testing to failure of 8 full-scale simply-supported one-way HSC panels, to examine the influences of different parameters including the slenderness ratio, load eccentricity, and reinforcement arrangement and ratio. The mathematical formulation is presented first, followed by the description of the experimental study. The results obtained from the tests and theoretical model are then discussed and compared. Comparisons of the theoretical, experimental results, and predictions of the design codes are also included, and the proposed model is further verified through comparison with other test results from the literature.

3.2 THEORETICAL FORMULATION

The mathematical formulation includes the derivations of the equilibrium equations, the constitutive relations, and the governing equations along with the solution procedure. The nonlinear model presented herein focuses on HSC panels in one-way action, but it serves as the basis for the development of the model for two-way panels. A smeared cracking modelling approach is used where a distinction is made between cracked and uncracked regions through the height of the panel. The model, as presented in Fig. 3.1 with its sign convention, is generalized to be able to account for axial and transverse loads and various combinations of boundary conditions. The kinematic relation of the panel considering large displacements is given by:

$$\varepsilon_{xx} = \frac{\mathrm{d}u_0}{\mathrm{d}x} - z\frac{\mathrm{d}^2 w}{\mathrm{d}x^2} + \frac{1}{2}\left(\frac{\mathrm{d}w}{\mathrm{d}x}\right)^2 \tag{3.1}$$

where ε_{xx} is the normal strain, u_0 and w are the longitudinal axial displacement and the out-of-plane deflection, and d/dx denotes a derivative with respect to x. The third term in Eq. (3.1) denotes the axial shortening strain due to bending (Chen and Lui 1987). The equilibrium equations of a beam-column structure can be found in many textbooks of structural mechanics and they read:

$$\frac{\mathrm{d}N_{xx}}{\mathrm{d}x} = -n_x \tag{3.2}$$

$$\frac{\mathrm{d}^2 M_{xx}}{\mathrm{d}x^2} = -q_z - \frac{\mathrm{d}}{\mathrm{d}x}\left(N_{xx}\frac{\mathrm{d}w}{\mathrm{d}x}\right) \tag{3.3}$$

where N_{xx} and M_{xx} are the internal axial force and bending moment, respectively; q_z and n_x are external transversely and longitudinally distributed loads (see Fig. 3.1(a)). The general boundary conditions at $x = 0$ and $x = H$ are given by

$$N_{xx} = \lambda N_i \qquad \text{or} \qquad u_0 = \bar{u}_0 \tag{3.4}$$

$$\frac{\mathrm{d}M_{xx}}{\mathrm{d}x} + N_{xx}\frac{\mathrm{d}w}{\mathrm{d}x} = \lambda P_i \qquad \text{or} \qquad w = \bar{w} \tag{3.5}$$

$$M_{xx} = -\lambda M_i \qquad \text{or} \qquad \frac{\mathrm{d}w}{\mathrm{d}x} = \bar{\varphi} \tag{3.6}$$

where $\bar{u}_0$, $\bar{w}$ and $\bar{\varphi}$ are external deformations at the edges; N_i, P_i, and M_i (i = 0 or H) are concentrated external forces and moments at the edges (Fig. 3.1(a)); λ = -1 for x = 0 and λ = 1 for $x = H$.

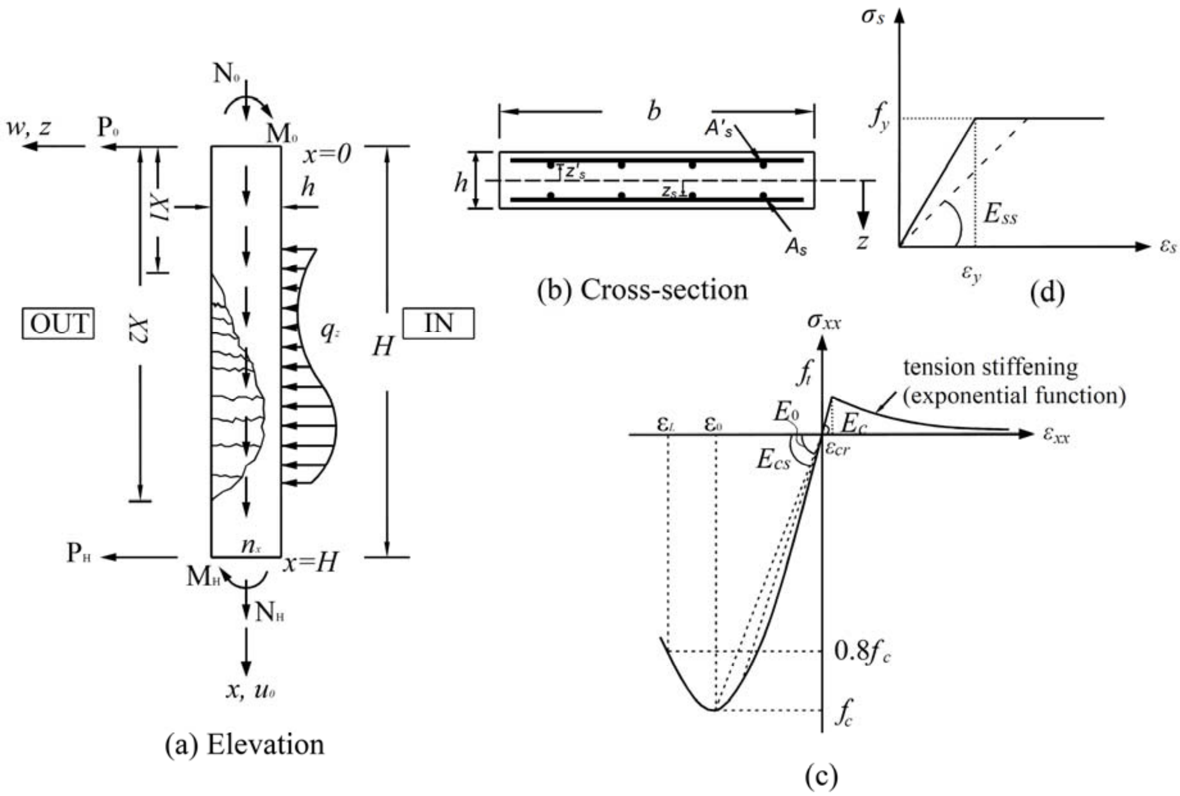

Fig. 3.1 Sign conventions of the model: (a) Panel geometry, loads, coordinates and displacements; (b) Cross-section of the panel; (c) Stress-strain curve of the concrete; (d) Absolute stress-strain curve of the steel;

3.2.1 Constitutive relations at the material point level

The constitutive relationship of the concrete accounts for cracking, tension-stiffening, and strain softening in compression. For this, the empirical compressive stress-strain curve proposed by Lu and Zhao (2010) is adopted, while the tension-stiffening effect is introduced through the model of Fields and Bischoff (2004) that takes the form of a descending exponential relation between stress and strain in tension after the peak stress in tension, as shown in Fig. 3.1(c). Note that the modelling approach proposed here can also handle other potential constitutive relations. The constitutive relation of concrete in compression adopted here is given as:

$$\sigma_{xx} = \begin{cases} f_c \left\{ 1 + 0.25 \left(\dfrac{\varepsilon_{xx} / \varepsilon_0 - 1}{\varepsilon_L / \varepsilon_0 - 1} \right)^{1.5} \right\}^{-1} & \text{for } \varepsilon_{xx} \le \varepsilon_L \\ f_c \left\{ \dfrac{\left(E_c / E_0\right)\left(\varepsilon_{xx} / \varepsilon_0\right) - \left(\varepsilon_{xx} / \varepsilon_0\right)^2}{1 + \left(E_c / E_0 - 2\right)\left(\varepsilon_{xx} / \varepsilon_0\right)} \right\} & \text{for } \varepsilon_L \le \varepsilon_{xx} \text{ and } \varepsilon_{xx} < 0 \end{cases} \tag{3.7}$$

in which,

$$\varepsilon_0 = -700 f_c^{0.31} \times 10^{-6}; \; E_0 = f_c / \varepsilon_0 \tag{3.8}$$

$$\varepsilon_L = \varepsilon_0 \left\{ \left(0.1 E_c / E_0 + 0.8\right) + \sqrt{\left(0.1 E_c / E_0 + 0.8\right)^2 - 0.8} \right\} \tag{3.9}$$

where σ_{xx} is the normal stress in concrete, E_c and f_c (in MPa) are the elastic modulus and compressive strength of concrete, ε_L is the concrete strain corresponding to the stress level of $0.8 f_c$ on the descending branch of the stress-strain curve, ε_0 and E_0 are the strain and secant modulus, respectively, that correspond to the concrete compressive strength f_c. The tensile part of the constitutive relation of concrete is given by:

$$\sigma_{xx} = \begin{cases} E_c \varepsilon_{xx} & \text{for } \; 0 \le \varepsilon_{xx} \text{ and } \varepsilon_{xx} \le \varepsilon_{cr} \\ e^{-0.8(\varepsilon_{xx} - \varepsilon_{cr}) \times 10^3} E_c \varepsilon_{cr} & \text{for } \; \varepsilon_{cr} < \varepsilon_{xx} \end{cases} \tag{3.10}$$

where ε_{cr} is the cracking strain, which is determined as f_t/E_c with f_t being the flexural tensile strength of concrete. The steel reinforcement is modelled as elastic-perfectly plastic, and its constitutive law under both tension and compression is shown in Fig. 3.1(d) and given by:

$$\sigma_{st} = \begin{cases} E_s \varepsilon_{st} & \text{for } \left|\varepsilon_{st}\right| \le \varepsilon_y \\ E_s \varepsilon_y & \text{for } \varepsilon_y < \varepsilon_{st} \\ -E_s \varepsilon_y & \text{for } \varepsilon_{st} < -\varepsilon_y \end{cases} \tag{3.11}$$

where σ_{st} and ε_{st} are the stress and strain of the steel reinforcement, E_s and ε_y are the elastic modulus and yielding strain of the steel, respectively.

3.2.2 Constitutive relations at the section level

The constitutive relations at the section level are formulated using the classical definitions of the stress resultants and using Eq. (3.1). The secant modulus approach is implemented here to account for the material nonlinearities of concrete and steel reinforcement. The stress resultants are given by:

$$N_{xx} = \int_{-\frac{h}{2}}^{\frac{h}{2}} bE_{cs}\varepsilon_{xx}\mathrm{d}z + E_{ss}A_s\varepsilon_s + E'_{ss}A'_s\varepsilon'_s \tag{3.12}$$

$$M_{xx} = \int_{-\frac{h}{2}}^{\frac{h}{2}} bE_{cs}\varepsilon_{xx}z\mathrm{d}z + E_{ss}A_s\varepsilon_s z_s + E'_{ss}A'_s\varepsilon'_s z'_s \tag{3.13}$$

where b and h are the width and thickness of the HSC panel, respectively; ε_s, A_s and z_s are the strain, area and distance to the panel mid-thickness of the steel reinforcement at the outer face of the panel; ε'_s , A'_s and z'_s are the strain, area and distance to the panel mid-thickness of the steel reinforcement at inner face of the panel (Fig. 3.1(b)); E_{cs}, E_{ss}

and E'_{ss} are the secant moduli of concrete and steel reinforcements at the outer and inner faces of the panel respectively (Fig. 3.1(c)-(d)), which take the following forms:

$$E_{cs} = \frac{\sigma_{xx}(\varepsilon_{xx})}{\varepsilon_{xx}}; \quad E_{ss} = \frac{\sigma_s(\varepsilon_s)}{\varepsilon_s}; \quad E'_{ss} = \frac{\sigma'_s(\varepsilon'_s)}{\varepsilon'_s} \tag{3.14}$$

where σ_s, and σ'_s are the stresses in the reinforcements at the outer and inner faces of the panel, respectively. Note that the secant moduli depend on the strain level at each material point, and they vary through the thickness and height of the panel. By substituting the kinematic relation (Eq. (3.1)) into Eqs. (3.12)-(3.13) the stress resultants become:

$$N_{xx} = A_{11}\left(\frac{\mathrm{d}u_0}{\mathrm{d}x} + \frac{1}{2}\left(\frac{\mathrm{d}w}{\mathrm{d}x}\right)^2\right) - B_{11}\frac{\mathrm{d}^2 w}{\mathrm{d}x^2} \tag{3.15}$$

$$M_{xx} = B_{11}\left(\frac{\mathrm{d}u_0}{\mathrm{d}x} + \frac{1}{2}\left(\frac{\mathrm{d}w}{\mathrm{d}x}\right)^2\right) - D_{11}\frac{\mathrm{d}^2 w}{\mathrm{d}x^2} \tag{3.16}$$

where A_{11}, B_{11} and D_{11} are the extensional, extensional-flexural, and flexural rigidities of the section, and they are given by:

$$A_{11} = \int_{-\frac{h}{2}}^{\frac{h}{2}} bE_{cs}\mathrm{d}z + E_{ss}A_s + E'_{ss}A'_s \tag{3.17}$$

$$B_{11} = \int_{-\frac{h}{2}}^{\frac{h}{2}} bE_{cs}z\mathrm{d}z + E_{ss}A_s z_s + E'_{ss}A'_s z'_s \tag{3.18}$$

$$D_{11} = \int_{-\frac{h}{2}}^{\frac{h}{2}} bE_{cs}z^2\mathrm{d}z + E_{ss}A_s z_s^2 + E'_{ss}A'_s \left(z'_s\right)^2 \tag{3.19}$$

3.2.3 Governing equations

The governing equations are derived by substituting the stress resultants (Eqs. (3.15) and (3.16)) into the equilibrium equations (Eqs. (3.2) and (3.3)) For convenience, they are presented as a set of 6 first-order differential equations as follows,

$$\frac{\mathrm{d}w}{\mathrm{d}x} = \phi \tag{3.20}$$

$$\frac{\mathrm{d}\phi}{\mathrm{d}x} = \frac{A_{11}M_{xx} - B_{11}N_{xx}}{B_{11}^2 - A_{11}D_{11}} \tag{3.21}$$

$$\frac{\mathrm{d}M_{xx}}{\mathrm{d}x} = S_{xx} - N_{xx}\frac{\mathrm{d}w}{\mathrm{d}x} \tag{3.22}$$

$$\frac{\mathrm{d}S_{xx}}{\mathrm{d}x} = -q_z \tag{3.23}$$

$$\frac{\mathrm{d}N_{xx}}{\mathrm{d}x} = -n_x \tag{3.24}$$

$$\frac{\mathrm{d}u_0}{\mathrm{d}x} = \frac{B_{11}M_{xx} - D_{11}N_{xx}}{B_{11}^2 - A_{11}D_{11}} - \frac{1}{2}\left(\frac{\mathrm{d}w}{\mathrm{d}x}\right)^2 \tag{3.25}$$

where S_{xx} is the shear force.

3.2.4 Solution procedure

At each load step, Eqs. (3.20)-(3.25) present a set of nonlinear differential equations due to the material nonlinearity that is introduced through the dependency of the rigidities on the unknown deformations and strains via Eqs. (3.17)-(3.19) and also due to the geometric nonlinearity (Eqs. (3.22) and (3.25)). In general, the rigidities are not uniform but they vary along the height of the panel because of cracking and/or stress levels. To simplify the analysis, the variation of the rigidities along the height of the cracked region is assumed to follow that of the out-of-plane deflection and they are assumed to be constant through the height of the uncracked region. This assumption results in two types of unknowns that need to be determined at each load step, namely: the rigidities at the critical section, and the start and end points of the cracked region ($X1$ and $X2$, see Fig. 3.1(a)). Here, an iterative procedure is used to determine these parameters at each load step, combined with the use of the numerical nonlinear shooting method (Stoer and Bulirsch (2002)) for the solution of the governing equations at each iteration. The arc length numerical continuation method, in which the formulation basically follows Sundararajan and Noah (1997) is also adopted in order to trace the buckling point and obtain the complete nonlinear equilibrium path. This method adds the following constraint to the set of governing equations,

$$L(Y,\lambda) = \left\{ \frac{\mathrm{d}Y_0}{\mathrm{d}s} \right\} \left(Y - Y_0 \right) + \left\{ \frac{\mathrm{d}\lambda}{\mathrm{d}s} \right\} \left(\lambda - \lambda_0 \right) - \Delta s = 0 \tag{3.26}$$

where $\{Y_0, \lambda_0\}$ is a point on the equilibrium path, Y is the vector of the unknowns, λ is the load parameter, and Δs is the arc length. The iterative procedure follows these steps:

Step 1. Initial guess. At the first iteration of the first load step, the panel is assumed uncracked. However, for the subsequent load steps, the solution from the previous load step is used as the initial guess for the current step.

Step 2. Analysis of the structure. Using the rigidities calculated in the initial guess or in the previous iteration (step 3), as well as the calculated locations of the start and end points of the cracked region, the governing equations are solved using the nonlinear shooting method.

Step 3. Analysis of the critical section (at the location of maximum bending moment). Based on the solution obtained in step 2, the strain at each material point across the critical section are determined using the kinematic relations appeared in Eq. (3.1). Once the strain distribution is calculated, the rigidities are updated through Eqs. (3.17)-(3.19) and $X1$ and $X2$ are also determined using the strain distribution at the tensioned face of the panel. The integrations in Eqs. (3.17)-(3.19) are numerically calculated to account for the material nonlinearity.

Step 4. Convergence criteria. If the norm of the relative difference between the magnitudes of the rigidities as well as $X1$ and $X2$ in two consecutive iterations is sufficiently small, the iterative procedure stops and the updated arc length is calculated. The analysis for the next load step is then carried out based on the updated arc length. Otherwise, the procedure returns to Step 2 with the updated rigidities determined in Step 3.

3.3 EXPERIMENTAL STUDY

As discussed in the Introduction, the test data available for model validation is limited. Thus, an experimental study was undertaken to extend the pool of data to validate the proposed theoretical model, as well as to examine the influences of various parameters on the failure behaviour of one-way HSC wall panels. It includes testing to failure of eight full-scale one-way HSC panels under symmetric eccentric axial loads on the top and bottom edges. Table 3.1 summarizes the details of the tested panels together with the experimental and theoretical failure loads. All panels have two layers of reinforcement, as shown in Fig. 3.1(b), except ST2 which has only one reinforcement layer being placed at the mid-thickness of the panel. Panel ST1 serves as a control (reference) specimen.

Table 3.1 Details for the experimental program and results

Panel No.[3]	h (mm)	Eccentricity (mm) Designed (e)	Test (top) (e_T)	Test (bottom) (e_B)	ρ_v (%)	[2]Φ (mm)	Failure load (kN) Test	Model	Column design AS3600 (2009)	Wall design AS3600 (2009)	Column design ACI318 (2008)	Wall design ACI318 (2008)
ST1	100	16.7	16.5	16.5	0.233	4.77	795	806	508	492	413	593
[1]ST2	100	16.7	16.8	16.8	0.233	6.75	804	786	260	485	399	593
ST3	100	8.3	6.9	7.7	0.233	4.77	1274	1216	508	740	413	593
ST4	100	33.3	35.2	36.6	0.233	4.77	297	378	508	---	413	593
ST5	130	21.7	23.0	23.0	0.284	6	1427	1464	1267	1293	933	1549
ST6	160	26.7	33.4	32.8	0.292	6.75	1882	1882	2560	1883	1772	2379
ST7	100	16.7	17.5	17.5	0.164	4	846	818	520	465	410	593
ST8	100	16.7	17.9	15.3	0.592	7.6	839	855	474	489	423	593

[1] – The panel has only one layer of steel reinforcement, placed at mid-thickness;
[2] – Diameter of steel mesh, with a spacing of 200 mm;
[3] - All panels are 2700 mm tall

The parameters that are examined for the different panels compare the reference specimen (ST1 in Table 3.1) to changes in the location of reinforcement (comparing ST1 to ST2), load eccentricity (comparing ST1 to ST3 and ST4), slenderness ratio (comparing ST1 to ST5 and ST6) and vertical reinforcement ratio ρ_v (comparing ST1 to ST7 and ST8). The designed eccentricities (e) are $h/12$ for specimen ST3, $h/3$ for specimen ST4 and $h/6$ for the rest specimens, where h is the thickness of each individual panel. The actual eccentricities in the experiment for ST1 to ST8 at the top (e_T) and bottom (e_B) ends are also given in Table 3.1, which are computed from the measured strains at the end sections (see the Section 3.4.1). Steel mesh was used as the reinforcement in all specimens with wire spacing of 200 mm in each orthogonal direction. The layout of the reinforcement is given in Fig. 3.2, in which a representative cross-section of ST1 is shown. The concrete cover is 20 mm for all specimens except ST2 in which only one single layer of reinforcement was used and placed at mid-thickness of the panel. All panels are 2700 mm high and 460 mm wide. The thickness varies per Table 3.1.

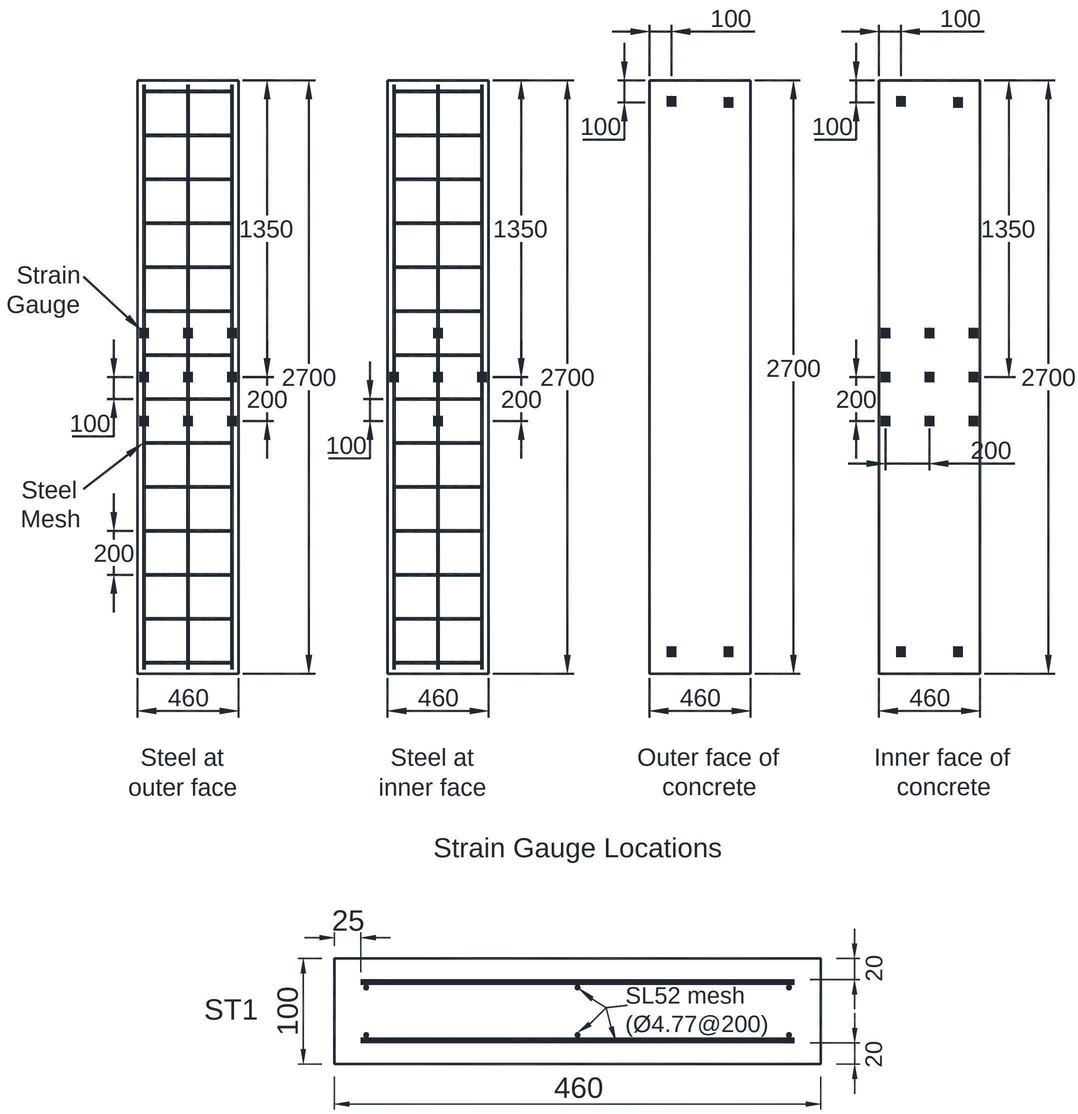

Fig. 3.2 Strain gauge locations and typical cross-section of the panel

3.3.1 Cast and curing of the specimens

All specimens were cast using a commercial ready-mixed high-strength concrete on the same day. The set-up of formwork is shown in Fig. 3.3(a). After casting, the panels were covered with wet hessian (burlap) and plastic sheets. They were kept moist in moulds for 7 days before stripping and then remained at ambient laboratory conditions until testing, as indicated in Fig. 3.3(b). The first panel was tested at the age of 42 days and, the other panels were tested subsequently one by one every two working days.

(a) Set-up of formwork

(b) Stripping formwork

Fig. 3.3 Preparation and demoulding of specimen

3.3.2 Material properties

Concrete cylinders of 100 mm diameter and 200 mm height and prisms of 100x100x500 mm were cast and cured with the panels. The concrete cylinders were tested in compression to measure the full stress-strain behaviour and the prisms were tested under 4-point bending to determine the flexural tensile strength of the concrete. A typical experimental stress-strain curve of the concrete is presented in Fig. 3.4(a); the initial modulus of elasticity was E_c = 38.4 GPa and the compressive strength was f_c = 81.4 MPa. The flexural tensile strength of the concrete was measured as f_t = 6.8 MPa. Samples of the reinforcing steel were tested to determine the stress-strain properties, with a typical result shown in Fig. 3.4(b). As the reinforcement used in the experiment was cold-formed steel, a yielding point is not precisely defined. In the analysis, 0.2% was adopted as the yielding strain (Eq. (3.11)). The elastic modulus was measured as 206 GPa.

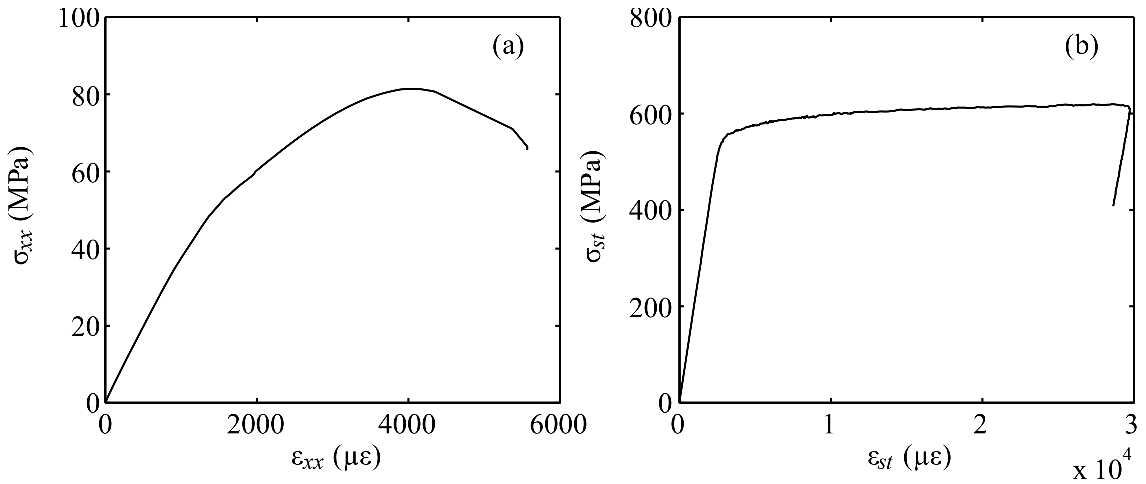

Fig. 3.4 Experimentally obtained compressive stress-strain curve: (a) Concrete; (b) Steel

3.3.3 Test setup and instrumentation

All panels were loaded under a deformation control up to failure using a 5000 kN capacity testing frame. The test setup is shown in Fig. 3.5. The loading and supporting mechanisms at each panel end consisted of a rotatable hinge to provide simply-supported boundary conditions. The net height of the panels was 2700 mm and the centre to centre distance between the steel pin connections was 2800 mm. The out-of-plane displacements were measured by displacement laser sensors at 5 locations symmetrically along the panel height. The panel strains were measured with 34 strain gauges, some of which were mounted on the steel reinforcement and the others on the concrete surfaces of each panel (Fig. 3.2).

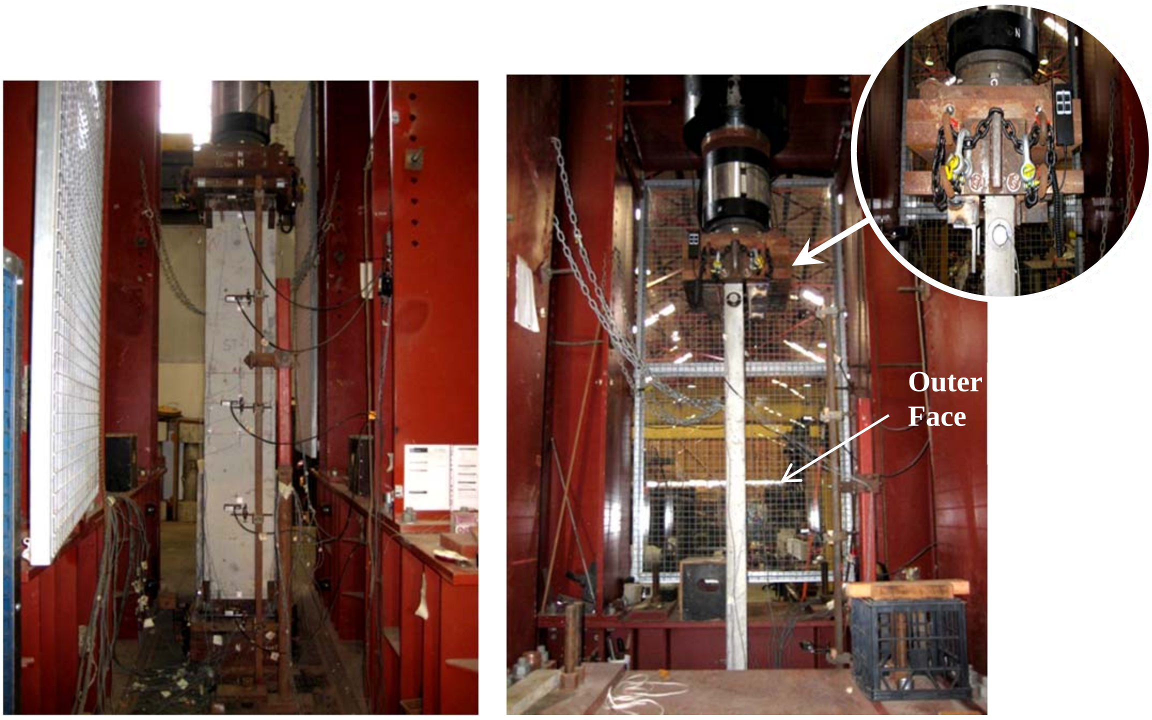

(a) Front View (Outer Face) (b) Side View

Fig. 3.5 Test Setup

3.4 RESULTS AND DISCUSSION

The experimental results are presented and discussed here. The theoretical model results are compared with the experimental test results reported here and with other test results from the literature. A comparison is also made with predictions according to design codes.

3.4.1 Experimental and theoretical results

The test results are summarized in Table 3.1, in conjunction with the corresponding failure loads predicted by the proposed model and by both wall and column design methods in AS3600 (2009) and ACI318 (2008) codes, respectively. Table 3.2 shows the model/experimental failure load ratio of all panels, which reveals a mean value of 1.029 and a standard deviation of 0.102.

The measured and predicted load-deflection curves of ST1 to ST6 are presented in Fig. 3.6, where w_c is the deflection at mid-height of the panel.

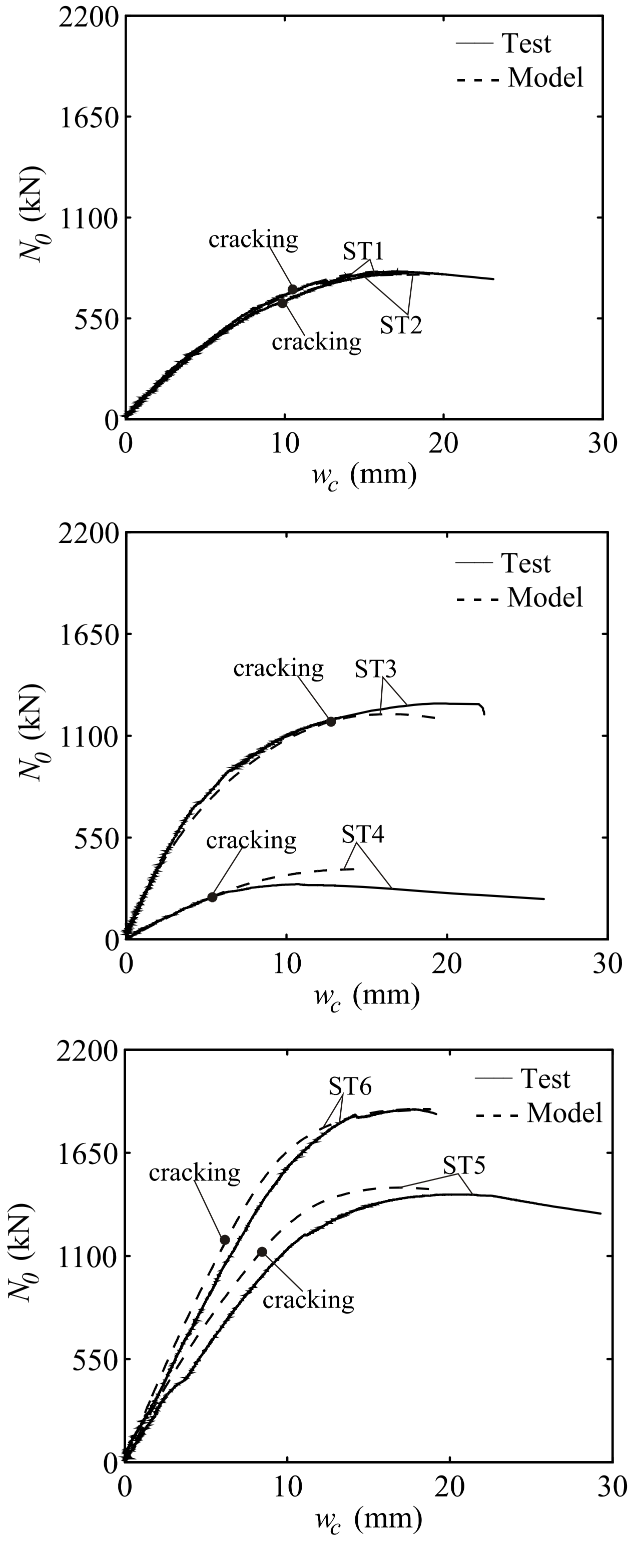

Fig. 3.6 Load vs. deflections at the centre-height of the panel for ST1-ST6

Due to variations in the panel thickness and possible errors during panel setting up, the actual eccentricity at the panel top and bottom might not achieve exactly the designed value. In the theoretical model analyses, the actual eccentricities at the top and bottom of a tested panel are used, which are calculated from the concrete strains measured near the panel ends on both panel surfaces as follows (assuming a linear strain distribution through the panel thickness and a linear material behaviour):

$$e_{test} = \frac{E_c I_{eff}}{N_{test}} \frac{\varepsilon_{cout-}\varepsilon_{cin}}{h} \tag{3.27}$$

where e_{test} is the actual eccentricity in the test at the top edge (e_T) or the bottom edge (e_B) (see Table 3.1); N_{test}, I_{eff}, ε_{cout} and ε_{cin} are the experimental axial load, effective moment of inertia obtained using the transformed section method, concrete strain on outer face and inner face of the panel, respectively. The geometric nonlinearity is neglected in Eq. (3.27) as the out-of-plane deflections at the locations near the panel ends are small. The mean values of the experimental eccentricities, which were determined at a load level equal to 30% the failure load are used here.

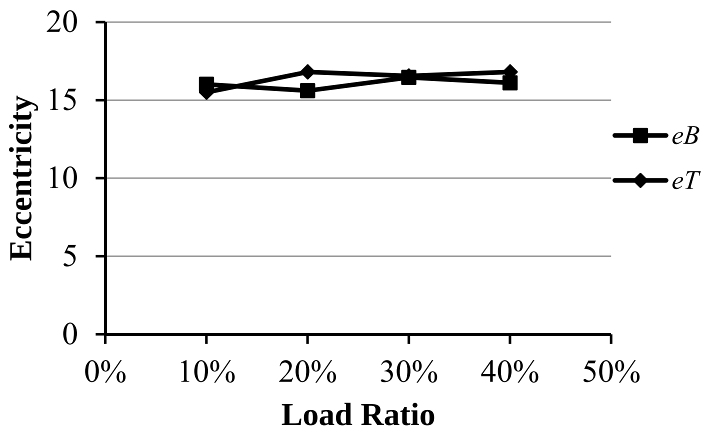

Fig. 3.7 Variation of Measured eccentricity with load ratio for Panel ST1

Similar eccentricities were achieved by applying Eq. (3.27) at the load level equal to 10%, 20%, 30% and 40% of the peak load, as shown in Fig. 3.7. So the eccentricities at the load level equal to 30% of the peak load for each individual panel were used in the theoretical model. The experimental compressive stress-strain curve as presented in Fig. 3.4(a), as well as the experimental tensile strength (f_t) of the HSC concrete are used in the theoretical model.

It is seen in Fig. 3.6 that the panels ST1-ST6 exhibited a nonlinear behavior with a limit point that characterizes their failure mode. As observed in the test, cracks were almost symmetrically developed around the panel centre. A representative crack pattern of ST4 is illustrated in Fig. 3.8. The cracking load predicted by the theoretical model is marked in the theoretical curves in Fig. 3.5. As indicated in the strain measurement results, all eight panels failed by buckling before crushing of concrete or yielding of reinforcement. Thus, unlike elastic beam-columns where instability failures are characterized by a bifurcation point in the load-deflection curve which is asymptotic to the Euler buckling load, cracking and material nonlinearity actually change the instability failure of slender HSC panels to a limit-point mode, where the load drops in the post-buckling stage (Chen and Lui 1987). It is observed that the predicted responses correlate closely with those from the tests. Due to the brittleness of high-strength concrete and the relatively small percentage of reinforcing steel used in the test samples, the reinforcement in all panels, except in Panel ST8, fractured at the failure load and the panels broke into two parts.

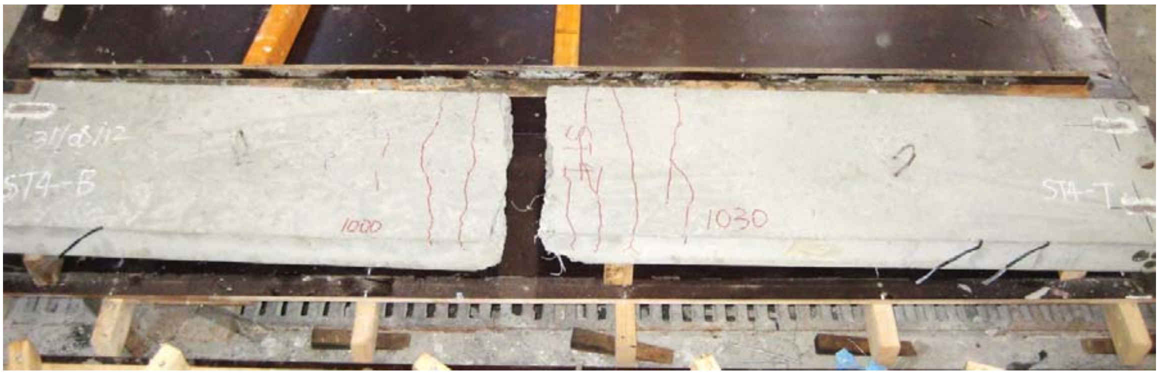

Fig. 3.8 Crack pattern of Specimen ST4 at failure

Specimens ST7 and ST8 were designed to investigate the influence of reinforcement ratio on the ultimate strength of HSC panels. Table 3.1 shows that the failure loads of ST7 and ST8 were close to that of ST1. Hence, the capability of reinforcement ratio to increase the buckling strength of HSC panels is limited. It was also found that the responses of ST7 and ST8 are comparable to that of ST1 and, therefore, for brevity their load-deflection curves are not presented here. Nevertheless, since ST8 is designed with nearly double the amount of reinforcement of ST1, it exhibited a more ductile failure as the reinforcement did not fracture at the peak load and more closely-spaced cracks were observed along the panel height. This observation implies that the minimum reinforcement ratio as prescribed in some design codes (0.15% in AS3600 (2009) and 0.12% in ACI318 (2008), which are both smaller than the one in ST1), may need to be further examined in the design of HSC panels to ensure some post-peak ductility.

Fig. 3.9 compares the measured and predicted strains of the reinforcement and concrete at the inner face around the mid-height for panels ST1 to ST6. The model is found to predict the strains in the HSC panel with good accuracy. Fig. 3.9 also shows that the measured peak strains of the concrete and reinforcement at failure loads are smaller than the ultimate strain of concrete and the yielding strain of the reinforcement, which indicates that buckling is the failure mode of all panels. The experimental and predicted strain distributions of ST1-ST6 over the panel thickness at the mid-height section and at 100 mm away from top of the panel are shown in Fig. 3.10 and Fig. 3.11 at three different load levels. It can be seen that with the increase of the load level, the neutral axis moves towards the inner face because of cracking and material nonlinearity, which is more dominant near the mid-height.

The deflection profiles of the panels measured from five laser displacement sensors at three load levels are shown in Fig. 3.12 along with the predicted profiles from the theoretical model. It can be seen that the increase of the out-of-plane displacement with the increase of the load level is nonlinear due to the geometric and material nonlinearities, which are well predicted by the proposed model.

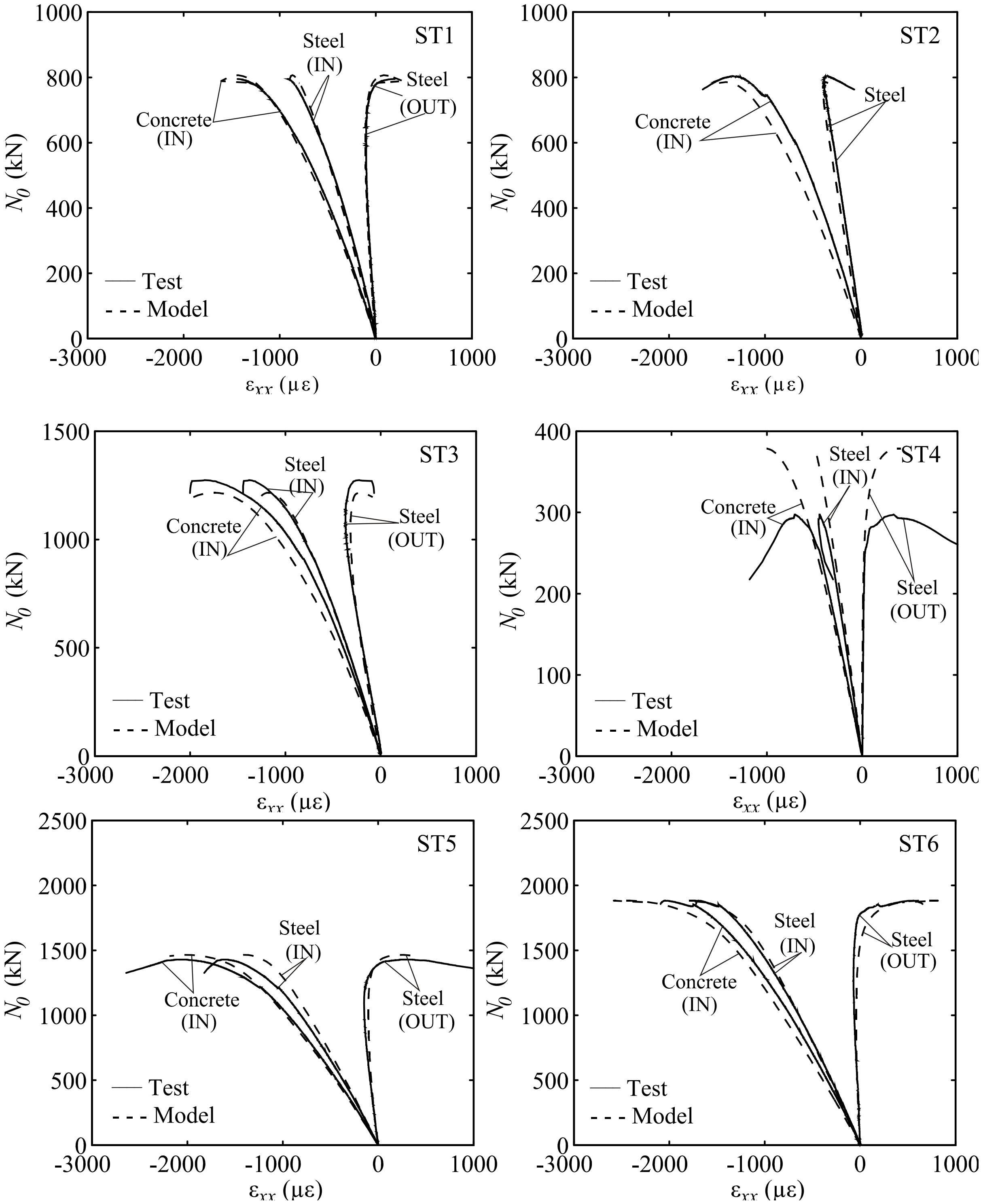

Fig. 3.9 Load vs. Strains at mid-height section for ST1-ST6

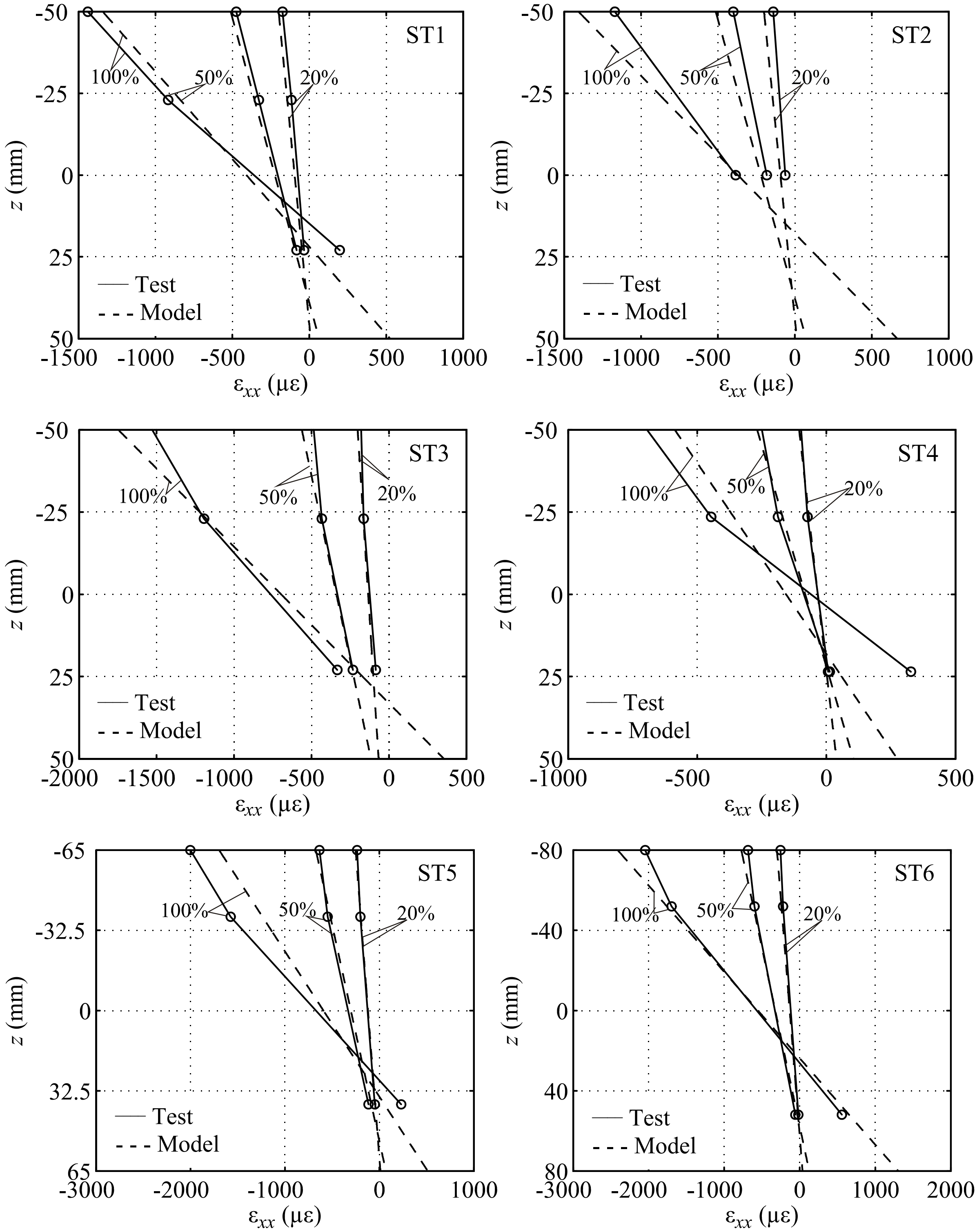

Fig. 3.10 Normal strain distributions at mid-height section for ST1-ST6 at three different load levels: 20%, 50% and 100% of test failure loads

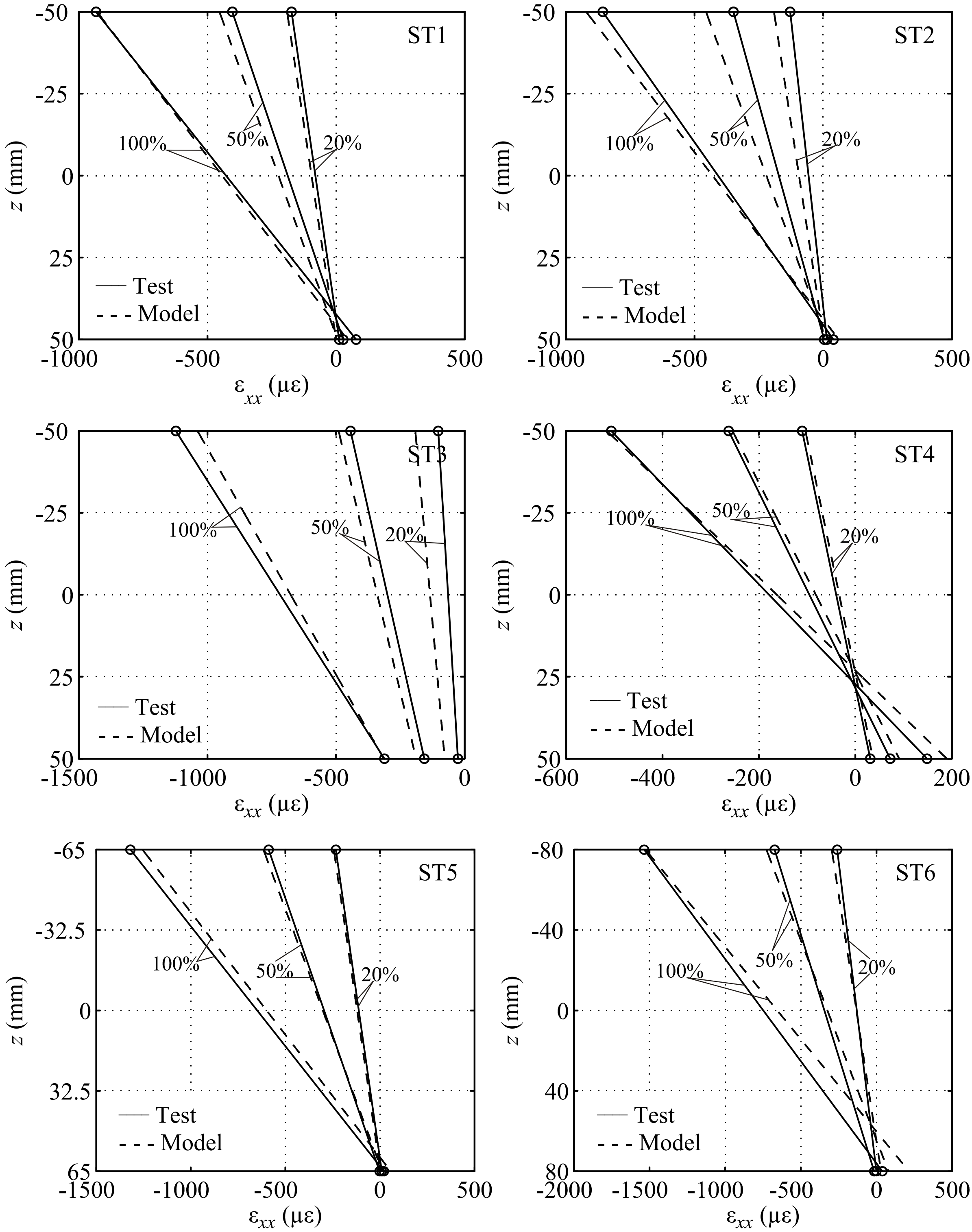

Fig. 3.11 Normal strain distribution at end section for ST1-ST6 at three different load levels: 20%, 50% and 100% of test failure loads

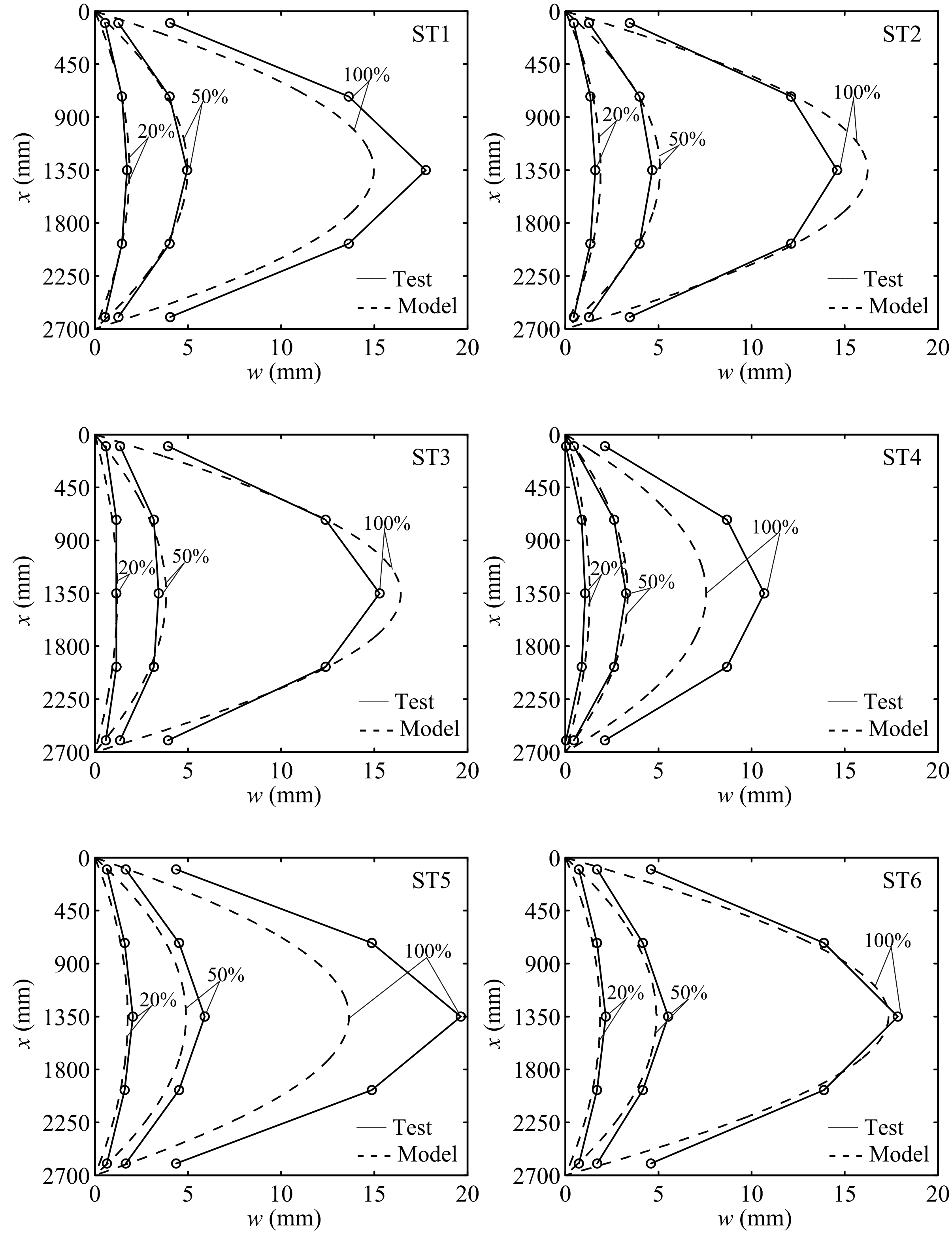

Fig. 3.12 Deflection distribution at three load levels: 20%, 50% and 100% of test failure loads

3.4.2 Parametric Study

The load-deflection curves of ST1 and ST2 (shown in Fig. 3.6) are examined to determine the effect of the location of reinforcement on the nonlinear behavior of HSC panels; panels ST1 and ST2 have nearly the same reinforcement ratios but the reinforcement is placed on both faces in ST1 and at the mid-thickness as a single layer in ST2. It can be seen that the different arrangements of reinforcement have a negligible influence on the failure loads of the panel, mainly because the failure mode is governed by buckling and because cracking was not significant. Fig. 3.9 shows that the steel reinforcement in ST1 are essentially subjected to compression forces throughout the loading history, despite cracking of the panel. This indicates that cracking took place only within the concrete cover region. This was also the case for ST2. It is also observed in Fig. 3.10 that the neutral axis depths in ST1 and ST2 are comparable.

The effect of load eccentricity on the HSC panel behavior is illustrated in Fig. 3.6 for ST3 and ST4, which is compared to the control panel ST1. Panel ST3, with about 1/5 of the eccentricity of ST4, exhibited a more rigid response and significantly higher buckling strength (more than 4 times) than that of ST4. Similarly, ST1 with approximately half the eccentricity of ST4 had a capacity of 2.7 times that of ST4. Fig. 3.9 reveals that due to the small eccentricity, the reinforcement and concrete of the tension face in ST3 are all in compression throughout the loading history until failure, which results in a large neutral axis depth, as seen in Fig. 3.10. For ST4, however, the reinforcement on the tension face is in tension because of the large eccentricity.

Panels ST5 and ST6 were tested to examine the effect of slenderness ratio on the performance of HSC panels. The definition of slenderness ratio (λ) for a column is adopted here, which is equal to H/r where r is the radius of gyration ($r = \sqrt{I_{eff} / A_{eff}}$, A_{eff} is the effective area of the section). The slenderness ratios for ST1, ST5 and ST6 are 94, 72 and 58, respectively. As expected, it is seen in Fig. 3.6 that the smaller the slenderness ratio, the higher the load-carrying capacity of the HSC panel, because it is dominated by buckling. Nevertheless, it is interesting to see that the decrease in the failure load is not proportional to $1/\lambda^2$ as in the elastic analysis. This is mainly due to the cracking and material nonlinearity, which are combined with the geometric nonlinearity and have a significant influence on the buckling failure load of HSC panels.

The influence of the slenderness ratio on the performance of HSC panels is further studied in Fig. 3.13. The same material characteristics of concrete and steel as well as the same width and height of the panel as those in the test are used here to predict capacity in Fig. 3.13. The thickness of the panel is varied in order to achieve different slenderness ratios. The panel is loaded eccentrically on both ends with an eccentricity of 20 mm. The reinforcement ratio for the panel is 0.256% regardless of the panel thickness. Both geometrically linear and nonlinear analyses are carried out using the proposed theoretical model, in which the linear analysis neglects the P-Δ effect and is conducted by omitting the nonlinear terms in Eqs. (3.21) and (3.25). The ratio of the failure load of the panel obtained from the geometrically nonlinear analysis (N_u^{non}) over the one obtained from the geometrically linear analysis (N_u^{lin}) is plotted with respect to the slenderness ratio in Fig. 3.13. It is seen that with the increase of the slenderness ratio, the ratio of the nonlinear failure load to the linear one decreases significantly, indicating the significant influence of the geometric nonlinearity. In panels with small slenderness ratios (less than 27), the linear and nonlinear analyses yield close results because the failure mode is characterized by material failure. For slenderness ratio between 27 and 62, although the predicted failure mode is crushing of concrete, the geometrically nonlinear model predicts a significantly smaller failure load, which are 66% to 95% of the failure loads that obtained by the geometrically linear analysis. In this portion of Fig. 3.13 the combined effects of the geometric and material nonlinearities accelerate the failure of the HSC panel. For slenderness ratio greater than 62, buckling dominates the failure of the panels.

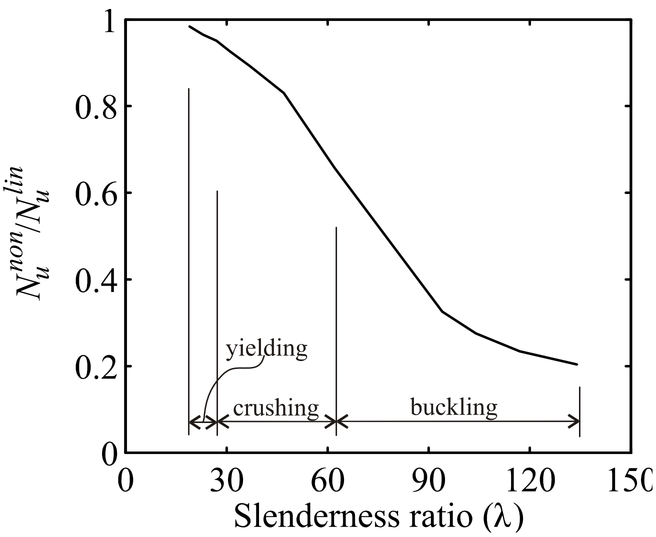

Fig. 3.13 Predicted ultimate strength (load per unit area) of HSC panels vs. slenderness ratio

3.4.3 Comparisons of Test, Model, and Code Equations

As the one-way HSC panel can be treated either as a wall or column, the calculated capacities by the design codes are based on two methods: the column design method (Chapter 10 in AS3600 (2009) and ACI318 (2008)) and wall design method (Chapter 11 in AS3600 (2009) and Chapter 14 in ACI318 (2008)). In the calculation of the capacity, the capacity reduction factor is taken as $\phi = 1.0$. It can be seen in Table 3.1 that in contrast to the model predictions, the predictions by both methods in AS3600 (2009) and ACI318 (2008) are generally significantly lower than the test results. Table 3.2 shows the code/experimental failure load ratios of all panels based on wall and column designs. Depending on the adopted design concept and code, the mean values range between 0.664 to 0.963, which are smaller than the mean model/test ratio of 1.029, and the standard deviations range between 0.182 to 0.486, which are significantly higher than the standard deviation of the model/test ratio (0.102).

Table 3.2 Predicted to test ratios for high strength concrete tests reported in this chapter

Panel No.	Model / Test	Column design AS3600 (2009) / Test	Wall design AS3600 (2009) / Test	Column design ACI 318 (2008) / Test	Wall design ACI 318 (2008) / Test
ST1	1.014	0.639	0.619	0.519	0.746
ST2	0.978	0.323	0.603	0.496	0.738
ST3	0.954	0.399	0.581	0.324	0.465
ST4	1.273	1.71	---	1.391	1.997
ST5	1.026	0.888	0.906	0.654	1.085
ST6	1	1.36	1.001	0.942	1.264
ST7	0.967	0.615	0.55	0.485	0.701
ST8	1.019	0.565	0.583	0.504	0.707
Average	1.029	0.812	0.692	0.664	0.963
Standard Deviation	0.102	0.486	0.182	0.345	0.486

The wall design methods in both codes are based on empirical or semi-empirical formulae that do not consider the geometrical and material nonlinearity appropriately. The wall design method in AS3600 (2009) even fails to predict the capacity of Panel ST4 which has the largest eccentricity in all specimens. The reason for the large gap between the predictions by the column design methods and the test is that the codes do not consider the influence of load eccentricity in the calculation of the buckling load for slender columns. ACI318 (2008) adopts an effective rigidity approach and AS3600 (2009) uses the rigidity of the section when the balanced failure happens. However, the section (and the neutral axis depth) at failure on which the effective rigidity is evaluated is actually determined by the combined axial load and bending moment, which depends on the load eccentricity and slenderness ratio. Therefore, it is recommended that these factors need to be incorporated into the calculation of the rigidities for the buckling load of HSC panels.

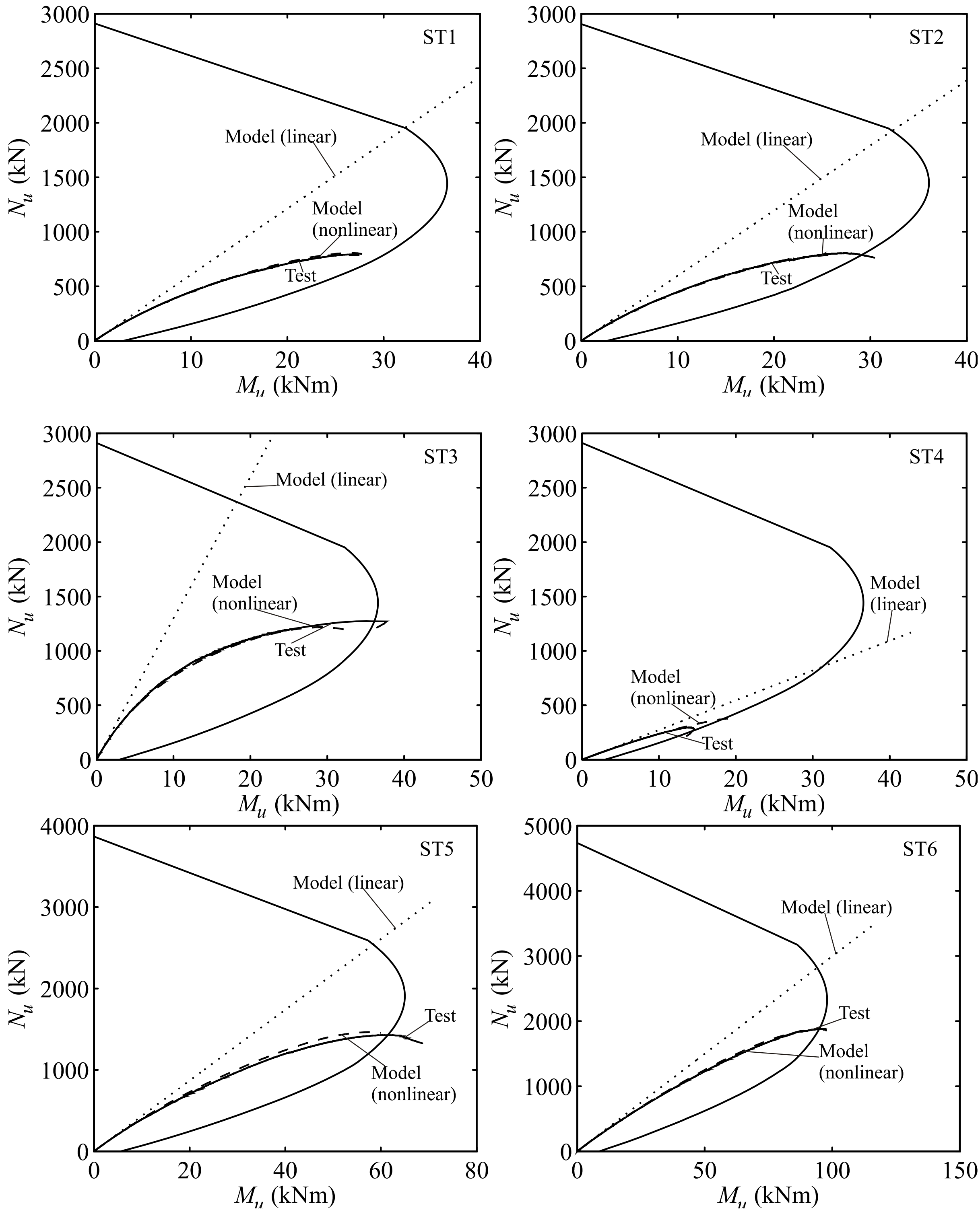

Fig. 3.14 Loading paths and section capacity lines of ST1-ST6

Fig. 3.14 presents the panel interaction section capacity curves for ST1-ST6 which are obtained according to the column design method in AS3600 (2009). Superimposed on the section capacity curve is the test loading path and the predicted load paths by the proposed theoretical model based on geometrically linear and nonlinear analyses. The figures clearly reveal that the load-carrying capacities of all the panels predicted by the geometric linear analysis significantly overestimate the capacity from the one predicted by the geometric nonlinear analysis, which, however, correlate well with the test results. The buckling failures of all the test panels are characterized by a limit-point, which in most cases develop before the test load path curve intersected the section capacity envelop.

3.4.4 Comparisons of Model Results with Test Results in the Literature

The capabilities of the proposed theoretical model are further examined by comparing the model prediction to other test results available in the literature. As the available test data on HSC panels are limited, the comparison study is extended to NSC panels. The test results of Saheb and Desayi (1989) and Fragomeni and Mendis (1998) are included here and the details of their experiments along with the corresponding theoretical failure loads as predicted by the proposed model are presented in Table 3.3. All the panels were simply-supported and were tested in one-way action under eccentric compression loading. Only the compressive strength was reported in each study and, therefore, the elastic modulus and tensile strength used in the model are evaluated based on AS3600 (2009), while the constitutive relations follow Eqs. (3.7)-(3.9). The panels have a single layer of reinforcement with 4 mm wires placed at the mid-thickness in Saheb and Desayi (1989), while in Fragomeni and Mendis (1998), the panels are reinforced at both faces where the diameter of the reinforcement is 2 mm.

As seen in Table 3.3, the theoretical failure loads correlate reasonably well with the test ones with a mean model/experimental failure load ratio of 0.985 and a standard deviation of 0.126. All panels were predicted to fail by buckling using the proposed model.

Table 3.3 Comparison of test results in the literature with the predictions of the proposed model

Literature	Panel No.	Dimensions			λ	e (mm)	f_c (MPa)	ρ_v (%)	Failure load (kN)		Model / Test
		H (mm)	b (mm)	h (mm)					Test	Model	
Fragomeni and Mendis (1998)	1a	1000	200	50	70	8.3	40.7	0.250	162	156	0.963
	1b	1000	200	50	70	8.3	58.9	0.250	187	202	1.080
	2a	1000	300	50	70	8.3	42.4	0.250	232	241	1.039
	2b	1000	300	50	70	8.3	65.4	0.250	264	324	1.277
	3a	1000	200	40	87	6.7	37.1	0.310	100	91	0.910
	4b	1000	300	40	87	6.7	54	0.210	217	173	0.797
	5a	1000	500	40	87	6.7	35.7	0.250	201	223	1.109
Saheb and Desayi (1989)	WAR-1	600	900	50	42	8.3	17.9	0.173	484	463	0.957
	WAR-2	600	600	50	42	8.3	17.9	0.173	315	304	0.965
	WAR-3	600	400	50	42	8.3	17.9	0.173	198	206	1.040
	WAR-4	600	300	50	42	8.3	17.9	0.173	147	154	1.048
	WSR-1	450	300	50	31	8.3	17.3	0.165	214	206	0.963
	WSR-2	600	400	50	42	8.3	17.3	0.165	254	200	0.787
	WSR-3	900	600	50	62	8.3	17.3	0.165	299	256	0.856
										Aeverage	0.982
										Standard Deviation	0.121

3.5 CONCLUSIONS

A nonlinear theoretical model has been developed for the failure analysis of one-way slender reinforced high-strength concrete panels. The model accounts for concrete cracking, tension-stiffening, nonlinearity in compression and yielding of the steel, as well as the geometric nonlinearity. It describes the entire equilibrium path of HSC panels through the use of the arc-length method. The model has been validated by an experimental study which has provided more insight into the behaviour of HSC panels. All the tested panels exhibited nonlinear responses due to the geometric and material nonlinearities and they failed dominantly by buckling. The buckling load is influenced by cracking and nonlinear material softening in compression. As a result, instability failure of HSC panels has shifted from the bifurcation buckling for the case of elastic panels to a limit-point buckling mode.

The influences of reinforcement ratio and location, load eccentricity, and slenderness ratio on the performance of HSC panels have been examined in the experimental study. The results have revealed that the reinforcement ratio and location has an insignificant influence on the buckling load of slender HSC panels with normal load eccentricities ($e \leq h/6$), but increasing the reinforcement ratio and reinforcing the panel at both faces can result in a more ductile failure. On the other hand, the behaviour of the HSC panel is substantially influenced by the load eccentricity and the slenderness ratio. Estimations of the load capacities of the tested HSC panels using a column design approach and simplified models for walls in the design codes showed considerable deviation from the test results. In general, the design models are conservative compared to the nonlinear model proposed in this chapter. The main reason for the conservative prediction is that for wall design, the formulae in the codes are empirical or semi-empirical that do not properly consider the material and geometrical nonlinearities, and the design codes exclude the influence of load eccentricity in the calculation of the effective rigidity in the column design approach, which is used to determine the buckling load. The capability of the proposed theoretical model was further demonstrated through comparison between test results available in the literature and predictions of the model, which has shown a good correlation between the results. Therefore, these simplified formulae in the codes should be reconsidered.

Finally, it can be concluded that the failure mode of HSC panels with typical slenderness ratios, as commonly used in practice, is characterized by brittle and sudden buckling failure that is sensitive to the slenderness ratio and to uncertainties regarding the magnitude of load eccentricity, which should be carefully considered in their design. The test results have shown that the brittle failure can be partially controlled by increasing the amount of reinforcement in the panel. These aspects have been well demonstrated by the proposed model, which also has shown and explained the interaction between the geometric and material nonlinearities.

CHAPTER 4 THEORETICAL STUDY OF THE LONG-TERM BEHAVIOR OF GENERAL ONE-WAY VISCOELASTIC PANELS WITHOUT CONSIDERING CRACKING

4.1 INTRODUCTION

The instantaneous response, particularly the buckling failure response of slender one-way HSC panels was studied in Chapter 3. It was shown that the coupling effect of geometric and material nonlinearities along with the imposed axial loads significantly reduced the buckling capacity of one-way HSC panels compared to classical buckling of elastic panels. Buckling failures may also occur to slender panels under sustained axial loads due to the additional weakening caused by creep and shrinkage of concrete. In such cases, buckling failures may occur over time under a sustained load that is significantly smaller than the instantaneous buckling load, a phenomenon typically referred to as creep buckling. The creep buckling failure is characterized by sudden loss of structural stability at a certain point of time after the panel being loaded. Such behavior was observed in reinforced concrete (RC) columns and shells (Bažant 1968; Bockhold and Petryna 2008; Hamed et al. 2011). On the other hand, the creep deformations may not necessarily lead to buckling failure but they may increase the internal stresses and decrease the residual strength of the wall when additional loads are to be applied. The dependence of the creep strains on the level of stresses that may vary with time, their interaction with shrinkage and thermal strains, and the nonlinear geometrical and material response, make accurate prediction of the creep behavior of HSC panels a challenging and difficult task.

It has been shown in Chapter 2 that the instantaneous buckling and failure behavior of NSC and HSC panels have been extensively investigated in the literature (Oberlender and Everard 1977; Saheb and Desayi 1989; Fragomeni and Mendis 1997). However, studies that focused on the buckling behavior of HSC panels including the influence of creep and shrinkage could not be found in the open literature.

Therefore, the long-term behavior of the one-way HSC panel is investigated in Chapter 4, 5 and 6. This chapter focuses on the theoretical examination of general viscoelastic panels, where material nonlinearities of concrete and steel reinforcement, shrinkage and aging of concrete are not considered. A more comprehensive theoretical investigation of the long-term response of the HSC one-way panel under the influences of creep and shrinkage is conducted in the next chapter that takes into account the concrete cracking and tension-stiffening effect, aging of concrete and yielding of steel reinforcement. An experimental long-term study of the HSC panels is carried out in Chapter 6 to validate the theoretical model presented in Chapter 5.

In this chapter, a nonlinear theoretical model is developed based on a step-by-step time analysis, which takes into account the variation of the internal stresses and deformations with time. A rheological material model that is based on the generalized Maxwell chain is used for modelling the creep of the concrete. The incremental governing equations are derived, and their solution at each time step is achieved numerically. The mathematical formulation of the model is presented next, followed by numerical and parametric studies.

4.2 MATHEMATICAL FORMULATION

The variational principle of virtual work ($\delta U + \delta W = 0$, δ is the variational operator) is used for the formulation of the incremental equilibrium equations along with the boundary conditions. The sign conventions for the coordinates, loads, and displacements are shown in Fig. 4.1(a). The time of concern t is subdivided into n_t discrete time steps with $\Delta t_r = t_r - t_{r-1}$ (r = 1,2,…n_t), and the virtual work of the internal stresses at time $t_{r-1}+\Delta t_r$ reads

$$\delta U = -\int (\sigma_{xx} + \Delta\sigma_{xx})\delta\Delta\varepsilon_{xx} dV \tag{4.1}$$

where σ_{xx} and ε_{xx} are the in-plane normal stress and strain respectively, Δ is the incremental time operator, and V is the volume of the panel.

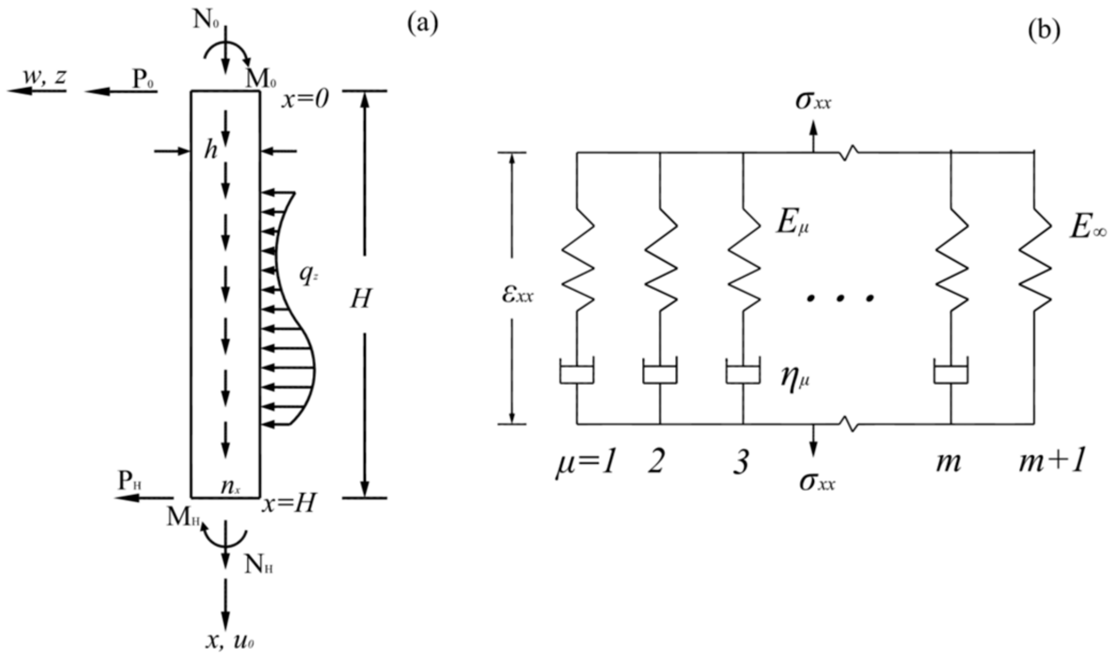

Fig. 4.1 (a) Panel geometry, loads, coordinates, and displacement (b) Maxwell chain

The stress and strain are functions of the independent coordinates x and z (Fig. 4.1(a)) and time t_{r-1}, which for brevity are omitted here. The incremental kinematic relation is:

$$\Delta\varepsilon_{xx}(t_r) = \Delta u_{0,x}(t_r) - z\Delta w_{,xx}(t_r) + \frac{1}{2}\Delta w_{,x}^2(t_r) + w_{,x}(t_{r-1})\Delta w_{,x}(t_r) \tag{4.2}$$

where u_0 and w are the longitudinal displacement and out-of-plane deflection, and $(\ )_{,x}$ denotes a derivative with respect to x. The virtual work of the external loads applied at time $t_r+\Delta t_r$ is:

$$\delta W = \int_{x=0}^{x=L} \left[\left(q_z + \Delta q_z \right) \delta \Delta w + \left(n_x + \Delta n_x \right) \delta \Delta u_0 \right] dx + (N_0 + \Delta N_0) \delta \Delta u_0 (x=0)$$
$$+ (P_0 + \Delta P_0) \delta w (x=0) + (M_0 + \Delta M_0) \delta \Delta w_{,x} (x=0) + (N_H + \Delta N_H) \delta \Delta u_0 (x=H) \quad (4.3)$$
$$+ (P_H + \Delta P_H) \delta w (x=H) + (M_H + \Delta M_H) \delta \Delta w_{,x} (x=H)$$

where q_z and n_x are external distributed loads; N_0, P_0, and M_0 are external loads and bending moment at the top of the panel (x=0), N_H, P_H and M_H are loads and moment at the bottom of the panel (x=H) (see Fig. 4.1(a)). Using Eqs. (4.1)-(4.3), the incremental equilibrium equations read

$$\Delta N_{xx,x} = -\Delta n_x \quad (4.4)$$

$$\Delta M_{xx,xx} = -\Delta q_z - \left[\left(N_{xx} + \Delta N_{xx} \right) \Delta w_{,x} \right]_{,x} - \left(\Delta N_{xx} w_{,x} \right)_{,x} \quad (4.5)$$

where N_{xx} and M_{xx} are the axial force and bending moment, respectively.

4.2.1 Constitutive relations

A differential-type form of Boltzmann's principle of superposition Bažant and Wu (1974) is adopted here. For simplicity, aging is not considered. The constitutive relation is derived in an incremental form using the generalized Maxwell model, as shown in Fig. 4.1(b). For this, the relaxation function is expanded into Dirichlet series, as follows

$$R(t,t') \approx \overline{R}(t,t') = \sum_{\mu=1}^{m} E_\mu e^{-(t-t')/\tau_\mu} + E_\infty \quad (4.6)$$

where $R(t,t')$ is the relaxation function, $\overline{R}(t,t')$ is the approximated relaxation function, t' is the time at application of loading, t is the time since first loading, E_μ is the modulus of the μth Hookean spring in the Maxwell chain, m is the number of units, τ_μ is the relaxation time of the μth unit and E_∞ is the modulus of the m+1 spring that is not coupled to any dashpot (see Fig. 4.1(b)). The moduli of the springs in the Maxwell chain are determined using least squares method to fit test data or a known expression of $R(t,t')$, assuming $\tau_\mu = \eta_\mu / E_\mu$ (η_μ is the viscosity of the μth dashpot). The incremental constitutive relation is as follows Bažant and Wu (1974):

$$\Delta\varepsilon_{xx}(t_r) = \frac{\Delta\sigma_{xx}(t_r)}{E_c''(t_r)} + \Delta\varepsilon''(t_r) \tag{4.7}$$

$$E_c''(t_r) = \sum_{\mu=1}^{m} \left(1 - e^{-\Delta t_r/\tau_\mu}\right) \frac{\tau_\mu}{\Delta t_r} E_\mu + E_\infty \tag{4.8}$$

where $\Delta\varepsilon''$ is the incremental creep strain, and E_c'' is quasi-elastic modulus. After obtaining the solution at time t_r, the stresses at each Maxwell unit are determined as follows:

$$\sigma_\mu(t_r) = e^{-\Delta t_r/\tau_\mu}\sigma_\mu(t_{r-1}) + E_\mu \Delta\varepsilon_{xx}(t_r)\left(1 - e^{-\Delta t_r/\tau_\mu}\right)\tau_\mu / \Delta t_r \tag{4.9}$$

The stress resultants are formulated by substitution of the kinematic relation Eq. (4.2) into Eq. (4.7) and integration throughout the cross-sectional area:

$$\Delta N_{xx}(t_r) = E_c''(t_r) A_{eff} \left[\Delta u_{0,x} + \frac{1}{2}\Delta w_{,x}^2 + w_{,x}\Delta w_{,x} - \Delta\tilde{\varepsilon}(t_r)\right] \tag{4.10}$$

$$\Delta M_{xx}(t_r) = -E_c''(t_r) I_{eff}\left[\Delta w_{,xx} - \Delta\tilde{\kappa}(t_r)\right] \tag{4.11}$$

$$\Delta\tilde{\varepsilon}(t_r) = \frac{1}{E_c''(t_r) A_{eff}} \left\{\sum_{\mu=1}^{m}\left(1 - e^{-\Delta t_r/\tau_\mu}\right) N_\mu(t_{r-1})\right\} \tag{4.12}$$

$$\Delta\tilde{\kappa}(t_r) = -\frac{1}{E_c''(t_r) I_{eff}} \left\{\sum_{\mu=1}^{m}\left(1 - e^{-\Delta t_r/\tau_\mu}\right) M_\mu(t_{r-1})\right\} \tag{4.13}$$

where $\Delta\tilde{\varepsilon}(t_r)$ and $\Delta\tilde{\kappa}(t_r)$ are the incremental membrane creep strain and change of curvature, A_{eff} and I_{eff} are the effective cross-sectional area and moment of inertia considering the steel reinforcement. Note that the modular ratio used here is $n = E_s / E_c''(t_r)$ which varies with time (E_s is the elastic modulus of steel).

4.2.2 Governing equations

The governing equations are formulated using the equilibrium equations (Eqs. (4.4)-(4.5)) and the stress resultants (Eqs. (4.10)-(4.13)). They are presented as a set of 6 first-order differential equations in terms of the unknown deformations and forces. Note that terms of high order product may be neglected due to the use of sufficiently small time increments:

$$\Delta w_{,x}(t_r) = \Delta\varphi(t_r) \tag{4.14}$$

$$\Delta\varphi_{,x}(t_r) = \Delta\tilde{\kappa}(t_r) - \Delta M_{xx}(t_r) \big/ E_c''(t_r) I_{eff} \tag{4.15}$$

$$\Delta M_{xx,x}(t_r) = \Delta S_{xx}(t_r) - N_{xx}(t_{r-1})\Delta w_{,x}(t_r) - \Delta N_{xx}(t_r) w_{,x}(t_{r-1}) \tag{4.16}$$

$$\Delta S_{xx,x}(t_r) = -q_z(t_r) \tag{4.17}$$

$$\Delta N_{xx,x}(t_r) = -\Delta n_x(t_r) \tag{4.18}$$

$$\Delta u_{0,x} = -w_{,x}(t_{r-1})\Delta w_{,x}(t_r) + \Delta N_{xx}(t_r) \big/ E_c''(t_r) A_{eff} + \Delta\tilde{\varepsilon}(t_r) \tag{4.19}$$

where S_{xx} is the shear force of the panel and φ is the rotation of the cross-section of the panel. The boundary conditions are:

$$\Delta N = \lambda \Delta N_i \ \left(i = 0,\ H\right) \qquad \text{or} \qquad \Delta u_0 = \Delta\bar{u}_0 \tag{4.20}$$

$$\Delta M_{,x} + \left(N + \Delta N\right)\Delta w_{,x} + \Delta N w_{,x} = \lambda \Delta P_i \ \left(i = 0,\ H\right) \qquad \text{or} \qquad \Delta w = \Delta\bar{w} \tag{4.21}$$

$$\Delta M = -\lambda \Delta M_i \left(i = 0,\ H\right) \qquad \text{or} \qquad \Delta w_{,x} = \Delta\bar{\varphi} \tag{4.22}$$

where $\Delta\bar{u}_0$, $\Delta\bar{w}$ and $\Delta\bar{\varphi}$ are external deformations. $\lambda = -1$ for x=0 and $\lambda = 1$ for x=H. Here Eqs. (4.14)-(4.19) are solved by the numerical multiple shooting method.

4.2.3 Creep properties

The relaxation function of concrete takes the following approximated expression Bažant and Kim (1979):

$$R(t,t')=\frac{1-\Delta_0}{J(t,t')}-\frac{0.115}{J(t,t-1)}\left(\frac{J(t-\Delta,t')}{J(t,t'+\Delta)}-1\right) \tag{4.23}$$

$$J(t,t')=\frac{1+\phi(t,t')}{E_c} \tag{4.24}$$

where $\Delta=(t-t')/2$, $\Delta_0\approx 0.008$, $J(t,t')$ is the compliance function of concrete, and $\varphi(t,t')$ is the creep coefficient which is evaluated based on AS3600 (2009) as:

$$\phi(t,t')=k_2k_3k_4k_5\phi_{\mathrm{cc.b}} \tag{4.25}$$

where $\varphi_{cc,b}$ is the basic creep coefficient and k_2, k_3, k_4, and k_5 are factors that depend on the age and strength of the concrete, geometry of the structure, time of loading, and the environmental conditions.

4.3 NUMERICAL STUDY

4.3.1 Numerical example

The panel investigated in this study is 5.0 m high by 1.5 m wide and 150 mm thick. The compressive strength and elastic modulus of the concrete are f_c' = 80 MPa and E_c = 39.6 GPa, respectively. The number of units in the Maxwell model (m) equals 5 in this example. The panel is assumed to be loaded at the age of 28 days. Following AS3600 (2009), the creep coefficient is given by

$$\varphi(t,28)=\frac{1.403(t-28)^{0.8}}{(t-28)^{0.8}+20.45} \tag{4.26}$$

The vertical steel reinforcement ratio is taken as 0.0015 and its elastic modulus is E_s=200 GPa. The panel is simply supported at both ends and is loaded by an eccentric sustained load. The variation of the out-of-plane deflection with time for the case of N_0 = 3300 kN and eccentricity e=7.5 mm is shown in Fig. 4.2. The axial load actually equals 50% of the classical Euler buckling load (P_{cr}=6628 kN) and the eccentricity is 0.05 of the thickness (*h*). As can be seen, the out-of-plane deflection increases with time as a result of creep and tends to increase to infinity at certain time. Due to the difficulties in generating a criterion for creep buckling, Hoff (1958) and Bažant and Cedolin (1991) suggested the use of maximum allowable deflection as a creep buckling criterion. Here, the maximum deflection is limited to 1.5*h*, and the corresponding time is defined as "critical time", which equals 663 days in Fig. 4.2.

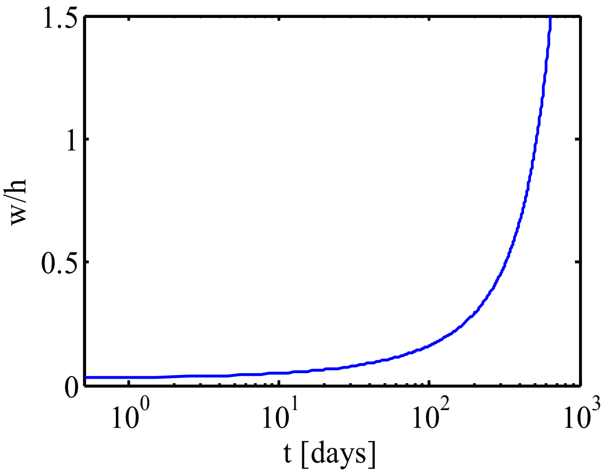

Fig. 4.2 Variation of maximum out-of-plane deflection with time of examined panel

The distributions of the deflection and the bending moment through the height of the panel at three different times are shown in Fig. 4.3. The results show that the increase in the deflection is associated with a significant increase and redistribution of the bending moment with time. These magnified moments may lead to cracking of the concrete, which may further weaken the structure and reduce its buckling capacity.

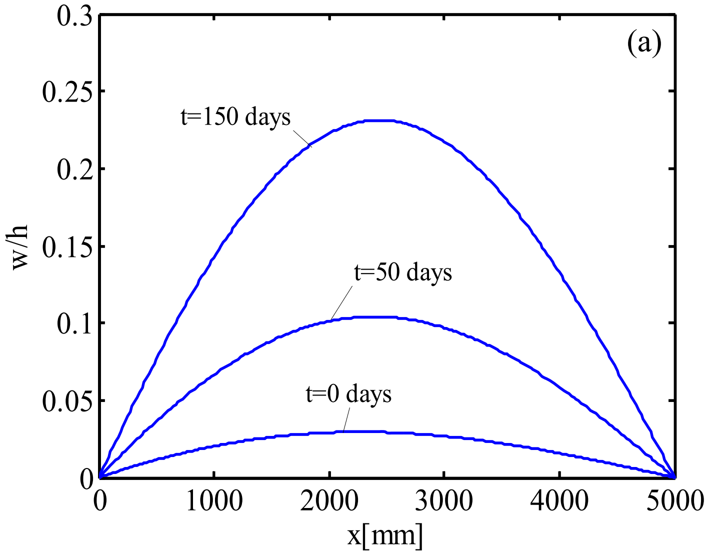

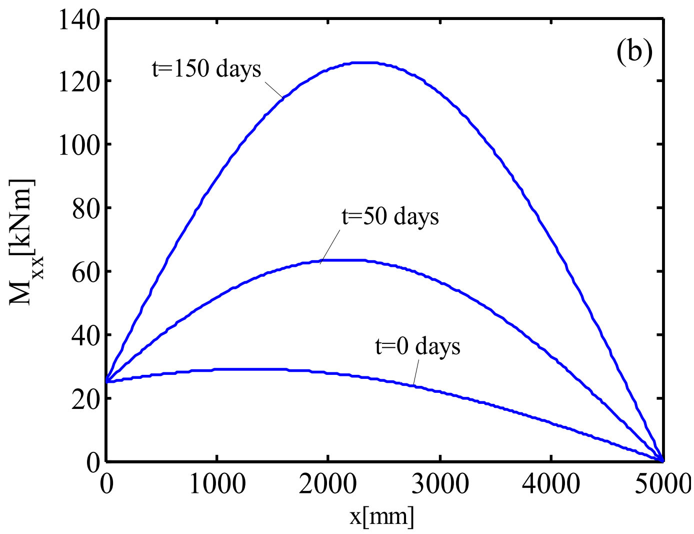

Fig. 4.3 Distribution of the out-of-plane deflection (a) and bending moment (b) at three different times

4.3.2 Parametric study

The influence of the magnitude of the sustained load is studied in Fig. 4.4. As expected, the critical time at which creep buckling occurs decreases with increasing initial load. Nevertheless, Fig. 4.4(b) shows that this decrease is exponentially proportional to the applied pressure. This exponential relation can be expressed in the following form

$$\frac{t_c}{t_0} = Ce^{\alpha N_0/P_{cr}} \tag{4.27}$$

where C and α are parameters that depend on the geometry and material of the panel, t_c is the critical time to be predicted and t_0 is the critical time that corresponds to the minimum N_0 for which buckling occurs ($N_0^{\min}$). In this case, $N_0^{\min} = 0.42P_{cr}$, which defines the long-term buckling load of the panel under this eccentricity and t_0=6157.3 days. This result is in accordance with that obtained using the simplified Effective Modulus Method (EMM) approach. In the latter, $N_0^{\min} = \pi^2 \overline{E} I_{eff} / H^2$ with $\overline{E} = E_c / [1 + \varphi(t,t')]$ which yields $N_0^{\min} = 0.42P_{cr}$ and provides a level of validation to the proposed model. However, the model developed here is more general and comprehensive than the EMM model, as it accounts for gradual loading of the structure and provides a basis for more comprehensive models that include cracking and material nonlinearity to be developed.

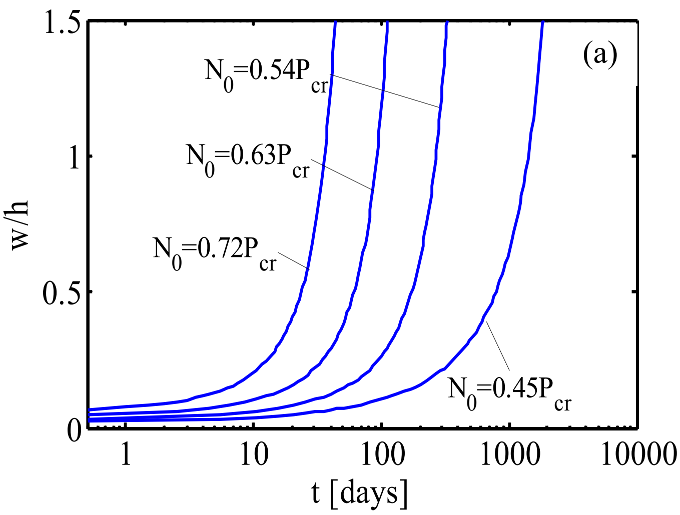

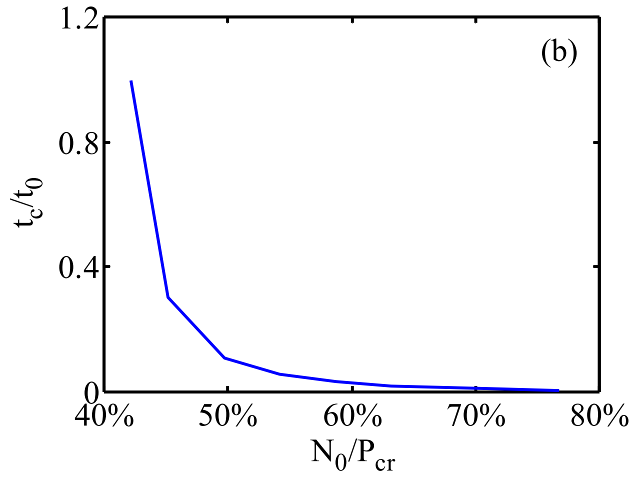

Fig. 4.4 Response of viscoelastic panel with e=0.05h: (a) Maximum out-of-plane deflection response with time; (b) Critical time versus axial load

The influence of the eccentricity under N_0 = 0.5P_{cr} is studied in Fig. 4.5 (t_e is the critical time of the panel loaded with e=0). Fig. 4.5 shows that t_c is also very sensitive to variations in the eccentricity. Unlike classical buckling that is determined based on the magnitude of the applied load, creep buckling is determined based on the magnitude of the time-dependent deflection. Hence, the results reveal that the structural stability over time needs to be carefully investigated as small variations in the eccentricity may initiate creep buckling. To clarify this, the time response of the panel under N_0 = 0.38P_{cr}, for which creep buckling is not expected to occur based on Fig. 4.5 is investigated for different values of e. The results, which for brevity are not presented here, reveal that once e exceeds 0.5h, buckling occurs. It is therefore important to take into account the coupling effect of the eccentricity and loading level in the creep buckling analysis of slender one-way panels.

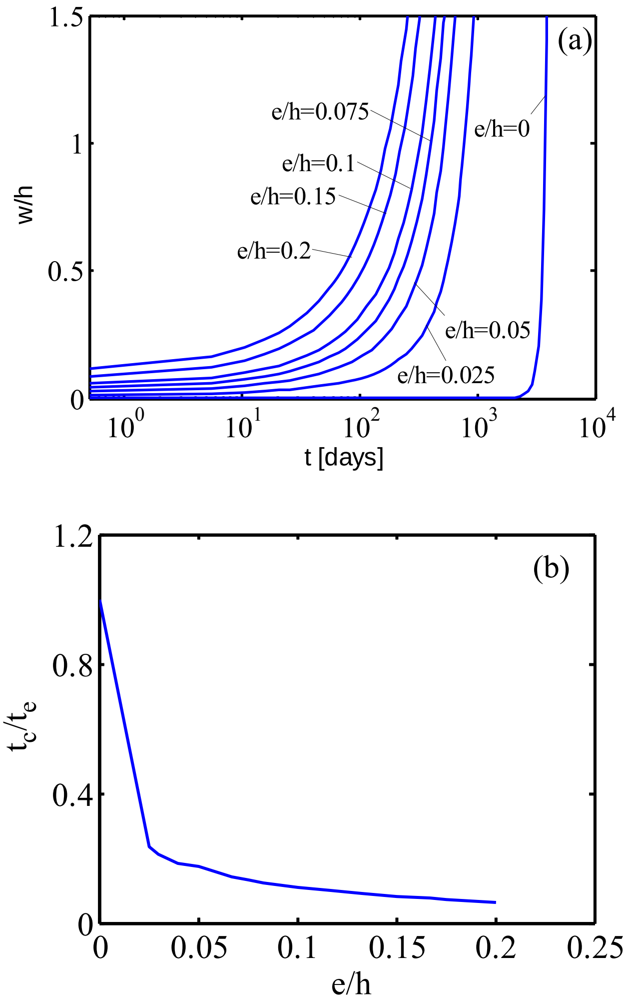

Fig. 4.5 Response of viscoleastic panel with N_0=0.5P_{cr}: (a) Maximum out-of-plane deflection response with time; (b) Critical time versus eccentricity

4.4 CONCLUSIONS

A nonlinear theoretical model has been presented in this chapter to study the time-dependent performance of viscoelastic panels. The model is based on one-way modeling of the panel, and accounts for the large-displacement kinematics and for the variation of the internal stresses and geometry with time. The present model can effectively predict the creep buckling response of the panel with different eccentricities and boundary conditions. The sensitivity of the critical time to cause creep buckling to the applied load and eccentricity has been revealed and quantitatively described by the proposed model. This chapter provides a basis for further and more detailed studies that account for cracking and material nonlinearity.

CHAPTER 5 THEORETICAL STUDY OF THE LONG-TERM BEHAVIOR OF ONE-WAY HSC PANELS

5.1 INTRODUCTION

The theoretical model presented in the last chapter considers concrete as a viscoelastic material, which sets up a foundation for a more comprehensive and sophisticated study of the long-term response of the HSC panel. In this chapter, the nonlinear model is re-developed, which accounts for combined effects of creep, shrinkage, aging of concrete, geometric nonlinearity, cracking and tension-stiffening through the step-by-step time analysis. The rheological material model that is based on the generalized Maxwell chain is used for modelling all the aforementioned material behavior through strain- and time-dependent springs and dashpots. The solution of the incremental governing equations of the panel at each time step is achieved numerically, combined with the use of a smeared cracking model and an iterative procedure for the determination of the sections rigidities and the creep strains. The model presented is a general one that is applicable for various combinations of boundary conditions, load scenarios, material and section properties. The mathematical formulation of the model is presented next, followed by numerical and parametric studies, and a comparison of the model with test results appeared in the literature.

5.2 MATHEMATICAL FORMULATION

The mathematical formulation includes the derivation of the incremental equilibrium equations, the constitutive relations, and the governing equations. In general, the wall panel can be either under one-way or two-way actions. However, in many cases, the aspect ratio of the wall (height/length), the type of connections to the adjacent members, and the load force a one-way action of the wall through its height. Hence, the model developed here focuses on one-way panels, but it serves as the basis for the development of models for two-way panels. A smeared cracking modelling approach is adopted along with a distinction between the cracked and the uncracked regions through the height of the panel. The sign conventions for the coordinates, loads, and displacements are shown in Fig. 5.1(a) and 1(b).

In order to describe the time-dependent variation of the internal stresses, as well as the time-dependent cracking and increase of the deformations due to the influence of creep and shrinkage, an incremental time-stepping analysis is implemented. For this, the time of concern t, which is measured from the time of first loading, is subdivided into n_t discrete time steps with $\Delta t_r = t_r - t_{r-1}$ ($r = 1,2,\ldots,n_t$). The incremental kinematic relation of the panel takes the following form considering large displacements:

$$\Delta\varepsilon_{xx}(t_r) = \Delta u_{0,x}(t_r) - z\Delta w,_{xx}(t_r) + \frac{1}{2}\left(\Delta w,_{x}(t_r)\right)^2 + w,_{x}(t_{r-1})\Delta w,_{x}(t_r) \qquad (5.1)$$

where ε_{xx} is the total strain that includes the viscoelastic strain ε_{xx}^{v} (instantaneous strain ε_{xx}^{ins} + creep strain ε_{xx}^{cp}) and the stress-independent shrinkage strain ε_{xx}^{sh}; u_0 and w are the longitudinal vertical displacement and the out-of-plane deflection, and $(\ )_{,x}$ denotes a derivative with respect to x. The basic equilibrium equations of the panel are similar to a beam-column member, which can be found in many textbooks of structural mechanics. The derivations of the incremental form of these equations and their boundary conditions were presented in detail in the last chapter using the variational principle of virtual work, which are therefore omitted herein. Yet, in the last chapter, the creep buckling response of HSC panels was preliminary investigated without the consideration of cracking and shrinkage of the concrete, which can significantly affect the buckling capacity. The incremental equilibrium equations read:

$$\Delta N_{xx,x} = -\Delta n_x \tag{5.2}$$

$$\Delta M_{xx,xx} = -\Delta q_z - \left[\left(N_{xx} + \Delta N_{xx} \right) \Delta w,_x \right],_x - \left(\Delta N_{xx} w,_x \right),_x \tag{5.3}$$

where N_{xx} and M_{xx} are the axial force and bending moment, respectively; q_z and n_x are external distributed loads (see Fig. 5.1(a)). Note that functions that appear without the Δ operator are known functions from the previous time step. The general boundary conditions at $x = 0$ and $x = H$ are given by

$$\Delta N_{xx} = \lambda \Delta N_i \qquad \text{or} \qquad \Delta u_0 = \Delta \overline{u}_0 \tag{5.4}$$

$$\Delta M_{xx,x} + \left(N_{xx} + \Delta N_{xx} \right) \Delta w,_x + \Delta N_{xx} w,_x = \lambda \Delta P_i \qquad \text{or} \qquad \Delta w = \Delta \overline{w} \tag{5.5}$$

$$\Delta M_{xx} = -\lambda \Delta M_i \qquad \text{or} \qquad \Delta w,_x = \Delta \overline{\varphi} \tag{5.6}$$

where $\overline{u}_0$, $\overline{w}$ and $\overline{\varphi}$ are external deformations at the edges; N_i, P_i, and M_i (i = 0 or H) are concentrated external forces and moments at the edges (Fig. 5.1(a)); λ = -1 for $x = 0$ and λ = 1 for $x = H$.

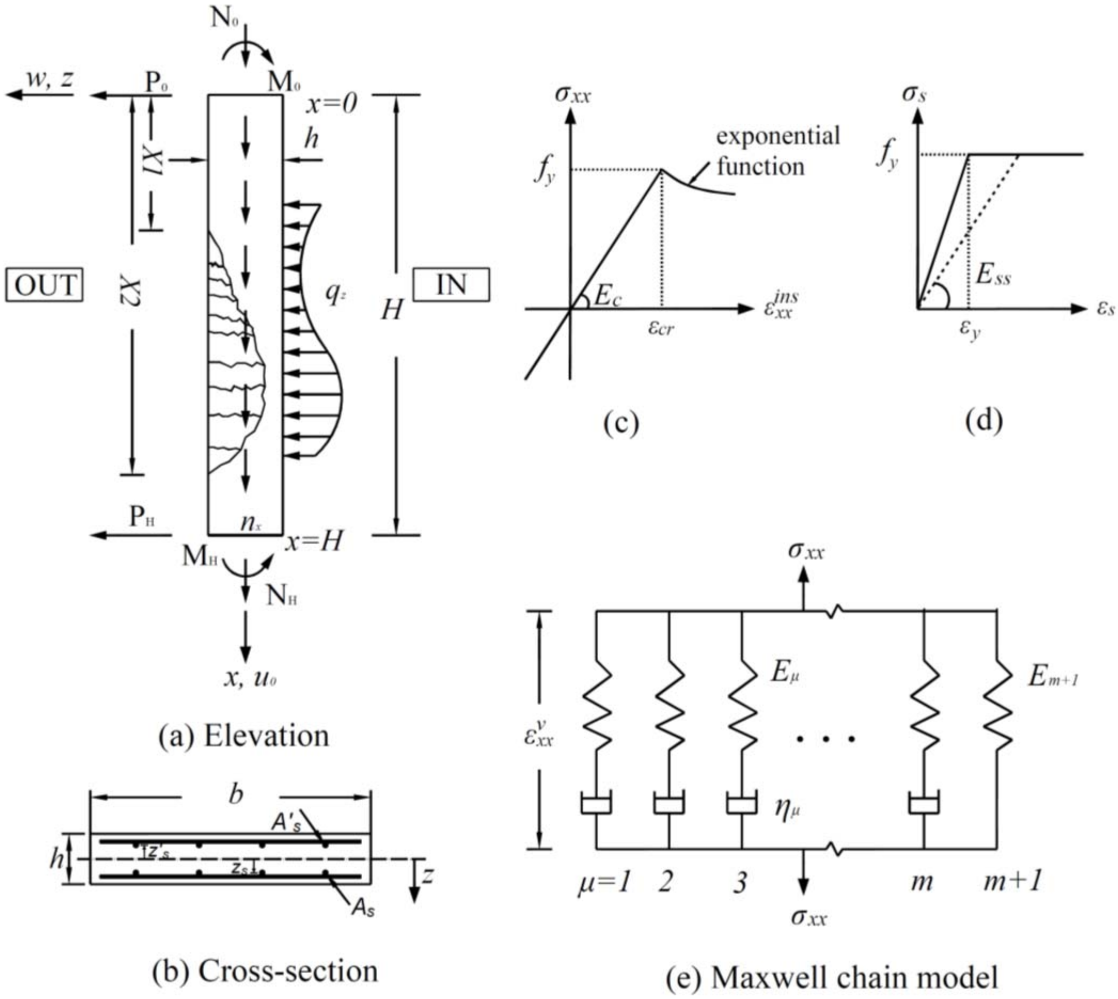

Fig. 5.1 Sign conventions of the model: (a) Panel geometry, loads, coordinates and displacements; (b) Cross-section of the panel; (c) Instantaneous stress-strain curve of the concrete; (d) Instantaneous absolute stress-strain curve of the steel; (e) Maxwell chain model

5.2.1 Constitutive relations at the material point level

The constitutive relations account for creep, shrinkage, aging and cracking of the concrete, while the steel is considered elastic-perfectly plastic. The concrete is considered linear viscoelastic in compression and nonlinear viscoelastic in tension due to the cracking and tension-stiffening. The nonlinearity of the concrete in compression is not considered because in most practical cases the level of stresses under sustained loads is relatively small and within the linear range, bearing in mind that the stress-strain curve in HSC is linear up to almost 70% of the compressive strength. The instantaneous constitutive relation of the concrete at initial loading ($t = t_0$) is presented first, from which the long-term constitutive relation is derived. The model proposed by Fields and Bischoff (2004), which is shown in Fig. 5.1(c), is used to model the tension-stiffening effect, although the modelling approach presented in this chapter can be used for various tension-stiffening models:

$$\sigma_{xx} = \begin{cases} E_c \varepsilon_{xx}^{ins} & \text{for} \quad \varepsilon_{xx}^{ins} \le \varepsilon_{cr} \\ e^{-0.8(\varepsilon_{xx}^{ins} - \varepsilon_{cr}) \times 10^3} E_c \varepsilon_{cr} & \text{for} \quad \varepsilon_{cr} < \varepsilon_{xx}^{ins} \end{cases} \tag{5.7}$$

where σ_{xx} is the normal stress in the concrete, E_c is the elastic modulus of the concrete at the time of loading, ε_{cr} is the cracking strain under instantaneous loading, which is determined as f_t / E_c with f_t being the flexural tensile strength of concrete. Note that f_t, E_c and ε_{cr} vary with time due to aging.

The constitutive relation of the steel reinforcement under both tension and compression is shown in Fig. 5.1(d) and is given by:

$$\sigma_s = \begin{cases} E_s \varepsilon_s & \text{for } \left|\varepsilon_s\right| \le \varepsilon_y \\ E_s \varepsilon_y & \text{for } \varepsilon_y < \varepsilon_s \\ -E_s \varepsilon_y & \text{for } \varepsilon_s < -\varepsilon_y \end{cases} \tag{5.8}$$

\where σ_s and ε_s are the stress and strain of the steel reinforcement, E_s and ε_y are the elastic modulus and yielding strain of the steel.

A rheological model which is based on the generalized Maxwell chain is used to formulate the long-term constitutive relation of concrete as presented in Bažant and Wu (1974) for linear cases (see Fig. 5.1(e)). However, in order to account for cracking, tension-stiffening and aging, strain and age dependent spring and dashpot constants are introduced here (Carol and Murcia 1989; Hamed and Bradford 2012). Yet, for these constants to be determined, the relaxation modulus needs to be defined first. Using Eq. (5.7), along with replacing ε_{xx}^{ins} with ε_{xx}^{v} and defining the secant modulus E_{sc} as $\sigma_{xx}/\varepsilon_{xx}^{v}$ to account for the nonlinear constitutive relation in tension, the relaxation modulus $R(\varepsilon_{xx}^{v},t,t')$ can be approximated as follows, assuming the same creep characteristics in both tension and compression (Gilbert 1988):

$$R(\varepsilon_{xx}^{v},t,t') = \frac{E_{sc}(\varepsilon_{xx}^{v},t')}{1+\varphi(t,t')} = \begin{cases} \dfrac{E_c(t')}{1+\varphi(t,t')} & \text{for} \quad \varepsilon_{xx}^{v} \le \varepsilon_{cr} \\ \dfrac{E_c(t')}{1+\varphi(t,t')} \dfrac{e^{-0.8(\varepsilon_{xx}^{v}-\varepsilon_{cr})\times 10^3}\varepsilon_{cr}}{\varepsilon_{xx}^{v}} & \text{for} \quad \varepsilon_{cr} < \varepsilon_{xx}^{v} \end{cases} \tag{5.9}$$

where $\varphi(t,t')$ is the creep coefficient of the concrete at time t for a load applied at time t'. In general, the viscoelastic characteristics of concrete depend on both the stress level and the viscoelastic strain and not just on the latter as described by Eq. (5.9). However, studies reveal that creep in tension may produce high levels of cracking and material softening over time (creep rupture) although the levels of stresses or instantaneous strains can be smaller than the peak tensile capacity (Carpinteri et al. 1996; Di Luzio 2009). In addition, many studies and design codes including Gilbert and Wu (2009) and CEB-FIP (1990) indicate that tension-stiffening can decrease to about 50% with time due to progressive cracking and bond slip. Therefore, in order to approximately simulate these two weakening effects with time, and due to the lack of accurate data regarding the effect of creep on the tension-stiffening effect, the relaxation modulus in Eq. (5.9) is defined as a function of the total viscoelastic strains ε_{xx}^{v} rather than the instantaneous strain or the stress level. In this approximated approach, cracking and material softening are assumed to occur once the viscoelastic strain reaches the cracking strain although the instantaneous strain is smaller than the cracking one, which may predict earlier cracking at some material points but can still simulate the creep rupture and the influence of creep on reducing the tension-stiffening effect (Hamed and Bradford 2012). The relaxation modulus is then expanded into a Dirichlet series, which describes a generalized Maxwell model (Fig. 5.1(e)), as follows:

$$R_{xx}(\varepsilon_{xx}^{v},t,t') \approx \bar{R}_{xx}(\varepsilon_{xx}^{v},t,t') = \sum_{\mu=1}^{m} E_{\mu}(\varepsilon_{xx}^{v},t')e^{-(t-t')/\tau_{\mu}} + E_{m+1}(\varepsilon_{xx}^{v},t') \tag{5.10}$$

where $\bar{R}_{xx}$ is the approximated relaxation modulus, $E_{\mu}(\varepsilon_{xx}^{v},t')$ is the modulus of the μth spring in the Maxwell chain, m is the number of units, τ_μ is the relaxation time of the μth unit. Note that the spring moduli and the dashpot constants ($\eta_{\mu}(\varepsilon_{xx}^{v},t') = \tau_{\mu}E_{\mu}(\varepsilon_{xx}^{v},t')$) are strain and age-dependent, which in general require the expansion of the relaxation modulus into a Dirichlet series at different ages and at different strain levels for their evaluation due to the variation of the internal stresses with time. This computational difficulty is treated in the subsequent.

The aging of concrete is introduced through an aging function $v(\varepsilon_{xx}^{ins},t')$ that describes the increase in the secant modulus with time and which is presented ahead. It was shown in Carol and Bazant (1993) that the use of rheological Maxwell or Kelvin models with spring constants that increase proportionally to the same function $v(t')$ is equivalent to the solidification theory developed in Bažant and Prasannan (1989a) that accounts for aging of the concrete. In the linear (strain-independent) case considered in Carol and Bazant (1993), the function $v(t')$ actually describes the increase in the macroscopic elastic modulus over time, while here it is assumed to describe the macroscopic secant modulus due to the nonlinearity introduced by the tension-stiffening effect. Thus, the spring modulus in the Maxwell unit can then be expressed as $E_{\mu}(\varepsilon_{xx}^{v},t') = v(\varepsilon_{xx}^{ins},t')E_{\mu}(\varepsilon_{xx}^{v})$. Hence, the calculation of the spring moduli at different ages of loading is avoided, while $E_{\mu}(\varepsilon_{xx}^{v})$ still needs to be determined at different levels of viscoelastic strain.

Eq. (5.9) shows that the relaxation modulus can be separated into two functions: one that is a function of strain only, and one that is a function of time only. Hence, the spring moduli can be determined by curve fitting of $\overline{R}_{xx}$ with R_{xx} for a chosen strain level, while their variation with cracking follows that of the secant modulus (Hamed and Bradford 2012). Here, the spring moduli are calculated for $\varepsilon_{xx}^{v} \leq \varepsilon_{cr}$ in Eq. (5.9), yielding $E_{\mu}(\varepsilon_{xx}^{v}) = E_{\mu}^{0}$. The variation of the spring moduli with the increase of the viscoelastic strain becomes:

$$E_{\mu}(\varepsilon_{xx}^{v}) = \begin{cases} E_{\mu}^{0} & \text{for} \quad \varepsilon_{xx}^{v} \leq \varepsilon_{cr} \\ E_{\mu}^{0} \dfrac{e^{-0.8(\varepsilon_{xx}^{v}-\varepsilon_{cr})\times 10^{3}} \varepsilon_{cr}}{\varepsilon_{xx}^{v}} & \text{for} \quad \varepsilon_{cr} < \varepsilon_{xx}^{v} \end{cases} \tag{5.11}$$

Following the subdivision of the time of concern into a number of time steps, the incremental constitutive relations can be formulated, which are based on a numerical time integration assuming a constant strain rate and a constant aging function and spring modulus at each time increment (Bažant and Wu 1974; Hamed 2012) as follows:

$$\Delta\varepsilon_{xx} = \frac{\Delta\sigma_{xx}}{E_{c}''\left(\varepsilon_{xx}^{v}(t_{r})\right)} + \Delta\varepsilon_{c}''\left(\varepsilon_{xx}^{v}(t_{r})\right) \tag{5.12}$$

in which E_{c}'' is the pseudo normal modulus, and $\Delta\varepsilon_{c}''$ is the incremental prescribed normal strain that includes the effects of both creep and shrinkage. These are given by:

$$E_{c}''\left(\varepsilon_{xx}^{v}(t_{r})\right) = v\left(\varepsilon_{xx}^{ins}(t_{r}),t_{r}\right)\left[\sum_{\mu=1}^{m}(1-e^{-\Delta t/\tau_{\mu}})\frac{\tau_{\mu}}{\Delta t}E_{\mu}\left(\varepsilon_{xx}^{v}(t_{r})\right) + E_{m+1}\left(\varepsilon_{xx}^{v}(t_{r})\right)\right] \tag{5.13}$$

$$\Delta\varepsilon_{c}''\left(\varepsilon_{xx}^{v}(t_{r})\right) = \frac{1}{E_{c}''\left(\varepsilon_{xx}^{v}(t_{r})\right)}\sum_{\mu=1}^{m}(1-e^{-\Delta t/\tau_{\mu}})\sigma_{\mu}(t_{r-1}) + \Delta\varepsilon_{xx}^{sh} \tag{5.14}$$

$$\sigma_\mu(t_r) = e^{-\Delta t/\tau_\mu}\sigma_\mu(t_{r-1}) + (1-e^{-\Delta t/\tau_\mu})\frac{\tau_\mu}{\Delta t}v\left(\varepsilon_{xx}^{ins}(t_r),t_r\right)E_\mu\left(\varepsilon_{xx}^{v}(t_r)\right)\Delta\varepsilon_{xx}^{v} \tag{5.15}$$

where σ_μ is the stress in the μth Maxwell unit.

In the numerical study of Section 5.3, the creep coefficient and shrinkage strain are assumed to follow AS3600 (2009), yielding:

$$\varphi(t,t') = (1.0+1.12e^{-0.008t_h})\frac{t^{0.8}}{t^{0.8}+0.15t_h}k_3k_4k_5\varphi_{\mathrm{cc.b}} \tag{5.16}$$

$$\varepsilon_{xx}^{sh} = \varepsilon_{xx}^{cse} + \varepsilon_{xx}^{csd} \tag{5.17}$$

where $t_h = 2A_g/u_e$ is the size factor of the specimen, with A_g as the gross cross-sectional area and u_e as the perimeter of the cross-section that is exposed to the atmosphere; k_3 and k_4 are coefficients that introduce the influence of the age of concrete at the time of loading (t') and the environmental effects; $\varphi_{cc,b}$ is the basic creep coefficient that depends on the characteristic strength; k_5 is a factor that reflects the influence of the concrete strength, which takes the following form

$$k_5 = \begin{cases} 1.0 & \text{for } f_c' \le 50 \text{ MPa} \\ (2.0-\alpha_3)-0.02(1.0-\alpha_3)f_c' & \text{for } 50 \text{ MPa} < f_c' \le 100 \text{ MPa} \end{cases} \tag{5.18}$$

where $\alpha_3 = 0.7/\left(k_4(1.0+1.12e^{-0.008t_h})\right)$, and f_c' is the characteristic compressive strength of concrete at 28 days; ε_{xx}^{cse} and ε_{xx}^{csd} in Eq. (5.17) are the chemical and drying shrinkage strains, respectively, which depend on the characteristic compressive strength as well. They are given as follows:

$$\varepsilon_{xx}^{cse} = (0.06f_c'-1)\times 50\times 10^{-6}\times(1-e^{-0.1(t+\tilde{t})}) \tag{5.19}$$

$$\varepsilon_{xx}^{csd} = (0.8+1.2e^{-0.005t_h})\frac{(t+\tilde{t})^{0.8}}{(t+\tilde{t})^{0.8}+0.15t_h}(1-0.008f_c')k_4\varepsilon_{csd.b}^{*} \tag{5.20}$$

where $\varepsilon_{csd.b}^{*}$ is the final drying basic shrinkage strain that depends on the quality of the aggregates, and $\tilde{t}$ refers to the time elapsed since termination of curing.

The effect of aging on the nonlinear relaxation modulus and the spring constants is introduced through the development of E_c, f_t, and ε_{cr} with time following CEB-FIP (1990), and assuming that the development of the tensile strength with time follows that of the compressive strength:

$$f_t(t) = f_t(28)\exp\left\{0.25\left[1-\left(\frac{28}{t}\right)^{1/2}\right]\right\} \tag{5.21}$$

$$E_c(t) = E_c(28)\exp\left\{0.25\left[1-\left(\frac{28}{t}\right)^{1/2}\right]\right\}^{1/2} \tag{5.22}$$

The aging function can then be determined as the ratio between the time-dependent secant modulus with respect to its value at the time of initial loading t_0:

$$v(\varepsilon_{xx}^{ins}, t') = E_{sc}(\varepsilon_{xx}^{ins}, t') / E_{sc}(\varepsilon_{xx}^{ins}, t_0) \tag{5.23}$$

5.2.2 Constitutive relations at the section level

The constitutive relations at the cross-section level of the panel are determined using the classical definition of the stress resultants and using Eq. (5.12) as follows:

$$\Delta N_{xx} = \int_{-\frac{h}{2}}^{\frac{h}{2}} bE_c''\ (\Delta\varepsilon_{xx} - \Delta\varepsilon_c''\ )\mathrm{d}z + E_{ss}A_s\Delta\varepsilon_s + E_{ss}'A_s'\ \Delta\varepsilon_s' \tag{5.24}$$

$$\Delta M_{xx} = \int_{-\frac{h}{2}}^{\frac{h}{2}} bE_c''\ (\Delta\varepsilon_{xx} - \Delta\varepsilon_c''\ )z\mathrm{d}z + E_{ss}A_s\Delta\varepsilon_s z_s + E_{ss}'A_s'\ \Delta\varepsilon_s'\ z_s' \tag{5.25}$$

where b and h are the width and thickness of the HSC panel, respectively; E_{ss}, ε_s, and A_s are the secant modulus of elasticity, strain and area of the steel reinforcement at the outer face of the panel, respectively (see Fig. 5.1); E_{ss}', ε_s', and A_s' are the secant modulus of elasticity, strain and area of the steel reinforcement at the inner face of the panel, respectively; z_s and z_s' are the distances of the steel reinforcement from the mid-thickness of the panel (see Fig. 5.1(b)). Note that E_c'' and $\Delta\varepsilon_c''$ depend on the strain level at each material point, and they vary through the thickness and height of the panel. By substituting the kinematic relation Eq. (5.1) into Eqs. (5.24) and (5.25), the stress resultants become

$$\Delta N_{xx} = A_{11}\left(\Delta u_{0,x} + \frac{1}{2}\Delta w,_x^2 + w,_x(t_{r-1})\Delta w,_x\right) - B_{11}\Delta w,_{xx} - \Delta\bar{N} \tag{5.26}$$

$$\Delta M_{xx} = B_{11}\left(\Delta u_{o,x} + \frac{1}{2}\Delta w,_x^2 + w,_x(t_{r-1})\Delta w,_x\right) - D_{11}\Delta w,_{xx} - \Delta\bar{M} \tag{5.27}$$

where A_{11}, B_{11} and D_{11} are the extensional, extensional-flexural, and flexural viscoelastic rigidities of the panel, and $\Delta\bar{N}$ and $\Delta\bar{M}$ are the incremental effective force and bending moment that introduce the effects of creep and shrinkage. The viscoelastic rigidities and the effective force and bending moment take the following form:

$$A_{11} = \int_{-\frac{h}{2}}^{\frac{h}{2}} bE_c''\,\mathrm{d}z + E_{ss}A_s + E_{ss}'A_s' \tag{5.28}$$

$$B_{11} = \int_{-\frac{h}{2}}^{\frac{h}{2}} bE_c''\,z\mathrm{d}z + E_{ss}A_s z_s + E_{ss}'A_s'\,z_s' \tag{5.29}$$

$$D_{11} = \int_{-\frac{h}{2}}^{\frac{h}{2}} bE_c''\,z^2\mathrm{d}z + E_{ss}A_s z_s^2 + E_{ss}'A_s'\,\left(z_s'\right)^2 \tag{5.30}$$

$$\Delta\bar{N}(t_r) = \int_{-\frac{h}{2}}^{\frac{h}{2}} b\left[\sum_{\mu=1}^{m}(1-e^{-\Delta t/T_\mu})\sigma_\mu(t_{r-1})\right]\mathrm{d}z + \left(A_{11} - E_{ss}A_s + E_{ss}'A_s'\right)\Delta\varepsilon_{xx}^{sh} \tag{5.31}$$

$$\Delta\bar{M}(t_r) = \int_{-\frac{h}{2}}^{\frac{h}{2}} b\left[\sum_{\mu=1}^{m}(1-e^{-\Delta t/T_\mu})\sigma_\mu(t_{r-1})\right]z\mathrm{d}z + \left(B_{11} - E_{ss}A_s z_s + E_{ss}'A_s'\,z_s'\right)\Delta\varepsilon_{xx}^{sh} \tag{5.32}$$

5.2.3 Incremental governing equations

The incremental governing equations are derived by substituting the stress resultants (Eqs. (5.26) and (5.27)) into the equilibrium equations (Eqs. (5.2) and (5.3)), noting that terms of higher product of the incremental displacements and forces are neglected due to the use of sufficiently small time increments. For convenience, the equations are presented as a set of first-order differential equations:

$$\Delta w,_x(t_r) = \Delta\phi(t_r) \tag{5.33}$$

$$\Delta\phi(t_r) = \frac{A_{11}\left(\Delta M_{xx}(t_r) + \Delta\bar{M}(t_r)\right) - B_{11}\left(\Delta N_{xx}(t_r) + \Delta\bar{N}(t_r)\right)}{B_{11}^2 - A_{11}D_{11}} \tag{5.34}$$

$$\Delta M_{xx,x}(t_r) = \Delta S_{xx}(t_r) - N_{xx}(t_{r-1})\Delta w,_x(t_r) - \Delta N_{xx}(t_r)w,_x(t_{r-1}) \tag{5.35}$$

$$\Delta S_{xx,x}(t_r) = -\Delta q_z(t_r) \tag{5.36}$$

$$\Delta N_{xx,x}(t_r) = -\Delta n_x(t_r) \tag{5.37}$$

$$\Delta u_{o,x}(t_r) = \frac{B_{11}\left(\Delta M_{xx}(t_r) + \Delta\bar{M}(t_r)\right) - D_{11}\left(\Delta N_{xx}(t_r) + \Delta\bar{N}(t_r)\right)}{B_{11}^2 - A_{11}D_{11}} - \Delta w,_x(t_r)w,_x(t_{r-1}) \tag{5.38}$$

where S_{xx} is the shear force.

5.2.4 Solution procedure

At each time step, Eqs. (5.33)-(5.38) present a set of nonlinear differential equations due to the dependency of the viscoelastic rigidities on the unknown deformations via Eqs. (5.28)-(5.30). These rigidities are uniform along the uncracked region but they vary along the cracked region. To simplify the analysis, the variation of the rigidities along the cracked region is assumed to follow that of the out-of-plane deflections, which actually determines the distribution of the nonlinear bending moment. This assumption results in two types of unknowns that need to be determined at each time step, namely: the rigidities at the critical section, and the start and end points of the cracked region

($X1$ and $X2$, see Fig. 5.1(a)). Here, an iterative procedure is used to determine these parameters at each time step, combined with the use of the numerical multiple shooting method (Stoer and Bulirsch 2002) for the solution of the incremental governing equations at each iteration. The iterative procedure follows these steps:

Step 1. Initial guess. At the first iteration of the instantaneous loading, the panel is assumed uncracked. However, for the subsequent time steps, the solution from the previous time step is used as the initial guess for the current step.

Step 2. Analysis of the structure. Using the rigidities calculated in the initial guess or in the previous iteration (step 3.3), as well as the calculated locations of the start and end points of the cracked region, the incremental governing equations become linear ones with variable coefficients in space, which are solved numerically.

Step 3. Analysis of the critical section (at the location of maximum bending moment). Based on the solution obtained in step 2, the equivalent rigidities of the critical section are determined as follows:

3.1 The incremental strain at time t_r is calculated at each material point across the critical section using the kinematic relation appears in Eq. (5.1). The total strain $\varepsilon_{xx}(t_r)$ is obtained by adding the incremental strain $\Delta\varepsilon_{xx}$ to the total strain accumulated in time t_{r-1}, i.e., $\varepsilon_{xx}(t_{r-1})$.

3.2 The total viscoelastic strain is obtained as

$$\varepsilon_{xx}^{v} = \varepsilon_{xx} - \varepsilon_{xx}^{sh} \tag{5.39}$$

3.3 Once the normal strain distribution is determined in step 3.2, the spring moduli of each point through the thickness of the panel are determined via Eq. (5.11). Consequently, the viscoelastic rigidities and the incremental effective forces due to creep and shrinkage are determined through Eqs. (5.28)-(5.32) and the normal stresses are updated using Eq. (5.15). The integrals in Eqs. (5.28)-(5.32) are numerically solved due to the material nonlinearity.

Step 4. Convergence Criteria. If the norm of the relative difference between the magnitudes of the viscoelastic rigidities as well as *X1* and *X2* in two consecutive iterations is sufficiently small, the iterative procedure stops. Otherwise, the procedure returns to step 2 with the updated rigidities of step 3.3.

The analysis is conducted up to a certain time (the critical time) where the deformations of the system exceed a prescribed limit (Hoff 1958; Bažant and Cedolin 1991). In general, the incremental exponential form of the creep law outlined above allows increasing the time step interval throughout the analysis (Bažant and Wu 1974). However, the time step is kept relatively small throughout the analysis here because the rate of creep is relatively high at the early stages of loading and at unknown times for which buckling with time may occur. A proper time step is selected for a given load level in the way that the difference between the predicted critical times of creep buckling for the selected time-step and one-half of it is of minor significance.

5.3 NUMERICAL STUDY

The numerical study includes a numerical example along with a parametric study, and a comparison with test results available in the literature, which demonstrate the capabilities of the proposed theoretical model.

5.3.1 Numerical Example

A one-way HSC panel that is subjected to an eccentric sustained axial load is investigated. The panel is simply supported at the top and bottom edges as shown in Fig. 5.2. Deformed bars of 5.0 mm diameter with spacing of 230 mm and a concrete cover of 20 mm are used, which result in a total vertical reinforcement ratio of $\rho_v = (A_s + A_s')/bh =$ 0.2%. The yielding strength and elastic modulus of the steel are 500 MPa and 200 GPa, respectively. The panel is assumed to be loaded at the age of 28 days after casting with N_0 = 794.2 kN, which equals to 30% of the instantaneous elastic Euler buckling load (P_{cr} = 2647.3 kN). The load is applied with an eccentricity of e = h/6 = 16.7 mm, which results in edge moments of M_0 = 13.2 kNm and M_H = -13.2 kNm (Fig. 5.1). Curing of the concrete is assumed to terminate after 7 days since casting, and the shrinkage from 7 to 28 days is considered as prescribed initial strain at first loading. The development with time of the shrinkage strain and the creep coefficient follow Eqs. (5.16)-(5.20) with k_3 = 1.1, k_4 =0.65, $\varepsilon^*_{csd.b} = -800 \times 10^{-6}$ and t_h = 90.9 mm as follows:

$$\varepsilon_{xx}^{sh}(t) = -1.9 \times 10^{-4}\left(1 - e^{-0.1(t+21)}\right) - \frac{2.92 \times 10^{-4}(t+21)^{0.8}}{(t+21)^{0.8} + 13.63} \tag{5.40}$$

$$\varphi(t) = \frac{1.53t^{0.8}}{t^{0.8} + 13.63} \tag{5.41}$$

The number of Maxwell units (m) used to model the viscoelastic behavior of concrete is taken as 5 in this example with $\tau_\mu = 5^{\mu-1}$ (days).

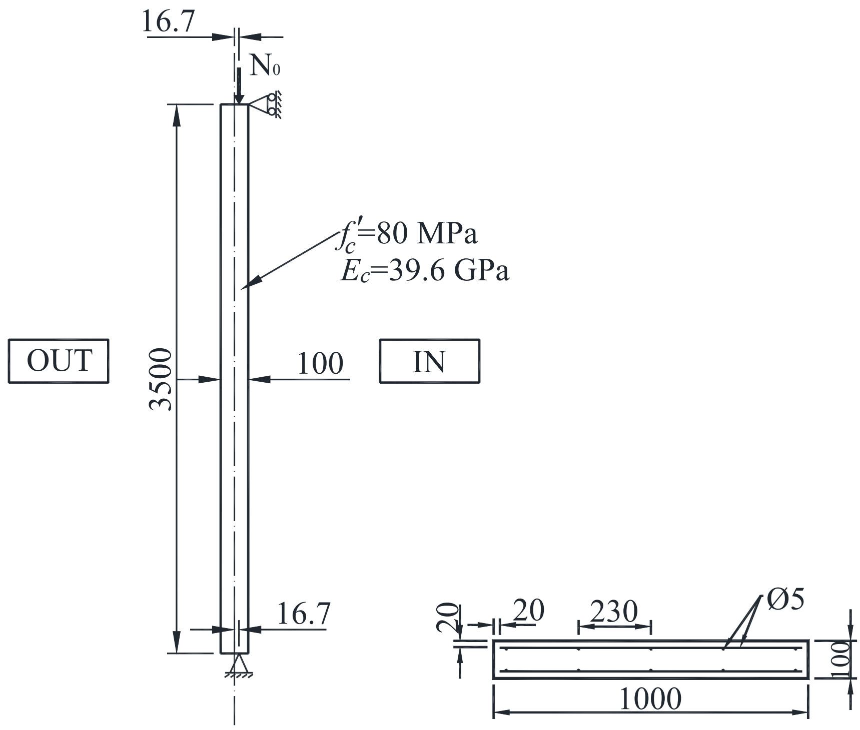

(a) Elevation (b) Cross-section

Fig. 5.2 Geometry, material properties and loads of the panel investigated in the numerical study

The time-dependent variation of the deflection and the bending moment at mid-height are shown in Fig. 5.3. The deflection is normalized with respect to the thickness of the panel *h*. It can be seen that the panel undergoes increasing deflection with time due to the effects of creep, shrinkage, and cracking of the concrete. This increased deflection leads to an increase in the bending moment at mid-height due to the geometric nonlinearity of the member (P-Δ effect). As shown in Fig. 5.3, beyond a certain time, the out-of-plane deflection as well as the bending moment tends to asymptotically increase towards infinity. Nevertheless, due to the brittleness of the concrete and its limited ability to undergo large deformations, a buckling failure criterion that is based on a maximum normalized out-of-plane deflection (w/h) of 0.4 is adopted in this case (Hoff 1958; Bažant and Cedolin 1991). Other creep buckling criteria may also apply, but it was found in this numerical example that beyond this deflection limit, the deformations, stresses, and strains dramatically increase. Hence, the analysis is stopped at t=171 days, which refers to the critical time for buckling that is predicted to occur under an axial load that equals to only 30% of the instantaneous elastic buckling load.

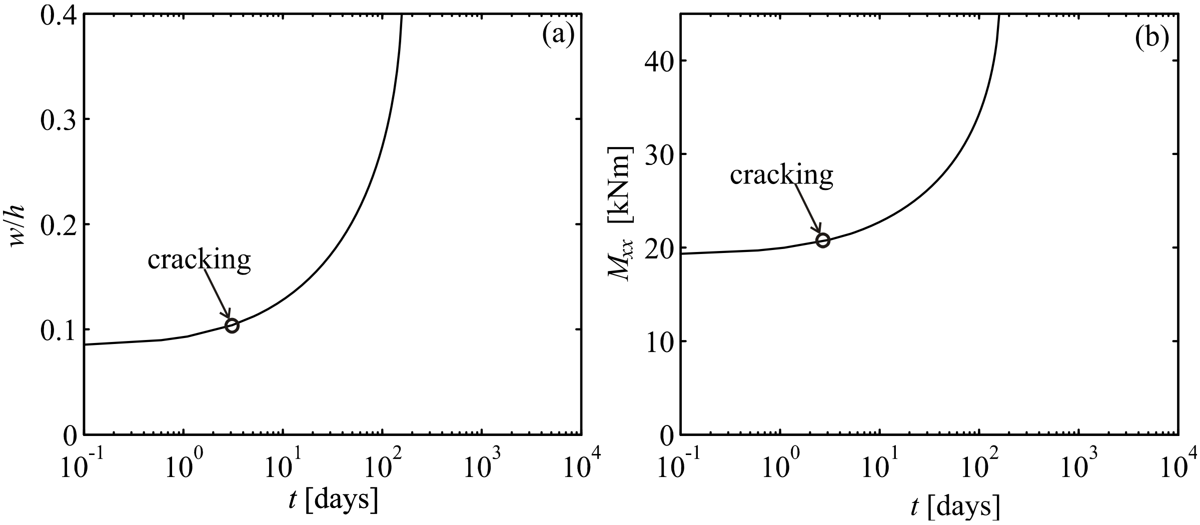

Fig. 5.3 Variation of the out-of-plane deflection (a) and bending moment (b) with time at mid-height

Under instantaneous loading, no cracking of the concrete is predicted. However, the results reveal that cracking appears at 3 days after initial loading as a result of shrinkage and creep effects (Fig. 5.3). The cracks propagate with time from mid-height towards the top and bottom edges with $X1$ = 125.7 mm and $X2$ = 3374 mm (see Fig. 5.1(a)) at t = 171 days. Fig. 5.4 shows the distribution of the out-of-plane deflection and bending moment through the height of the panel at various times, which exhibit the importance of the long-term geometric nonlinear effects, and the ability of the model to describe the structural response at different times.

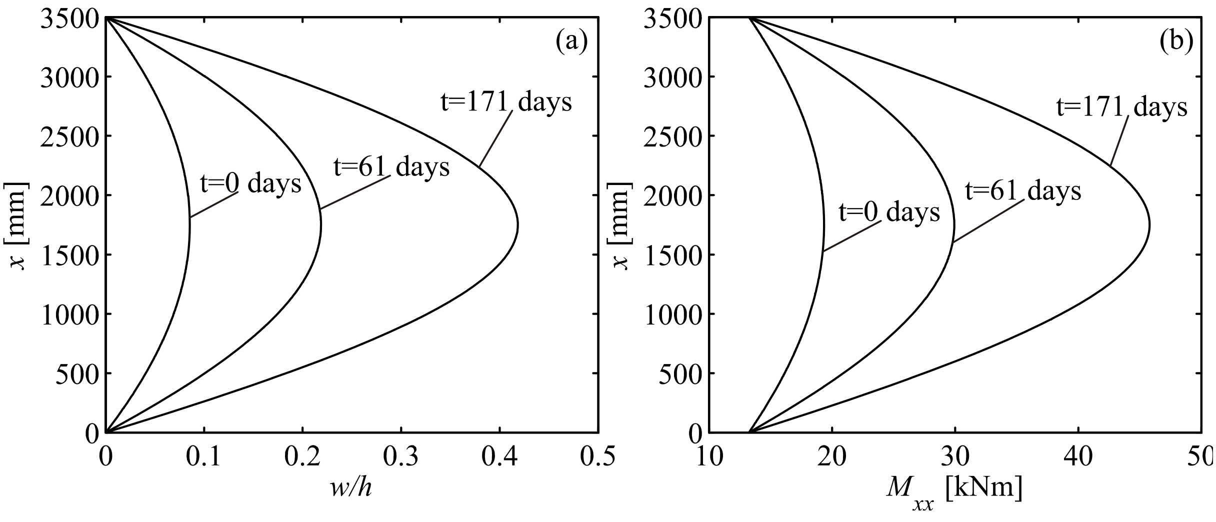

Fig. 5.4 Deflection (a) and bending moment (b) distribution through the height at three different times

Fig. 5.5 shows the distribution of the instantaneous and long-term total normal strains and stresses through the thickness of the critical section at mid-height. In flexural RC members under sustained loading but with no geometric nonlinear effects, relaxation of the compressive stresses occurs with time along with an increase in the compressed depth due to the restraint provided by the steel reinforcement. Here, the compressive stresses continuously increase with time and the neutral axis is shifting inwards toward the compressed face, as was also reported in the experimental study of Tatsa (1989). Fig. 5.6 shows a very small relaxation of the compressive stress provided by the reinforcement because the section at the edge is uncracked and has a zero magnification of the bending moment due to the geometric nonlinearity.

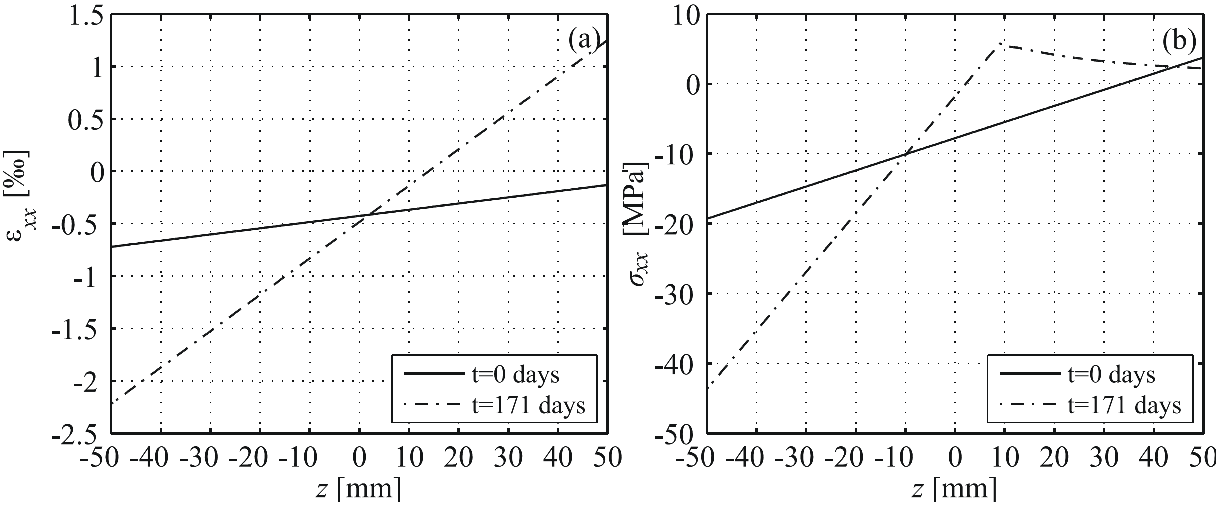

Fig. 5.5 Normal total strain (a) and stress (b) distribution at mid-height section at two different times

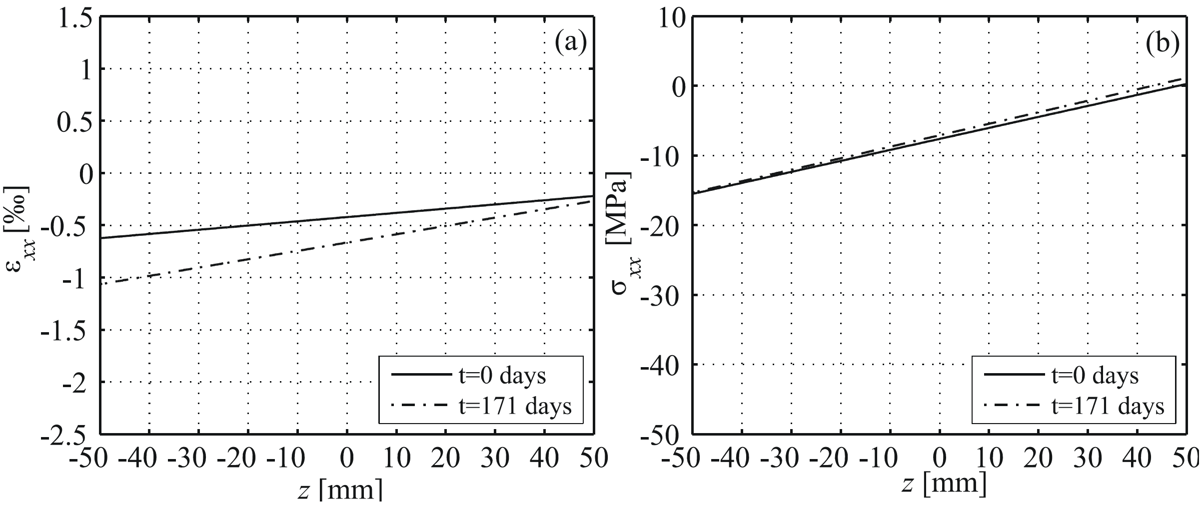

Fig. 5.6 Normal total strain (a) and stress (b) distribution at the edge section at two different times

The variation with time of the peak stresses and strains of the concrete and the steel reinforcement are shown in Fig. 5.7 and Fig. 5.8, respectively. It can be seen that the compressive and tensile strains of the concrete continuously increase with time. The compressive stress in the concrete at the critical time (t = 171 days, where the deformation starts to increase rapidly) is -43.5 MPa, which is within the linear viscoelastic range of behavior of the concrete as assumed by the model. The tensile stress in the concrete starts to decrease after cracking as shown in Fig. 5.7(d) along with tension-stiffening effects. Fig. 5.8 shows that the stresses in the steel reinforcements on both sides of the panel tend to increase with time. The increase is induced by the restraint of the creep and shrinkage deformations of the concrete, and by the additional bending moment due to the geometric nonlinearity. The stress in the reinforcement at the critical time for which buckling is predicted to happen is less than the yielding strength. These results indicate that in this case, no material failure in steel or concrete is expected to occur before buckling.

It can be seen that the model is capable of describing the nonlinear time-dependent response of the structure, including the distribution of stresses and strains at different times and different locations. Although concrete is still elastic in compression when buckling failure is predicted to happen; in other cases, crushing or softening of the concrete or yielding of the steel may occur before buckling. Thus, the creep and shrinkage effects may also lead to premature material failures with time due to their coupling with the geometric nonlinear effects that significantly increase the stresses. Such aspects of structural behavior should also be considered in the design of HSC panels, as well as in estimating their design life.

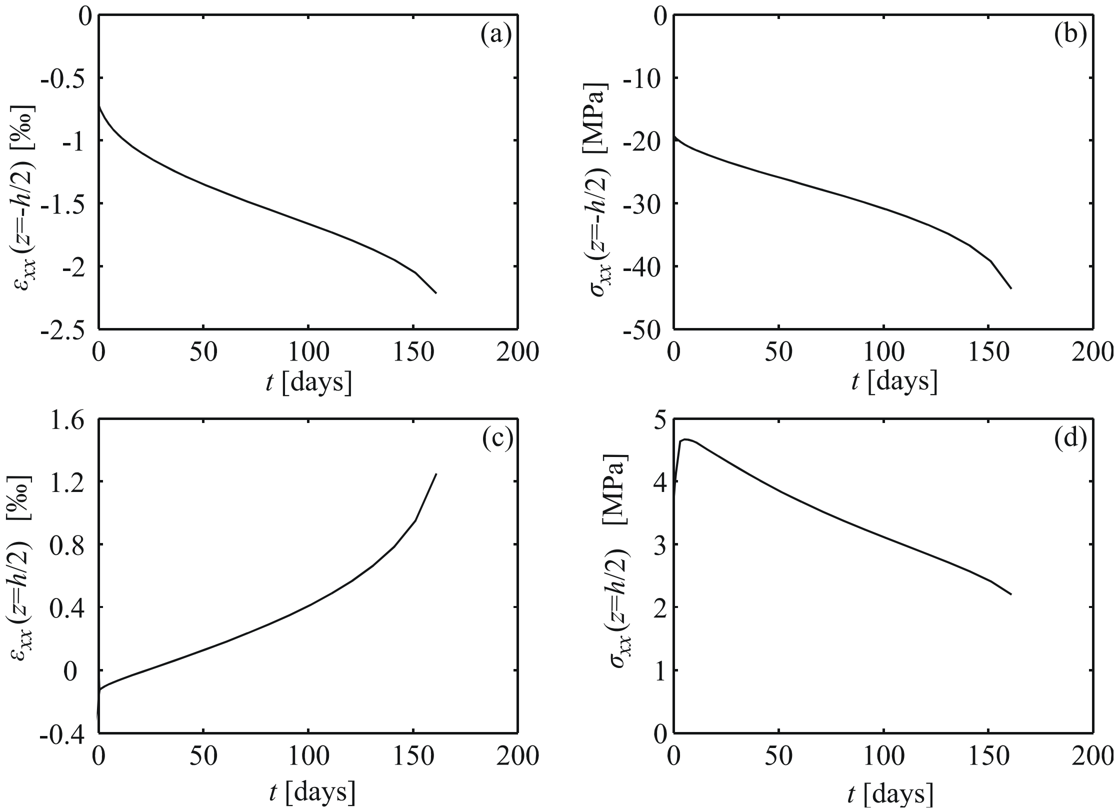

Fig. 5.7 Variation of total strain and stress in the extreme fibers of concrete at mid-height section: (a) Strain at inward face; (b) Stress at inward face; (c) Strain at outward face; (d) Stress at outward face

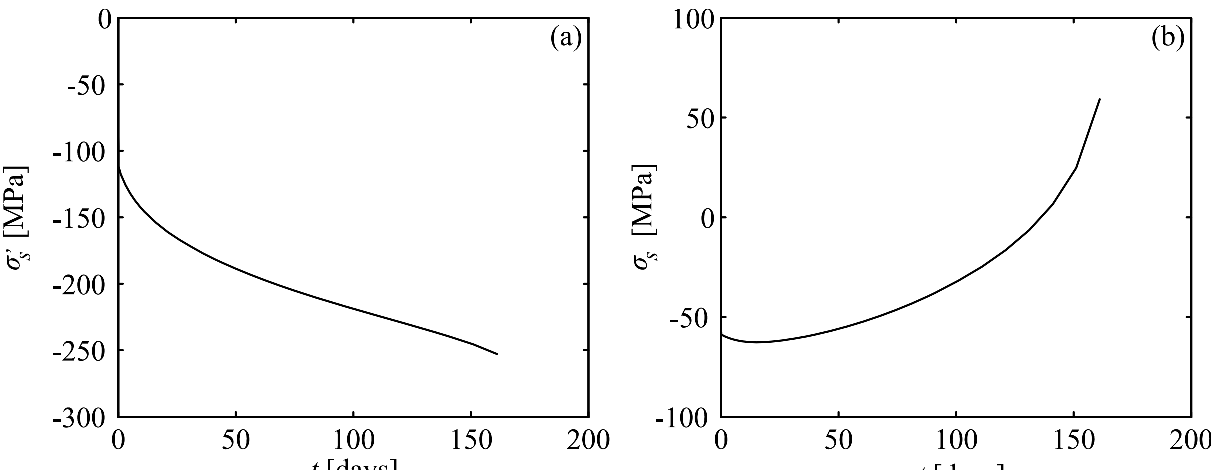

Fig. 5.8 Variation of stresses in the steel reinforcement at mid-height section: (a) Reinforcement close to the inward surface; (b) Reinforcement close to the outward surface

5.3.2 Parametric study

A parametric study is conducted here to investigate the influences of some of the parameters that govern the nonlinear time-dependent response. Three parameters are investigated, which include the magnitude and eccentricity of the sustained load, and the steel reinforcement ratio. The panel investigated in Section 3.1 is used as a reference one with $N_0 = 0.3P_{cr}$ = 794.2kN, $e = h/6$ and ρ_v = 0.2%. Thus, when one parameter is changed, the other two are kept constant. The results are summarized in Table 5.1 and are presented in Fig. 5.9 and Fig. 5.10.

Table 5.1 Results of parametric study

Parameters Examined	N_0	e	ρ_v (%)	t_{cr} (days)
Magnitude of Sustained Load	$0.2P_{cr}$	$h/6$	0.2	Stable
	$0.3P_{cr}$	$h/6$	0.2	171.1
	$0.35\ P_{cr}$	$h/6$	0.2	55.1
	$0.4\ P_{cr}$	$h/6$	0.2	20.6
Load Eccentricity	$0.3\ P_{cr}$	$h/3$	0.2	6.5
	$0.3\ P_{cr}$	$h/6$	0.2	171.1
	$0.3\ P_{cr}$	$h/9$	0.2	1421
	$0.3\ P_{cr}$	$h/12$	0.2	Stable
Reinforcement Ratio	$0.3\ P_{cr}$	$h/6$	0.2	171.1
	$0.3\ P_{cr}$	$h/6$	0.8	211.1
	$0.3\ P_{cr}$	$h/6$	1.6	341.1
	$0.3\ P_{cr}$	$h/6$	4.0	Stable

Note: P_{cr} = 2647.3 kN, $h = 100$ mm

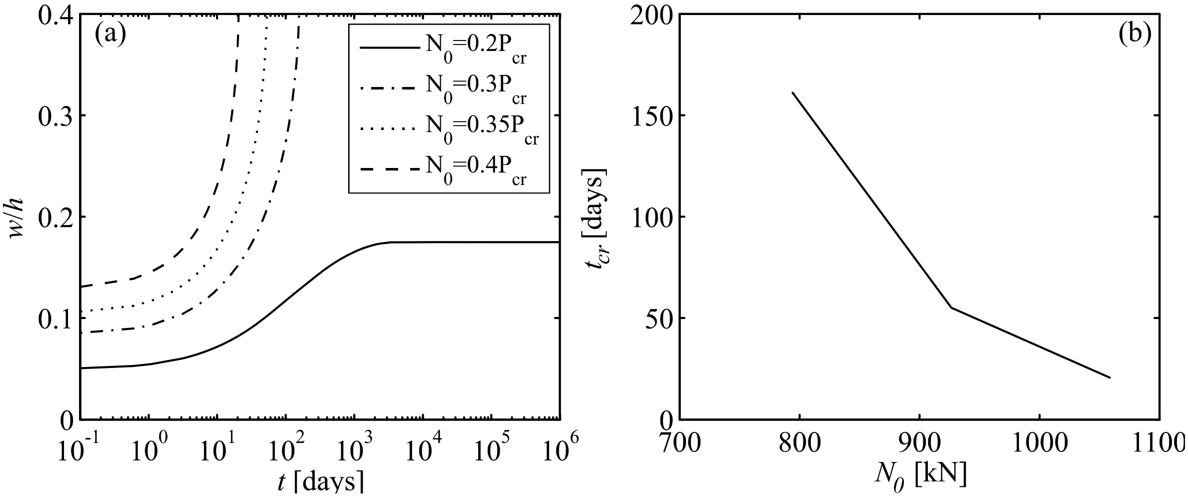

Fig. 5.9 Influence of load level on the long-term behavior of the HSC panel ($e = h/6$, $\rho_v = 0.2\%$); (a) Variation of the out-of-plane deflection at mid-height with time; (b) Critical time versus load level

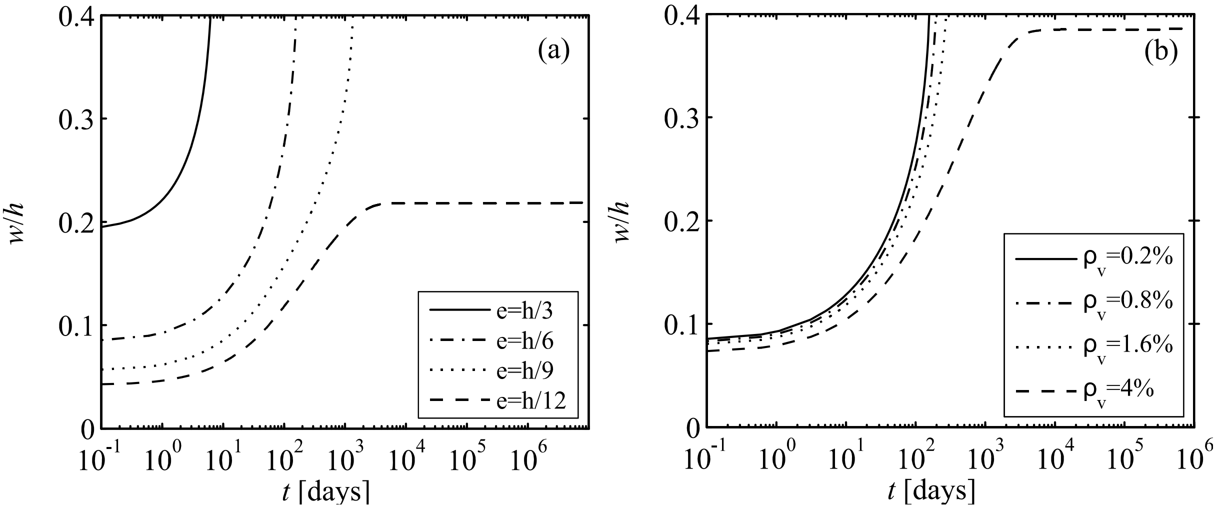

Fig. 5.10 Influences of load eccentricity ($N_0 = 0.3P_{cr}$, $\rho_v = 0.2\%$) (a) and reinforcement ratio ($N_0 = 0.3P_{cr}$, $e = h/6$) (b) on the long-term behavior of the HSC panel

The influence of the magnitude of the sustained load on the buckling with time is shown in Fig. 5.9. The eccentricity and reinforcement ratio are $h/6$ and 0.2% respectively for all load levels. As expected, the increase of the imposed load causes earlier buckling of the panel (reduction of the critical time). However, it can be seen in Fig. 5.9(b) that the critical time is very sensitive to small changes in the magnitude of the applied load, and the relation between the two is nonlinear. It can also be seen in Fig. 5.9 that no buckling is predicted for the case of $N_0 = 0.2P_{cr}$ as the deflection-time curve becomes almost constant after a certain time, which indicates a stable behavior. The minimum magnitude of sustained load that leads to buckling with time of the panel (defined as P_{crl} here) equals $0.24P_{cr}$. Thus, the buckling capacity of the panel is reduced by 76% due to the combined effects of creep, shrinkage and cracking, which is critical in the design of HSC panels. This result is different from the corresponding result calculated using the commonly used and simplified Effective Modulus Method. In this method, $P_{crl} = \pi^2 \bar{E} I_{eff} / H^2$, with $\bar{E}$ as the effective elastic modulus that is given by $\bar{E} = E_c / [1 + \varphi(t,t')]$, and I_{eff} as the moment of inertia of the transformed gross cross-section, which yields $P_{crl} = 0.4P_{cr}$. Those differences can be even larger for different boundary conditions, as shown in Chapter 4, which indicate that such simplified methods should be carefully considered for the design and analysis of slender RC structures with geometric nonlinearity (Hamed et al. 2010b).

The effect of the load eccentricity on the time-dependent response of the HSC panel is investigated in Fig. 5.10(a) and Table 5.1, in which $N_0 = 0.3P_{cr}$ and $\rho_v = 0.2\%$. Also here, the sensitivity of the behavior upon changes in the load eccentricity is revealed, where small variations of the eccentricity may trigger earlier long-term buckling failures. Fig. 5.10(a) shows that the change of the critical time with the load eccentricity is also nonlinear. These results reveal the importance of considering different load scenarios in the design of slender HSC panels, as inaccuracies in estimating the actual load eccentricity (which is very common) may have a critical influence on the predicted behavior.

The effect of the reinforcement ratio is shown in Fig. 5.10(b) and Table 5.1. $N_0 = 0.3P_{cr}$ and the eccentricity is $h/6$ for all cases. It can be seen that the critical time of the HSC panel increases with the increase of the reinforcement ratio, and for $\rho_v > 4\%$, no creep buckling occurs. Thus, in addition to the role of the tensile reinforcement in carrying tensile stresses at the cracked region, the increase in both the tensile and compressive reinforcement ratio can significantly restrain the creep deformations of the concrete and can prevent buckling of the panel with time. These results reveal a potential way of controlling the long-term buckling of the panel with time without the need to change its geometry, which can be effective for slender panels.

5.3.3 Comparison to test results from the literature

A comprehensive experimental study regarding the creep buckling response of HSC panels could not be found in the literature. Nevertheless, in order to provide some level of validation to the proposed theoretical model, a comparison with the test results of Tatsa (1989) that include creep testing of NSC panels without buckling is presented. The compressive strength of the concrete used by Tatsa (1989) is 24.3 MPa, and the dimensions of the panel are 145 mm thickness, 300 mm wide and 2500 mm high. The one-way panel is simply-supported at the top and bottom edges and is subjected to eccentric sustained loads at 50 mm eccentricity at both edges. The panel is symmetrically reinforced on both faces with a reinforcement ratio of 1.04%, and it was loaded at 28 days. Shrinkage is assumed to commence at 7 days after casting. As no data was reported regarding the creep and shrinkage properties of the concrete, they are estimated based on AS3600 (2009) considering the different dimensions, age and strength of concrete, as well as the different exposure to atmosphere at laboratory conditions compared to the numerical example presented in sections 3.1 (Eqs. (5.16)-(5.22)). They are given as follows,

$$\varphi(t) = \frac{4.69t^{0.8}}{t^{0.8} + 14.66} \tag{5.42}$$

$$\varepsilon_{xx}^{sh}(t) = 2.29\times10^{-5}\left(1-e^{-0.1(t+21)}\right)+\frac{8.04\times10^{-4}(t+21)^{0.8}}{(t+21)^{0.8}+14.66} \tag{5.43}$$

The comparison of the predicted out-of-plane deflection of the panel at mid-height with the test results appears in Fig. 5.11. It can be seen that the theoretical results generally agree well with the test results although the predicted instantaneous deflection is slightly smaller than the actual one. Some small discrepancies can also be observed at the delayed stages after loading (t > 60 days) which can be partially attributed to different actual creep and shrinkage properties than the ones used in the model. Nevertheless, the comparison provides a level of validation to the proposed model. Yet, further verifications of the model through comparison with creep tests including buckling need to be conducted, which is considered for further study by the authors.

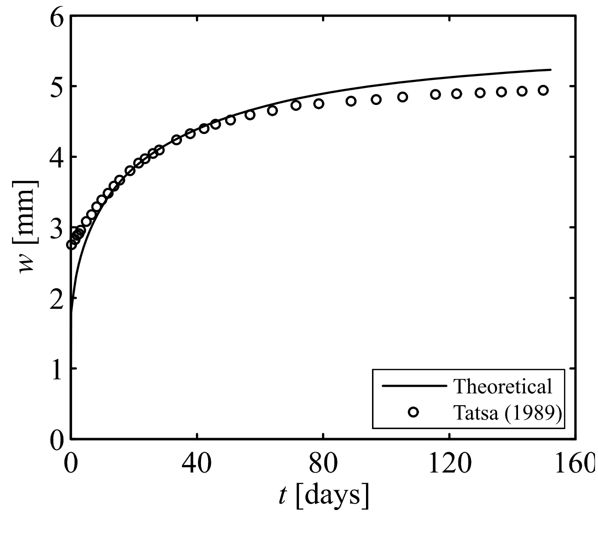

Fig. 5.11 Comparison of the theoretical model with experimental results

5.4 CONCLUSIONS

A theoretical model has been developed for the one-way time-dependent analysis of reinforced high-strength concrete panels. The model accounts for creep, shrinkage and aging of the concrete, as well as for cracking and tension-stiffening through a rheological viscoelastic model that is based on the generalized Maxwell chain. It considers the geometric nonlinearity and describes the variation of the internal stresses and deformations with time through a time-stepping analysis.

The capabilities of the theoretical model have been examined and demonstrated through numerical examples and parametric studies, which have shown the increase of the out-of-plane deflection of the HSC panel with time, and the change of the strain and stress distributions at different cross-sections. Most importantly, it has been shown that the long-term effects of creep and shrinkage can cause premature buckling of the panel with time. The predicted load that leads to buckling with time can be much smaller than the elastic buckling load, which shows the importance of considering these long-term effects in the design of HSC panels.

It has been shown that the change in the deflection of the panel is accompanied by shifting of the neutral axis towards the compression side, and by a continuous growth of the compressive and tensile stresses in the concrete and the steel reinforcement. Such increase in the stresses may lead to material failures by concrete crushing or steel yielding even before buckling occurs. It has also been shown that even though the concrete may not be cracked under instantaneous loading, creep and shrinkage may lead to time-dependent cracking that can significantly decrease the buckling capacity of the panel. The parametric study has shown that the time-dependent buckling behaviour is very sensitive to key parameters, such as the load magnitude and eccentricity, and that in some cases, creep buckling failures can be prevented by providing sufficient reinforcement.

Finally, it can be concluded that the model developed here sets a theoretical basis for the nonlinear time-dependent analysis of HSC panels including the effects of creep and shrinkage. It also clarifies the important roles these parameters can have on the buckling capacity, and it provides a tool for their quantitative evaluation. Yet, further aspects of the structural behaviour including the two-way action, temperature effects, and the material nonlinearity in compression need to be investigated.

CHAPTER 6 EXPERIMENTAL STUDY OF THE LONG-TERM BEHAVIOR OF ONE-WAY HSC PANELS

6.1 INTRODUCTION

This chapter presents experimental results of the long-term behavior of one-way HSC panels subjected to eccentric uniaxial in-plane loads. The experimental program consisted of five HSC panels simply-supported along the two short edges only and tested under sustained loading. Two panels failed by creep buckling under the sustained loads, whereas the other three panels were loaded to failure at some time after initial loading without the release of the sustained loads. The influences of the loading age, eccentricity, and level of the in-plane load on the time-dependent behavior are investigated in the test. The experimental study conducted herein aims to validate the proposed model as presented in Chapter 5 and to improve the understanding of the time-dependent behaviour of one-way HSC panels. Moreover, as there appears to be a shortage of reliable test data reported for one-way HSC panel under sustained eccentric in-plane loading in the open literature, the test findings represent a benchmark database that can be used for further long-term stability study of HSC panels. The experimental program is described firstly in the chapter, followed by a comparison of the test results with the model results.

6.2 EXPERIMENTAL PROGRAM

6.2.1 Test specimens

In the experimental investigation, five slender high-strength concrete panels were tested under sustained in-plane compression load that was eccentrically applied on the two short edges. All panels were simply supported on the loading edges and loaded horizontally. They possess the same dimensions, where the height (H), width (b) and thickness (h) are 2700 mm, 460 mm and 100 mm, respectively. These dimensions are similar to the ones used in the short-term experimental study presented in Chapter 3, which provides the basis for this study. Moreover, they were all equally reinforced at the outer and inner layers in the in-plane load direction with the total reinforcement ratio equal to 0.22%. SL52 welded steel mesh with bar diameter of 4.77 mm in two orthogonal directions was used as the reinforcements. The geometric configuration and layout of reinforcement of the panels are depicted in Fig. 6.1. The concrete cover is 20 mm for all specimens. The specimens were prepared, casted and cured in the same way as the short-term experiment study described in Chapter 3.

Three parameters were examined in the tests, that include the loading age, eccentricity and level of load. The details of the loading conditions are reported in Table 6.1. The eccentricities presented here are the actual ones, which were determined using the concrete strains measured near to the edges of the specimens in test and following Eq. (3.27). The load level for each panel is determined as the ratio of the measured sustained load divided by the corresponding short-term load-carrying capacity predicted by the proposed short-term theoretical model using the tested material properties and eccentricities. As the short-term model was validated comprehensively by comparing with test results generated in the short-term experimental study and with others from the literature, and also because the tested long-term specimens have the same dimensions, concrete strength, steel reinforcement and loading eccentricities, as the specimens tested under short-term loading in Chapter 3, its predicted failure loads are considered to be reliable.

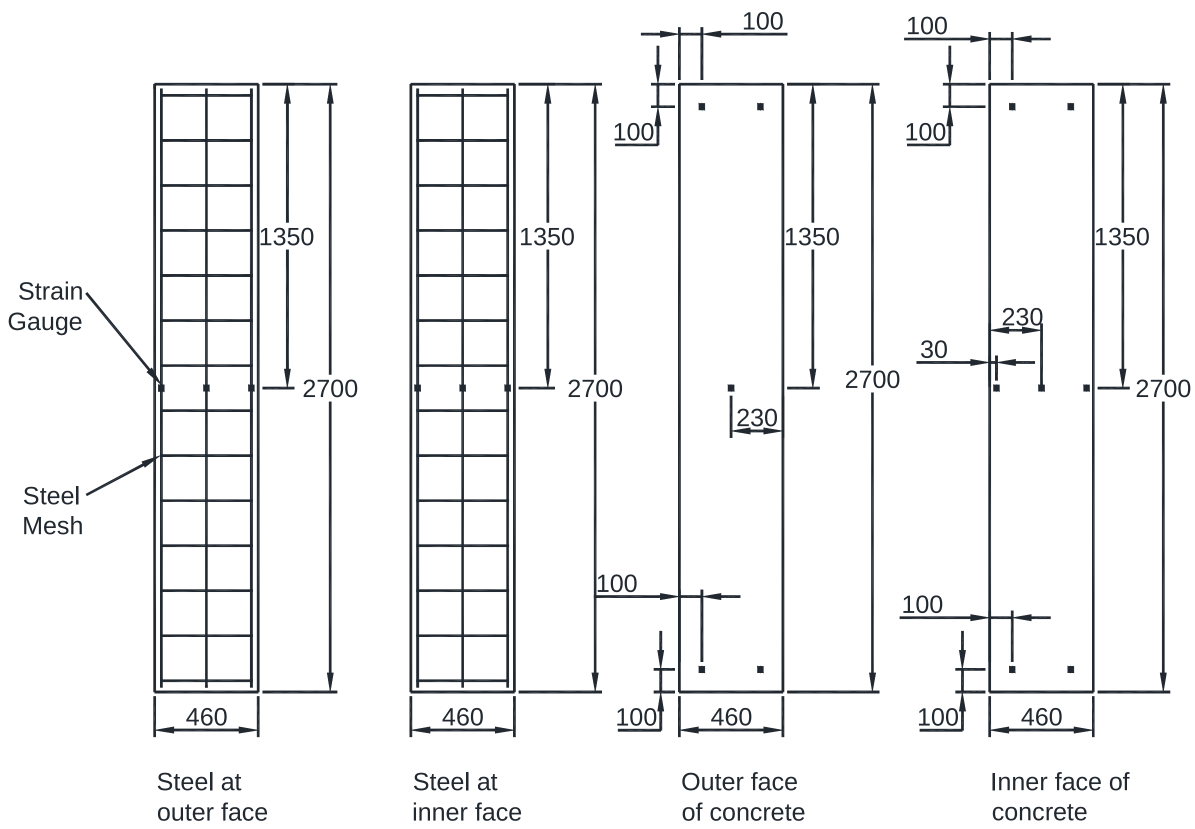

(a) Strain gauge locations in the long-term test

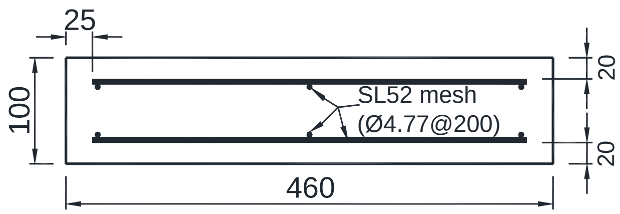

(b) Cross-section of tested panel

Fig. 6.1 Strain gauge location and cross-section of all panel specimens

Panels LT2 and LT3 were tested at an old age, whereas the other specimens were all loaded at the same concrete age of 22 days. The effect of loading age was investigated by comparing the test results of Specimen LT3 to those of LT5 because both have the same eccentricity. The eccentricity was varied between Specimen LT2 and LT3 to examine role of the load eccentricity. Specimen LT1 and LT5 were designed to study the influence of the in-plane load level on the long-term performance of HSC panels. Specimen LT4 was initially loaded to 75% of its predicted short-term failure load, followed by an unloading stage until the load was dropped to 62% of the failure load, which was kept constant with time after that.

Table 6.1 Details of loading conditions

Panel No.	Loads (kN)			Eccentricity (mm)		
	Sustained load (kN)	Predicted short-term failure load (kN)	Sustained load level	[1] e_L (mm)	[2] e_R (mm)	[3] e_{design}/h
LT1	591	638	93%	22.5	21.9	1/6
LT2	320	436	73%	31.1	37.5	1/3
LT3	615	820	75%	19.1	18.8	1/6
LT4	369	593	62%	24.1	27.8	1/4
LT5	548	764	72%	19.6	21.4	1/6

[1]–Eccentricity measured in the test at left edge;
[2]–Eccentricity measured in the test at right edge;
[3]–Designed eccentricity;

6.2.2 Preparation of test specimens

The formworks of the panel specimens were built using structural grade plywood and laid horizontally on the ground in the structural laboratory. The SL52 mesh was cut to the required dimension and placed at the top and bottom layers that were held in place by steel bar chairs. The formwork and details of the reinforcement are illustrated in Fig. 6.2. The specimens were cast using a commercially mixed high-strength concrete. The casting of specimens as well as the testing was done in pairs, in the order of LT1, LT2 and LT3, LT4 and LT5. After casting, the panels were covered with wet hessian and wrapped with plastic sheets at the outside of the hessian. They were kept moist in the formwork for 14 days before stripping and remained in the ambient laboratory conditions until the day of loading.

(a) Set-up of formwork

(b) Details of reinforcing mesh

Fig. 6.2 Preparation of test specimen

6.2.3 Test setup and instrumentation

The HSC panels were tested horizontally in a universal testing frame with hydraulic jack at one end and two load cells at the other end. The load was applied and monitored to remain constant through the hydraulic jack. The test setup is shown in Fig. 6.3 and Fig. 6.4.

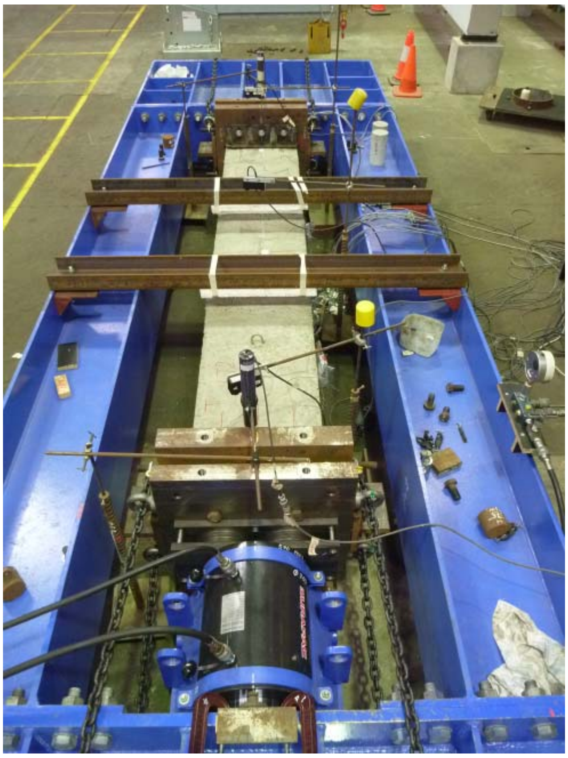

(a) Top view

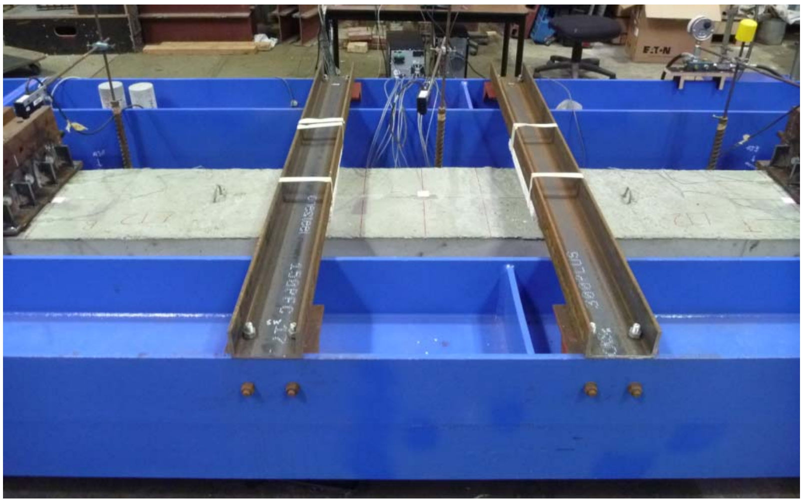

(b) Side view

Fig. 6.3 Long-term test set-up

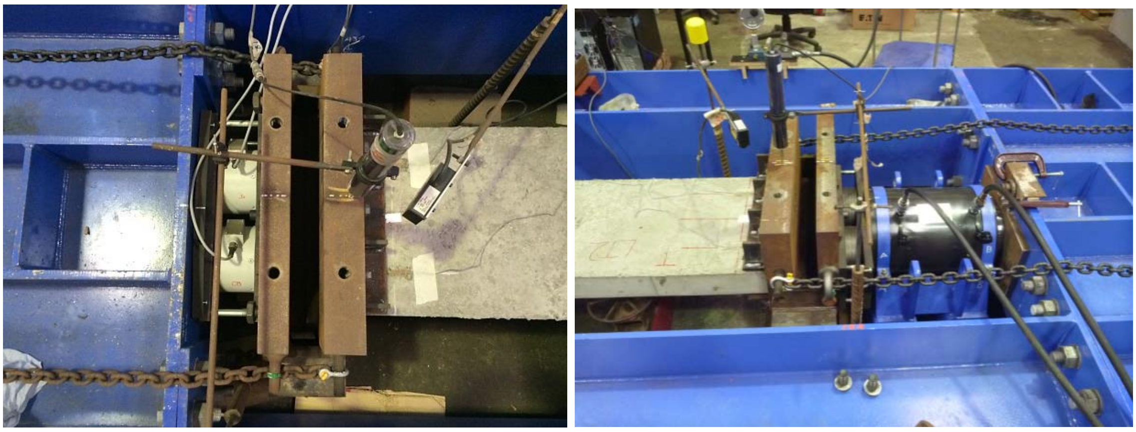

(a) Left end: load cell (b) Right end: hydraulic jack

Fig. 6.4 Details of test setup

A number of spring plates with high load-carrying capacity were inserted between the jack and the end support plate so as to minimize the dropping of the axial sustained load with time. The loading and supporting mechanisms at each panel end consisted of a rotatable hinge to provide simply-supported boundary condition (See Fig. 6.4). The load eccentricity was set up in a way that the panel would deform upwards under loading. The two external load cells were installed to measure the applied load throughout the entire test, as shown in Fig. 6.4. The out-of-plane displacements were measured by laser displacement sensors at 3 points of the outer (top) face of the panel that were symmetrically distributed along its length, i.e. at x = 100 mm, x = 1350 mm, and x = 2600 mm. 18 strain gauges were mounted on the surfaces of steel and concrete at the critical locations as shown in Fig. 6.1(a). The displacements of the hinge plates on the two ends were monitored using the linear strain conversion transducer (LSCT), as shown in Fig. 6.3.

6.2.4 Test procedure

The panel specimens were loaded by a hydraulic pump. Each panel was loaded up to the desired load level first, and then once the load level had been reached, the valve on the jack was closed to prevent further loading and then the pump was released. The process of applying the instantaneous loads ordinarily last less than half an hour. The sustained load tended to drop as a result of concrete creep. The dropping was fairly remarkable especially at the first few hours after the sustained load was applied. So the load was topped up from time to time as needed, to maintain at the constant level throughout the test. The procedure of adjusting the load is as follows: first, use the hydraulic pump to load the pressure to the desired level which can be read directly from a pressure gauge connected to the oil hose; then, the valve was opened so that the pump was connected through to the jack; finally, the load was topped up by driving the jack through the pump. As aforementioned, two specimens were failed by creep buckling under the sustained load. The other three panels were loaded to failure at some time after initial loading by increasing the imposed load level without the release of the existing loads, since they displayed long-term stable behaviours.

6.2.5 Material properties

Concrete cylinders of 100 mm diameter and 200 mm height as well as concrete prisms of 100x100x500 mm were cast and cured along with the panels. Five concrete cylinders were tested in compression to measure the compressive strength and elastic modulus of concrete and three prisms were tested under 4-point bending to determine the flexural tensile strength of the concrete. These material properties were measured at the commencement and completion of the panel test, as reported in Table 6.2. The development of the material properties of concrete with time was determined using the interpolation method, as their difference at the beginning and end of test were fairly small.

Two standard concrete prisms of 75x75x280 mm with gauge studs mounted on both ends were cast and cured for each pair of specimens as well in order to measure the shrinkage strain following AS1012.13 (1992). The measurement of the shrinkage strain commenced immediately after the test specimens were demoulded at 14 days using the vertical comparator as shown in Fig. 6.5, and stopped once the panel was failed. The measured data is shown in Fig. 6.7.

Fig. 6.5 Measurement of shrinkage strain

Fig. 6.6 Creep rig setup

Three cylinders were placed in a standard creep rig under a sustained stress of 30 MPa for each pair of panels, as presented in Fig. 6.6. The stresses were applied hydraulically at the same time of the test of corresponding specimens and adjusted to remain constant due to the occurrence of creep and shrinkage. The total strains which included the elastic strain, the shrinkage strain and creep strain were measured from the three cylinders using Demec strain gauges. The shrinkage strains were measured from two unloaded companion cylinders with the same dimensions as the creep cylinders. The creep strains were then determined by subtracting the sum of the measured shrinkage strain and instantaneous elastic strain from the total strains. The creep coefficient, determined as the ratio of measured average creep strain to the measured average elastic strain, is shown in Fig. 6.8.

Since the same steel reinforcement as in the short-term test was used here, the material properties of the steel reinforcement determined in the short-term test was adopted, where the yielding strain was 0.2% and the measured elastic modulus was 206 GPa. The stress-strain relation is the same as presented in Fig 3.3(b).

Table 6.2 Material properties of concrete at the start and end of panel testing

Panel No.	Concrete Age (Days)	f'_c (MPa)	E_c (GPa)	f_t (MPa)	Event on the timeline
LT1	22	80.9	36.4	5.3	Initial loading
	38	89.5	37.3	6.4	Failure
LT2 & LT3	99	91.7	40.25	6.9	Initial loading of LT2
	203	95	39.3	7	Failure of LT3
LT4 & LT5	22	101	39.5	5.9	Initial loading of LT4 & LT5
	91	103.5	39.8	8.9	Failure of LT5
	126	103	40.5	8.9	Failure of LT4

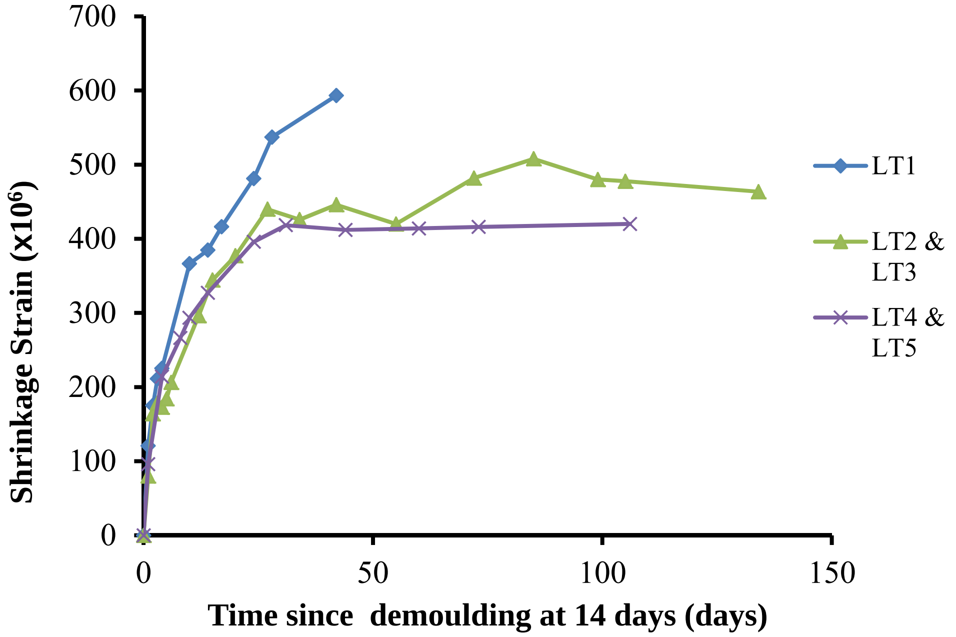

Fig. 6.7 Shrinkage strain measured in the tests

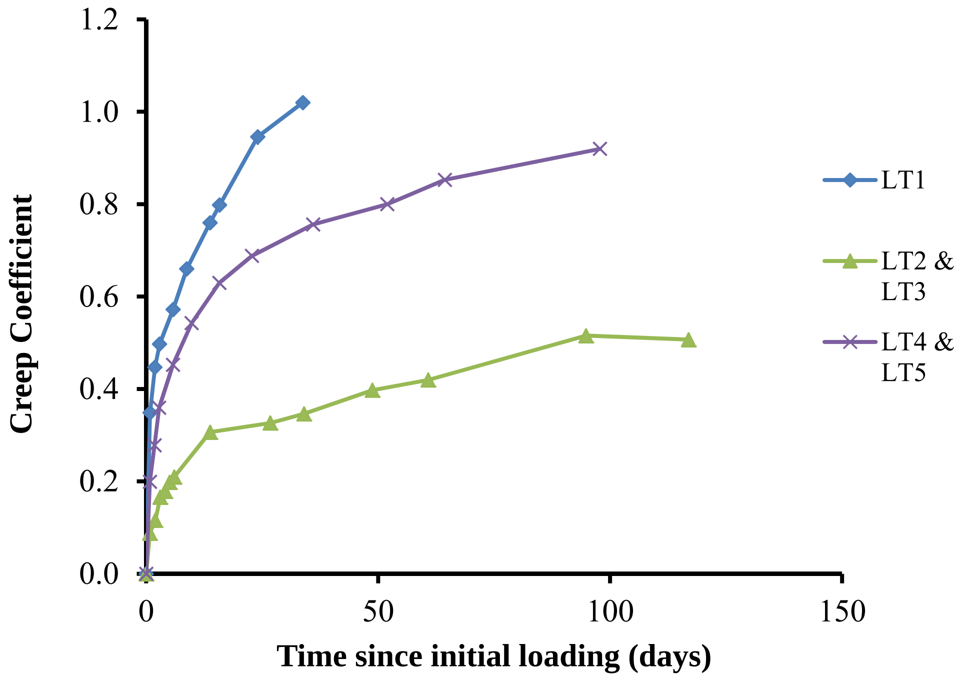

Fig. 6.8 Creep coefficient measured in the tests

6.3 EXPERIMENTAL RESULTS AND DISCUSSIONS

The experimental results as well as the predictions by the long-term theoretical model are summarized in Table 6.3. As mentioned earlier, the predicted short-term failure loads are obtained by using the short-term theoretical model in Chapter 3 along with employing the experimental material properties and loading conditions. The concrete is assumed to be linear viscoelastic in compression and nonlinear in tension in the long-term model, where cracking and tension-stiffening which follows the rule proposed by Fields and Bischoff (2004) as in Chapter 5 are considered. The self-weight of the panel is not considered in the long-term model as the positive bending moments caused by the self-weight is negligible compared to the negative bending moments produced by the eccentric in-plane loading. The measured material properties are incorporated into the long-term theoretical model, in which the aging effect of the concrete for the elastic modulus and strength is modelled via interpolating the experimental data with time. The creep coefficients attained in the experiment are also used in the theoretical model. By means of using the least square method to fit the experimental relaxation modulus as determined in Eq. (5.9), the spring moduli in the expanded relaxation modulus are determined. Since Specimens LT1, LT4 and LT5 were cast using the same concrete mixture and cured under similar conditions, and they were loaded at the same age, their material properties including strength, elastic modulus, creep coefficient and shrinkage are considered to be the same and the average values are used in the model. The number of Maxwell units (m) used to model the viscoelastic behavior of concrete is taken as 5 with $\tau_\mu = 5^{\mu-1}$(days) in the model. The spring constants for Panels LT1, LT4 and LT5 obtained by the least squares methods are: E_1 = 9313 MPa, E_2 =4573 MPa, E_3 =3982 MPa, E_4 =3097 MPa, E_5 =2889 MPa, E_6 =15200 MPa. The creep properties of the aged Panels LT2 and LT3 were different from the other three panels. So the associated springs constants are E_1 = 3494 MPa, E_2 = 3661 MPa, E_3 = 2650 MPa, E_4 = 4849 MPa, E_5 = 5493 MPa, E_6 = 20058 MPa.

Table 6.3 Comparison of test results to predicted results by the theoretical model

Panel No.	Test				Prediction		
	Concrete age upon loading (t_0) (days)	Load duration (t) (days)	Failure mode	Ultimate failure load (kN)	Critical time (t)	Failure mode	Short-term failure load (kN)
LT1	22	13	Creep buckling	591	18	Creep buckling	638
LT2	146	57	Stable (crushed)	373	N/A	Stable	436
LT3	99	42	Stable (crushed)	794	N/A	Stable	820
LT4	22	104	Stable (crushed)	466	N/A	Stable	593
LT5	22	69	Creep buckling	548	107	Creep buckling	764

Cracking occurred to all specimens during or right after the instantaneous loading as predicted by the theoretical model, which firstly started in the middle spans and then propagated to the two edges with loading and time. All panel specimens collapsed in buckling failure modes either with time (creep buckling) or after continuous instantaneous loading to failure (crushed), since they were all slender panels that had identical geometric configurations. The cracking regions generally concentrated within the middle one-third span of the specimens. A typical buckling failure mode is shown in Fig. 6.9. Panel LT1 and LT5 failed by creep buckling under the sustained load, whereas the other three specimens were crushed at a certain time after initial loading since they exhibited long-term stable responses.

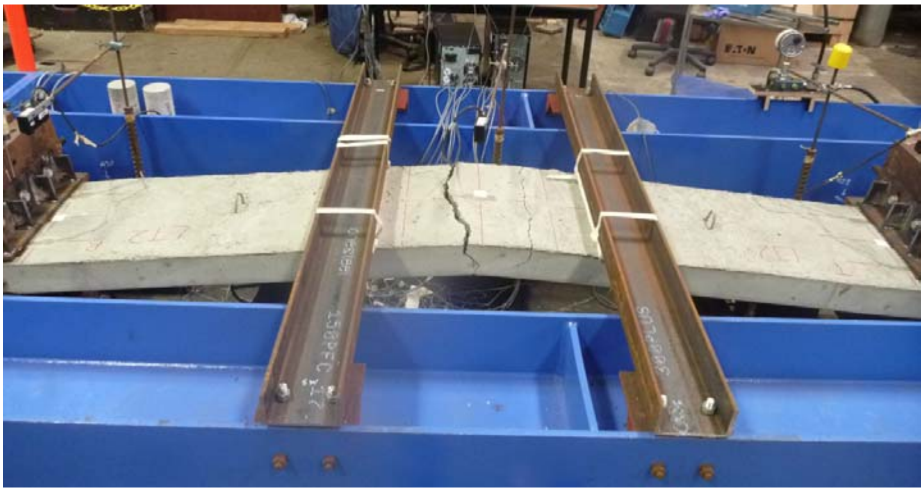

Fig. 6.9 Representative buckling failure mode

The variation of the center deflections versus time is plotted in Fig. 6.10-Fig. 6.13 for all panels, where both experimental and predicted results are shown. It can be seen that in general the model results show close correlations with the test results, which demonstrates the capability of the theoretical model in predicting the time-dependent performance of HSC panels.

Fig. 6.10 investigates the effect of loading age on the long-term behavior of one-way HSC panel under the same level of eccentric in-plane loads. LT3 is loaded at 99 days whereas LT5 is loaded at 22 days. The test load levels and eccentricities of these two specimens appeared not to be completely identical as it was very difficult to control the sustained load level and eccentricity in such long-term buckling test. Nevertheless, the load levels and eccentricities of both panels were close enough for comparison with each other. It can be observed that both specimens experienced increased out-of-plane deflections with time due to the combined effects of creep, shrinkage and geometric nonlinearity. In addition, the early-loaded Specimen LT5 showed a softer behavior with a larger deflection compared to Specimen LT3 that was tested in an old age. This is within the expectation since aged concrete creeps less. The predicted curves agree fairly well with the measured ones until the failure of the specimens. Specimen LT5 is characterized by a sudden buckling failure under the sustained load at 69 days after initial loading. On the contrary, Specimen LT3 was predicted to be long-term stable and the change of tested deflection with time clearly validated the prediction. Hence, the panel was loaded to failure at t = 42 days by increasing the existing in-plane load. The panel failed by buckling as well with the ultimate failure load equal to 794 kN that is fairly close but slightly smaller than the predicted short-term load-carrying capacity. Based on the results of this panel, the creep and shrinkage seem to have almost no influence on the residual strength of the panel.

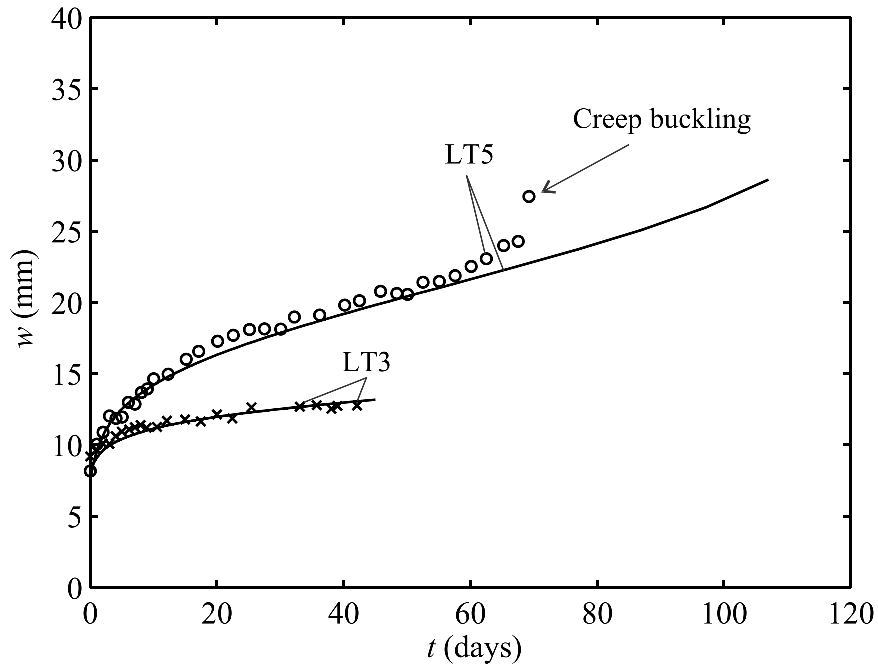

Fig. 6.10 Effect of loading age: variation with time of the center out-of-plane displacement of Specimen LT3 and LT5 (ooo and xxx Test; —— Model)

The experimental and theoretical deflections of Specimens LT2 and LT3 are plotted against time in Fig. 6.11 for the examination of the influence of the eccentricity of the in-plane load on the time-dependent response of HSC panels. Panel LT2 was tested under an eccentricity that equals to 1/3h while Panel LT3 was loaded with a load eccentricity of 1/6h. There was a time lag in the loading age of the two specimens.

However, since the two panels were cast using the same batch of concrete and they were loaded in an old age at which there is no siginifciant variation of material properties with time, the material properties of these two specimens including the creep, elastic modulus and strength are considered to be the same in this study. It can be seen that tas long as no creep buckling failure happens with time, then changes in the eccentricity have a minor influnce on the creep response. Due to different load levels in the two panels, but with almost the same sustained load to failure load ratio, the instantaneous defleciton of Panel LT3 is larger, and the creep responses are very similar as predicted by the model. Similiar to LT3, Specimen LT2 was going to reach a stable state eventurally as predicted by the long-term theoretical model (see Table 6.3). So it was loaded to failure at 57 days with the ultimate failure load achieved at 373 kN, which is around 17% smaller than the predicted short-term capacity. Thus, the long-term effects of creep and shrinkage may reduce the residual strength of HSC panels, which need to be considered in their design.

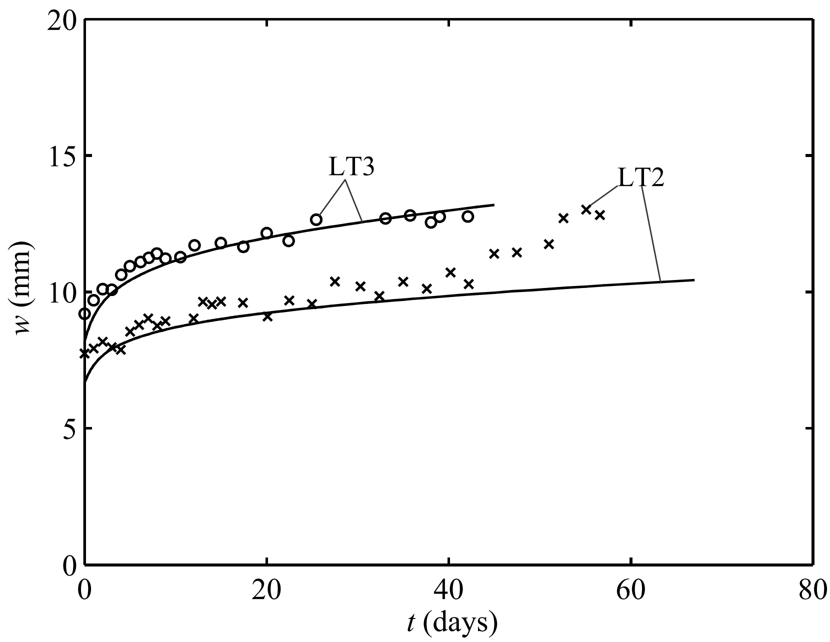

Fig. 6.11 Effect of in-plane load eccentricity: variation with time of the center out-of-plane displacement of Specimen LT2 and LT3 (ooo and xxx Test; —— Model)

Fig. 6.12 investigates the influence of the in-plane load level on the time-dependent performance of HSC panels. Specimen LT1 and LT5 were tested under 93% and 72% of the corresponding short-term failure loads, respectively, and they both failed by creep buckling at different times. It can be seen that the theoretical result of LT1 correlates with the test result reasonably well and apparently, the centre deflection of Specimen LT1 which was subjected to the higher axial loads increased more rapidly than that of Specimen LT5. Consequently, Specimen LT1 failed more rapidly as well, characterized by a brittle creep buckling failure that occurred at 13 days in contrast to 69 days for Panel LT5. Good correlation also appears for LT5. It was shown in Chapter 5 that the critical time to cause creep buckling is very sensitive to the load level. This theoretical observation is also validated here and it explains to some extent the difference between the predicted critical time and the observed one for LT5. The load ratio used in the model was 72%, but Fig. 6.12 shows that increasing the load level slightly by 3% or 5% can dramatically influence the time-dependent behavior and the predicted critical times, which equal to 96 days and 70 days, respectively, for the load levels that corresponds to 75% and 77% of the short-term load-carrying capacity of LT5. This 3% or 5% difference between the two applied loads in the model can be within the typical tolerances of any testing of RC structures, but the results of the long-term test investigated here are very sensitive to this parameter.

As mentioned earlier, Panel LT4 was first loaded to 75% of its predicted short-term failure load. The load was then dropped to 62% of its failure load and remained constant with time. The panel exhibited a typical stable behaviour with time. Yet, in order to highlight the influence of this loading history, where residual plastic deformation exist before creep due to the unloading stage, and which may reflect real loading scenario in practice, the load versus deflection for LT4 is shown in Fig. 6.13. It shows the entire loading history of loading, unloading, creep under sustained load, and reloading to failure. The instantaneous load deflection curved as predicted by the theoretical model is also shown for comparison. The panel exhibited a stable behaviour under the sustained load and therefore, it was loaded to failure after 104 days since first loading. The measured ultimate strength of the panel was 466 kN, compared to 593 kN for the predicted short-term load capacity. Thus, it can be seen that under this loading scenario, creep may have a more significant impact on the residual strength of the panel, which dropped by about 21% from the short-term strength. Similar figures are also presented for LT2 and LT3.

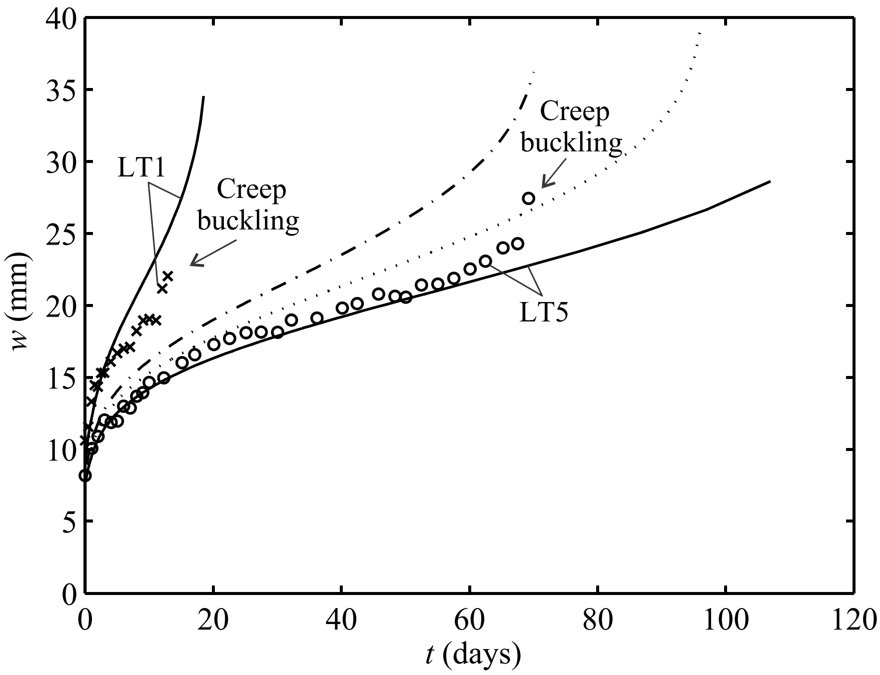

Fig. 6.12 Effect of in-plane load level: variation with time of the center out-of-plane displacement of Specimen LT1 and LT5 (ooo and xxx Test; —— Model; · · · · · · Model results for Panel LT5 with load equals to 75% of the failure load; — · — · Model results for Panel LT5 with load equals to 77% of the failure load)

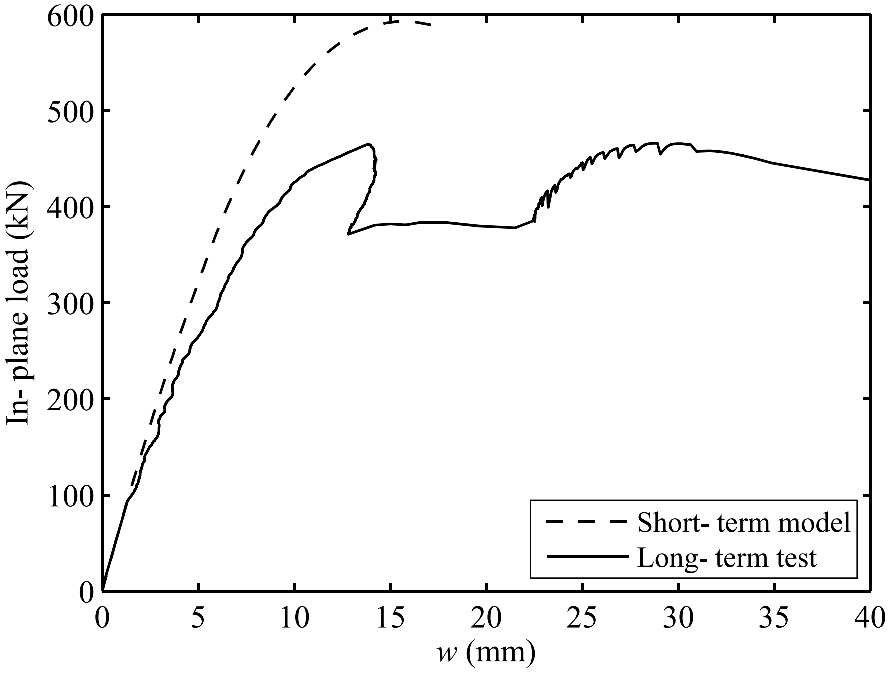

Fig. 6.13 In-plane load vs. out-of-plane center deflection of Specimen LT4

The load versus the centre out-of-plane deflections for Specimens LT2 and LT3 are plotted in Fig. 6.14-Fig. 6.15. It can be seen that the instantaneous behaviour of the tested panel is well captured and described by the short-term theoretical model, whose capability in predicting the short-term performance of HSC panels has already been validated and demonstrated in Chapter 3. The magnitudes of the deflections at the maximum load were comparable to those under the short-term loading. It is found that the residual strength of Panel LT3 is close to the prediction while there is a perceptible reduction for the residual strength of Panel LT2, which has larger load eccentricity.

The tested and predicted compressive strains of steel and concrete at the inner face of mid-span section for Panel LT1, LT2, LT3 and LT5 versus time are given in Fig. 6.16-Fig. 6.19. Generally, the strains are well predicted by the long-term theoretical model. It can be seen that the absolute value of the compressive strains in the steel and concrete increase with time due to the long-term effects of creep and shrinkage and geometric nonlinearity. The steel strains at the time of failure were all less than the yielding strain 0.2%, indicating that no yielding happened to the reinforcement, and indicating that failure has actually occurred due to buckling.

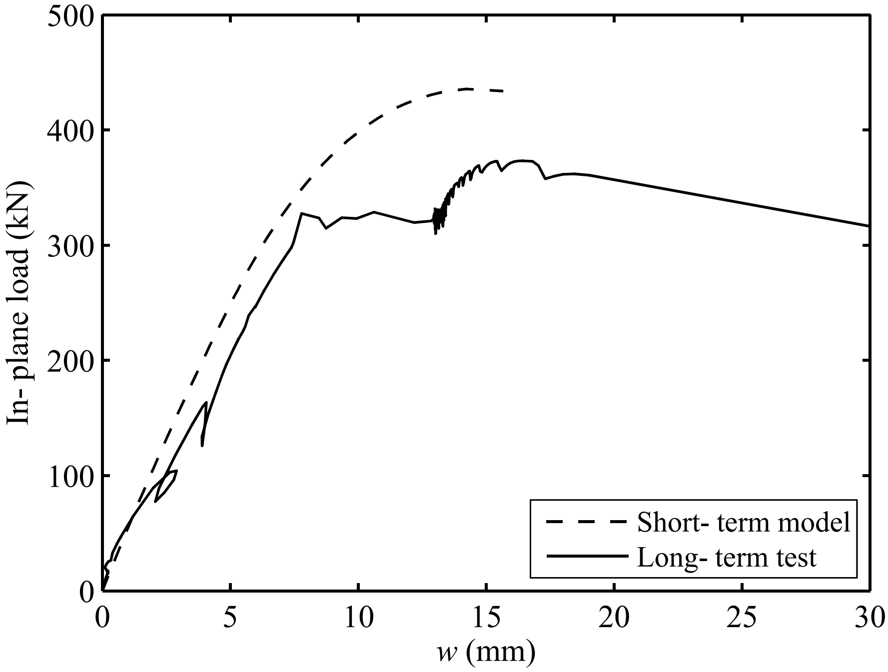

Fig. 6.14 In-plane load vs. out-of-plane center deflection of Specimen LT2

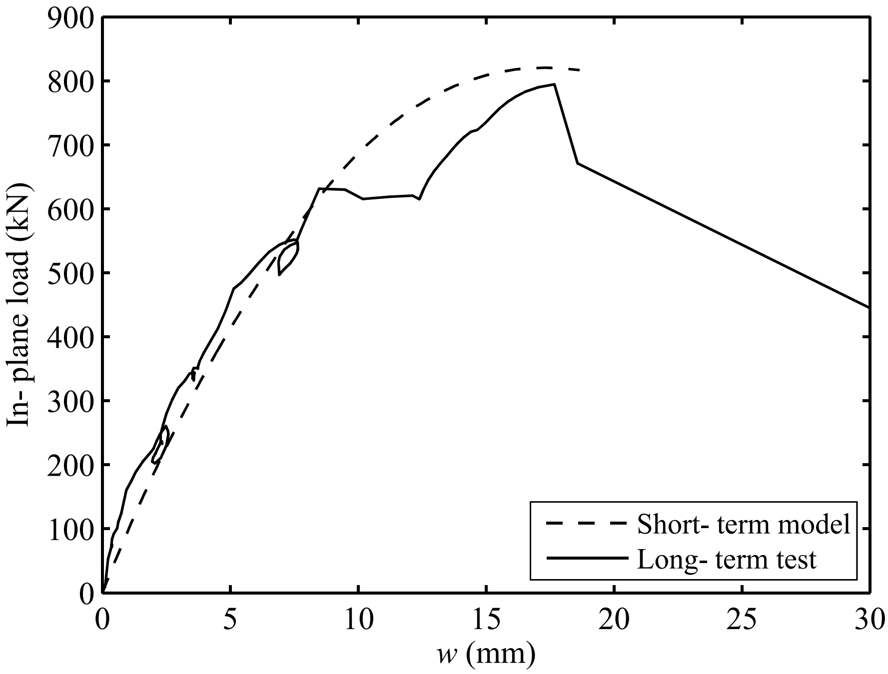

Fig. 6.15 In-plane load vs. out-of-plane center deflection of Specimen LT3

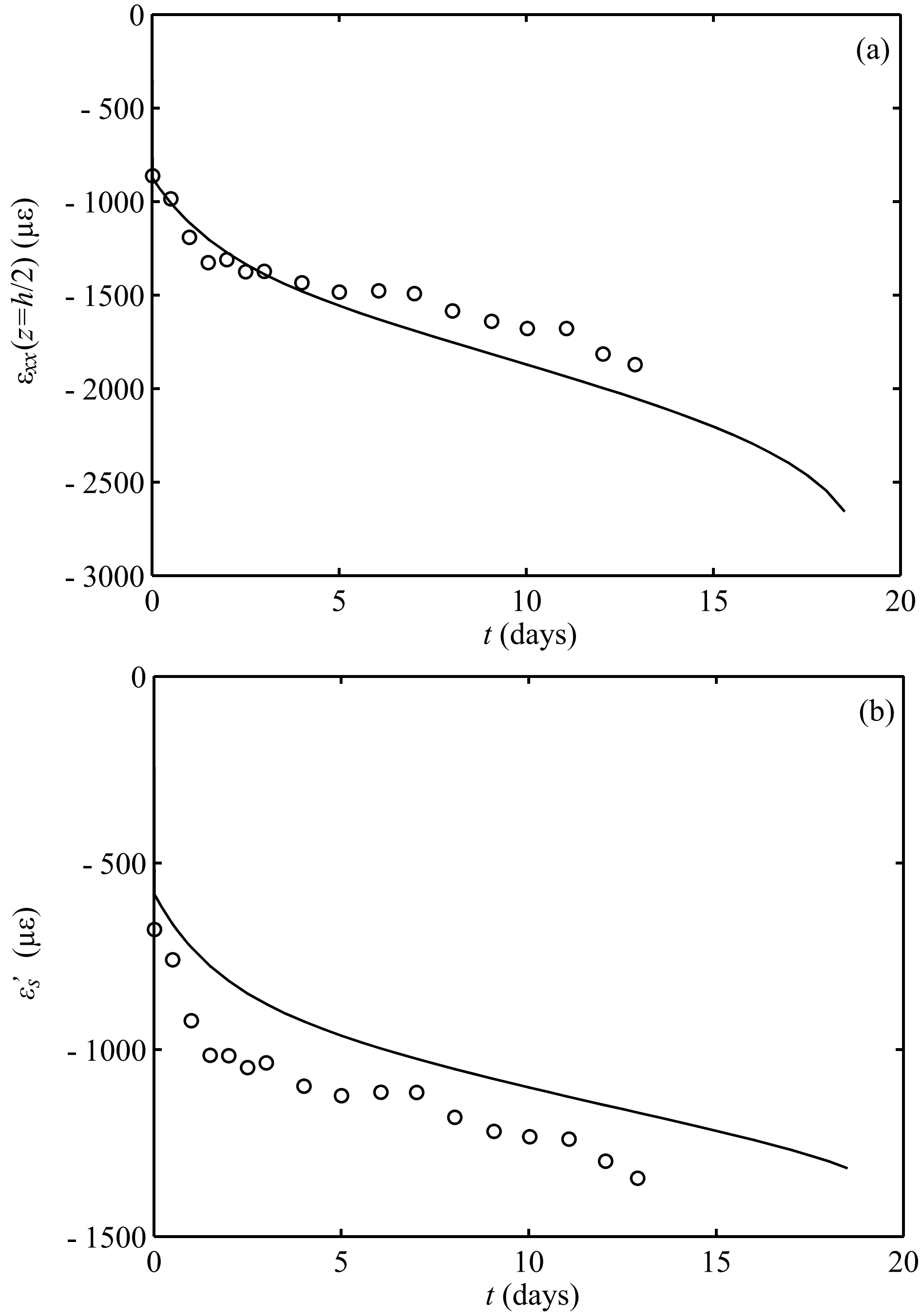

Fig. 6.16 Variation with time of compressive strains at the mid-height section of Specimen LT1 (a) concrete at the bottom surface; (b) steel in compression (ooo Test; —— Model)

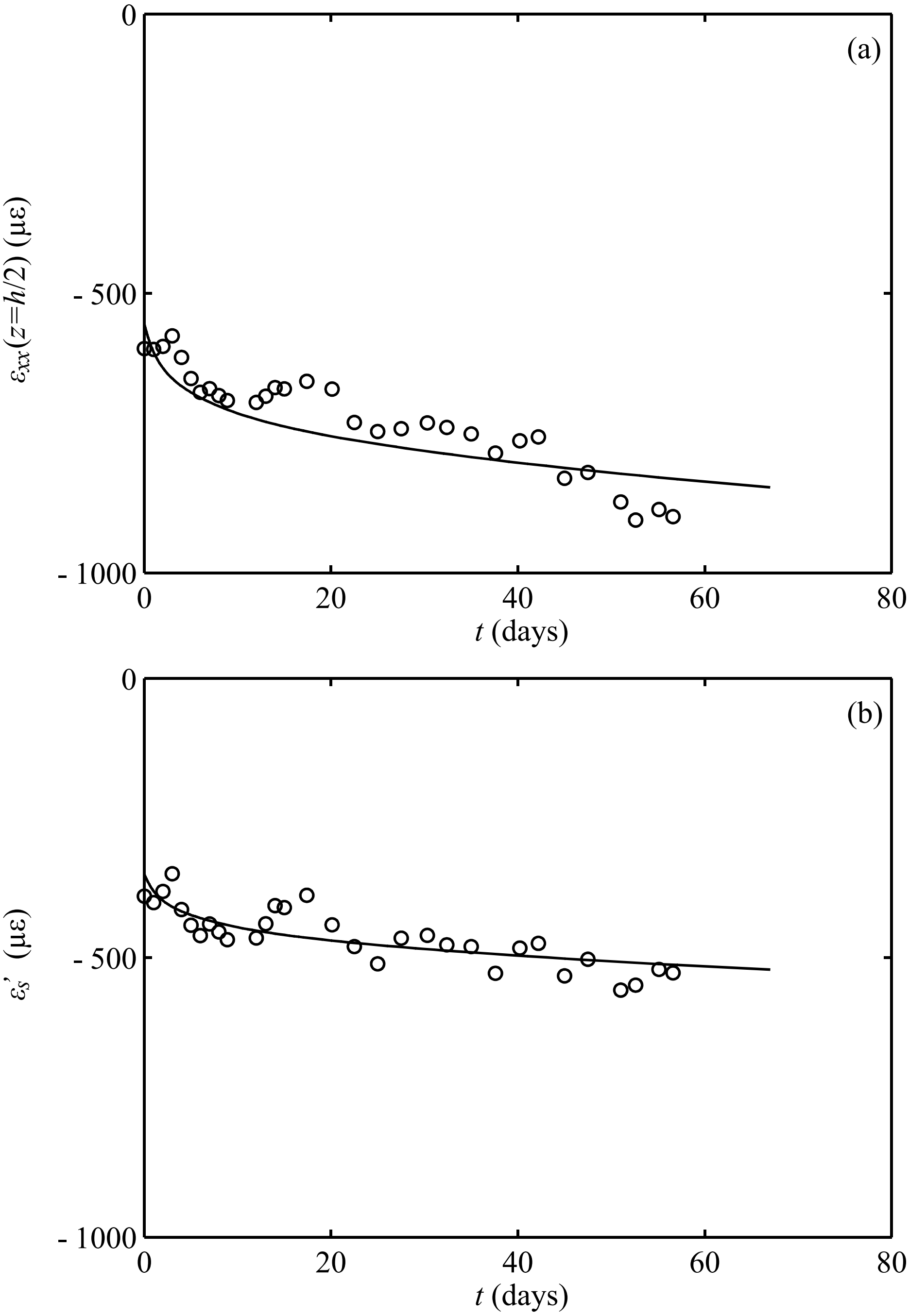

Fig. 6.17 Variation with time of compressive strains at the mid-height section of Specimen LT2 (a) concrete at the bottom surface; (b) steel in compression (ooo Test; —— Model)

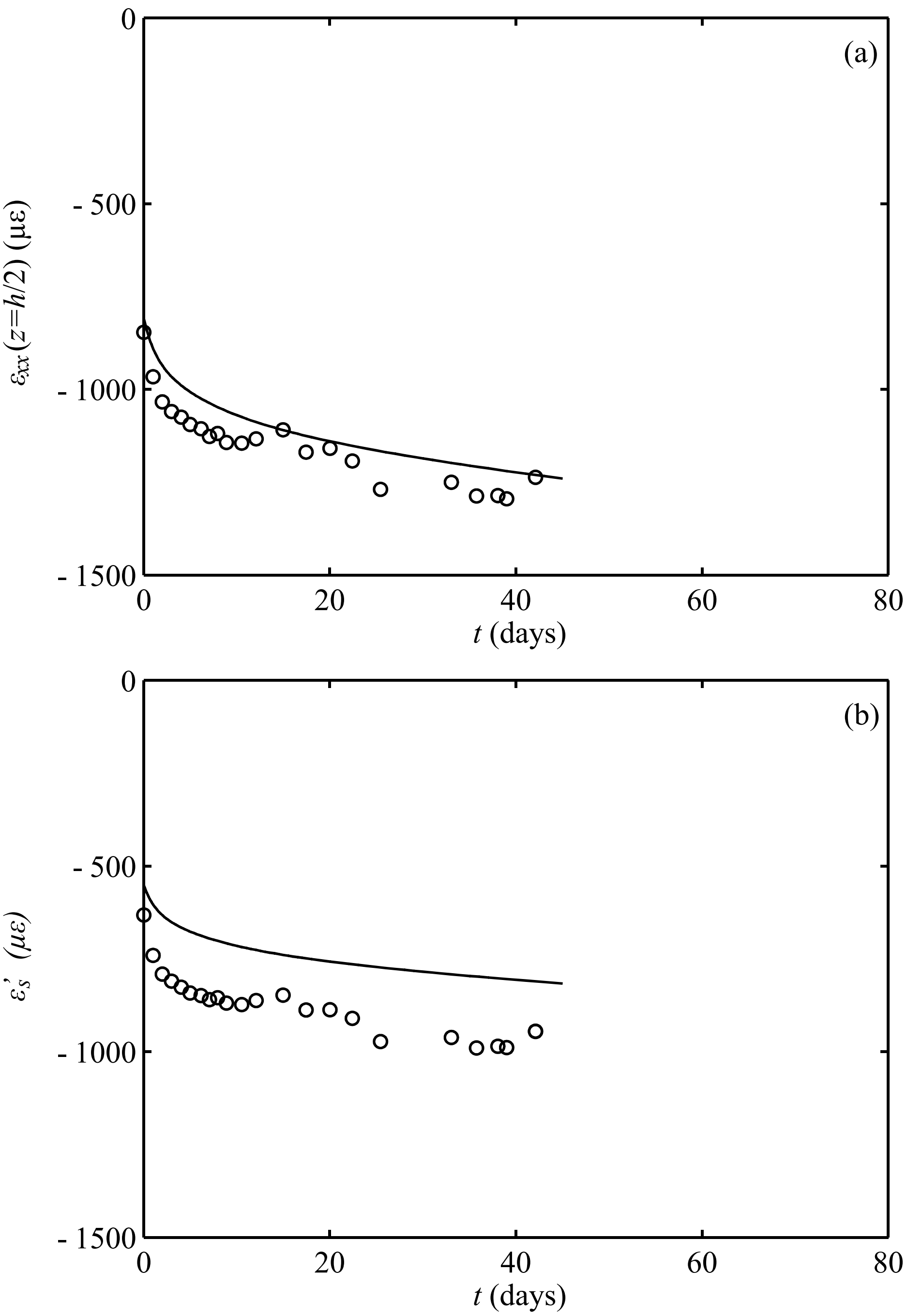

Fig. 6.18 Variation with time of compressive strains at the mid-height section of Specimen LT3 (a) concrete at the bottom surface; (b) steel in compression (ooo Test; —— Model)

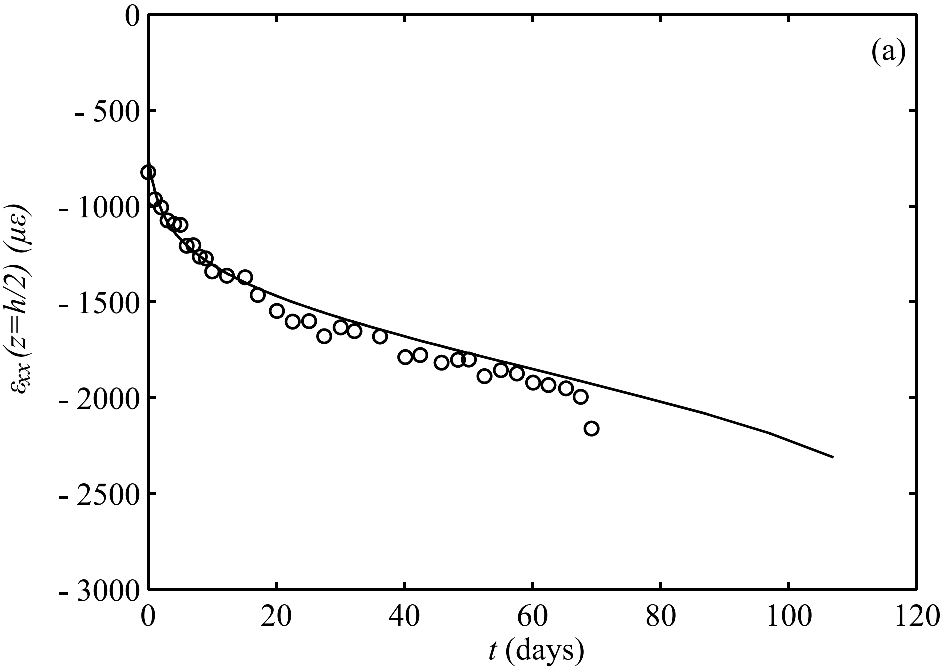

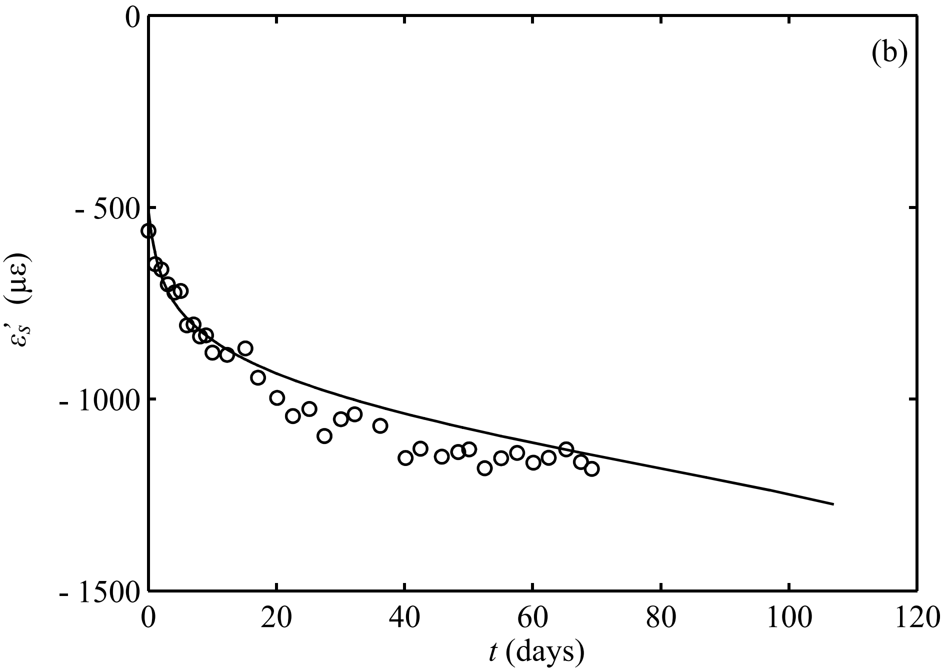

Fig. 6.19 Variation with time of compressive strains at the mid-height section of Specimen LT5 (a) concrete at the bottom surface; (b) steel in compression (ooo Test; —— Model)

6.4 SUMMARY AND CONCLUSIONS

An experimental study that consisted of testing 5 slender HSC panels to failure under sustained loading is conducted in this chapter to investigate the time-dependent behaviour of HSC one-way panels and the influence of creep on the residual strength of the panel. The panels were subjected to in-plane eccentric compression loads and simply supported along the short edges. It was found in this study that the out-of-plane deflections along with the strains in steel and concrete continuously increase with time due to the combined effect of creep, shrinkage, cracking of concrete and geometric nonlinearity. Two panels were collapsed by creep buckling under the sustained load and the other three panels exhibited long-term stable response and therefore were loaded to failure at some time after loading without the release of the existing load.

Three factors that can substantially affect the response of the panels were examined in the study, including the loading age, the magnitude and eccentricity of the in-plane load. It is found in this long-term study that the loading age is crucial. The specimen tested at an older age showed smaller instantaneous and long-term deflections and exhibited stable response. On the other hand, creep buckling failure occurred to the panel that was loaded at the earlier age under the same load level. Furthermore, the long-term behaviour of the HSC panels is significantly affected and very sensitive to the in-plane load level. The higher load resulted in larger instantaneous deflection of the specimen and more rapid increase of it with time, which eventually led to earlier creep buckling. It is also found in this study that small difference in the load level such as 3% or 5%, which exists within the typical tolerance in any reinforced concrete structure testing, can give rise to notable variation in terms of the critical time of slender HSC panels.

Finally, as seen in the present experiment, the time-dependent effects of creep and shrinkage, coupled with the geometric nonlinearity, has caused reductions of the residual strength of HSC panels to varying degrees. This reduction should be carefully considered and treated in the design of slender HSC wall panels, as their ultimate carrying capacities after being loaded over time under the sustained service loads will be smaller than that under the instantaneous loads.

CHAPTER 7 THEORETICAL STUDY OF LONG-TERM BEHAVIOR OF TWO-WAY HSC PANELS

7.1 INTRODUCTION

All the investigations carried out so far regarding the long-term behavior of high-strength concrete (HSC) panels have focused on their one-way actions. However, in practice, the panels can be restrained to a certain degree on more than two edges, which enforce the panel to behave in a two-way action. Such panels are referred to as two-way panels. Similar to one-way panels, slender two-way concrete panels may undergo increasing in-plane and out-of-plane deformations with time under eccentric sustained in-plane and/or out-of-plane loads due to the combined effects of geometric nonlinearity and long-term creep. This may cause excessive deflection and cracking when the structure is in serviceable state or may eventually lead to creep buckling failures.

Although the long-term effects may result in similar type of problems as in one-way concrete panels, the two-way behavior in terms of moment redistributions, cracking and buckling are significantly different. Therefore, a new theoretical model that utilizes the mechanics of thin plates is developed in this chapter for the analysis and prediction of the long-term response of HSC panels. A time-stepping analysis is used to account for the effect of creep. A rheological material model is adopted, which is based on the generalized Maxwell chain. In order to highlight the long-term effects only, a linear viscoelastic material behavior is assumed at the first part of the study. In the second part, the concrete is considered to be linear viscoelastic in compression, but with cracking and brittle behavior in tension being accounted for using a smeared cracking approach. The incremental governing equations are solved numerically at each time step based on a Fourier series expansion of the deformations and loads in one direction, and using the numerical multiple shooting method in the other direction. An iterative procedure is developed at each time step to determine the section rigidities and creep strains when the cracking of the concrete is accounted for. The mathematical formation of the model is presented first, followed by numerical and parametric studies.

7.2 MATHEMATICAL FORMULATION

In this section, the panel is considered to behave viscoelastic where cracking is not accounted for. The general governing equations derived here are applicable to any combination of external loads and boundary conditions. Concrete cracking is introduced into the model in a simplified way as shown in Section 7.3.2.

As in the one-way theoretical model, a time-stepping analysis approach is adopted in order to account for the time-dependent change of the internal stresses and the increase of the deformations of the structure with time. The mathematical formulation consists of the development of the incremental equilibrium equations, the constitutive relations and the governing equations. The sign conventions for the coordinates, loads and displacement are shown in Fig. 7.1. The middle plane of the panel is taken as the xy plane, where the x and y axes are directed along the edges. The z axis is taken normal to the middle plane and measured positive downwards. The forces and bending moments at the boundaries as well as the lateral loads are also presented in Fig. 7.1. The torsional moments at the boundaries are not shown in the figure for brevity and clarity.

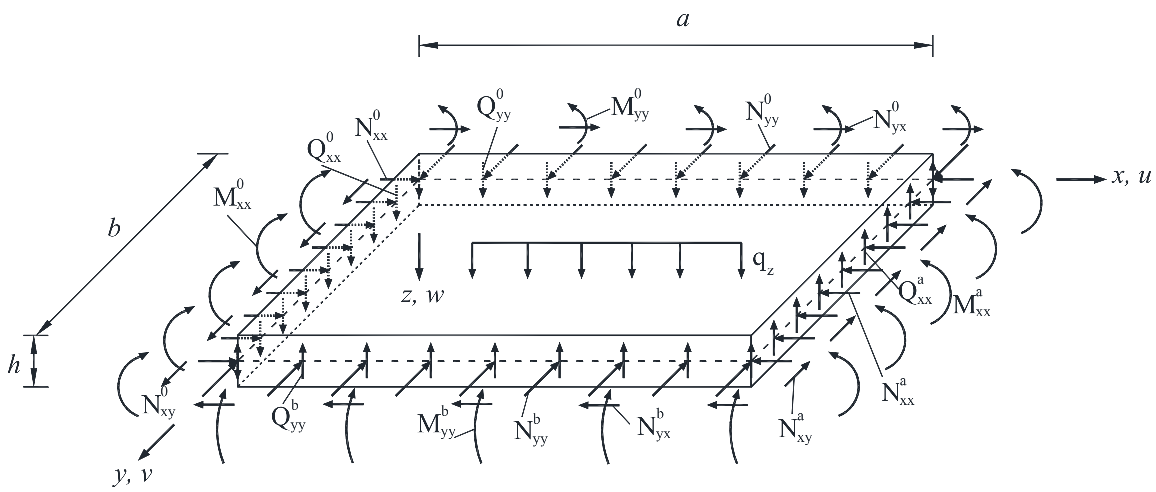

Fig. 7.1 Sign conventions of the investigated panel

7.2.1 Kinematic relations

In typical HSC panels, the dimensions in the *z* direction are much smaller than those in the other two directions. Therefore, a plane stress condition is adopted, where the stresses in the *z* direction including the normal and shear stresses are equal to zero. The theoretical model is based on Von Karman plate theory where the large displacement theory is applied. The incremental kinematic relations of the plate then read

$$
\begin{aligned}
\Delta\varepsilon_{xx}(t_r) &= \frac{\partial \Delta u(t_r)}{\partial x} + \frac{1}{2}\left(\frac{\partial \Delta w(t_r)}{\partial x}\right)^2 + \frac{\partial w(t_{r-1})}{\partial x}\frac{\partial \Delta w(t_r)}{\partial x} - z\frac{\partial^2 \Delta w(t_r)}{\partial x^2} \\
\Delta\varepsilon_{yy}(t_r) &= \frac{\partial \Delta v(t_r)}{\partial y} + \frac{1}{2}\left(\frac{\partial \Delta w(t_r)}{\partial y}\right)^2 + \frac{\partial w(t_{r-1})}{\partial y}\frac{\partial \Delta w(t_r)}{\partial y} - z\frac{\partial^2 \Delta w(t_r)}{\partial y^2} \\
\Delta\gamma_{xy} &= \frac{\partial \Delta u(t_r)}{\partial y} + \frac{\partial \Delta v(t_r)}{\partial x} - 2z\frac{\partial^2 \Delta w(t_r)}{\partial x \partial y} + \frac{\partial w(t_{r-1})}{\partial y}\frac{\partial \Delta w(t_r)}{\partial x} + \frac{\partial w(t_{r-1})}{\partial x}\frac{\partial \Delta w(t_r)}{\partial y} \\
&\quad + \frac{\partial \Delta w(t_r)}{\partial x}\frac{\partial \Delta w(t_r)}{\partial y}
\end{aligned}
\tag{7.1}
$$

where ε_{xx} and ε_{yy} are the total normal strains in the *x* and *y* directions; γ_{xy} is the total shear strain in the *xy* planes. Each total strain has two components: the instantaneous strain and the creep strain. *u* and *v* are the in-plane displacements along *x* and *y* directions, and *w* is the out-of-plane deflection along *z* axis, and $\dfrac{\partial}{\partial x}$ and $\dfrac{\partial}{\partial y}$ denote the partial derivative with respect to x and y, respectively; Δ represents the incremental operator and note that any displacement that appear without the Δ operator are the accumulated known quantity from the previous time step.

7.2.2 Equilibrium equations

The variational principle of virtual work is used to derive the nonlinear incremental equilibrium equations along with the boundary conditions, which leads to

$$\delta U + \delta W = 0 \tag{7.2}$$

where δU and δW are the internal virtual work and external virtual work and δ is the variational operator. The internal virtual work is

$$\delta U = \int_{\mathrm{V}} \left(\sigma_{xx} + \Delta\sigma_{xx}\right)\delta\Delta\varepsilon_{xx} + \left(\sigma_{yy} + \Delta\sigma_{yy}\right)\delta\Delta\varepsilon_{yy} + \left(\sigma_{xy} + \Delta\sigma_{xy}\right)\delta\Delta\gamma_{xy}\mathrm{dV} \tag{7.3}$$

where σ_{xx} and σ_{yy} are the normal stresses in the x and y directions; σ_{xy} is the shear stress in the xy plane; V is the volume of the panel. Note that all the stresses and strains are functions of space and time, which for brevity are not included in the formulation. By substituting Eq.(7.1) into Eq.(7.3) and making integration with respect to z as well as integration by parts with respect to x and y, the internal virtual work becomes

$$
\begin{aligned}
\delta U = & -\int_0^a\int_0^b \left[\frac{\partial\left(N_{xx}+\Delta N_{xx}\right)}{\partial x}+\frac{\partial\left(N_{xy}+\Delta N_{xy}\right)}{\partial y}\right]\delta\Delta u\,\mathrm{d}x\mathrm{d}y \\
& -\int_0^a\int_0^b \left[\frac{\partial\left(N_{yy}+\Delta N_{yy}\right)}{\partial y}+\frac{\partial\left(N_{xy}+\Delta N_{xy}\right)}{\partial x}\right]\delta\Delta v\,\mathrm{d}x\mathrm{d}y \\
& -\int_0^a\int_0^b \left\{\begin{array}{l}\dfrac{\partial}{\partial x}\left[\left(N_{xx}+\Delta N_{xx}\right)\left(\dfrac{\partial w}{\partial x}+\dfrac{\partial \Delta w}{\partial x}\right)\right] \\ +\dfrac{\partial}{\partial y}\left[\left(N_{yy}+\Delta N_{yy}\right)\left(\dfrac{\partial w}{\partial y}+\dfrac{\partial \Delta w}{\partial y}\right)\right]\end{array}\right\}\delta\Delta w\,\mathrm{d}x\mathrm{d}y \\
& -\int_0^a\int_0^b \left\{\begin{array}{l}\dfrac{\partial}{\partial x}\left[\left(N_{xy}+\Delta N_{xy}\right)\left(\dfrac{\partial w}{\partial y}+\dfrac{\partial \Delta w}{\partial y}\right)\right] \\ +\dfrac{\partial}{\partial y}\left[\left(N_{xy}+\Delta N_{xy}\right)\left(\dfrac{\partial w}{\partial x}+\dfrac{\partial \Delta w}{\partial x}\right)\right]\end{array}\right\}\delta\Delta w\,\mathrm{d}x\mathrm{d}y \\
& -\int_0^a\int_0^b \left[\frac{\partial^2\left(M_{xx}+\Delta M_{xx}\right)}{\partial x^2}+\frac{\partial^2\left(M_{yy}+\Delta M_{yy}\right)}{\partial y^2}+2\frac{\partial^2\left(M_{xy}+\Delta M_{xy}\right)}{\partial x\partial y}\right]\delta\Delta w\,\mathrm{d}x\mathrm{d}y \\
& +\int_0^b \left(N_{xx}+\Delta N_{xx}\right)\delta\Delta u\Big|_{x=0}^{x=a}\mathrm{d}y+\int_0^a \left(N_{yy}+\Delta N_{yy}\right)\delta\Delta v\Big|_{y=0}^{y=b}\mathrm{d}x \\
& +\int_0^b \left(N_{xy}+\Delta N_{xy}\right)\delta\Delta v\Big|_{x=0}^{x=a}\mathrm{d}y+\int_0^a \left(N_{xy}+\Delta N_{xy}\right)\delta\Delta u\Big|_{y=0}^{y=b}\mathrm{d}x \\
& +\int_0^a \left[\left(N_{yy}+\Delta N_{yy}\right)\left(\frac{\partial w}{\partial y}+\frac{\partial \Delta w}{\partial y}\right)+\left(N_{xy}+\Delta N_{xy}\right)\left(\frac{\partial w}{\partial x}+\frac{\partial \Delta w}{\partial x}\right)\right]\delta\Delta w\Big|_{y=0}^{y=b}\mathrm{d}x \\
& +\int_0^a \left[\frac{\partial\left(M_{yy}+\Delta M_{yy}\right)}{\partial y}+2\frac{\partial\left(M_{xy}+\Delta M_{xy}\right)}{\partial x}\right]\delta\Delta w\Big|_{y=0}^{y=b}\mathrm{d}x \\
& +\int_0^b \left[\left(N_{xx}+\Delta N_{xx}\right)\left(\frac{\partial w}{\partial x}+\frac{\partial \Delta w}{\partial x}\right)+\left(N_{xy}+\Delta N_{xy}\right)\left(\frac{\partial w}{\partial y}+\frac{\partial \Delta w}{\partial y}\right)\right]\delta\Delta w\Big|_{x=0}^{x=a}\mathrm{d}y \qquad (7.4) \\
& +\int_0^b \left[\frac{\partial\left(M_{yy}+\Delta M_{yy}\right)}{\partial x}+2\frac{\partial\left(M_{xy}+\Delta M_{xy}\right)}{\partial y}\right]\delta\Delta w\Big|_{x=0}^{x=a}\mathrm{d}y \\
& -\int_0^a \left(M_{yy}+\Delta M_{yy}\right)\frac{\partial\delta\Delta w}{\partial y}\Big|_{y=0}^{y=b}\mathrm{d}x-\int_0^b \left(M_{xx}+\Delta M_{xx}\right)\frac{\partial\delta\Delta w}{\partial x}\Big|_{x=0}^{x=a}\mathrm{d}y \\
& -2\left(M_{xy}+\Delta M_{xy}\right)\delta\Delta w\Big|_{x=0}^{x=a}\Big|_{y=0}^{y=b}
\end{aligned}
$$

where N_{xx} and N_{yy} are the internal axial forces in the x and y directions and N_{xy} are the internal shear force in the xy plane; M_{xx} and M_{yy} are the internal bending moments along

x and y axes and M_{xy} is the internal torsional bending moment; a and b are the length and width of the panel (see Fig. 7.1). The external virtual work is given by

$$
\begin{aligned}
\delta V = & -\int_0^a\int_0^b \left(q_z + \Delta q_z\right)\delta\Delta w \mathrm{d}x\mathrm{d}y \\
& + \int_0^b \left(N_{xx}^i + \Delta N_{xx}^i\right)\delta\Delta u(x,y)\Big|_{x=0}^{x=a}\mathrm{d}y + \int_0^a \left(N_{yy}^i + \Delta N_{yy}^i\right)\delta\Delta v(x,y)\Big|_{y=0}^{y=b}\mathrm{d}x \\
& + \int_0^b \left(N_{xy}^i + \Delta N_{xy}^i\right)\delta\Delta v(x,y)\Big|_{x=0}^{x=a}\mathrm{d}y + \int_0^a \left(N_{yx}^i + \Delta N_{yx}^i\right)\delta\Delta u(x,y)\Big|_{y=0}^{y=b}\mathrm{d}x \\
& + \int_0^b \left(M_{xx}^i + \Delta M_{xx}^i\right)\frac{\partial\delta\Delta w}{\partial x}(x,y)\Big|_{x=0}^{x=a}\mathrm{d}y + \int_0^a \left(M_{yy}^i + \Delta M_{yy}^i\right)\frac{\partial\delta\Delta w}{\partial y}(x,y)\Big|_{y=0}^{y=b}\mathrm{d}x \\
& + \int_0^b \left(Q_{xx}^i + \Delta Q_{xx}^i\right)\delta\Delta w(x,y)\Big|_{x=0}^{x=a}\mathrm{d}y + \int_0^a \left(Q_{yy}^i + \Delta Q_{yy}^i\right)\delta\Delta w(x,y)\Big|_{y=0}^{y=b}\mathrm{d}x
\end{aligned}
\tag{7.5}
$$

where q_z is the out-of-plane distributed load applied perpendicular to the top surface of the panel throughout the whole area; N_{xx}^i, N_{xy}^i, M_{xx}^i and Q_{xx}^i are the external axial loads, in-plane shear forces, bending moments and shear forces applied at the boundaries $x = 0$ and $x = a$ ($i = 0$ at $x = 0$ and $i = a$ at $x = a$); N_{yy}^i, N_{yx}^i, M_{yy}^i and Q_{yy}^i are the external axial loads, in-plane shear forces, bending moments and shear forces applied at the boundaries $y = 0$ and $y = b$ ($i = 0$ at $y = b$ and $i = a$ at $y = b$). By substituting Eq.(7.4) and Eq.(7.5) back into Eq. (7.3), the incremental equilibrium equations can be obtained as

$$\frac{\partial\Delta N_{xx}}{\partial x} + \frac{\partial\Delta N_{xy}}{\partial y} = 0 \tag{7.6}$$

$$\frac{\partial\Delta N_{yy}}{\partial y} + \frac{\partial\Delta N_{xy}}{\partial x} = 0 \tag{7.7}$$

$$
\begin{aligned}
& N_{xx}\frac{\partial^2\Delta w}{\partial x^2} + \Delta N_{xx}\frac{\partial^2 w}{\partial x^2} + \Delta N_{xx}\frac{\partial^2\Delta w}{\partial x^2} + N_{yy}\frac{\partial^2\Delta w}{\partial y^2} + \Delta N_{yy}\frac{\partial^2 w}{\partial y^2} + \Delta N_{yy}\frac{\partial^2\Delta w}{\partial x^2} \\
& + 2N_{xy}\frac{\partial^2\Delta w}{\partial x\partial y} + 2\Delta N_{xy}\frac{\partial^2 w}{\partial x\partial y} + 2\Delta N_{xy}\frac{\partial^2\Delta w}{\partial x\partial y} + \frac{\partial^2\Delta M_{xx}}{\partial x^2} + \frac{\partial^2\Delta M_{yy}}{\partial y^2} + 2\frac{\partial^2\Delta M_{xy}}{\partial x\partial y} + q = 0
\end{aligned}
\tag{7.8}
$$

The general boundary conditions at $x = 0$ and $x = a$ are given by

$$\begin{aligned}
&\Delta N_{xx} + \Delta N^{i}_{xx} = 0 && \text{or} && \Delta u = \Delta \overline{u} \\
&\Delta N_{xy} + \Delta N^{i}_{xy} = 0 && \text{or} && \Delta v = \Delta \overline{v} \\
&\Delta M_{xx} - \Delta M^{i}_{xx} = 0 && \text{or} && \frac{\partial \Delta w}{\partial x} = \frac{\partial \Delta \overline{w}}{\partial x} \\
&N_{xx}\frac{\partial \Delta w}{\partial x} + \Delta N_{xx}\frac{\partial w}{\partial x} + \Delta N_{xx}\frac{\partial \Delta w}{\partial x} + N_{xy}\frac{\partial \Delta w}{\partial y} + \Delta N_{xy}\frac{\partial w}{\partial y} + \Delta N_{xy}\frac{\partial \Delta w}{\partial y} \\
&+\frac{\partial \Delta M_{xx}}{\partial x} + 2\frac{\partial \Delta M_{xy}}{\partial y} + \Delta Q^{i}_{xx} = 0 && \text{or} && \Delta w = \Delta \overline{w}
\end{aligned} \tag{7.9}$$

where $\overline{u}$, $\overline{v}$, and $\overline{w}$ are the external deformations at the edges; and $i = 0$ at $x = 0$ and $i = a$ at $x = a$. The general boundary conditions at $y = 0$ and $y = b$ are given by

$$\begin{aligned}
&\Delta N_{yy} + \Delta N^{i}_{yy} = 0 && \text{or} && \Delta v = \Delta \overline{v} \\
&\Delta N_{xy} + \Delta N^{i}_{yx} = 0 && \text{or} && \Delta u = \Delta \overline{u} \\
&\Delta M_{yy} - \Delta M^{i}_{yy} = 0 && \text{or} && \frac{\partial \Delta w}{\partial x} = \frac{\partial \Delta \overline{w}}{\partial x} \\
&N_{yy}\frac{\partial \Delta w}{\partial y} + \Delta N_{yy}\frac{\partial w}{\partial y} + \Delta N_{yy}\frac{\partial \Delta w}{\partial y} + N_{xy}\frac{\partial \Delta w}{\partial x} + \Delta N_{xy}\frac{\partial w}{\partial x} + \Delta N_{xy}\frac{\partial \Delta w}{\partial x} \\
&+\frac{\partial \Delta M_{yy}}{\partial y} + 2\frac{\partial \Delta M_{xy}}{\partial x} + \Delta Q^{i}_{yy} = 0 && \text{or} && \Delta w = \Delta \overline{w}
\end{aligned} \tag{7.10}$$

where $\overline{u}$, $\overline{v}$ and $\overline{w}$ are the external deformations at the edges; and $i = 0$ at $y = 0$ and $i = b$ at $y = b$.

7.2.3 Constitutive relations at material point level

As mentioned before, the concrete is considered to be linear viscoelastic in order to highlight the creep effects on the long-term behaviour of HSC panels. The steel reinforcement is modelled as elastic at this stage. A rheological model which is based on the generalized Maxwell chain is used to formulate the long-term constitutive relation of concrete (Bažant and Wu 1974). The relaxation moduli can be approximated as follows:

$$R_{xx}(t,t') = \frac{E_c}{(1-\nu)\left[1+\varphi(t,t')\right]} \tag{7.11}$$

$$R_{yy}(t,t') = \frac{E_c}{(1-\nu)\left[1+\varphi(t,t')\right]} \tag{7.12}$$

$$R_{xy}(t,t') = \frac{G_c}{1+\varphi(t,t')} \tag{7.13}$$

where $R_{xx}(t,t')$, $R_{yy}(t,t')$ and $R_{xy}(t,t')$ are the relaxation moduli in x and y directions and xy plane; $\varphi(t,t')$ is the creep coefficient of the concrete at time t for a load applied at time t'; E_c and G_c are the elastic and shear moduli of concrete, and their correlation is given by

$$G_c = \frac{E_c}{2(1+\nu)} \tag{7.14}$$

where ν is the Poisson's ratio, which is assumed to be time-independent in this study (Bazant 1988). Thus, due to the lack of experimental data regarding the creep behavior of concrete in shear, the latter is assumed to be similar to the creep behavior under normal stresses. The relaxation moduli can be expanded into Dirichlet series as follows (Bažant and Wu 1974):

$$R_{xx}(t,t') \approx \overline{R}_{xx}(t,t') = \sum_{\mu=1}^{m} E_\mu e^{-(t-t')/\tau_\mu} + E_{m+1} \tag{7.15}$$

$$R_{yy}(t,t') \approx \overline{R}_{yy}(t,t') = \sum_{\mu=1}^{m} E_\mu e^{-(t-t')/\tau_\mu} + E_{m+1} \tag{7.16}$$

$$R_{xy}(t,t') \approx \overline{R}_{xy}(t,t') = \sum_{\mu=1}^{m} G_\mu e^{-(t-t')/\tau_\mu} + G_{m+1} \tag{7.17}$$

where $\overline{R}_{xx}$, $\overline{R}_{yy}$ and $\overline{R}_{xy}$ are the approximated relaxation moduli; E_μ and G_μ are the moduli of the μth spring in the Maxwell chain for the modelling in the normal and shear directions; m is the number of units; τ_μ is the relaxation time of the μth unit. Note again that in this study, m and τ_μ are assumed to be identical in the normal and shear directions for simplicity, respectively.

Following the subdivision of the time of concern into a number of time steps, the incremental constitutive relations of plane stress state can be formulated as follows, which are based on numerical time integration

$$\Delta\sigma_{xx}(t_r) = \frac{E''(t_r)}{1-\nu^2}\left[\Delta\varepsilon_{xx}(t_r) - \Delta\varepsilon''_{xx}(t_r) + \nu\left(\Delta\varepsilon_{yy}(t_r) - \Delta\varepsilon''_{yy}(t_r)\right)\right] \tag{7.18}$$

$$\Delta\sigma_{yy}(t_r) = \frac{E''(t_r)}{1-\nu^2}\left[\Delta\varepsilon_{yy}(t_r) - \Delta\varepsilon''_{yy}(t_r) + \nu\left(\Delta\varepsilon_{xx}(t_r) - \Delta\varepsilon''_{xx}(t_r)\right)\right] \tag{7.19}$$

$$\Delta\sigma_{xy}(t_r) = G''(t_r)\left(\Delta\gamma_{xy}(t_r) - \Delta\gamma''_{xy}(t_r)\right) \tag{7.20}$$

where $E''_c\ (t_r)$ and $G''(t_r)$ are the pseudo normal and shear moduli, and $\Delta\varepsilon''_{xx}(t_r)$, $\Delta\varepsilon''_{yy}(t_r)$ and $\Delta\gamma''_{xy}(t_r)$ are the incremental prescribed normal strains in *x* and *y* directions and shear strain in the *xy* plane that includes the effects of creep and shrinkage. These are given by

$$E''(t_r) = \sum_{\mu=1}^{m}\left(1 - e^{-\Delta t_r/\tau_\mu}\right)\frac{\tau_\mu}{\Delta t_r}E_\mu + E_{m+1} \tag{7.21}$$

$$G''(t_r) = \sum_{\mu=1}^{m}\left(1 - e^{-\Delta t_r/\tau_\mu}\right)\frac{\tau_\mu}{\Delta t_r}G_\mu + G_{m+1} \tag{7.22}$$

$$\Delta\varepsilon''_{xx}(t_r) = \frac{1}{E''(t_r)}\sum_{\mu=1}^{m}\left(1 - e^{-\Delta t_r/\tau_\mu}\right)\left[\sigma_\mu^{xx}(t_{r-1}) - \nu\sigma_\mu^{yy}(t_{r-1})\right] + \Delta\varepsilon_{sh} \tag{7.23}$$

$$\Delta\varepsilon''_{yy}(t_r) = \frac{1}{E''(t_r)}\sum_{\mu=1}^{m}\left(1 - e^{-\Delta t_r/\tau_\mu}\right)\left[\sigma_\mu^{yy}(t_{r-1}) - \nu\sigma_\mu^{xx}(t_{r-1})\right] + \Delta\varepsilon_{sh} \tag{7.24}$$

$$\Delta\gamma''_{xy} = \frac{1}{G''(t_r)}\sum_{\mu=1}^{m}\left(1 - e^{-\Delta t_r/\tau_\mu}\right)\sigma_\mu^{xy}(t_{r-1}) \tag{7.25}$$

$$\sigma_\mu^{xx}(t_r) = e^{-\Delta t_r/\tau_\mu}\sigma_\mu^{xx}(t_{r-1}) + \frac{E_\mu}{1-\nu^2}\left[\Delta\varepsilon_{xx}(t_r) + \nu\Delta\varepsilon_{yy}(t_r)\right]\left(1 - e^{-\Delta t_r/\tau_\mu}\right)\frac{\tau_\mu}{\Delta t_r} \tag{7.26}$$

$$\sigma_\mu^{yy}(t_r) = e^{-\Delta t_r/\tau_\mu}\sigma_\mu^{yy}(t_{r-1}) + \frac{E_\mu}{1-\nu^2}\left[\Delta\varepsilon_{yy}(t_r) + \nu\Delta\varepsilon_{xx}(t_r)\right]\left(1 - e^{-\Delta t_r/\tau_\mu}\right)\frac{\tau_\mu}{\Delta t_r} \tag{7.27}$$

$$\sigma_\mu^{xy}(t_r) = e^{-\Delta t_r/\tau_\mu}\sigma_\mu^{xy}(t_{r-1}) + G_\mu\Delta\gamma_{xy}(t_r)\left(1 - e^{-\Delta t_r/\tau_\mu}\right)\frac{\tau_\mu}{\Delta t_r} \tag{7.28}$$

where σ_μ^{xx} , σ_μ^{yy} and σ_μ^{xy} are the stresses in the μth Maxwell unit and ε_{sh} is the shrinkage strain which is assumed to be uniform in the x and y directions, as well as through the thickness of the panel. Based on Eq. (7.14), the following relations are obtained for $G''(t_r)$ and G_μ

$$G''(t_r) = \frac{E''(t_r)}{2(1+\nu)} \tag{7.29}$$

$$G_\mu = \frac{E_\mu}{2\left(1+\nu\right)} \tag{7.30}$$

7.2.4 Constitutive relations at section level

The constitutive relations at the cross-section level of the panel are determined using the classical definition of stress resultants and using the constitutive relations Eq. (7.18)-(7.20) as follows:

$$\begin{aligned}\Delta N_{xx}(t_r) &= \int_{-\frac{h}{2}}^{\frac{h}{2}} \Delta\sigma_{xx}(t_r)\mathrm{d}z \\ &= \int_{-\frac{h}{2}}^{\frac{h}{2}} \frac{E''(t_r)}{1-\nu^2}\left[\Delta\varepsilon_{xx}(t_r) - \Delta\varepsilon''_{xx}(t_r) + \nu\left(\Delta\varepsilon_{yy}(t_r) - \Delta\varepsilon''_{yy}(t_r)\right)\right]\mathrm{d}z\end{aligned} \tag{7.31}$$

$$\begin{aligned}\Delta N_{yy}(t_r) &= \int_{-\frac{h}{2}}^{\frac{h}{2}} \Delta\sigma_{yy}(t_r)\mathrm{d}z \\ &= \int_{-\frac{h}{2}}^{\frac{h}{2}} \frac{E''(t_r)}{1-\nu^2}\left[\Delta\varepsilon_{yy}(t_r) - \Delta\varepsilon''_{yy}(t_r) + \nu\left(\Delta\varepsilon_{xx}(t_r) - \Delta\varepsilon''_{xx}(t_r)\right)\right]\mathrm{d}z\end{aligned} \tag{7.32}$$

$$\begin{aligned}\Delta N_{xy}(t_r) &= \int_{-\frac{h}{2}}^{\frac{h}{2}} \Delta\sigma_{xy}(t_r)\mathrm{d}z \\ &= \int_{-\frac{h}{2}}^{\frac{h}{2}} \frac{E''(t_r)}{2(1+\nu)}\left(\Delta\gamma_{xy}(t_r) - \Delta\gamma''_{xy}(t_r)\right)\mathrm{d}z\end{aligned} \tag{7.33}$$

$$\begin{aligned}\Delta M_{xx}(t_r) &= \int_{-\frac{h}{2}}^{\frac{h}{2}} \Delta\sigma_{xx}(t_r)z\mathrm{d}z \\ &= \int_{-\frac{h}{2}}^{\frac{h}{2}} \frac{E''(t_r)z}{1-\nu^2}\left[\Delta\varepsilon_{xx}(t_r) - \Delta\varepsilon''_{xx}(t_r) + \nu\left(\Delta\varepsilon_{yy}(t_r) - \Delta\varepsilon''_{yy}(t_r)\right)\right]\mathrm{d}z\end{aligned} \tag{7.34}$$

$$\begin{aligned}\Delta M_{yy}(t_r) &= \int_{-\frac{h}{2}}^{\frac{h}{2}} \Delta\sigma_{yy}(t_r)z\mathrm{d}z \\ &= \int_{-\frac{h}{2}}^{\frac{h}{2}} \frac{E''(t_r)z}{1-\nu^2}\left[\Delta\varepsilon_{yy}(t_r) - \Delta\varepsilon''_{yy}(t_r) + \nu\left(\Delta\varepsilon_{xx}(t_r) - \Delta\varepsilon''_{xx}(t_r)\right)\right]\mathrm{d}z\end{aligned} \tag{7.35}$$

$$\Delta M_{xy}(t_r) = \int_{-\frac{h}{2}}^{\frac{h}{2}} \Delta\sigma_{xy}z\mathrm{d}z = \int_{-\frac{h}{2}}^{\frac{h}{2}} \frac{E''(t_r)z}{2(1+\nu)}\left(\Delta\gamma_{xy}(t_r) - \Delta\gamma''_{xy}(t_r)\right)\mathrm{d}z \tag{7.36}$$

where h is the thickness of the panel. Note that the forces and bending moments are defined as the distributions of these quantities per unit length. By substituting the kinematic relations Eq.(7.1) into Eqs.(7.31)-(7.36), the stress resultants become

$$\Delta N_{xx}(t_r) = C''\left[\begin{array}{l}\dfrac{\partial\Delta u}{\partial x} + \dfrac{1}{2}\left(\dfrac{\partial\Delta w}{\partial x}\right)^2 + \dfrac{\partial w(t_{r-1})}{\partial x}\dfrac{\partial\Delta w}{\partial x} \\ +\nu\left(\dfrac{\partial\Delta v}{\partial y} + \dfrac{1}{2}\left(\dfrac{\partial\Delta w}{\partial y}\right)^2 + \dfrac{\partial w(t_{r-1})}{\partial y}\dfrac{\partial\Delta w}{\partial y}\right)\end{array}\right] - \Delta\bar{N}_{xx}(t_r) \tag{7.37}$$

$$\Delta N_{yy}(t_r) = C'' \left[\begin{array}{l} \dfrac{\partial \Delta v}{\partial y} + \dfrac{1}{2}\left(\dfrac{\partial \Delta w}{\partial y}\right)^2 + \dfrac{\partial w(t_{r-1})}{\partial y}\dfrac{\partial \Delta w}{\partial y} \\ +\nu\left(\dfrac{\partial \Delta u}{\partial x} + \dfrac{1}{2}\left(\dfrac{\partial \Delta w}{\partial x}\right)^2 + \dfrac{\partial w(t_{r-1})}{\partial x}\dfrac{\partial \Delta w}{\partial x}\right) \end{array} \right] - \Delta \bar{N}_{yy}(t_r) \tag{7.38}$$

$$\Delta N_{xy}(t_r) = \frac{1-\nu}{2} C'' \left[\begin{array}{l} \dfrac{\partial \Delta u}{\partial y} + \dfrac{\partial \Delta v}{\partial x} + \dfrac{\partial w(t_{r-1})}{\partial x}\dfrac{\partial \Delta w}{\partial y} \\ + \dfrac{\partial w(t_{r-1})}{\partial y}\dfrac{\partial \Delta w}{\partial x} + \dfrac{\partial \Delta w}{\partial x}\dfrac{\partial \Delta w}{\partial y} \end{array} \right] - \Delta \bar{N}_{xy}(t_r) \tag{7.39}$$

$$\Delta M_{xx}(t_r) = -D''\left(\frac{\partial^2 \Delta w}{\partial x^2} + \nu \frac{\partial^2 \Delta w}{\partial y^2}\right) - \Delta \bar{M}_{xx}(t_r) \tag{7.40}$$

$$\Delta M_{yy}(t_r) = -D''\left(\frac{\partial^2 \Delta w}{\partial y^2} + \nu \frac{\partial^2 \Delta w}{\partial x^2}\right) - \Delta \bar{M}_{yy}(t_r) \tag{7.41}$$

$$\Delta M_{xy}(t_r) = -(1-\nu) D'' \frac{\partial^2 \Delta w}{\partial x \partial y} - \Delta \bar{M}_{xy}(t_r) \tag{7.42}$$

where C'' and D'' are axial and flexural viscoelastic rigidities of the two-way panel; $\Delta\bar{N}_{xx}(t_r)$, $\Delta\bar{N}_{yy}(t_r)$ are the incremental effective axial forces in the x and y directions and $\Delta\bar{N}_{xy}(t_r)$ is the incremental effective shear force in the xy plane; $\Delta M_{xx}(t_r)$ and $\Delta M_{yy}(t_r)$ are the incremental effective bending moments along x and y axis and $\Delta M_{xy}(t_r)$ is the incremental effective torsional bending moment. The viscoelastic rigidities, which account for the internal reinforcement, are given by

$$C'' = \frac{E''}{1-\nu^2}\left[h + (n-1)A_{sx}/b + (n-1)A'_{sx}/b\right] \tag{7.43}$$

$$D'' = \frac{E''}{1-\nu^2}\left[\frac{h^3}{12} + (n-1)A_s z_{sx}^2/b + (n-1)A'_s z'^2_{sx}/b\right] \tag{7.44}$$

where $n = E_s / E''$, E_s is elastic modulus of steel reinforcement; A_{sx} and A'_{sx} are the areas of the steel reinforcements at the inner and outer faces of the panel in the x direction; z_{sx}

and z'_{sx} are the locations of the corresponding reinforcements measured from the mid-thickness of the panel. Note that the total reinforcement ratio and their locations in the x and y direction are assumed to be the same in this study. The effective forces and bending moments are given as

$$\begin{aligned}\Delta\bar{N}_{xx}(t_r) &= \int_{-\frac{h}{2}}^{\frac{h}{2}} \frac{E''(t_r)}{1-\nu^2}\left[\Delta\varepsilon''_{xx}(t_r)+\nu\Delta\varepsilon''_{yy}(t_r)\right]\mathrm{d}z \\ &= \int_{-\frac{h}{2}}^{\frac{h}{2}} \sum_{\mu=1}^{m}\left(1-e^{-\Delta t_r/\tau_\mu}\right)\sigma_\mu^{xx}(t_{r-1})\mathrm{d}z + \int_{-\frac{h}{2}}^{\frac{h}{2}} \frac{E''(t_r)}{1-\nu}\Delta\varepsilon_{sh}\mathrm{d}z \\ &= \sum_{\mu=1}^{m}\left(1-e^{-\Delta t_r/\tau_\mu}\right)N_\mu^{xx}(t_{r-1}) + \int_{-\frac{h}{2}}^{\frac{h}{2}} \frac{E''(t_r)}{1-\nu}\Delta\varepsilon_{sh}\mathrm{d}z\end{aligned} \tag{7.45}$$

$$\begin{aligned}\Delta\bar{N}_{yy}(t_r) &= \int_{-\frac{h}{2}}^{\frac{h}{2}} \frac{E''(t_r)}{1-\nu^2}\left[\Delta\varepsilon''_{yy}(t_r)+\nu\Delta\varepsilon''_{xx}(t_r)\right]\mathrm{d}z \\ &= \int_{-\frac{h}{2}}^{\frac{h}{2}} \sum_{\mu=1}^{m}\left(1-e^{-\Delta t_r/\tau_\mu}\right)\sigma_\mu^{yy}(t_{r-1})\mathrm{d}z + \int_{-\frac{h}{2}}^{\frac{h}{2}} \frac{E''(t_r)}{1-\nu}\Delta\varepsilon_{sh}\mathrm{d}z \\ &= \sum_{\mu=1}^{m}\left(1-e^{-\Delta t_r/\tau_\mu}\right)N_\mu^{yy}(t_{r-1}) + \int_{-\frac{h}{2}}^{\frac{h}{2}} \frac{E''(t_r)}{1-\nu}\Delta\varepsilon_{sh}\mathrm{d}z\end{aligned} \tag{7.46}$$

$$\begin{aligned}\Delta\bar{N}_{xy}(t_r) &= \int_{-\frac{h}{2}}^{\frac{h}{2}} \frac{E''(t_r)}{2\left(1+\nu\right)}\Delta\gamma''_{xy}(t_r)\mathrm{d}z \\ &= \int_{-\frac{h}{2}}^{\frac{h}{2}} \sum_{\mu=1}^{m}\left(1-e^{-\Delta t_r/\tau_\mu}\right)\sigma_\mu^{xy}(t_{r-1})\mathrm{d}z + \int_{-\frac{h}{2}}^{\frac{h}{2}} \frac{E''(t_r)}{2(1+\nu)}\Delta\varepsilon_{sh}\mathrm{d}z \\ &= \sum_{\mu=1}^{m}\left(1-e^{-\Delta t_r/\tau_\mu}\right)N_\mu^{xy}(t_{r-1}) + \int_{-\frac{h}{2}}^{\frac{h}{2}} \frac{E''(t_r)}{2(1+\nu)}\Delta\varepsilon_{sh}\mathrm{d}z\end{aligned} \tag{7.47}$$

$$\begin{aligned}\Delta\bar{M}_{xx}(t_r) &= \int_{-\frac{h}{2}}^{\frac{h}{2}} \frac{E''(t_r)}{1-\nu^2} z\left[\Delta\varepsilon''_{xx}(t_r)+\nu\Delta\varepsilon''_{yy}(t_r)\right]\mathrm{d}z \\ &= \int_{-\frac{h}{2}}^{\frac{h}{2}} \sum_{\mu=1}^{m}\left(1-e^{-\Delta t_r/\tau_\mu}\right)\sigma_\mu^{xx}(t_{r-1})z\mathrm{d}z + \int_{-\frac{h}{2}}^{\frac{h}{2}} \frac{E''(t_r)z}{1-\nu}\Delta\varepsilon_{sh}\mathrm{d}z \\ &= \sum_{\mu=1}^{m}\left(1-e^{-\Delta t_r/\tau_\mu}\right)M_\mu^{xx}(t_{r-1}) + \int_{-\frac{h}{2}}^{\frac{h}{2}} \frac{E''(t_r)z}{1-\nu}\Delta\varepsilon_{sh}\mathrm{d}z\end{aligned} \tag{7.48}$$

$$\begin{aligned}\Delta\bar{M}_{yy}(t_r) &= \int_{-\frac{h}{2}}^{\frac{h}{2}} \frac{E''(t_r)}{1-\nu^2} z\left[\Delta\varepsilon''_{yy}(t_r)+\nu\Delta\varepsilon''_{xx}(t_r)\right]\mathrm{d}z \\ &= \int_{-\frac{h}{2}}^{\frac{h}{2}} \sum_{\mu=1}^{m}\left(1-e^{-\Delta t_r/\tau_\mu}\right)\sigma_\mu^{yy}(t_{r-1})z\mathrm{d}z + \int_{-\frac{h}{2}}^{\frac{h}{2}} \frac{E''(t_r)z}{1-\nu}\Delta\varepsilon_{sh}\mathrm{d}z \\ &= \sum_{\mu=1}^{m}\left(1-e^{-\Delta t_r/\tau_\mu}\right)M_\mu^{yy}(t_{r-1}) + \int_{-\frac{h}{2}}^{\frac{h}{2}} \frac{E''(t_r)z}{1-\nu}\Delta\varepsilon_{sh}\mathrm{d}z\end{aligned} \tag{7.49}$$

$$\begin{aligned}\Delta\bar{M}_{xy}(t_r) &= \int_{-\frac{h}{2}}^{\frac{h}{2}} \frac{E''(t_r)}{2\left(1+\nu\right)} z\Delta\gamma''_{xy}(t_r)\mathrm{d}z \\ &= \int_{-\frac{h}{2}}^{\frac{h}{2}} \sum_{\mu=1}^{m}\left(1-e^{-\Delta t_r/\tau_\mu}\right)\sigma_\mu^{xy}(t_{r-1})z\mathrm{d}z + \int_{-\frac{h}{2}}^{\frac{h}{2}} \frac{E''(t_r)}{2(1+\nu)}\Delta\varepsilon_{sh}\mathrm{d}z \\ &= \sum_{\mu=1}^{m}\left(1-e^{-\Delta t_r/\tau_\mu}\right)M_\mu^{xy}(t_{r-1}) + \int_{-\frac{h}{2}}^{\frac{h}{2}} \frac{E''(t_r)z}{2(1+\nu)}\Delta\varepsilon_{sh}\mathrm{d}z\end{aligned} \tag{7.50}$$

By substituting Eqs. (7.26)-(7.28) into Eqs. (7.45)-(7.50) along with using Eqs. (7.18)-(7.20) and Eqs. (7.23)-(7.25), N_μ^{xx}, N_μ^{yy}, N_μ^{xy}, M_μ^{xx}, M_μ^{yy} and M_μ^{xy} can be determined as

$$N_\mu^{xx}(t_r) = e^{-\Delta t_r/\tau_\mu}N_\mu^{xx}(t_{r-1})+\left(1-e^{-\Delta t_r/\tau_\mu}\right)\frac{\tau_\mu}{\Delta t_r}\frac{E_\mu(t_r)}{E''(t_r)}\left[\Delta N_{xx}(t_r)+\Delta\bar{N}_{xx}(t_r)\right] \tag{7.51}$$

$$N_{\mu}^{yy}(t_r) = e^{-\Delta t_r/\tau_\mu} N_{\mu}^{yy}(t_{r-1}) + \left(1 - e^{-\Delta t_r/\tau_\mu}\right) \frac{\tau_\mu}{\Delta t_r} \frac{E_\mu(t_r)}{E''(t_r)} \left[\Delta N_{yy}(t_r) + \Delta \bar{N}_{yy}(t_r)\right] \quad (7.52)$$

$$N_{\mu}^{xy}(t_r) = e^{-\Delta t_r/\tau_\mu} N_{\mu}^{xy}(t_{r-1}) + \left(1 - e^{-\Delta t_r/\tau_\mu}\right) \frac{\tau_\mu}{\Delta t_{r\text{-}1}} \frac{E_\mu(t_r)}{E''(t_r)} \left[\Delta N_{xy}(t_r) + \Delta \bar{N}_{xy}(t_r)\right] \quad (7.53)$$

$$M_{\mu}^{xx}(t_r) = e^{-\Delta t_r/\tau_\mu} M_{\mu}^{xx}(t_{r-1}) + \left(1 - e^{-\Delta t_r/\tau_\mu}\right) \frac{\tau_\mu}{\Delta t_{r\text{-}1}} \frac{E_\mu(t_r)}{E''(t_r)} \left[\Delta M_{xx}(t_r) + \Delta \bar{M}_{xx}(t_r)\right] \quad (7.54)$$

$$M_{\mu}^{yy}(t_r) = e^{-\Delta t_r/\tau_\mu} M_{\mu}^{yy}(t_{r-1}) + \left(1 - e^{-\Delta t_r/\tau_\mu}\right) \frac{\tau_\mu}{\Delta t_r} \frac{E_\mu(t_r)}{E''(t_r)} \left[\Delta M_{yy}(t_r) + \Delta \bar{M}_{yy}(t_r)\right] \quad (7.55)$$

$$M_{\mu}^{xy}(t_r) = e^{-\Delta t_r/\tau_\mu} M_{\mu}^{xy}(t_{r-1}) + \left(1 - e^{-\Delta t_r/\tau_\mu}\right) \frac{\tau_\mu}{\Delta t_r} \frac{E_\mu(t_r)}{E''(t_r)} \left[\Delta M_{xy}(t_r) + \Delta \bar{M}_{xx}(t_r)\right] \quad (7.56)$$

7.2.5 Governing equations

The incremental governing equations are formulated by substitution of the stress resultants Eqs. (7.37)-(7.42) into the equilibrium equations (7.6)-(7.8), noting that terms of higher product of the incremental displacements and forces are neglected due to the use of sufficiently small time increments. The incremental governing equations are partial differential equations in terms of the unknown displacements:

$$\psi_p\left(\Delta u,\ \Delta v,\ \Delta w\right) = 0 \qquad \left(p = 1,\ 2,\ 3\right) \quad (7.57)$$

where ψ_p consists of differential operators. For brevity, the explicit form of these equations is not presented here.

7.2.6 Solution procedure

The set of incremental partial differential equations (7.57) and the boundary conditions (7.9)-(7.10) are reduced to a set of ordinary differential equations by a separation of variables and expansion into the truncated Fourier series (Hong and Teng 2002; Hamed et al., 2010a).

$$\{\Delta u(x,y),\ \Delta v(x,y),\ \Delta w(x,y)\} = \sum_{m=1}^{2F} \{\Delta u_m(x),\ \Delta v_m(x),\ \Delta w_m(x)\}\, g_m(y) \qquad (7.58)$$

where F = (F_u, F_v, or F_w) is the number of terms in the relevant Fourier series. The solution of the initial state or previous accumulated displacements and the external loads along the panel and at the boundaries take the forms

$$\{u(x,y),\ v(x,y),\ w(x,y)\} = \sum_{m=1}^{2F} \{u_m(x),\ v_m(x),\ w_m(x)\}\, g_m(y) \qquad (7.59)$$

$$\begin{aligned}
\begin{Bmatrix} Q^0_{xx}(x,y),\ Q^a_{xx}(x,y), N^0_{xx}(x,y), \\ N^a_{xx}(x,y), M^0_{xx}(x,y),\ M^a_{xx}(x,y) \end{Bmatrix} &= \sum_{m=1}^{2F} \begin{Bmatrix} Q^0_{xxm}(x),\ Q^a_{xxm}(x), N^0_{xxm}(x), \\ N^a_{xxm}(x), M^0_{xxm}(x),\ M^a_{xxm}(x) \end{Bmatrix} g_m(y) \\
\begin{Bmatrix} Q^0_{yy}(x,y),\ Q^b_{yy}(x,y), N^0_{yy}(x,y), \\ N^b_{yy}(x,y), M^0_{yy}(x,y),\ M^b_{yy}(x,y) \end{Bmatrix} &= \sum_{m=1}^{2F} \begin{Bmatrix} Q^0_{yym}(x),\ Q^b_{yym}(x), N^0_{yym}(x), \\ N^b_{yym}(x), M^0_{yym}(x),\ M^b_{yym}(x) \end{Bmatrix} g_m(y) \qquad (7.60) \\
q_z(x,y) &= \sum_{m=1}^{2F} q_{zm}(x) g_m(y)
\end{aligned}$$

The functions $g_m(y)$ are

$$g_m(y) = \begin{cases} \sin\left(\dfrac{m\pi}{b} y\right) & m = 1, 2, \dots, F \\ \cos\left[\dfrac{(m-F)\pi}{b} y\right] & m = F+1, F+2, \dots, 2F \end{cases} \qquad (7.61)$$

By minimizing the errors due to the truncated Fourier series by the Galerkin procedure with trigonometric weighting functions, the partial differential equations are converted into the linear ordinary differential equations in the x direction,

$$\Psi^m_p(x) = \int_0^b \psi_p(u,\ v,\ w)\, g_m(y) \mathrm{d}y \qquad (p = 1,\ 2,\ 3;\ \ m = 1, 2, \dots, 2F) \qquad (7.62)$$

The governing equations along with the boundary conditions are solved through the use of the multiple shooting method at each time step (Stoer and Bulirsch 2002). Similar to the analysis of one-way panel, the analysis presented here is also conducted up to a certain time (the critical time) where the deformations of the system exceed a prescribed limit (Hoff 1958; Bažant and Cedolin 1991). A proper time step is selected for a given load level in the way that the difference between the predicted critical times of creep buckling for the selected time-step and one-half of it is of minor significance.

7.3 NUMERICAL STUDY

The governing equations derived in Eq. (7.57) and the solution procedures proposed in Eqs. (7.58)-(7.61) are generally applicable for any combinations of loading scenarios and boundary conditions. Nevertheless, to demonstrate the capability of the proposed theoretical model in predicting the time-dependent behavior of HSC panels, a relatively simple case is selected in the numerical study in which the rectangular (or square) panel is simply-supported on four edges and subjected to an in-pane eccentric compression load in the x direction only, as shown in Fig. 7.2.

This section presents the numerical results of two panels where one is square and the other one is rectangular, as well as a parametric study that aims to investigate the effects of the aspect ratio, load level and eccentricity, slenderness ratio, cracking, reinforcement ratio and shrinkage. For simplicity also, only the first term of the Fourier series is considered in deriving the governing equations. For clarity, in all numerical and parametric studies, only the influence of creep is considered, while the effect of shrinkage is separately investigated in Section 7.3.3.8 as one of the parameters.

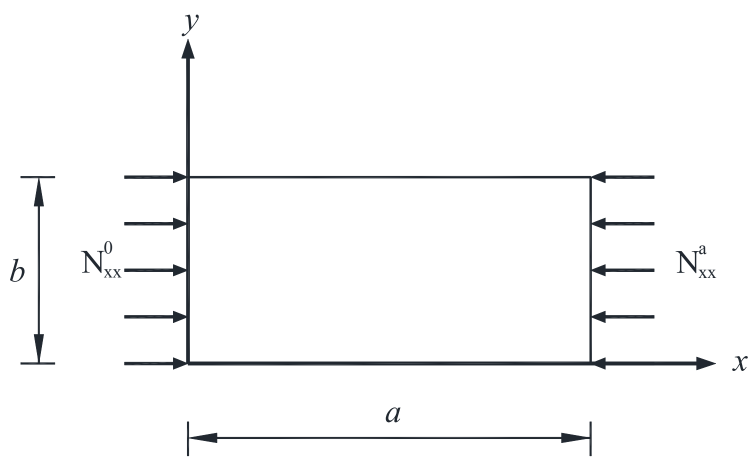

Fig. 7.2 HSC panel used in numerical study: simply-supported on four edges and loaded by uniformly distributed eccentric compression forces in the *x* direction

7.3.1 Numerical Example I: Simply-supported two-way square HSC panel

For a simply-supported rectangular panel subjected to uniform eccentric compression forces in the *x* direction only, the boundary conditions are given by $N^{0}_{xy} = N^{a}_{xy} = N^{b}_{xy} = N^{0}_{yy} = N^{b}_{yy} = 0$ and $N^{0}_{xx} = N^{a}_{xx} \neq 0$ (Fig. 7.2). The panel investigated here is a square one with the dimensions of 2000×2000×100 mm (a×b×h). There are two layers of steel reinforcement in both orthogonal directions, placed at top and bottom of the specimen. The reinforcement ratios in the *x* and *y* directions (ρ_x and ρ_y), where $\rho_x = (A_{sx} + A'_{sx})/bh$ and $\rho_y = (A_{sy} + A'_{sy})/ah$, are both 0.2% and the reinforcement at the top and bottom in each direction are equal. The concrete cover is 20 mm and the elastic modulus of the steel is 200 GPa, respectively. The panel is assumed to be loaded at the age of 28 days after casting with $N^{0}_{xx} = N^{a}_{xx}$ = 20.3 kN/mm, which equals to 60% of the instantaneous buckling load (P_{cr} = 33.9 kN/mm), that is determined according to the classical equation given as (Dym and Shame 2013):

$$P_{cr} = \frac{4D''\pi^2}{b^2} = \frac{4\pi^2}{b^2}\frac{E_c}{1-\nu^2}\left[\frac{h^3}{12} + (n-1)A_{sx}z_{sx}^2/b + (n-1)A'_{sx}z'^2_{sx}/b\right] \qquad (7.63)$$

The load is assumed to be applied at 28 days with an eccentricity of $e = h/6 = 16.7$ mm, which results in edge moments of $M_{xx}^{0} = M_{xx}^{a} = 339$ kNm/m (Fig. 7.1). The development with time of the creep coefficient follows AS3600 (2009) as in Chapter 5, which gives

$$\varphi(t) = \frac{1.45t^{0.8}}{t^{0.8} + 17} \tag{7.64}$$

The number of Maxwell units (m) used to model the viscoelastic behavior of concrete is taken as five in this example with $\tau_{\mu} = 5^{\mu-1}$ (days). The spring constants in the Maxwell model yielded by the least squares methods are $E_1 = 1684$ MPa, $E_2 = 7537$ MPa, $E_3 = 8674$ MPa, $E_4 = 4050$ MPa, $E_5 = 1199$ MPa, $E_6 = 16287$ MPa.

The time-dependent variation of the out-of-plane deflection and the bending moments at the center of the panel are shown in Fig. 7.3 and Fig. 7.4. The time t is measured since the time of first loading. The deflection is normalized with respect to the thickness of the panel h. It can be seen that the deflection of the panel and hence the bending moments M_{xx} and M_{yy} increase with time as a result of the combined effects of creep and geometric nonlinearity. Similar to the one-way panel, the out-of-plane deflection as well as the bending moment tends to asymptotically increase towards infinity beyond a certain time. The criterion for critical time of buckling failure adopted here follows the same definition as in the one-way panel where buckling considered to occur when the normalized out-of-plane deflection (w/h) reaches a given limit. The limit in this numerical study is taken as 4 and the corresponding time, referred to as the critical time, equals 1400 days in this case. As indicated in Fig. 7.4(b), the ratio of M_{xx}/M_{yy} also increases with time, which implies that stress redistribution occurs with time and the influence of the geometric nonlinearity becomes more pronounced in the x direction than in the y direction.

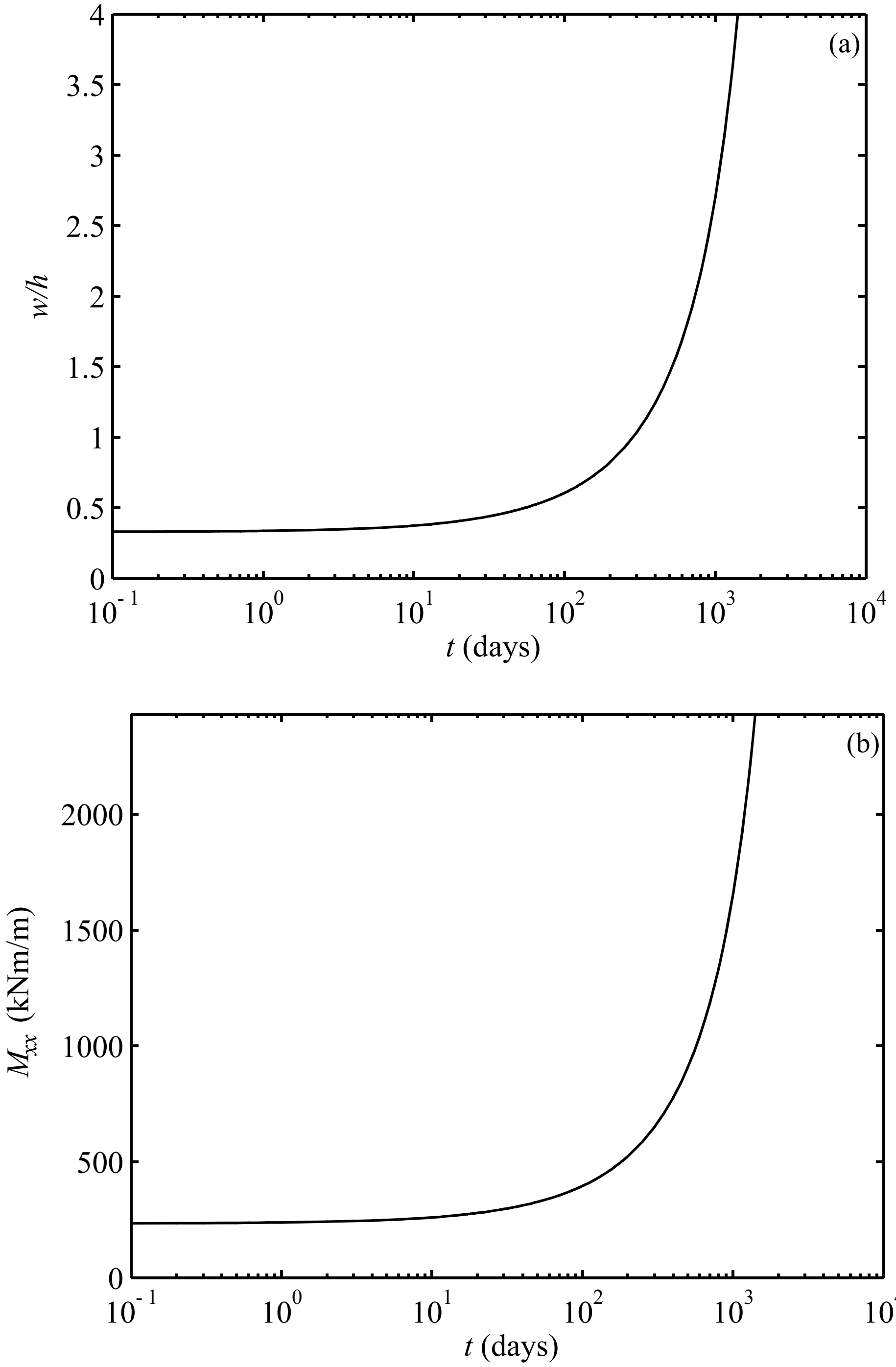

Fig. 7.3 Variation with time of the (a) out-of-plane deflection; (b) bending moment M_{xx} at the center of the panel

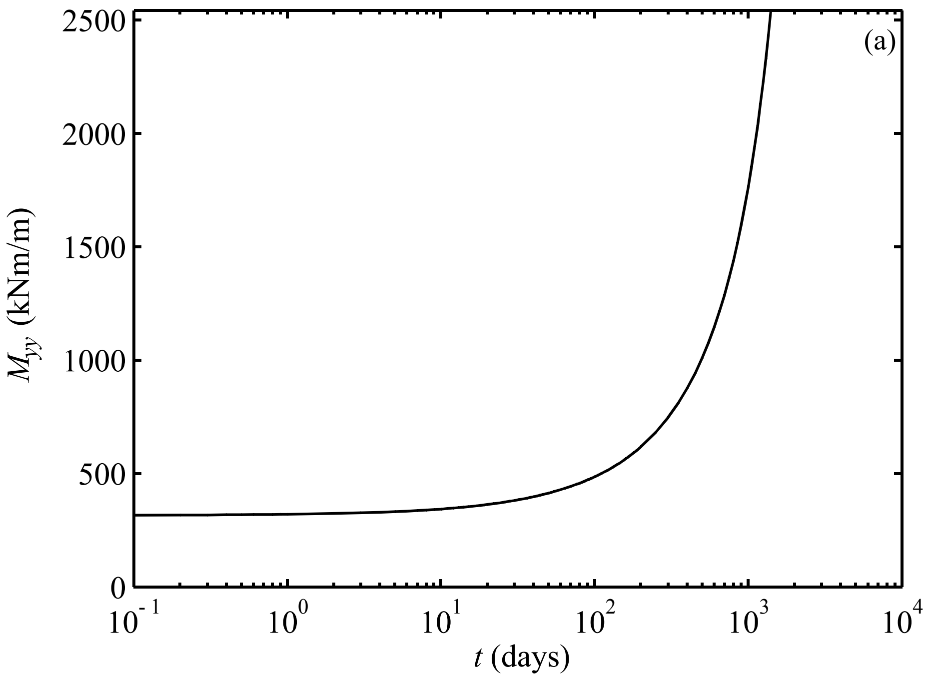

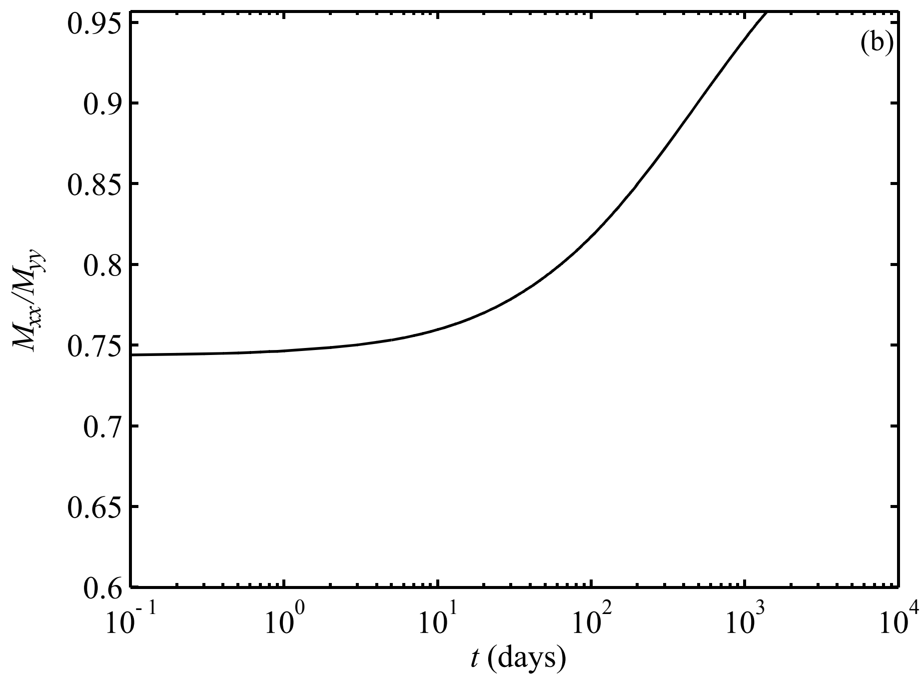

Fig. 7.4 Variation with time of the (a) bending moment M_{yy}; (b) the ratio of M_{xx}/M_{yy} at the center of the panel

7.3.2 Numerical Example II: Simply-supported two-way rectangular HSC panel

The second panel studied here is a more realistic and general one with the dimensions of 5000×3500×150 mm (a×b×h). The material properties, reinforcement ratios along with the boundary conditions are the same as in the first panel. The sustained load level is 60% of its own elastic buckling load, which equals 22.4 kN/mm. The eccentricities at both edges are $h/6$, which equals to 25 mm. The time-dependent variation of the out-of-plane deflection and the bending moments at the center of the panel are shown in Fig. 7.5 and Fig. 7.6. Similar to the first panel, this panel also undergoes increased deflection with time due to creep and geometric nonlinearity. It fails by creep buckling as well at t = 4900 days.

The out-of-plane deflection distribution and the bending moments M_{xx} and M_{yy} distribution along x and y directions at various times are shown in Fig. 7.7-Fig. 7.9. The result shows that the time-dependent increase of the out-of-plane deflection caused significant increase of bending moments in both x and y directions. It also demonstrates the ability of the proposed theoretical model in predicting and describing the time-dependent response of thin panels. It is clear by inspecting Fig. 7.8(a) that due to the creep and geometric nonlinearity, the bending moment M_{xx} is increasing with time and at some time, the maximum bending moment may appear at the center rather than at the edges which is the location of maximum M_{xx} for the panel under instantaneous loading. The shift of the maximum M_{xx} from the edges to the middle as time goes should be carefully taken into consideration in designing the concrete panels as the maximum bending moments in the x direction appear at different locations for short-term response and long-term response. Failure to do so may result in unexpected serviceability problems such as excessive deflection and concrete cracking etc., or even structural failure in the long run.

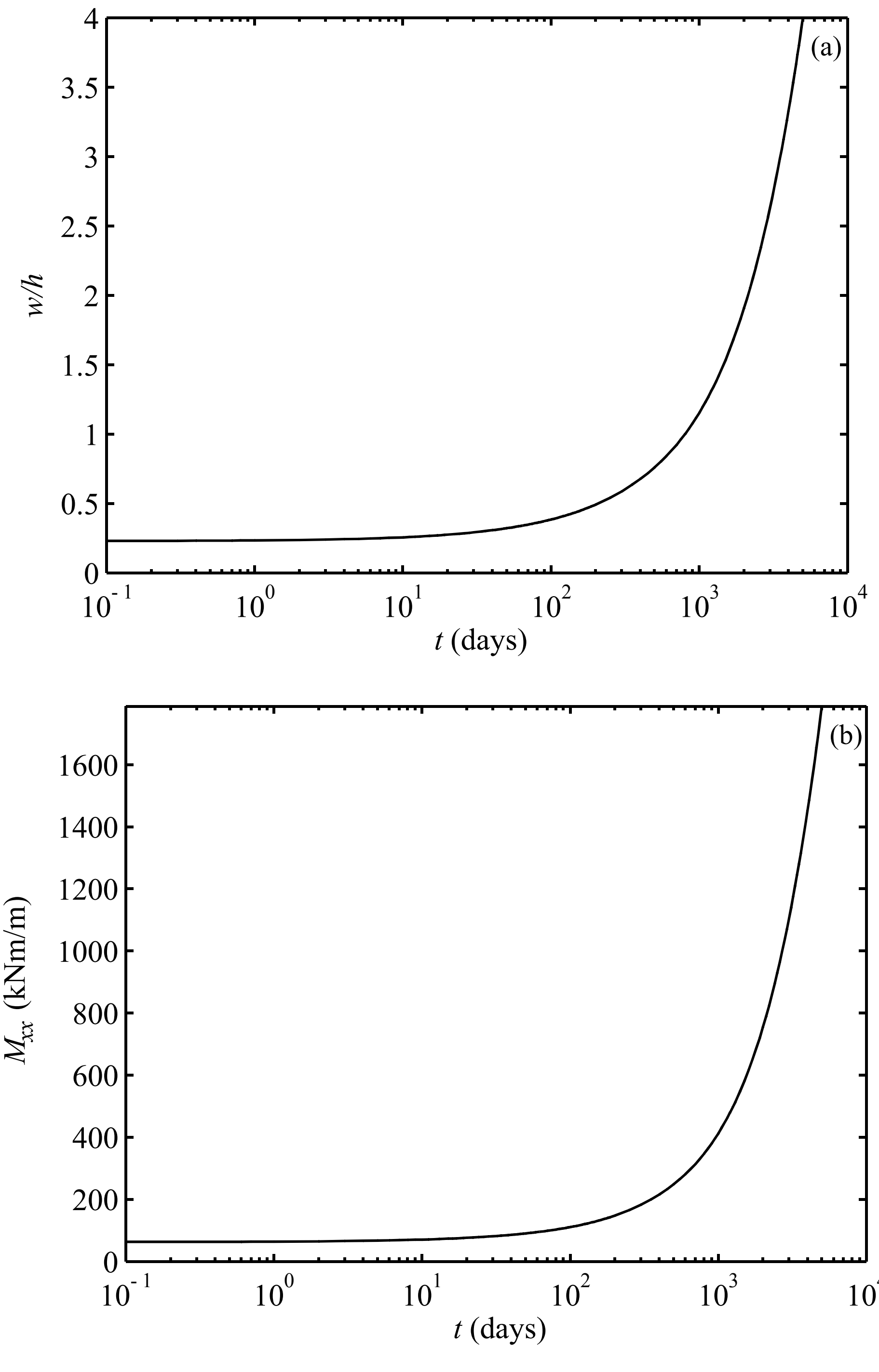

Fig. 7.5 Variation with time of the (a) out-of-plane deflection; (b) bending moment M_{xx} at the center of the panel

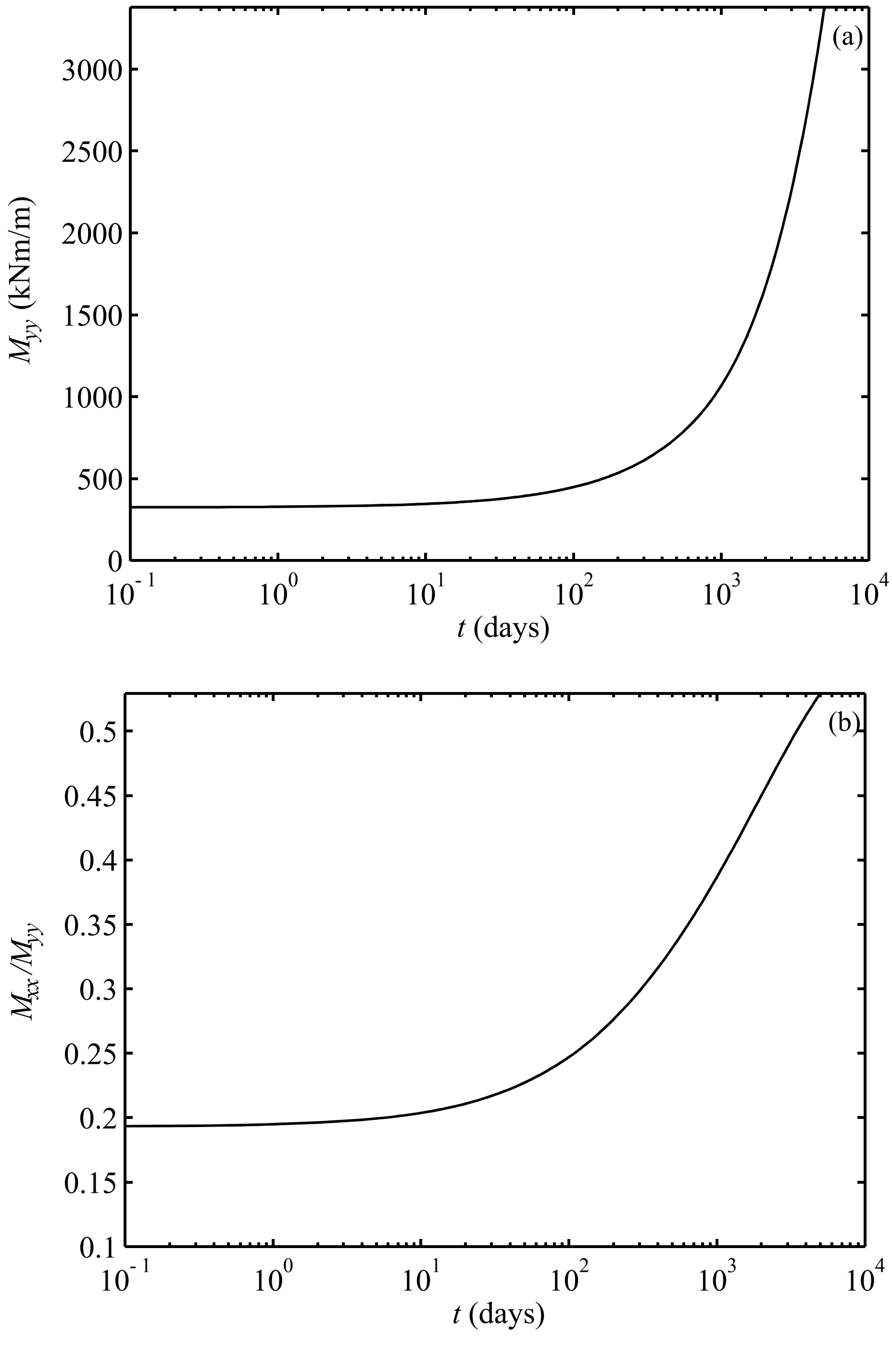

Fig. 7.6 Variation with time of the (a) bending moment M_{yy}; (b) the ratio of M_{xx}/M_{yy} at the center of the panel

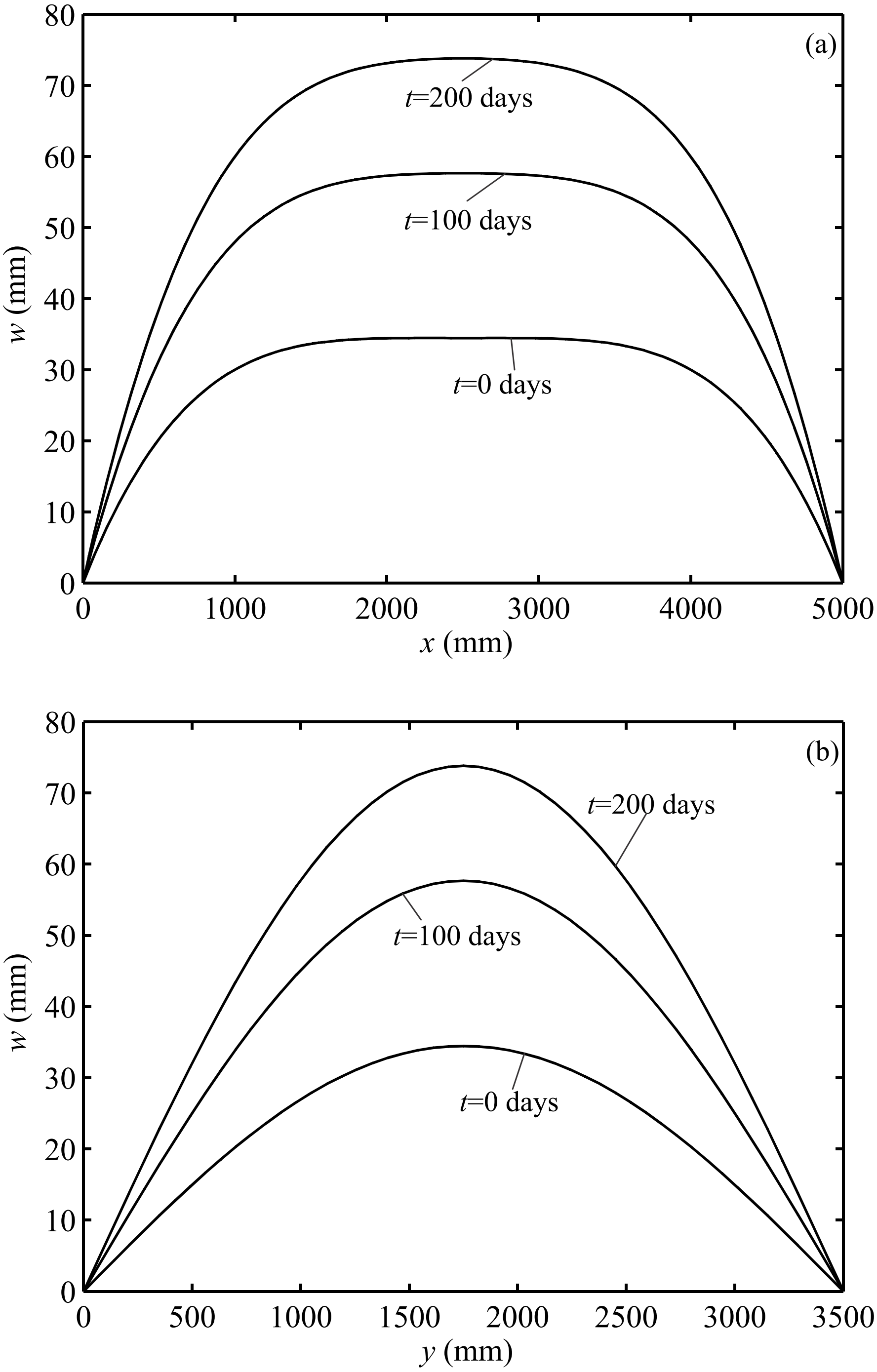

Fig. 7.7 Deflection distribution through x direction (a) and y direction (b) at three different times

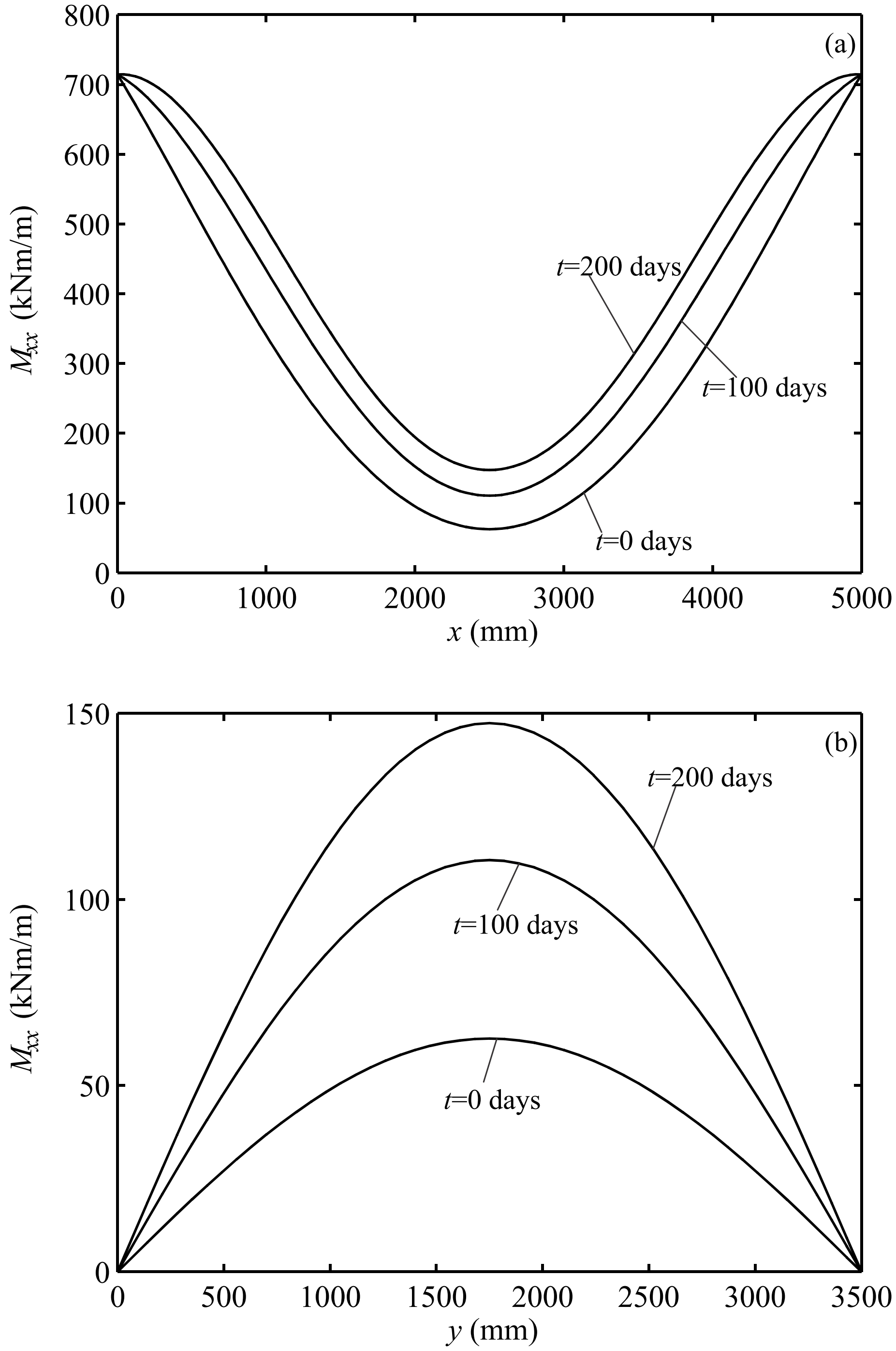

Fig. 7.8 Bending moment M_{xx} distribution through x direction (a) and y direction (b) at three different times

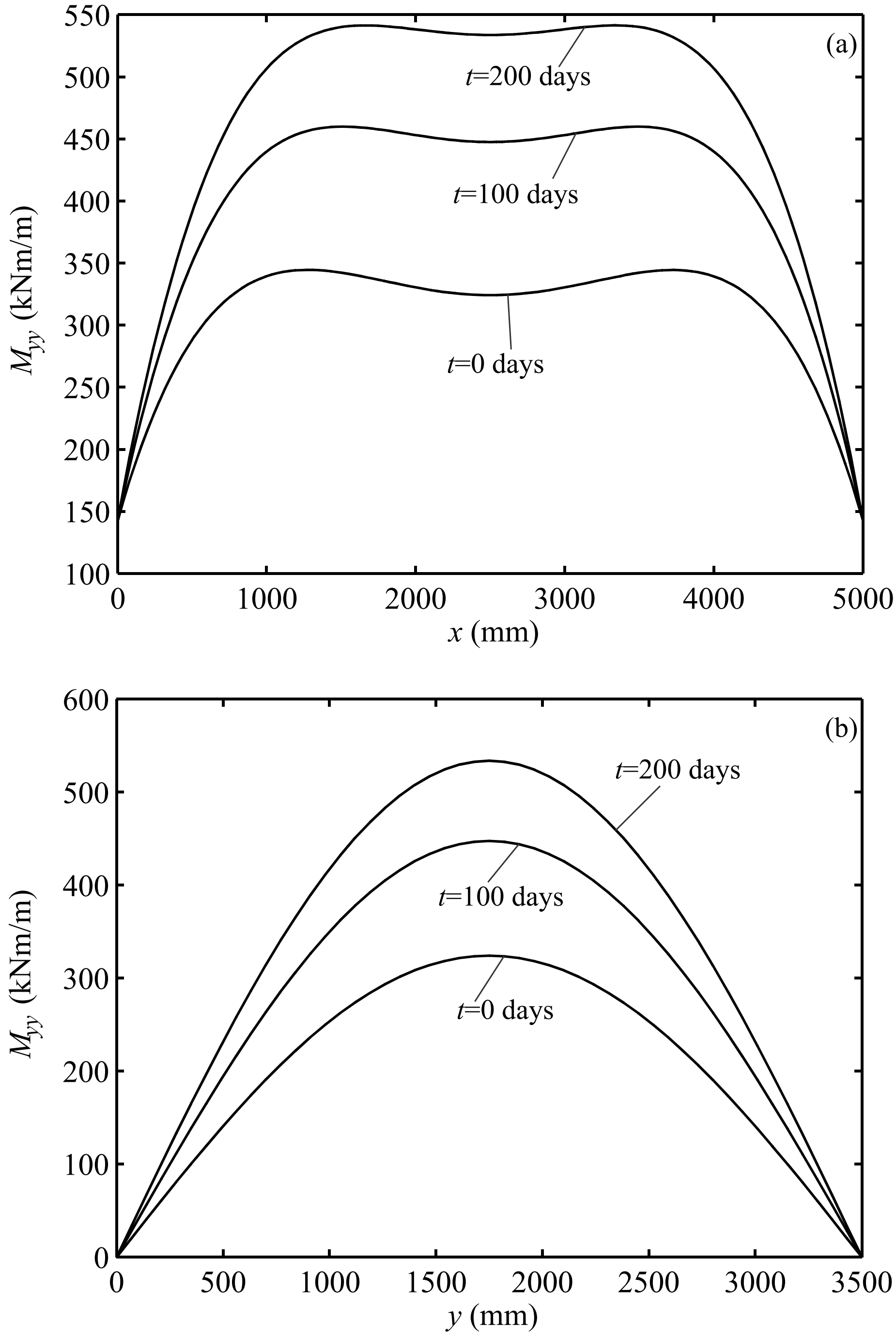

Fig. 7.9 Bending moment M_{yy} distribution through x direction (a) and y direction (b) at three different times

7.3.3 Parametric study

A parametric study is carried out in this section to examine the effects of the key factors on the time-dependent response of HSC panels. The factors include the magnitude and eccentricity of the sustained in-plane load (N_{xx}^{0}), the slenderness ratio defined as b/h, and the aspect ratio defined as a/b, boundary conditions, cracking, shrinkage and the steel reinforcement ratios (ρ_x and ρ_y). All the aforementioned factors are examined based on the viscoelastic material behaviour, except the shrinkage and reinforcement ratio, which are studied along with the consideration of cracking. The panel investigated in the first numerical example is used as a reference. All panels have the same dimensions as the reference panel unless specifically stated. Moreover, all the panels studied here contains equal reinforcement ratios in both orthogonal directions ($\rho_x = \rho_y$), and in each direction, the reinforcement are equally placed at the inner and outer layers.

7.3.3.1 Effect of load level

Fig. 7.10 presents the influence of the level of the sustained load on the time-dependent behaviour of the square two-way HSC panel that is simply-supported on four edges. For all load levels, the same dimensions, eccentricity, reinforcement ratios (ρ_x and ρ_y) and material properties as the reference panel are used. It can be seen that the increase of the imposed load level leads to earlier occurrence of buckling (shorter critical time). It can also be observed that the panel studied here is stable in the long run under load level that is lower than 50% of the elastic buckling load P_{cr}, as the increase in the out-of-plane deflection stops increasing and becomes almost constant after a certain time. The minimum load level to cause creep buckling for the examined panel is 51% of its elastic buckling load. This result is in accordance with that obtained using the simplified Effective Modulus Method (EMM), where E_c in Eq. (7.63) is replaced with

$E_c / \left[1+\varphi(t,t')\right]$. Nevertheless, if cracking is taken into account or biaxial loading scenarios are considered, the simplified effective modulus method might lead to inaccurate results.

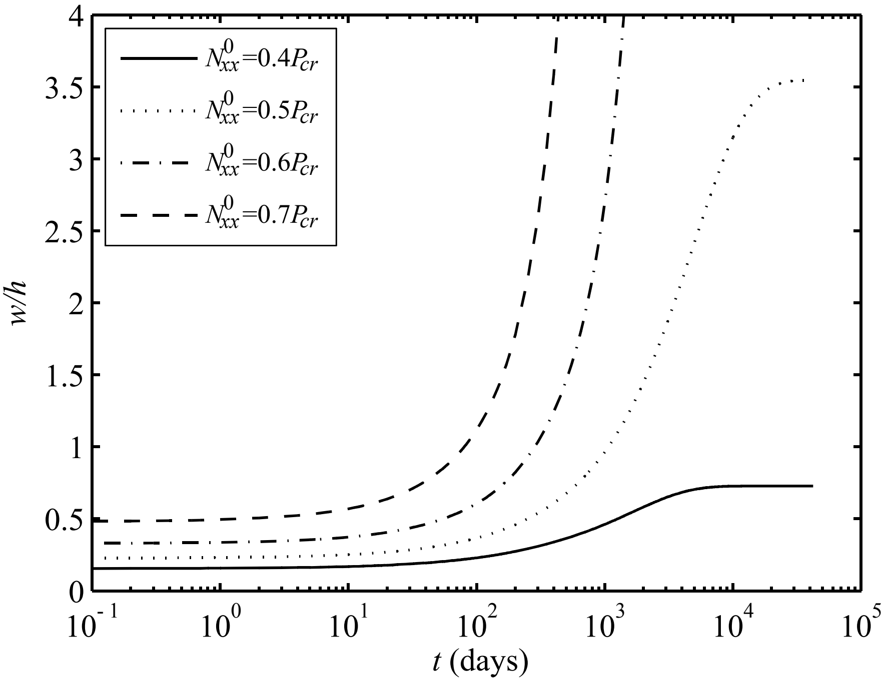

Fig. 7.10 Influence of load level on the long-term behavior of the HSC panel for the square panel ($e = h/6$, $[\rho_x, \rho_y] = 0.2\%$, $a \times b \times h = 2000 \times 2000 \times 100$ mm)

7.3.3.2 Effect of load eccentricity

Fig. 7.11 reveals the change of the out-of-plane deflection at the centre of the square panel with time under the in-plane compression load with different eccentricities. The load is equal to 52% of the elastic buckling load. As seen in the figure, the time-dependent behaviour is very sensitive to the eccentricity. Thus, it is essential in the design to consider different load scenarios as small inaccuracy in estimating the actual load eccentricity may result in catastrophic buckling failure in the long term.

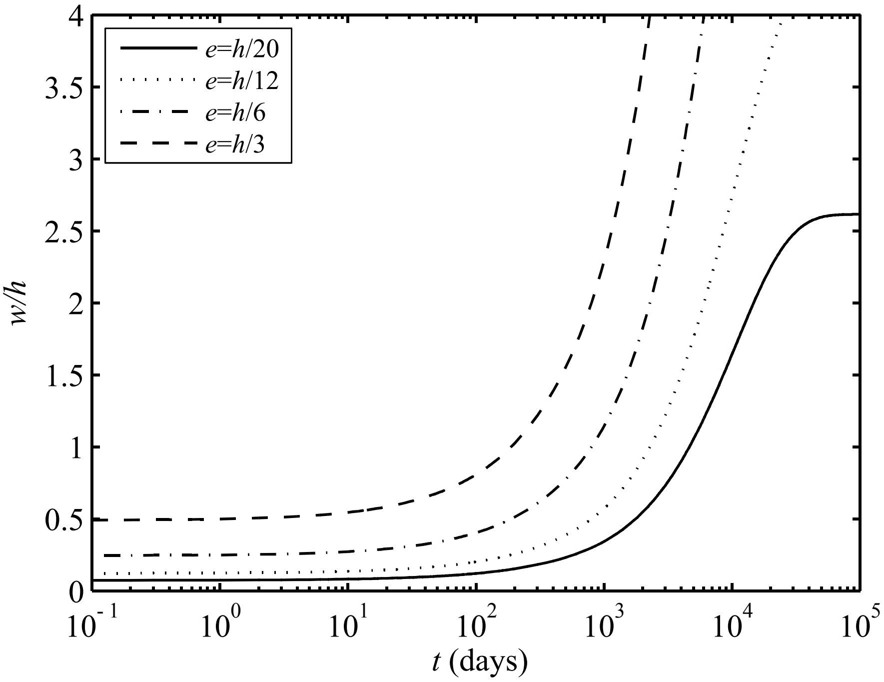

Fig. 7.11 Influence of eccentricity on the long-term behavior of the square HSC panel ($N^0_{xx} = 0.52P_{cr}$, $[\rho_x, \rho_y] = 0.2\%$, $a \times b \times h = 2000 \times 2000 \times 100$ mm)

7.3.3.3 Effect of slenderness ratio

The normalized deflection at the center of the panels with various thicknesses is plotted against the time in Fig. 7.12. The load level, the eccentricity as well as the reinforcement ratios in both orthogonal directions are $0.6P_{cr}$, $h/6$, and 0.2%, respectively, where P_{cr} is the elastic buckling load corresponding to the panel with 100 mm thickness in order to keep the load unchanged for the three different cases. The slenderness ratio is defined as *a/h*. Three different thicknesses 90 mm, 100 mm and 120 mm are investigated, which give the slenderness ratios of 22.2, 20 and 16.7. It can be seen that under the same magnitude of sustained load, the panels that are 90 mm and 100 mm thick are unstable whereas the panel with 120 mm thickness exhibits stable behavior. For the unstable panels, the critical time increases with increasing the thickness. Therefore, in practical design and use of the two-way panels, the creep buckling failure can be prevented by increasing the thickness of the panel.

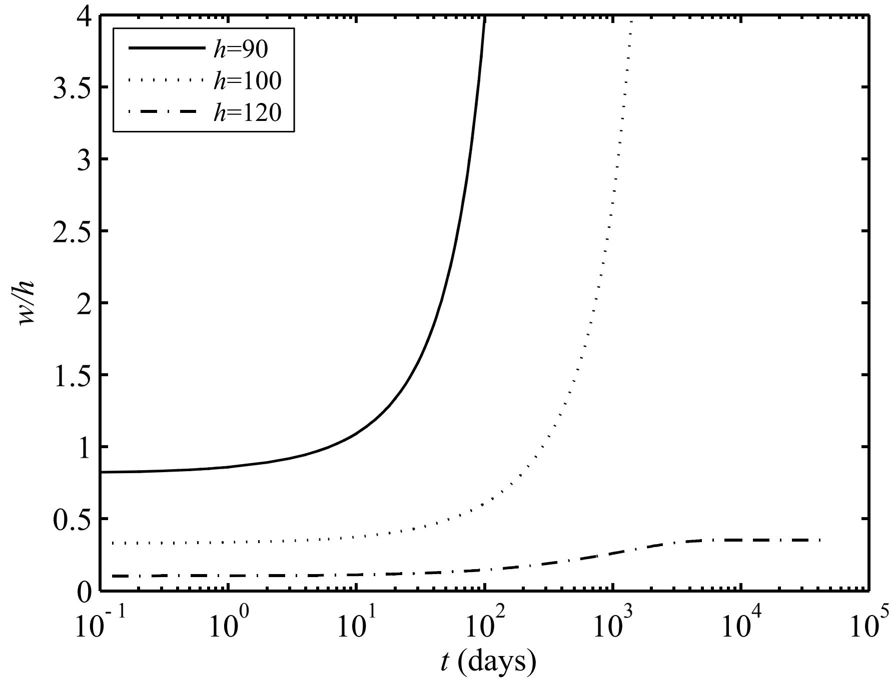

Fig. 7.12 Influences of slenderness on the long-term behavior of the square HSC panel (N_{xx}^0 = 0.6P_{cr}, $e = h/6$, $[\rho_x, \rho_y] = 0.2\%$, $a \times b$ = 2000×2000 mm)

7.3.3.4 Effect of boundary conditions

The support conditions are varied at the two loading edges ($x = 0$ and $x = a$), while the other two edges at $y = 0$ and $y = b$ remain simply-supported. Three different cases are investigated in this section, including simply-supported with eccentric loading at both loading edges (Case I), simply-supported at both loading edges with concentric loading at one edge and eccentric loading at the other (Case II), and fixed support at one loading edge and simply-supported with eccentric loading at the other (Case III). The details are given in Table 7.1. The panel has the same geometric and material properties as the reference panel.

Table 7.1 Details of boundary conditions and loads

	Boundary support condition				In-plane load	
	$x = 0$	$x = a$	$y = 0$	$y = b$	N_{xx}^{0}	N_{xx}^{a}
Case I	SS[1]	SS	SS	SS	Eccentric (e=h/6)	Eccentric (e=h/6)
Case II	SS	SS	SS	SS	Eccentric (e=h/6)	Concentric
Case III	Fixed	SS	SS	SS	N/A	Eccentric (e=h/6)

[1] – Simply-supported;

The variation of the center deflection with time for the three cases are depticed in Fig. 7.13. It can bee seen that creep buckling happens to both Case I and Case II. It can also be seen that Case I that is loaded eccentrically at both ends is more vulnerable to creep buckling. On the other hand, Case III is the stiffest one among the three cases due to the fixed support at one end, which leads to an ultimate stable state.

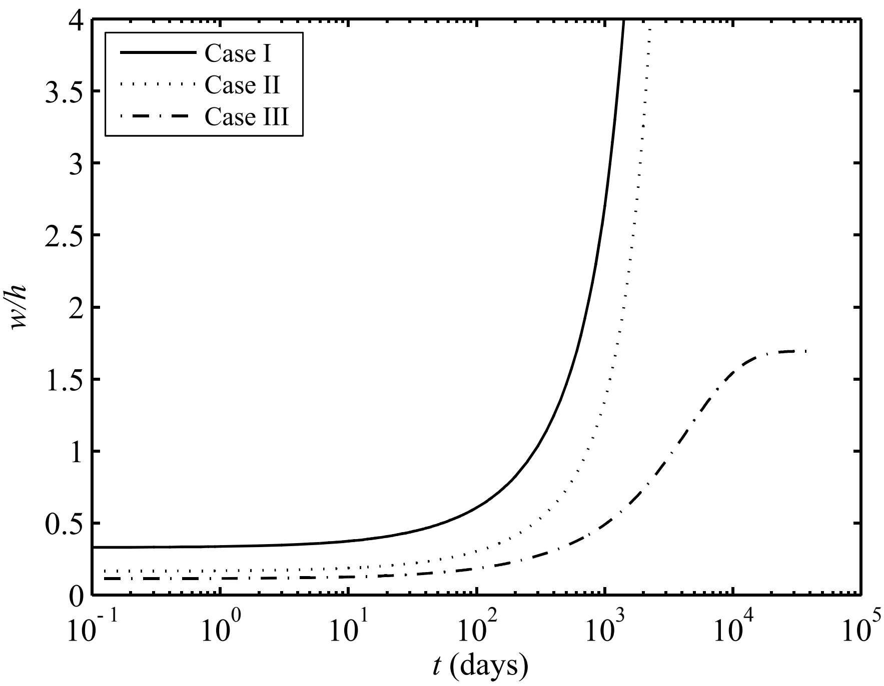

Fig. 7.13 Influences of boundary conditions on the long-term behavior of the square HSC panel (N_{xx}^{0} = 0.6P_{cr}, [ρ_x, ρ_y] = 0.2%, $a \times b \times h$ = 2000×2000×100 mm)

7.3.3.5 Effect of aspect ratio

The result for the effect of aspect ratio is shown in Fig. 7.14 where five aspect ratios namely 0.5, 0.75, 1, 1.5 and 2 are investigated. The aspect ratios are achieved by varying the length (a) of the panel whereas the width (b) and thickness (h) remain the same as the reference panel. All panels possess the same reinforcement ratio of 0.2% in both orthogonal directions, and under the in-plane compression load in the x direction with $N_{xx}^{0} = 0.6P_{cr}$ and $e = h/6$. The maximum deflections for the panels with aspect ratio from 0.5 to 1.5 appear at the center of the specimen, whereas for the panel with a/b=2, the maximum deflection occurs around a quarter of the length. It is observed in the figure that the long-term behavior of the two-way panel is substantially influenced by the aspect ratio and the panel with aspect ratio of 1 is the most critical case. The critical time decreases either with the increase of the aspect ratio as long as it is larger than 1 or with the decrease of the aspect ratio as long as it is smaller than 1. The increase of the critical time associated with the increase of aspect ratio can be explained by the fact that the panel with longer length (a) is stiffer and hence has smaller deflections under the same load level, which is obvious by observing the instantaneous deflection.

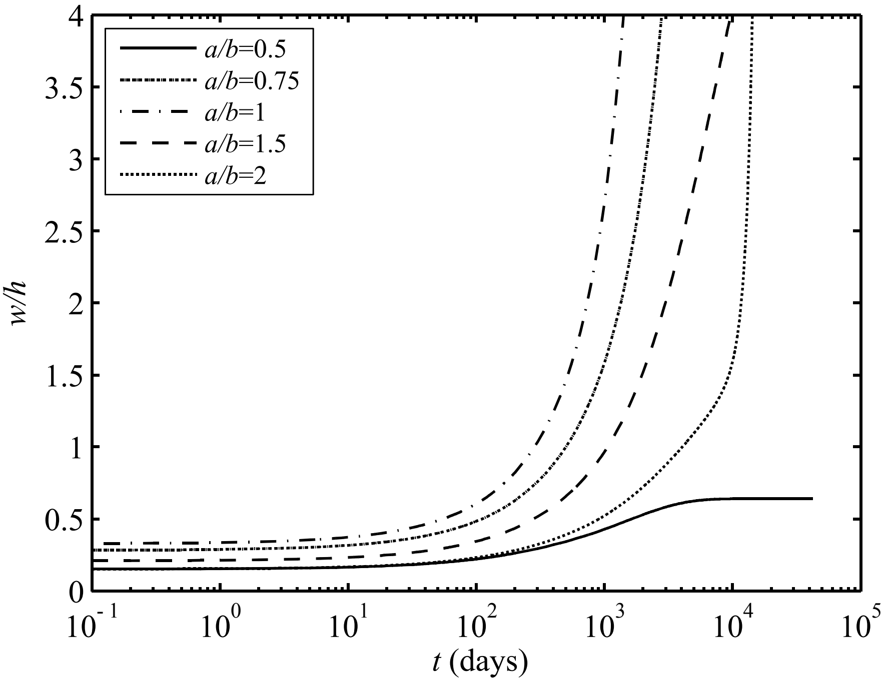

Fig. 7.14 Influence of aspect ratio on the long-term behavior of the HSC panel (N_{xx}^{0} = $0.6P_{cr}$, $e = h/6$, $[\rho_x, \rho_y] = 0.2\%$, $b \times h = 2000 \times 100$ mm)

The distribution of the center deflection, the bending moments M_{xx} and M_{yy} along x and y directions at various times are illustrated through Fig. 7.15 to Fig. 7.23 for the panels with aspect ratio equal to 0.5, 1 and 2, respectively. It can be observed that with the increase of the length (a) (and so the aspect ratio), the edge moments M_{xx}^{0} and M_{xx}^{a} have a smaller influence on the behavior of the two-way panel.

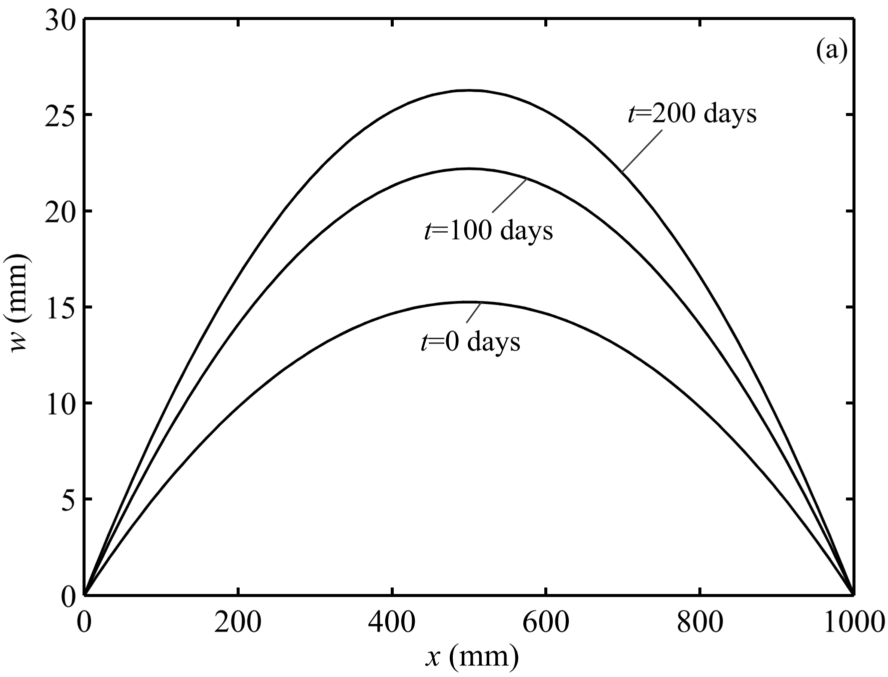

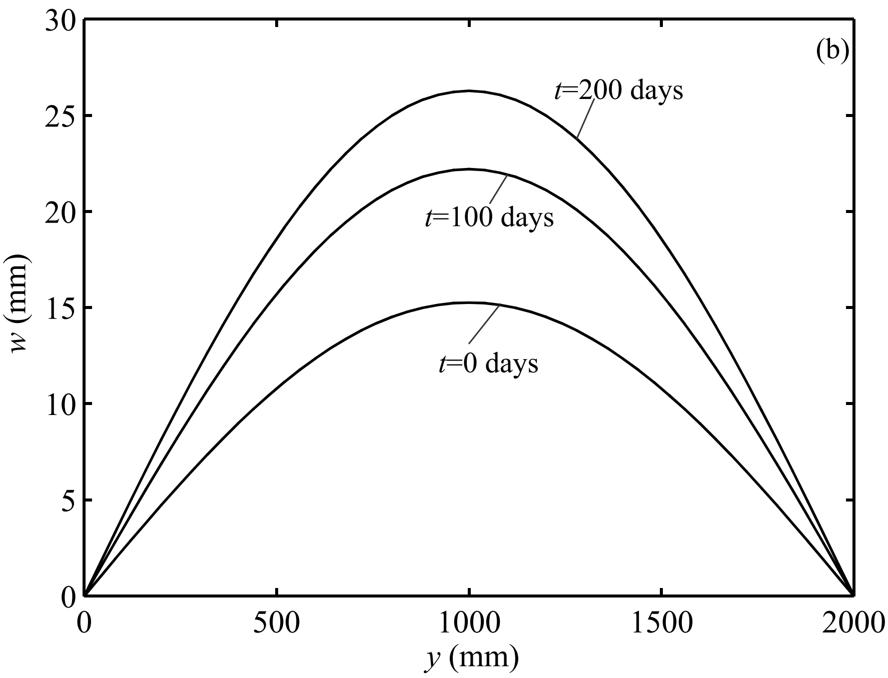

Fig. 7.15 Deflection distribution through x direction (a) and y direction (b) at three different times for the panel with aspect ratio equal to 0.5

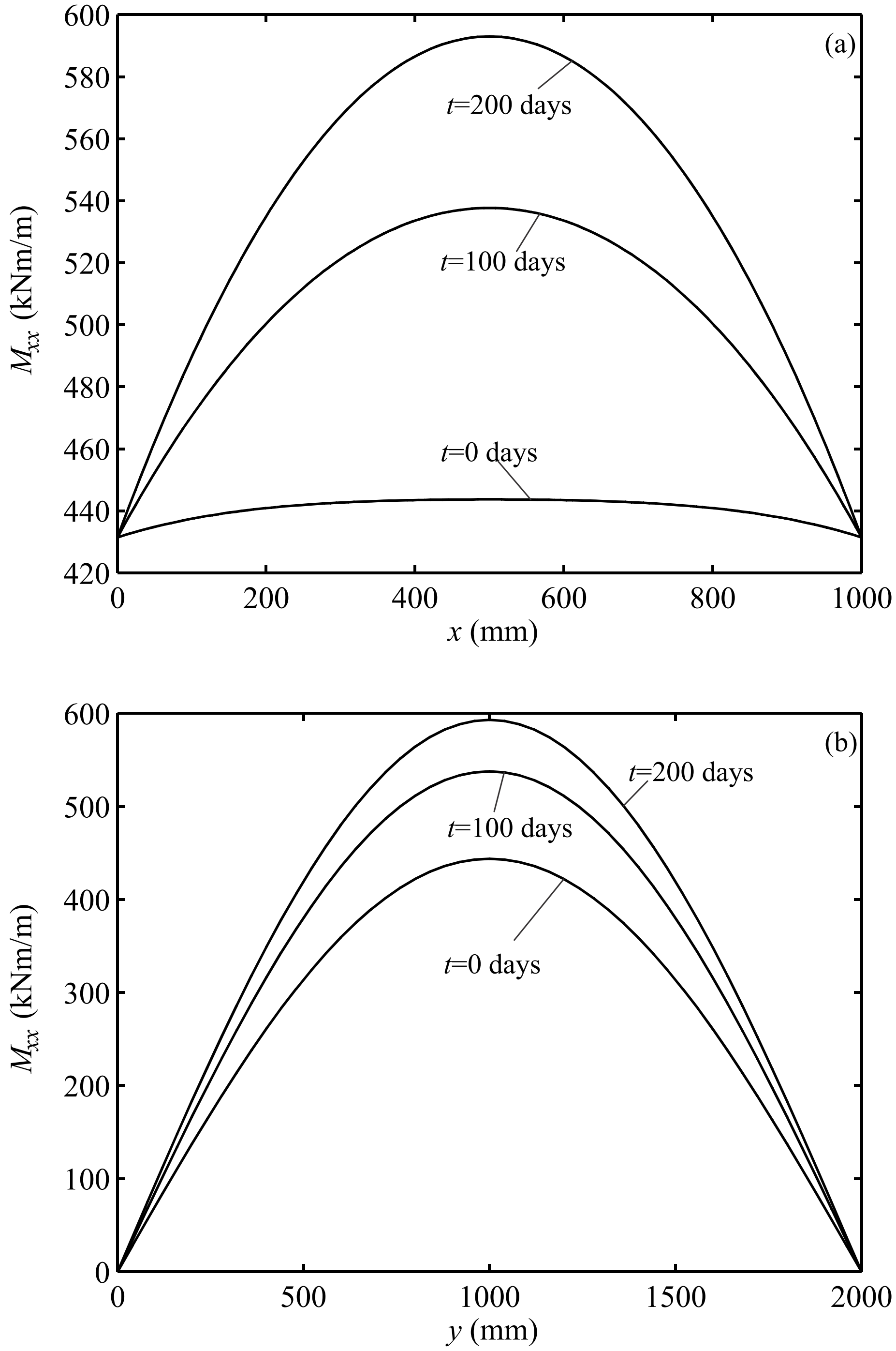

Fig. 7.16 Bending moment M_{xx} distribution through x direction (a) and y direction (b) at three different times for the panel with aspect ratio equal to 0.5

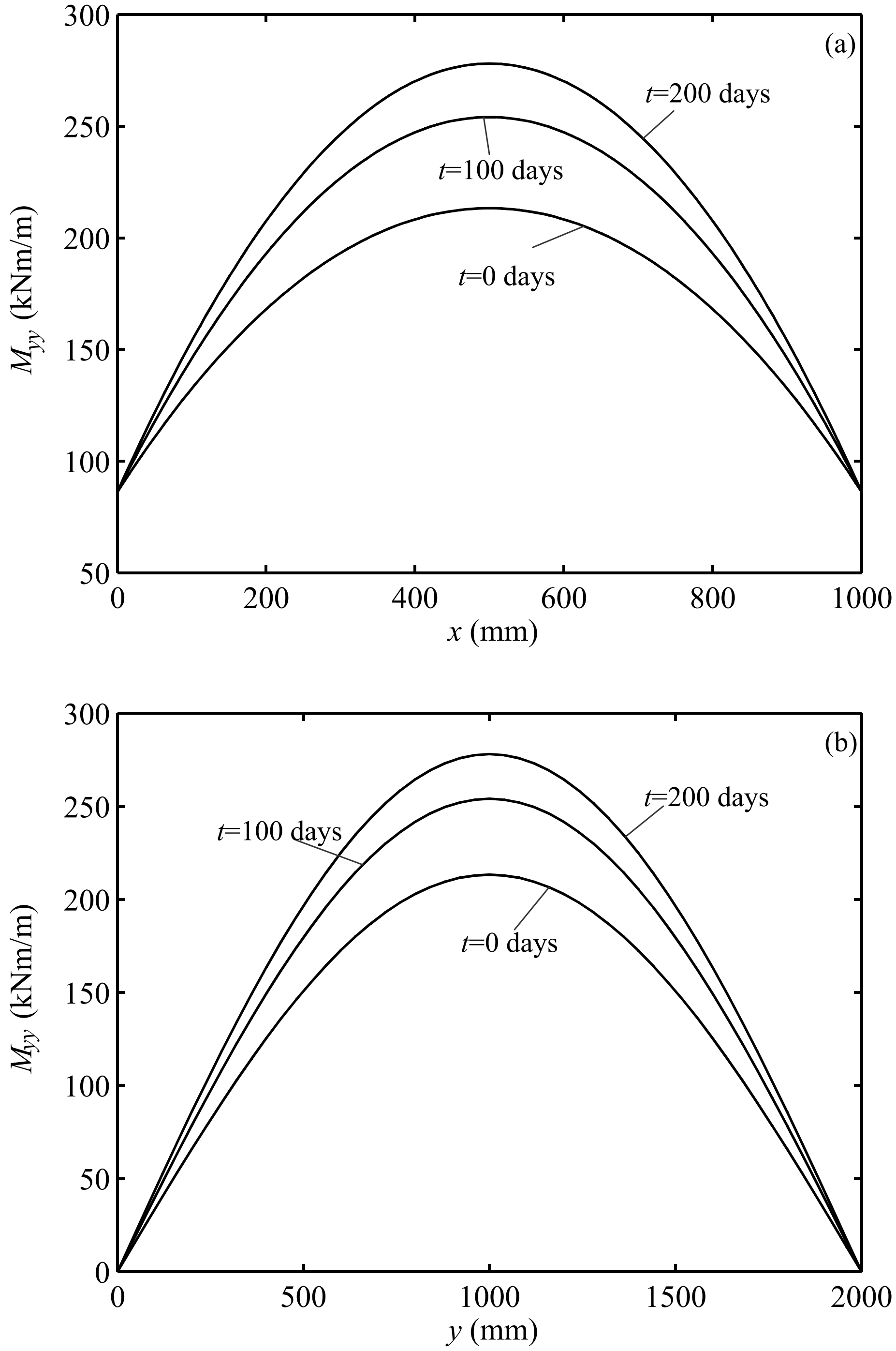

Fig. 7.17 Bending moment M_{yy} distribution through x direction (a) and y direction (b) at three different times for the panel with aspect ratio equal to 0.5

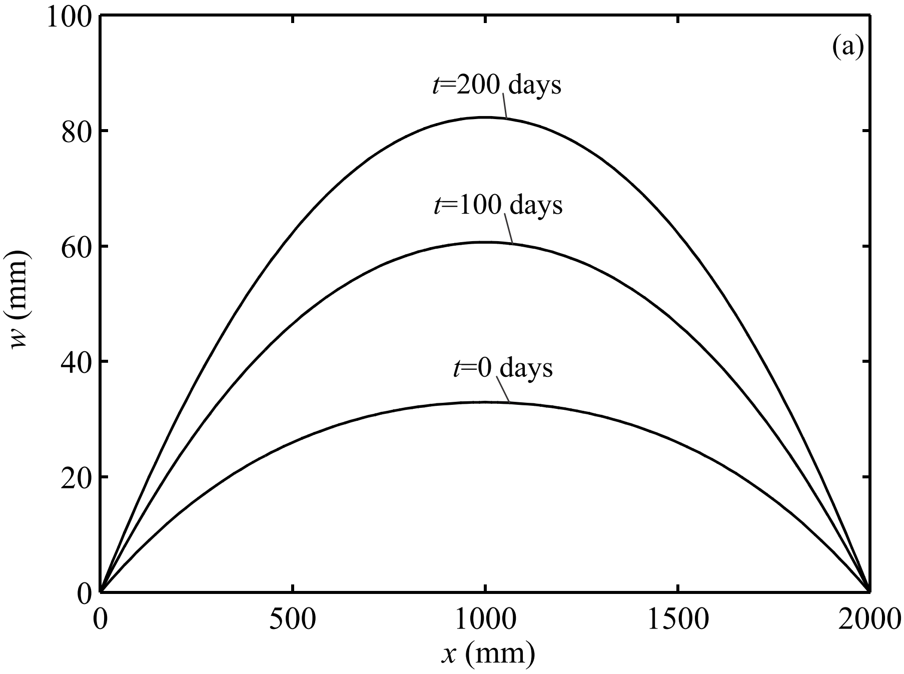

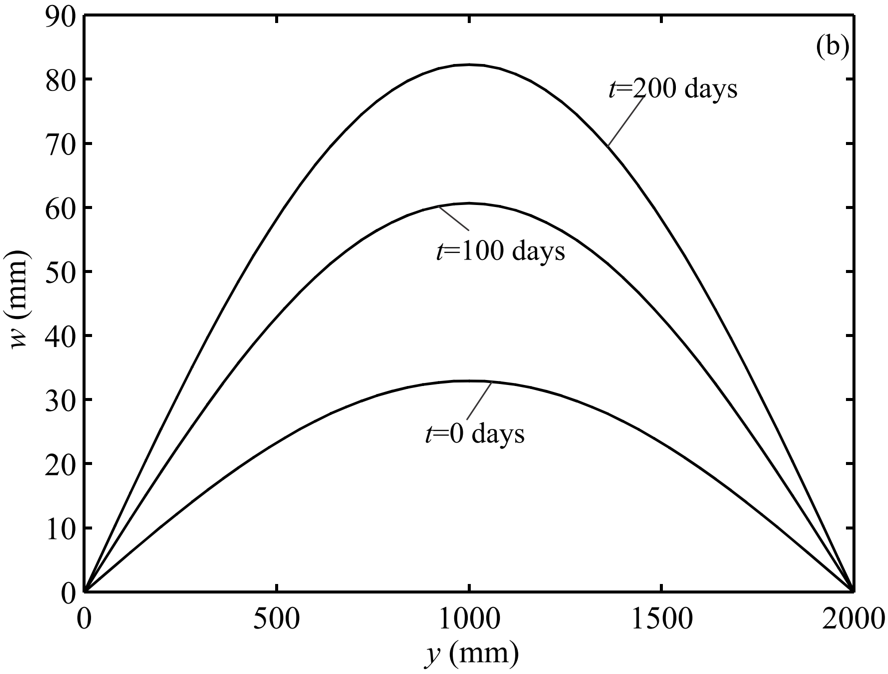

Fig. 7.18 Deflection distribution through x direction (a) and y direction (b) at three different times for the panel with aspect ratio equal to 1

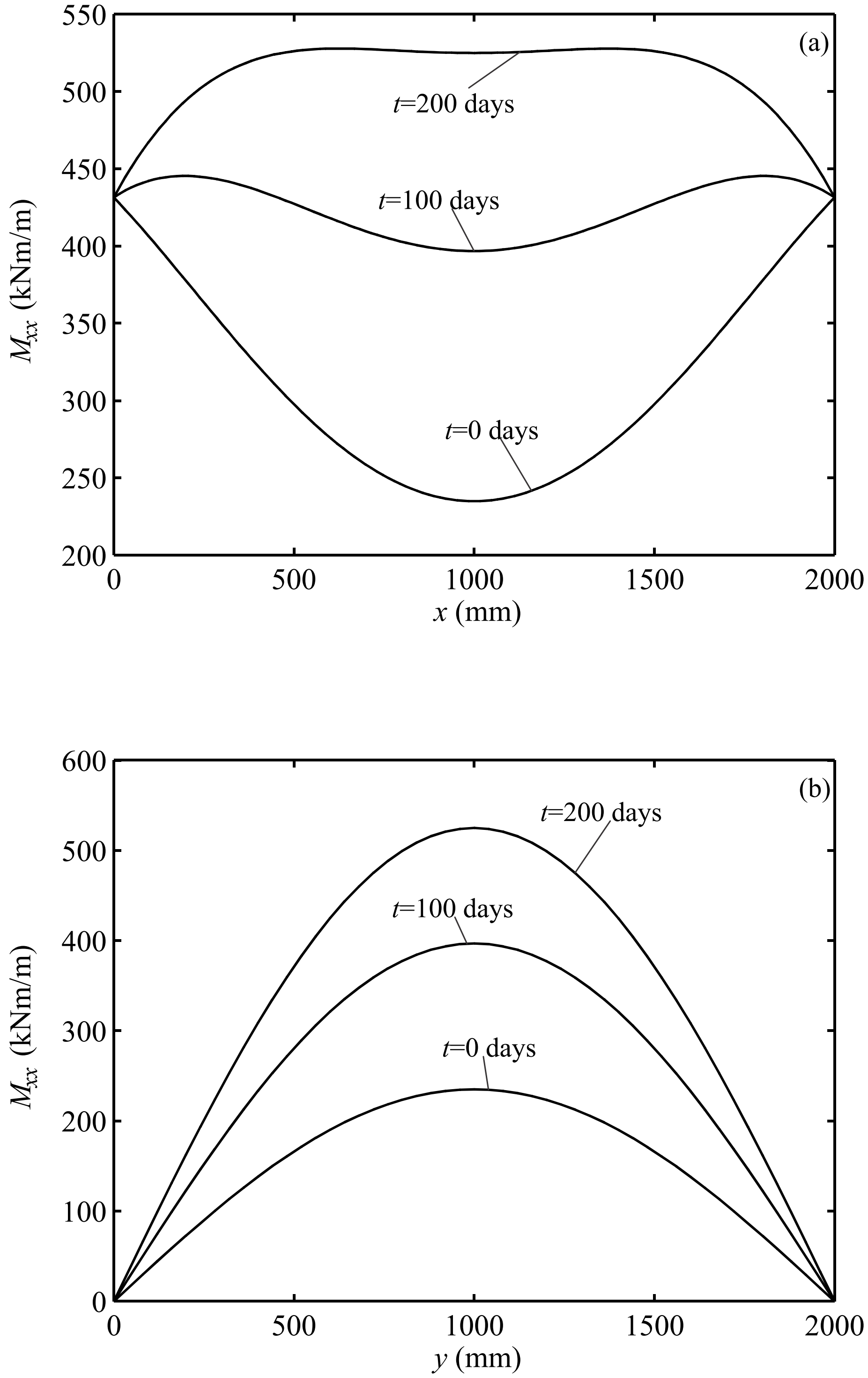

Fig. 7.19 Bending moment M_{xx} distribution through x direction (a) and y direction (b) at three different times for the panel with aspect ratio equal to 1

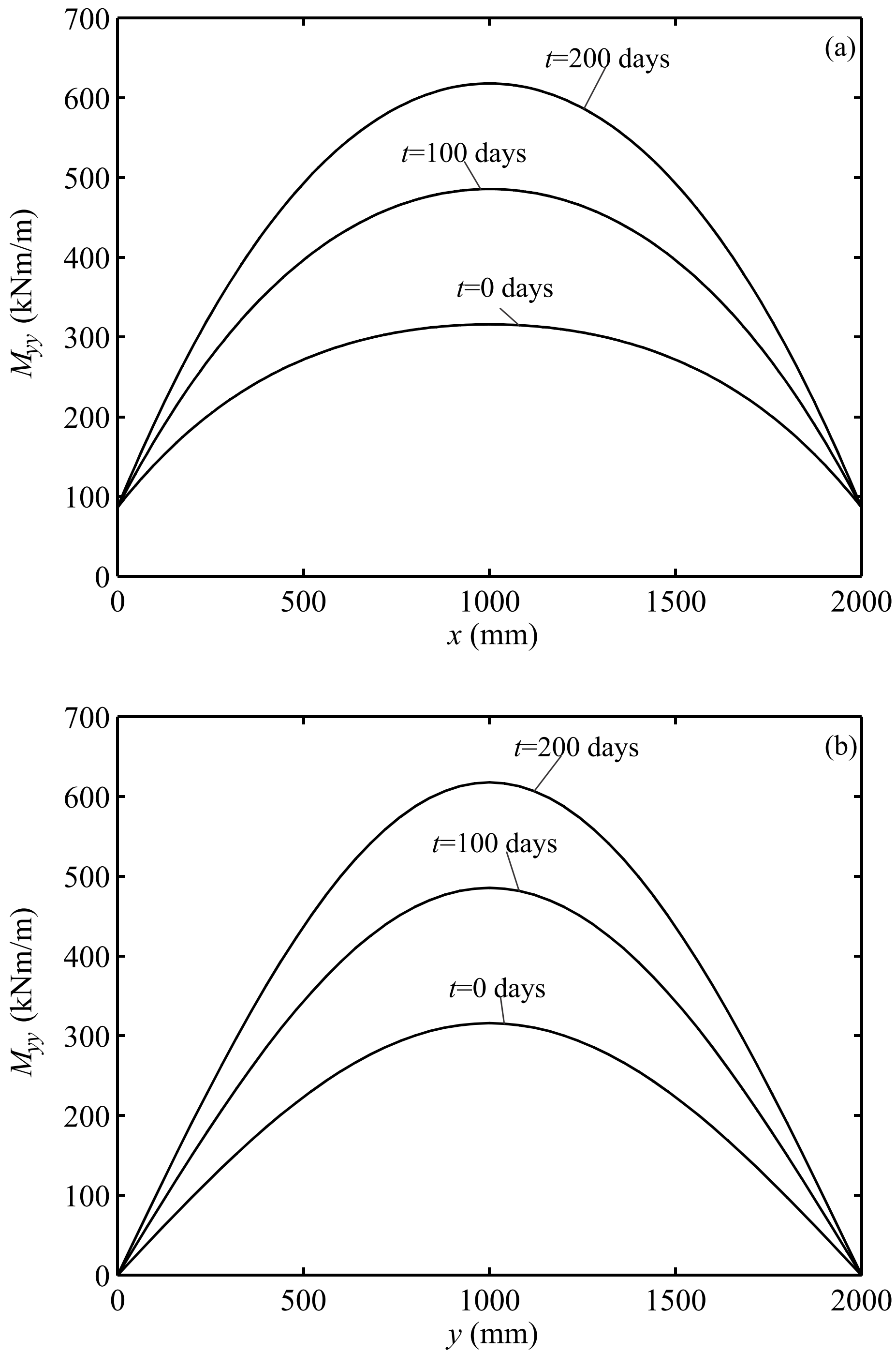

Fig. 7.20 Bending moment M_{yy} distribution through x direction (a) and y direction (b) at three different times for the panel with aspect ratio equal to 1

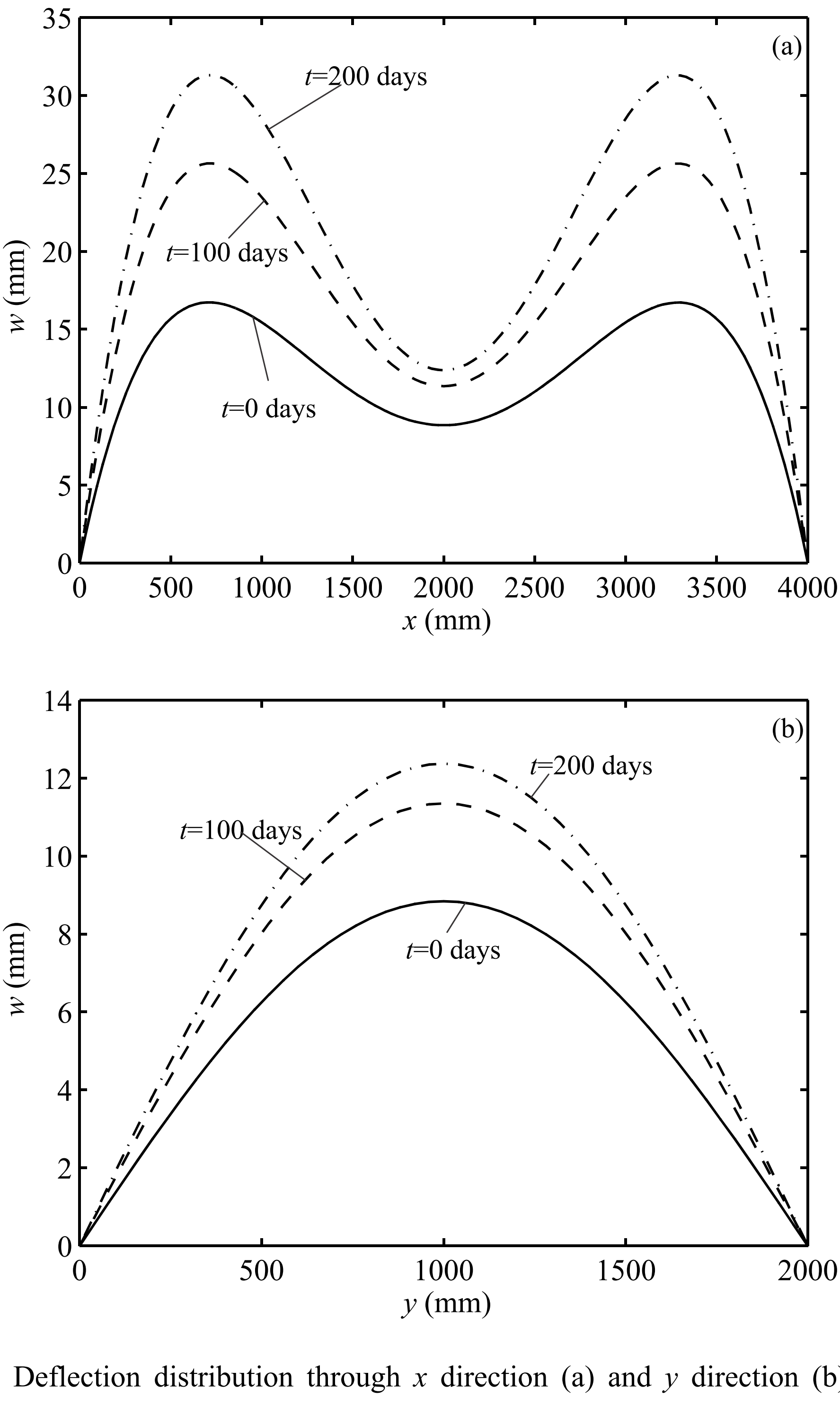

Fig. 7.21 Deflection distribution through x direction (a) and y direction (b) at three different times for the panel with aspect ratio equal to 2

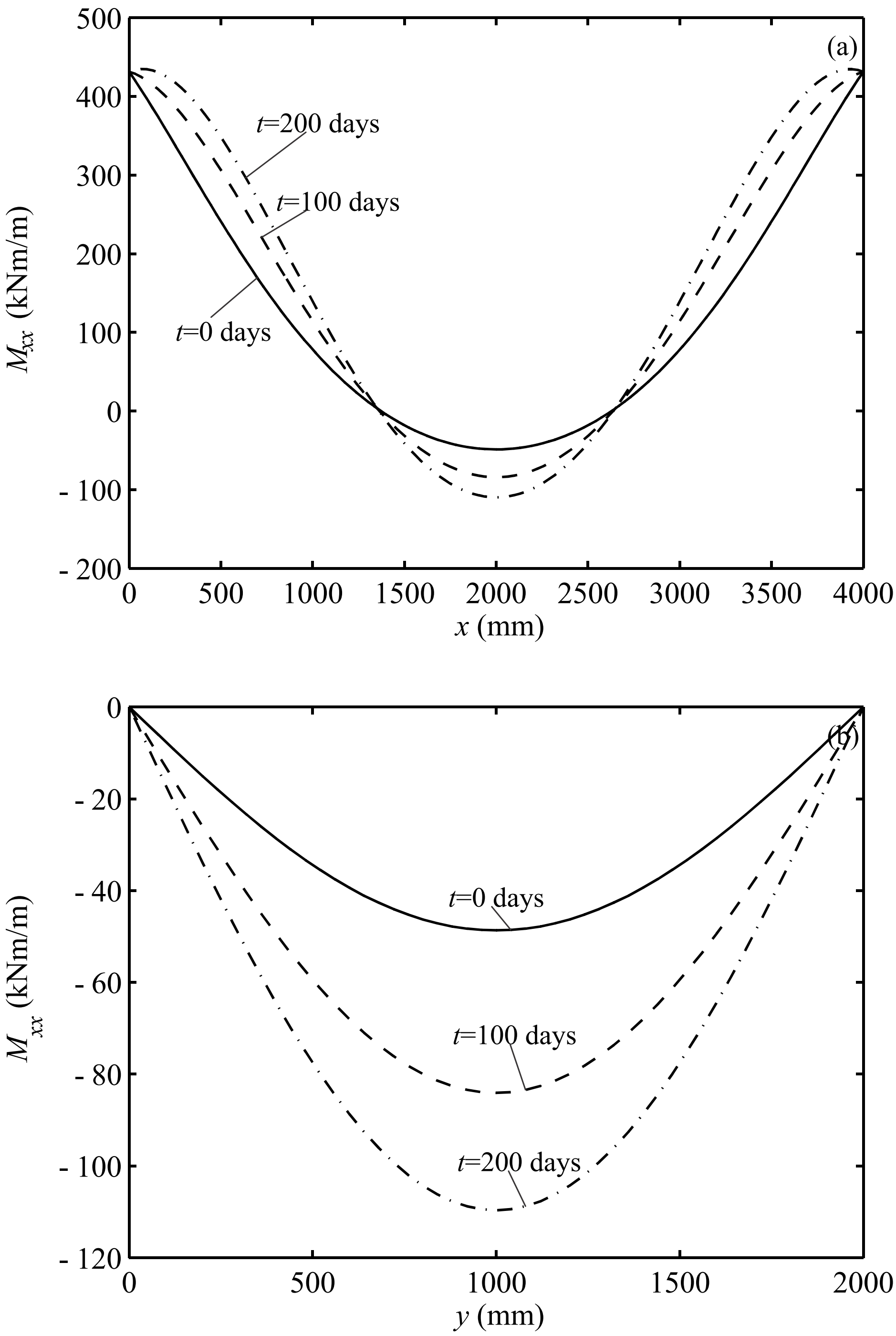

Fig. 7.22 Bending moment M_{xx} distribution through x direction (a) and y direction (b) at three different times for the panel with aspect ratio equal to 2

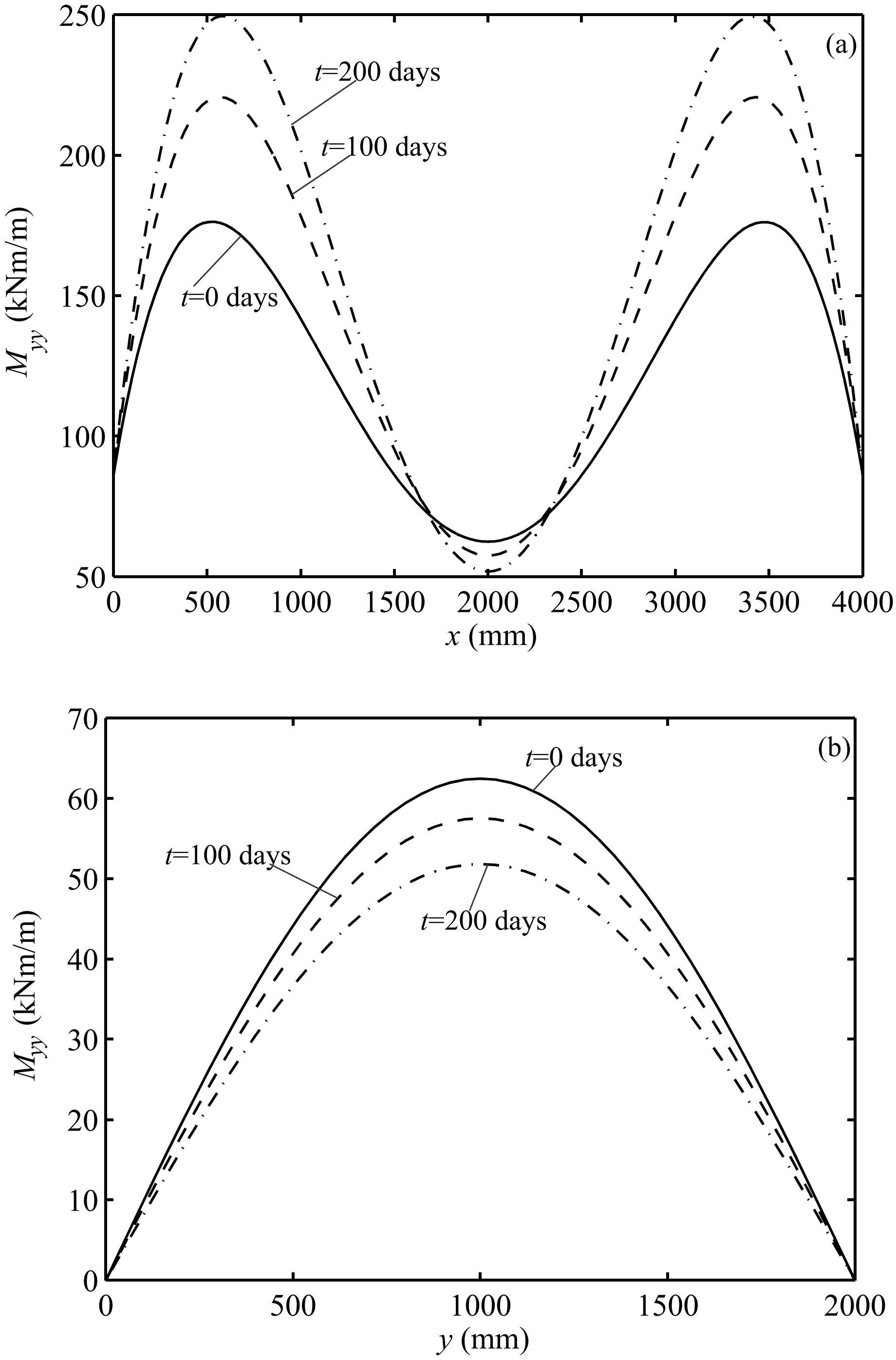

Fig. 7.23 Bending moment M_{yy} distribution through x direction (a) and y direction (b) at three different times for the panel with aspect ratio equal to 2

7.3.3.6 *Effect of cracking*

In the analysis presented in this section, the cracking of concrete is taken into account in the model. Although high-strength concrete possesses higher tensile strength than normal-strength concrete, it is still a brittle material and the cracking of the concrete imposes a significant impact on the short-term and long-term behaviour of HSC structures. Hence, in the theoretical model, the concrete is considered to be linear viscoelastic but brittle in tension due to cracking, and linear viscoelastic in compression, because the nonlinearity in the stress-strain relation for high-strength concrete under compression commences only at around 70% of the compressive stress. The tension-stiffening is not accounted here, and the effective Poisson's ratio of concrete is assumed to be zero once cracking appears (Ghoneim and MacGregor 1994). Following the above assumptions, the stress-resultants for the cracked panel can be derived based on Eqs. (7.40)-(7.42), which read

$$\Delta M_{xx}(t_r) = -D''_{cr}\frac{\partial^2 \Delta w}{\partial x^2} - \Delta\bar{M}_{xx}(t_r) \tag{7.65}$$

$$\Delta M_{yy}(t_r) = -D''_{cr}\frac{\partial^2 \Delta w}{\partial y^2} - \Delta\bar{M}_{yy}(t_r) \tag{7.66}$$

$$\Delta M_{xy}(t_r) = -D''_{cr}\frac{\partial^2 \Delta w}{\partial x \partial y} - \Delta\bar{M}_{xy}(t_r) \tag{7.67}$$

where D''_{cr} is the flexural cracked rigidity, which is given by

$$D''_{cr} = \int_{-d_n}^{h-dn} \frac{E''_z}{1-\nu^2} z^2 \mathrm{d}z + \frac{E''}{1-\nu^2}\left[nA_{sx}z_{sx}^2 / b + (n-1)A'_{sx}z'^2_{sx} / b\right] \tag{7.68}$$

$$E''_z = \begin{cases} E'' & \text{for} \quad \varepsilon_{xx}^{ins} < \varepsilon_{cr} \\ 0 & \text{for} \quad \varepsilon_{cr} <= \varepsilon_{xx}^{ins} \end{cases} \tag{7.69}$$

where d_n is the depth of the neutral axis depth measured from the top extreme fiber of the section; ε_{cr} is the concrete cracking strain where $\varepsilon_{cr} = f_t/E_c$, and f_t is the flexural tensile strength of the concrete obtained from uniaxial testing, as suggested by Chen (1982) for 2D problems under tension-tension state of stresses.

By substituting the Fourier series expansion of w into the Eqs. (7.65)-(7.67) and taking only the first term of the Fourier series for simplicity, the incremental bending moments for cracked section are given by

$$\Delta M_{xx}(t_r) = -D''_{cr}\sin\left(\frac{\pi y}{b}\right)\frac{\mathrm{d}\Delta w_1(x)}{\mathrm{d}x^2} - \Delta\bar{M}_{xx}(t_r) \tag{7.70}$$

$$\Delta M_{yy}(t_r) = D''_{cr}\sin\left(\frac{\pi y}{b}\right)\left(\frac{\pi}{b}\right)^2 \Delta w_1(x) - \Delta\bar{M}_{yy}(t_r) \tag{7.71}$$

$$\Delta M_{xy}(t_r) = -D''_{cr}\left(\frac{\pi}{b}\right)\cos\left(\frac{\pi y}{b}\right)\frac{\mathrm{d}\Delta w_1(x)}{\mathrm{d}x} - \Delta\bar{M}_{xy}(t_r) \tag{7.72}$$

At each time step, Eq. (7.57) presents a 4^{th}-order nonlinear differential equation due to the dependency of the viscoelastic rigidities on the unknown deformations via Eq. (7.68). It is assumed that the rigidity along the cracked region is uniform through its length, which equal to D''_{cr}. The rigidity along the uncracked region is also uniform and equals D''. This assumption results in two types of unknowns that need to be determined at each time step, namely: the rigidities at the critical section, and the start and end points of the cracked region $X1$ and $X2$ along x axis. Here, an iterative procedure is used to determine these parameters at each time step, combined with the use of the numerical multiple shooting method for the solution of the incremental governing equations at each iteration. The iterative procedure follows these steps:

Step 1. Initial guess. At the first iteration of the instantaneous loading, the panel is assumed uncracked. However, for the subsequent time steps, the solution from the previous time step is used as the initial guess for the current step.

Step 2. Analysis of the structure. Using the rigidities calculated in the initial guess or in the previous iteration (step 3.3), as well as the calculated locations of the start and end points of the cracked region, $X1$ and $X2$, the incremental governing equations become linear ones with variable coefficients in space, which are solved numerically using the shooting method.

Step 3. Analysis of the critical section and update the rigidities. The rigidity is evaluated at the location that has the maximum tensile strains.

3.1. Based on the solution obtained in step 2, the incremental bending moment at time t_r is calculated at the critical section by using the stress-resultants. The total bending moment is obtained by adding the incremental bending moments at time t_r to the total bending moments accumulated up to the step t_{r-1}.

3.2. The instantaneous strain at the critical section in the y direction (ε_{yy}^{ins}),is then calculated as follows:

$$\varepsilon_{yy}^{ins} = \frac{M_{yy} z}{D''_{cr}} \tag{7.73}$$

where z is measured from the neutral axis that is determined from the previous iteration as presented in Step 3.4.

3.3. Once the normal strain distribution is determined in Step 3.2, the neutral axis depth d_n is determined by taking the relative distance between the point of zero strain and the extreme fibre on the top surface. Consequently, the viscoelastic rigidities and the incremental forces due to creep are calculated.

3.4. *Update of z coordinates*: The z coordinate is updated in this step because of the shifting of the neutral axis with cracking. So the new location of the neutral axis is determined based on using the first moment of area as follows

$$z_{na} = \frac{\int_{-d_n}^{z_{cr}} z\mathrm{d}z + \left[nA_{sx} z_{sx} + (n-1) A'_{sx} z'_{sx} \right]}{(z_{cr} + d_n) + \left[nA_{sx} + (n-1) A'_{sx} \right]} \tag{7.74}$$

where z_{na} is the z coordinate of the neutral axis location and z_{cr} is the z coordinate where $\varepsilon_{yy}^{ins} = \varepsilon_{cr}$. Following the calculation of z_{na}, the origin of the z coordinates is then moved to this point and the new z coordinate system is then established along with updating z_{sx} and z'_{sx};

Step 4. Convergence Criteria. If the norm of the relative difference between the magnitudes of the viscoelastic rigidities as well as $X1$ and $X2$ in two consecutive iterations is sufficiently small, the iterative procedure stops. Otherwise, the procedure returns to step 2 with the updated rigidities and z coordinates obtained in step 3.3 and 3.4, respectively.

The panel studied in this section has the same dimensions and boundary conditions as the one in Section 7.3.1. The eccentric in-plane load level in x direction (N_{xx}^{0}) is $0.2P_{cr}$, where P_{cr} is the corresponding elastic buckling load. The eccentricity at both loading edges is $h/20$. The reinforcement ratios ρ_x and ρ_y are both 2%, which are equally distributed in the top and bottom layers in each direction. The concrete compressive strength, f_c', flexural tensile strength, f_t, and elastic modulus, E_c are 80 MPa, 5.4 MPa, and 39.6 GPa, respectively. The long-term results are shown in Fig. 7.24-Fig. 7.25. The results for the panel without considering cracking are also plotted in the figures for comparison. The limit of the normalized out-of-plane deflection for the criterion of the creep buckling is reduced to 1 in this study because of the limited ability of concrete structure to undergo large deformation. It can be observed in the figure that the out-of-plane deflection as well as the bending moments M_{xx} and M_{yy} and the ratio between them at the centre of the panel grow with the increase of time due to the combined effect of creep, concrete cracking and geometric nonlinearity. Creep buckling happens at the time t =235 days since the first application of the sustained load. In contrast, the linear viscoelastic plate loaded under the same loading conditions is much stiffer such that the out-of-plane deflection increases much less than the cracked panel. Moreover, creep bucking does not happen to the linear viscoelastic panel in such low load level. So it can be seen that the cracking of the concrete can significantly weaken the panel and enforce the panel to buckle under a low load level that would not cause any failure for the linear viscoelastic panel. Hence, it is essential to take the cracking of concrete into consideration in the analysis and design of the time-dependent behaviour of two-way HSC concrete panels.

The effect of in-plane load level is studied for the panel with cracking in Fig. 7.26, where three load levels 15%, 20% and 25% are investigated. It can be seen that with the consideration of cracking, the behaviour of the HSC panel becomes very sensitive to the variation of the load level such that a small change in the magnitude of the load can impose a significant influence on the time-dependent response. The minimum load that can induce creep buckling to the panel with cracking is found to be 17% of the instantaneous elastic buckling load, which is much smaller than that for the viscoelastic panel. The simplified EMM also fails in predicting this long-term buckling load.

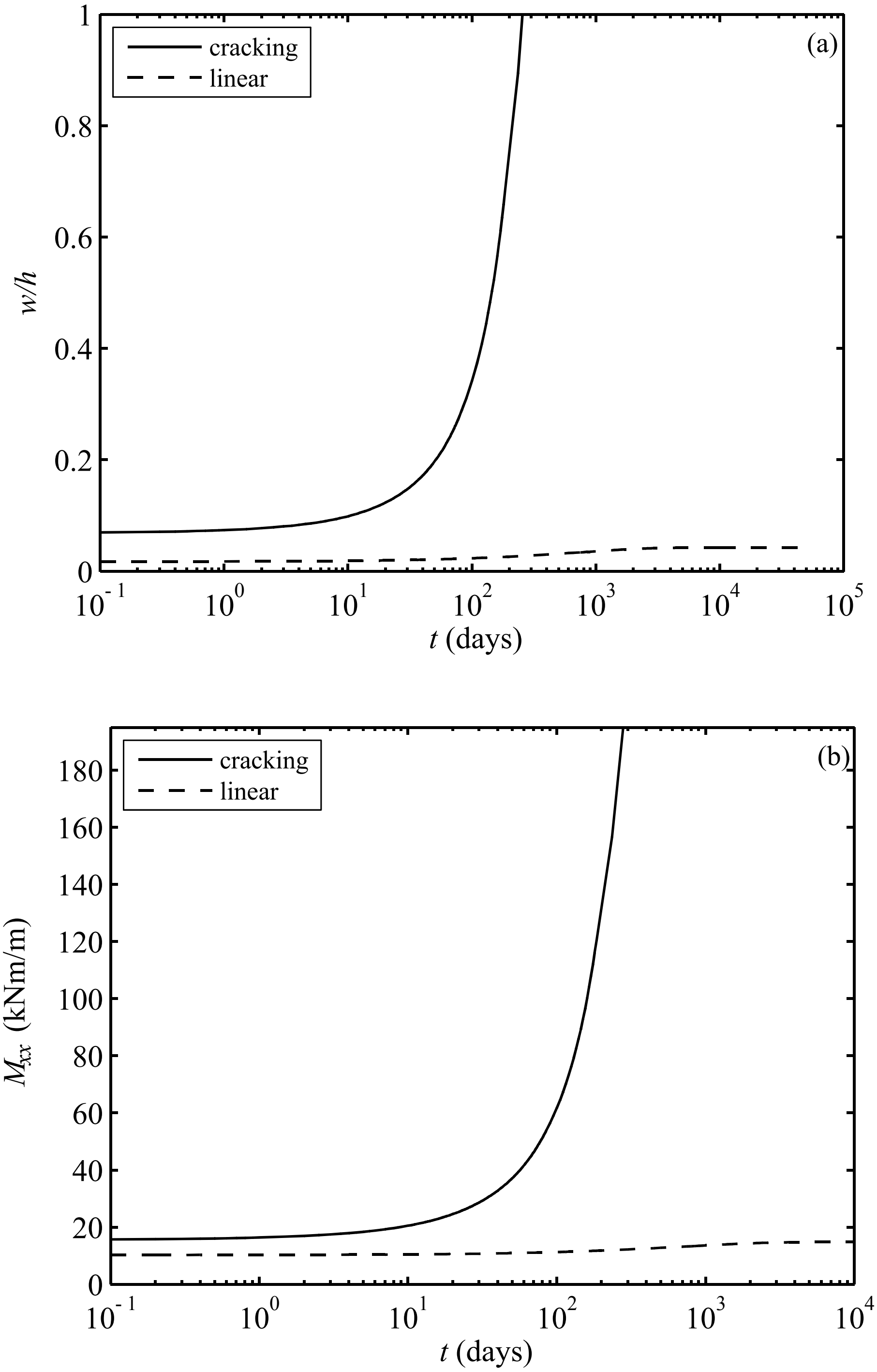

Fig. 7.24 Variation with time of the (a) out-of-plane deflection; (b) bending moment M_{xx} at the center of the panel

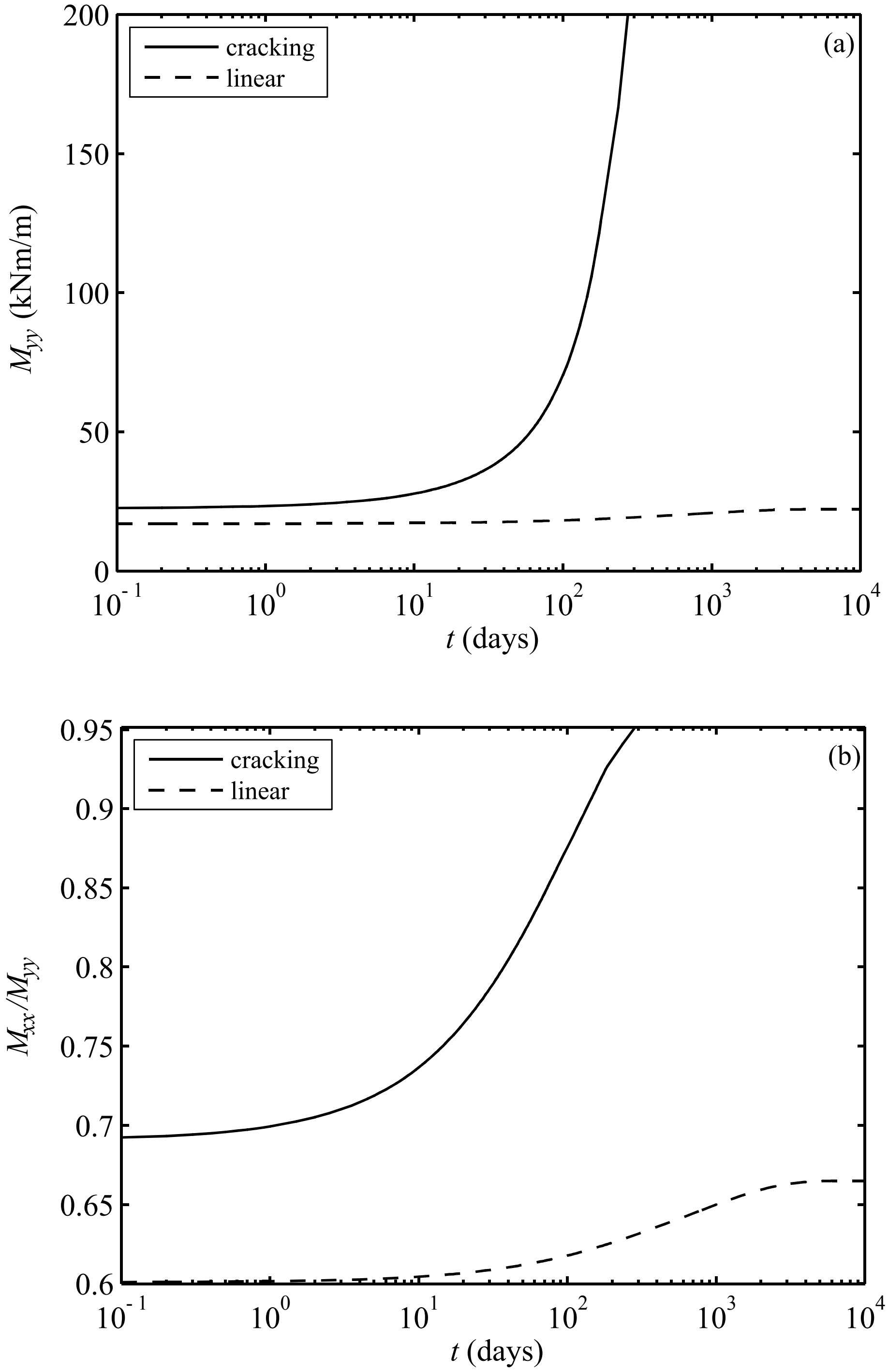

Fig. 7.25 Variation with time of the (a) bending moment M_{yy}; (b) the ratio of M_{xx}/M_{yy} at the center of the panel

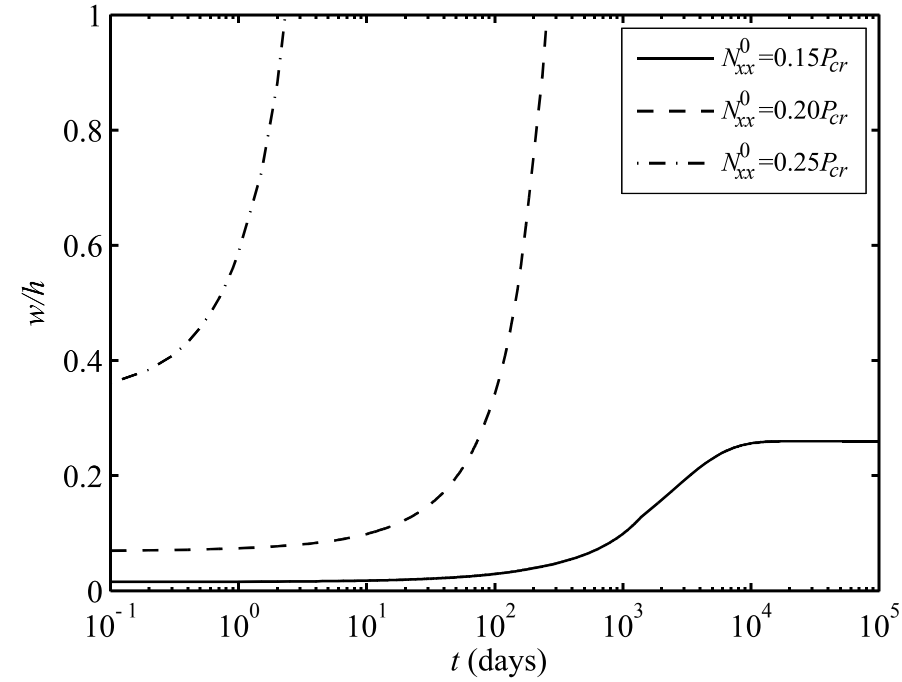

Fig. 7.26 Influence of load level on the long-term behavior of the HSC panel ($e = h/20$, $[\rho_x, \rho_y] = 2\%$, $a \times b \times h = 2000 \times 2000 \times 100$ mm)

7.3.3.7 Effect of reinforcement ratio

The effect of the reinforcement ratios is studied in Fig. 7.27 for the cracked panel where $N_{xx}^0 = 0.2P_{cr}$, and the eccentricity is $h/6$ for all cases. It is revealed that the time-dependent response of the cracked HSC panel is also very sensitive to the reinforcement ratio. The critical time of the HSC panel increases with the increase of the reinforcement ratio, and for the case where the reinforcement ratio equals to 3%, the panel exhibits a long-term stable behavior. The results reveal that the creep buckling can be potentially prevented by increasing the amount of reinforcement without changing the geometry of the panel.

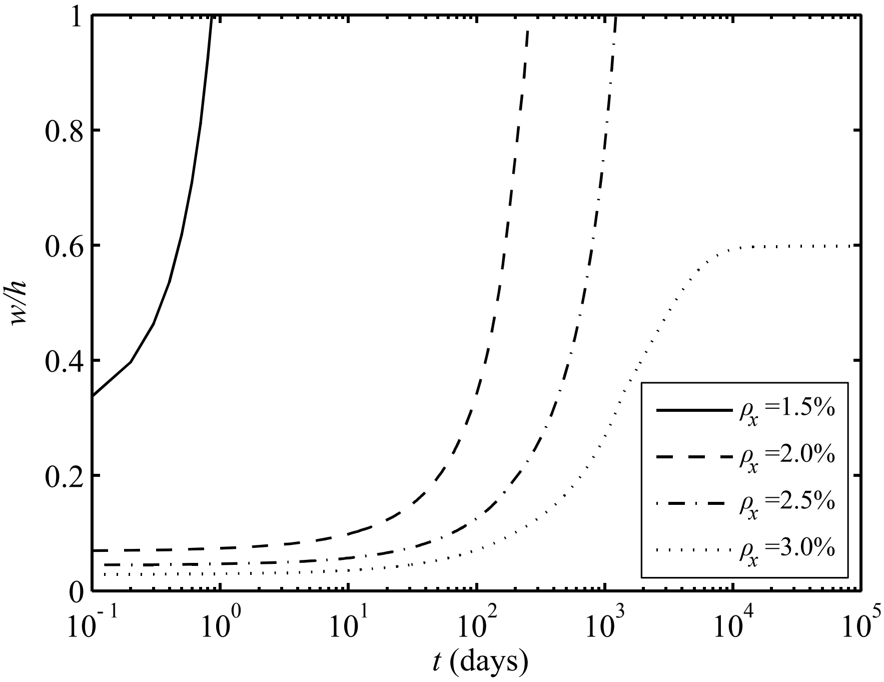

Fig. 7.27 Influence of reinforcement ratio on the long-term behavior of the HSC panel ($N_{xx}^0 = 0.2P_{cr}$, $e = h/20$, $[\rho_x, \rho_y] = 2\%$, $a\times b\times h = 2000\times2000\times100$ mm)

7.3.3.8 Effect of shrinkage

The influence of shrinkage on the long-term behavior of cracked HSC panels is investigated in Fig. 7.28. Two panels are examined in the figure, where one considers the effect of shrinkage while the other does not. The shrinkage is assumed to start at the age of 14 days and its development with time is in accordance with AS3600 (2009) as in Chapter 5, which is as follows:

$$\varepsilon_{xx}^{sh}(t) = -1.9\times10^{-4}\left(1-e^{-0.1(t+14)}\right) - \frac{2.75\times10^{-4}(t+14)^{0.8}}{(t+14)^{0.8}+17.3} \tag{7.75}$$

As shown in the figure, the shrinkage only slightly weakens the panel and a softer time-dependent response is obtained for the panel with shrinkage. Creep buckling failure occurs to both panels and the critical time reduces from 235 days to 225 days due to the effect of shrinkage.

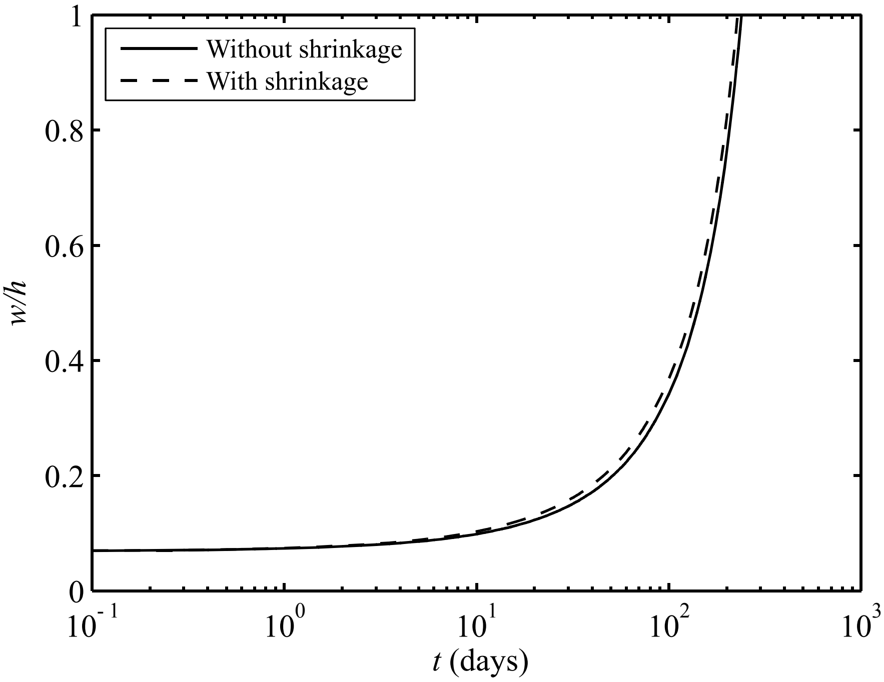

Fig. 7.28 Influence of shrinkage on the long-term behavior of the HSC panel (N_{xx}^{0} = $0.2P_{cr}$, $e = h/20$, $a \times b \times h$ = 2000×2000×100 mm)

7.4 SUMMARY AND CONCLUSIONS

A nonlinear theoretical model is developed in this chapter for the time-dependent analysis of two-way HSC panels. Creep, shrinkage and cracking of the concrete are accounted for through a rheological viscoelastic model. The model considers the geometric nonlinearity and describes the variation of the internal stresses with time through a step-by-step time analysis.

It has been shown in the numerical study for the linear viscoelastic panel that the out-of-plane deflection together with the internal bending moments increase with time as a result of the combined effects of creep and geometric nonlinearity, which may lead to creep buckling failures. The capabilities of the theoretical model for quantitatively describing the increase of the deflection and capturing ultimate failure are clearly demonstrated through the numerical examples.

A parametric study is also conducted in this chapter to investigate some vital factors that can potentially influence the time-dependent behavior of the HSC panel. It is found that the HSC panel undergoes smaller increase of deflection over time with the decrease of uniaxial load level, and eccentricity, or with the increase of the reinforcement ratio. The panel exhibits more rigid instantaneous and long-term responses with the fixed boundaries or concentric in-plane loading than with the eccentric in-plane loading. The investigation on the influence of aspect ratio shows that the HSC panel is most vulnerable when the aspect ratio equals to 1, where creep buckling failure happens earliest. Panels with aspect ratios other than 1 have larger critical times or stable long-term responses.

The simplified study carried out for the HSC panels considering cracking has suggested that the long-term performance of the panel is highly influenced by cracking where creep buckling could be happening under relatively low load levels. It also highlights the importance of considering the effect of cracking in the design of two-way HSC panels. It has been revealed that the shrinkage tends to slightly weaken the cracked HSC panel.

CHAPTER 8 SUMMARY, CONCLUSIONS AND RECOMMENDATIONS

8.1 SUMMARY AND CONCLUSIONS

The thesis presents theoretical and experimental investigations on the short-term and long-term responses of slender HSC panels under in-plane loading, with particular emphasis on their buckling behaviour. Both one-way and two-way panels are examined. Although the short-term behaviour of RC panels has been widely investigated in the literature, the existing studies have mainly focused on normal-strength concrete panels. Research works on HSC panels, especially the experimental studies are very limited and the problem of creep buckling has not been addressed yet.

At the first stage of this thesis, the short-term behaviour of HSC panels has been addressed both theoretically and experimentally. The model considers concrete cracking, tension-stiffening, strain-softening of the concrete in compression, and yielding of the steel reinforcement along with the geometric nonlinearity. It describes the entire equilibrium path of one-way HSC panel under eccentric in-plane loading through the use of the arc-length method. The model has been validated by an experimental study that has been conducted in this thesis and by other test results that appeared in the literature. The experimental study includes testing to failure of eight full-scale HSC panels. All the tested panels have showed nonlinear responses due to the geometric and material nonlinearities and failed dominantly by buckling characterized by a limit-point mode. A number of parameters are investigated in the experimental study, including the reinforcement ratio and location, load eccentricity and slenderness ratio. The results have shown that the load eccentricity and slenderness ratio have profound influences on the behaviour of HSC panels, but the influences of the reinforcement ratio and location are of minor importance. However, they play a more critical role in controlling the ductility of these panels. Estimations of the buckling loads of the tested HSC panels by the design codes have revealed considerable deviation from the experimental results, mainly because the codes do not properly consider the material and geometric nonlinearities, as well as the load eccentricity in the calculation of the effective rigidities. On the other hand, a good correlation has been achieved between the theoretical and the test results.

The creep buckling response of general slender one-way viscoelastic panels has been investigated first without considering cracking, in order to highlight and clarify the creep effects only. A nonlinear theoretical model has been developed in this regard, which accounts for the geometric nonlinearity and the variation of the internal stresses and deformations with time through a step-by-step time analysis. Creep is modelled by a rheological model that is based on the generalized Maxwell chain. The concrete has been considered to be linear viscoelastic. The effects of cracking, aging, and shrinkage have been considered in a more advanced model presented in a subsequent chapter. The results have shown that typical slender one-way panels subjected to sustained eccentric in-plane loading experience increased out-of-plane deflection with time, associated with a significant increase and redistribution of the bending moment, which may ultimately lead to creep buckling failures. The results of the parametric study reveal that the critical time at which the creep buckling happens is very sensitive to the magnitude and eccentricity of the applied load. The model is validated to some level by comparison to the simplified Effective Modulus Method (EMM). However, the model presented in this thesis is more general and comprehensive than the EMM model and it accounts for gradual loading of the structure and provides a basis for more comprehensive models that includes cracking, shrinkage, tension-stiffening and aging of the concrete.

A more sophisticated model has been developed in Chapter 5 for the time analysis of slender one-way HSC panels, which accounts for creep, shrinkage and aging of the concrete, as well as for cracking and tension-stiffening. The capabilities of the theoretical model have been examined and demonstrated through numerical examples and parametric studies, which show that the increase with time of the out-of-plane deflection is accompanied by shifting of the neutral axis towards the compression side, and by a continuing growth of the compressive and tensile stresses in the concrete and the steel reinforcement. The results also reveal that even though the concrete may not be cracked under instantaneous loading, creep and shrinkage may result in time-dependent cracking that can considerably reduce the buckling capacity of the panel. It has been shown that the long-term effects of creep and shrinkage can cause premature buckling of the panel with time, and that the long-term buckling loads can be smaller than the elastic buckling loads, which highlight the importance of considering these long-term effects in the design of HSC panels. The parametric study clarifies that the time-dependent behavior of one-way panels can be significantly influenced by the magnitude and eccentricity of the in-plane load and under given circumstances, creep buckling failure can be avoided by using sufficient reinforcement.

The long-term response of slender one-way HSC panels has been experimentally investigated in Chapter 6. The experimental program consists of testing five simply-supported one-way slender HSC panels under sustained eccentric in-plane loading. Two panels failed by creep buckling under the sustained load due to the combined effects of creep, shrinkage, cracking and geometric nonlinearity, and the other three panels showed long-term stable response and therefore were loaded to failure without releasing the existing load at some time after initial loading. Three parameters including the loading age, the magnitude and eccentricity of the in-plane load have been investigated in the experimental program. The results show that the loading age is a crucial factor affecting the behavior of HSC panels. Creep buckling failure occurred to the panels loaded at the earlier age, whereas panels loaded at an older age exhibited stable behavior. It has also been shown that the long-term response of slender HSC panels is very sensitive to the magnitude and eccentricity of the in-plane load and that the effects of creep and shrinkage lead to reductions of the residual strength to varying degrees. This reduction should be carefully considered in the design of HSC wall panels, as their ultimate strength after being loaded over time will be smaller than the one under instantaneous loads.

Chapter 7 presents a nonlinear theoretical model for the time-dependent analysis of slender HSC panels in two-way actions. The model considers creep, shrinkage and cracking of the concrete through a rheological viscoelastic model. Von Karman plate theory is used for deriving the incremental governing equations through variational principles. The equations are solved numerically at each time step based on a Fourier series expansion of the deformations and loads in one direction, and using the numerical multiple shooting method in the other direction. In the numerical study, the model has been demonstrated to be able to effectively predict the time-dependent behavior of two-way HSC panels, where the out-of-plane deflection along with the internal bending moments increase with time as a result of the combined effects of creep and geometric nonlinearity, which may ultimately lead to creep buckling failures. The parametric study has suggested that the long-term behavior of the two-way HSC panel can also be affected by many factors including the reinforcement ratio and the boundary conditions and so on. The results for the study on the aspect ratio have shown that the HSC panel is most vulnerable when the panel is square (aspect ratio equals 1). Panels with aspect ratio other than 1 have shown prolonged critical times or stable long-term behavior. The simplified study on the effect of cracking has revealed that the time-dependent behavior of HSC panels can be significantly weakened by cracking of the concrete, leading to earlier creep buckling and smaller long-term buckling load. Hence, it is of vital importance to consider the effect of cracking in the design and buckling analysis of two-way HSC panels. The HSC panel can be further weakened by shrinkage of concrete, as indicated in the study, resulting in larger increase of out-of-plane deflection and earlier buckling failure.

Finally, it can be concluded from the short-term study that the failure mode of HSC panels with typical slenderness ratio as commonly used in practice is characterized by brittle and sudden buckling failure that is very sensitive to the slenderness ratio and to uncertainties regarding the load eccentricity, which should be carefully considered in the design. The test results have shown that the brittle failure can be partially controlled by increasing the amount of reinforcement in the panel. These aspects have been well demonstrated by the proposed model, which also has shown and explained the interaction between the geometric and material nonlinearities. It can also be concluded from the long-term study that the time-dependent behavior of HSC panels in one-way and two-way actions are both significantly influenced by the long-term effects of creep and shrinkage. Buckling failures can occur at much lower load level than the elastic buckling load due to the combined effects of creep, shrinkage, and cracking, as observed in the experimental study and predicted in the model. The long-term models developed here set theoretical basis for the nonlinear time-dependent analysis of HSC panels, including the effects of creep and shrinkage. The study also clarifies the important roles that critical parameters can have on the buckling capacity of the panel, and it provides the tools for their quantitative evaluation. The long-term test on the one-way HSC panels provides benchmark database for future long-term stability study of HSC panels.

8.2 RECOMMENDATIONS FOR FUTURE RESEARCH

Based on the thesis presented above, the research goals that were established at the beginning of the study have been successfully accomplished. However, in the course of the study, a few areas have been identified that may be useful for future research and for extending and enhancing the current study. Scope for future studies is outlined in the following:

- It has been shown in Chapter 3 that the major codes of practice are not accurate in predicting the buckling capacity of slender one-way HSC panels. More accurate design formulae for one-way panels can be developed.
- The nonlinear long-term model developed for the one-way HSC panel can be extended to account for the material nonlinearity of concrete in compression, since more stocky panels can exist in practice than the ones examined in this study. In these cases, the instantaneous stress-strain relation in compression is nonlinear, the creep coefficient is stress-dependent, and the phenomenon of creep rupture needs to be taken into account.
- The interaction between creep, shrinkage and thermal strains, and their influence on the behaviour of HSC panels, especially on the time-dependent thermal buckling behaviour can be further investigated.
- The long-term model for two-way panel can be further developed to include the aging, tension-stiffening, and material nonlinearity in compression.

- The wall design guidelines in the codes for two-way panels can be reviewed and compared to the long-term theoretical model to account for the effects of creep and shrinkage in a more simplified way.

REFERENCE

ACI209 (1971). "Prediction of creep, shrinkage, and temperature effects in concrete structures." American Concrete Institute, Michigan

ACI209 (1992). "Prediction of creep, shrinkage, and temperature effects in concrete structures." American Concrete Institute, Michigan

ACI318 (1971). "Building code requirements for reinforced concrete." American Concrete Institute, Michigan

ACI318 (1977). "Building code requirements for reinforced concrete." American Concrete Institute, Michigan

ACI318 (1983). "Building code requirements for reinforced concrete." American Concrete Institute, Michigan

ACI318 (1989). "Building code requirements for reinforced concrete : With design applications." American Concrete Institute, Michigan

ACI318 (1992). "Building code requirements for reinforced concrete and commentary." American Concrete Institute, Michigan

ACI318 (1995). "Building code requirements for structural concrete and commentary." American Concrete Institute, Michigan

ACI318 (1999). "Building code requirements for reinforced concrete and commentary." American Concrete Institute, Michigan

ACI318 (2008). "Building code requirements for structural concrete and commentary." American Concrete Institute Michigan

ACI363 (1984). "State-of-the-art report on high-strength concrete." American Concrete Institute.

ACI363 (2010). "Report on high-strength concrete." American Concrete Institute.

Aghayere, A. O., and MacGregor, J. G. (1990a). "Analysis of concrete plates under combined in-plane and transverse loads." *ACI Structural Journal*, 87(5), 539-547.

Aghayere, A. O., and Macgregor, J. G. (1990b). "Tests of reinforced concrete plates under combined in-plane and transverse loads." *ACI Structural Journal*, 87(6), 615-622.

Amoushahi, H., and Azhari, M. (2013). "Static analysis and buckling of viscoelastic plates by a fully discretized nonlinear finite strip method using bubble functions." *Composite Structures*, 100, 205-217.

AS1012.13 (1992). "Methods of testing concrete - method 13: Determinatiion of tthe drying shrinkage of concrete for samples prepared iin the ffield or in tthe laboratory." Standards Australia, Sydney, Australia

AS3600 (1988). "Concrete structures." Standards Association of Australia, North Sydney

AS3600 (1994). "Concrete structures." Standards Association of Australia, North Sydney

AS3600 (2009). "Concrete structures." *AS3600-2009*, Standards Association of Australia, Sydney, Australia

Ashour, H. A. (1994). "Creep buckling of cylindrical panels under multiaxial loading." *Computers and Structures*, 52(1), 139-148.

Attard, M. M., Minh, N. G., and Foster, S. J. (1996). "Finite element analysis of out-of-plane buckling of reinforced concrete walls." *Computers & Structures*, 61(6), 1037-1042.

Bazant, Z. P. (1988). *Mathematical modelling of creep and shrinkage of concrete*, John Wiley and Sons, Chichester.

Bažant, Z. P. (1968). "Creep stability and buckling strength of concrete columns." *Magazine of Concrete Research*, 20(63), 85-94.

Bažant, Z. P. (1972). "Prediction of concrete creep effects using age-adjusted effective modulus method." *Journal of the American Concrete Institute*, 69(20), 212-217.

Bažant, Z. P., and Wu, S. T. (1974). "Rate-type creep law of aging concrete based on maxwell chain." *Materials and Structures*, 7(1), 45-60.

Bažant, Z. P., and Panula, L. (1978a). "Practical prediction of time-dependent deformations of concrete - part i: Shrinkage." *Materials and Structures*, 11(5), 307-316.

Bažant, Z. P., and Panula, L. (1978b). "Practical prediction of time-dependent deformations of concrete - part ii: Basic creep." *Materials and Structures*, 11(5), 317-328.

Bažant, Z. P., and Panula, L. (1978c). "Practical prediction of time-dependent deformations of concrete - part iii: Drying creep." *Materials and Structures*, 11(6), 415-424.

Bažant, Z. P., and Panula, L. (1978d). "Practical prediction of time-dependent deformations of concrete - part iv: Temperature effect on basic creep." *Materials and Structures*, 11(6), 424-434.

Bažant, Z. P., and Panula, L. (1979a). "Practical prediction of time-dependent deformations of concrete - part v: Temperature effect on drying creep." *Materials and Structures*, 12(3), 169-174.

Bažant, Z. P., and Panula, L. (1979b). "Practical prediction of time-dependent deformations of concrete - part vi: Cyclic creep, nonlinearity and statistical scatter." *Materials and Structures*, 12(3), 175-183.

Bažant, Z. P., and Kim, S. S. (1979). "Approximate relaxation function for concrete " *Journal of Structural Engineering*, 105(12), 1695-1705.

Bažant, Z. P., and Tsubaki, T. (1980). "Nonlinear creep buckling of reinforced concrete columns." *Journal of Structural Engineering*, 109(3), 866-884.

Bažant, Z. P., and Panula, L. (1984). "Practical prediction of creep and shrinkage of high strength concrete." *Materials and Structures*, 17(101), 375-378.

Bažant, Z. P., and Prasannan, S. (1989a). "Solidification theory for concrete creep. I: Formulation." *Journal of Engineering Mechanics*, 115(8), 1691-1703.

Bažant, Z. P., and Prasannan, S. (1989b). "Solidification theory for concrete creep. Ii: Verification and application." *Journal of Engineering Mechanics*, 115(8), 1704-1725.

Bažant, Z. P., and Cedolin, L. (1991). *Stability of structures: Elastic, inelastic, fracture and damage theories*, Oxford University Press, New York.

Behan, J. E., and O'Connor, C. (1982). "Creep buckling of reinforced concrete columns." *Journal of the Structural Division, Proceedings of the American Society of Civil Engineers*, 108(ST12), 2799-2818.

Birman, V., and Magid, M. G. (1995). "Creep buckling and rupture of columns with arbitrary symmetric cross section." *International Journal of Mechanical Sciences*, 37(8), 831-841.

Bockhold, J., and Petryna, Y. S. (2008). "Creep influence on buckling resistance of reinforced concrete shells." *Computers and Structures*, 86(7-8), 702-713.

BS8110 (1985). "British standard structural use of concrete part 1 - code of practice for design and construction." British Standards Institution, London

Carol, I., and Murcia, J. (1989). "A model for the non-linear time-dependent behaviour of concrete in compression based on a maxwell chain with exponential algorithm." *Materials and Structures*, 22(3), 176-184.

Carol, I., and Bazant, Z. P. (1993). "Viscoelasticity with aging caused by solidification of nonaging constituent." *Journal of Engineering Mechanics*, 119(11), 2252-2259.

Carpinteri, A., Valente, S., Zhou, F. P., Ferrara, G., and Melchiorri, G. (1996). "Tensile and flexural creep rupture tests on partially-damaged concrete specimens." *Materials and Structures/Materiaux et Constructions*, 30(199), 269-276.

CEB-FIP (1990). "Model code." Comite Euro-International du Beton, Switzerland

CEB-FIP (1999). "Module code for concrete structures, evaluation of the time dependent behavior of concrete." Comite Euro-International du Beton/Federation Internationale de la Precontrainte, Lausanne

Chang, W. P. (1986). "Creep buckling of nonlinear viscoelastic columns." *Acta Mechanica*, 60, 199-215.

Chen, W. F. (1982). *Plasticity in reinforced concrete*, McGraw-Hill Book Company, New York.

Chen, W. F., and Lui, E. M. (1987). *Structural stability: Theory and implementation* Prentice Hall, New York.

Claeson, C., and Gylltoft, K. (2000). "Slender concrete columns subjected to sustained and short-term eccentric loading." *ACI Structural Journal*, 97(1), 45-53.

Crisfield, M. A. (1983). "Arc-length method including line searches and accelerations." *International Journal for Numerical Methods in Engineering*, 19(9), 1269-1289.

Di Luzio, G. (2009). "Numerical model for time-dependent fracturing of concrete." *Journal of Engineering Mechanics*, 135(7), 632-640.

Distefano, J. N. (1965). "Creep buckling of slender columns." *Journal of the Structural Division, Proceedings of the American Society of Civil Engineers*, 91(ST3), 127-149.

Doh, J. H. (2002). "Experimental and theoretical studies of normal and high strength concrete wall panels." Doctor of Philosophy, Griffith University, Griffith.

Dym, C. L., and Shame, I. H. (2013). *Solid mechanics a variational approach* Springer Science+Business Media New York, Heidelberg, Dordrecht, London.

El-Metwally, S. E., F.Ashour, A., and Chen, W. F. (1990). "Instability analysis of eccentrically loaded concrete walls." *Journal of Structural Engineering*, 116(10), 2862-2881.

Eurocode2 (2005). "Design of concrete structures - part 1-1: General rules and rules for buildings." European Committee for Standardization, Brussels, Belgium

Farvashany, F. E., Foster, S. J., and Rangan, B. V. (2008). "Strength and deformation of high-strength concrere shearwalls." *ACI Structural Journal*, 105(1), 21-29.

Fields, K., and Bischoff, P. H. (2004). "Tension stiffening and cracking of high-strength reinforced concrete tension members." *ACI Structural Journal*, 101(4), 447-456.

Foster, S. (1992). "Application of the arc length method involving concrete cracking." *International Journal for Numerical Methods in Engineering*, 33(2), 269-285.

Fragomeni, S., and Mendis, P. A. (1997). "Instability analysis of normal- and high-strength reinforced-concrete walls." *Journal of Structural Engineering*, 123(5), 680-684.

Fragomeni, S., and Mendis, P. A. (1998). "Applicability of current aci318 wall design formula for high strength concrete walls." *Advances in Structural Engineering*, 2(2), 103-108.

Ghoneim, M. G., and MacGregor, J. G. (1994a). "Tests of reinforced concrete plates under combined inplane and lateral loads." *ACI Structural Journal*, 91(1), 19-30.

Ghoneim, M. G., and MacGregor, J. G. (1994b). "Behavior of reinforced concrete plates under combined inplane and lateral loads." *ACI Structural Journal*, 91(2), 188-197.

Ghoneim, M. G., and MacGregor, J. G. (1994c). "Prediction of the ultimate strength of reinforced concrete plates under combined inplane and lateral loads." *ACI Structural Journal*, 91(6), 688-696.

Gilbert, R., and Wu, H. (2009). "Time-dependent stiffness of cracked reinforced concrete elements under sustained actions." *Australian Journal of Structural Engineering*, 9(2), 151-158.

Gilbert, R. I. (1988). *Time effects in concrete structures*, Elsevier Science Publishers, Amsterdam.

Gilbert, R. I. (1989). "A procedure for the analysis of slender concrete columns under sustained eccentric loading." *Civil Engineering Transactions*, 1(39), 39-46.

Glanville, W. H. (1933). "Creep of concrete under load." *The Structural Engineer*, 11(2), 54-73.

Guan, H., Cooper, C., and Lee, D.-J. (2010). "Ultimate strength analysis of normal and high strength concrete wall panels with varying opening configurations." *Engineering Structures*, 32, 1341-1355.

Gupta, A., and Rangan, B. V. (1998). "High-strength concrete (hsc) structural walls." *ACI Structural Journal*, 95 (2), 194-205.

Hamed, E., Bradford, M. A., and Gilbert, R. I. (2010a). "Creep buckling of imperfect thin-walled shallow concrete domes." *Journal of Mechanics of Materials and Structures*, 5(1), 107-128.

Hamed, E., Bradford, M. A., and Gilbert, R. I. (2010b). "Nonlinear long-term behaviour of spherical shallow thin-walled concrete shells of revolution." *International Journal of Solids and Structures*, 47(2), 204-215.

Hamed, E., Bradford, M. A., Gilbert, R. I., and Chang, Z. T. (2011). "Analytical model and experimental study of failure behavior of thin-walled shallow concrete domes." *Journal of Structural Engineering*, 137(1), 88-99.

Hamed, E. (2012). "Nonlinear creep response of reinforced concrete beams." *Journal of Mechanics of Materials and Structures*, 7(5), 435-460.

Hamed, E., and Bradford, M. A. (2012). "Flexural time-dependent cracking and post-cracking behaviour of frp strengthened concrete beams." *International Journal of Solids and Structures*, 49(13), 1595-1607.

Han, N. (1996). "Time-dependent behavior of high-strength concrete." PhD Thesis, Delft University of Technology The Netherlands.

Hoff, N. J. (1956). "Creep buckling." *The Aeronautical Quarterly*, 7(1), 1-20.

Hoff, N. J. (1958). "A survey of the theories of creep buckling." *Proc.,3rd US National Congress of Applied Mechanics*, American Society of Mechanical Engineers, New York, United States, 29-49.

Hong, T., and Teng, J. G. (2002). "Non-linear analysis of shells of revolution under arbitrary loads." *Computers and Structures*, 80(18-19), 1547-1568.

Huang, N. C. (1976). "Creep buckling of imperfect columns." *Journal of Applied Mechanics*, 43(3), 131-136.

Hwee, Y. S., and Vijaya, R. (1990). "Studies on commercial high-strength concretes." *ACI Materials Journal*, 87(5), 440-445.

Jafari, N., Azhari, M., and Heidarpour, A. (2014). "Local buckling of rectangular viscoelastic composite plates using finite strip method." *Mechanics of Advanced Materials and Structures*, 21(4), 263-272.

JSCE (2002). "Standard specification for concrete structures, structural performance verification." Japan Society of Civil Engineers, Tokyo

Kirsanov, M. N. (1997). "Singular points of the creep deformation and buckling of a column." *International Journal of Engineering Science*, 35(3), 221-227.

Lee, Y., Lee, B. Y., Kwon, S. H., Kim, Y. Y., and Kim, J. K. (2008). "Long-term behavior of a reinforced concrete wall under compressive stress applied to part of the wall's entire width." *Magazine of Concrete Research*, 60(10), 759-768.

Lu, Z. H., and Zhao, Y. G. (2010). "Empirical stress-strain model for unconfined high-strength concrete under uniaxial compression." *Journal of Materials in Civil Engineering*, 22(11), 1181-1186.

Massicotte, B., MacGregor, J. G., and Elwi, A. E. (1990). "Behavior of concrete panels subjected to axial and lateral loads." *Journal of structural engineering New York, N.Y.*, 116(9), 2324-2343.

Mauch, S., and Holley, M. J. (1963). "Creep buckling of reinforced concrete columns " *Journal of the Structural Division, Proceedings of the American Society of Civil Engineers*, 89(ST4), 451-479.

Mazloom, M. (2008). "Estimating long-term creep and shrinkage of high-strength concrete." *Cement and Concrete Composites*, 30(4), 316-326.

Mickleborough, N. C., and Gilbert, R. I. (1991). "Creep buckling of uniaxially loaded reinforced concrete columns." *ACI Sepcial Publication*, 129, 39-55.

Minahen, T. M., and Knauss, W. G. (1993). "Creep buckling of viscoelastic strucutres." *International Journal of Solids and Structures*, 30(8), 1075-1092.

Mokhtarzadeh, A., and French, C. (2000). "Time-dependent properties of high-strength concrete with consideration for precast applications." *ACI Materials Journal*, 97(3), 263-271.

Ngab, A. S., Nilson, A. H., and Slate, F. O. (1981). "Shrinkage and creep of high strength concrete." *ACI Journal*, 78(4).

Oberlender, G. D., and Everard, N. J. (1977). "Investigation of reinforced concrete walls." *ACI Journal*, 74(6), 256-263.

Oliveira, B. F., and Creus, G. J. (2000). "Viscoelastic failure analysis of composite plates and shells." *Composite Structures*, 49(4), 369-384.

Rabotnov, G. N., and Shesterikov, S. A. (1957). "Creep stability of columns and plates." *Journal of Mechanics and Physics of Solids*, 6, 27-34.

Saheb, S. M., and Desayi, P. (1989). "Ultimate strength of rc wall panels in one-way in-plane action." *Journal of Structural Engineering*, 115(10), 2617-2630.

Saheb, S. M., and Desayi, P. (1990a). "Ultimate strength of r.C. Wall panels in two-way in-plane action." *Journal of Structural Engineering*, 116(5), 1384-1402.

Saheb, S. M., and Desayi, P. (1990b). "Ultimate strength of rc wall panels with openings." *Journal of Structural Engineering*, 116(6), 1565-1578.

Sanjayan, J. G., and Maheswaran, T. (1999). "Load capacity of slender high-strength concrete walls with side supports." *ACI Structural Journal*, 96(4), 571-577.

Selim, S., and Akbarov, S. D. (2003). "Fem analysis of the three-dimensional buckling problem for a clamped thick rectangular plate made of a viscoelastic composite." *Mechanics of Composite Materials*, 39(6), 531-540.

Shousha, H. M., El-Mihilmy, M. T., and Ghoneim, M. (2007). "Analysis of reinforced high-strength concrete slender walls under axial and transverse loads." *Journal of Engineering and Applied Science*, 54(1), 71-90.

Smadi, M. M., Slate, F. O., and Nilson, A. H. (1987). "Shrinkage and creep of high-, medium- and low-strength concretes, including overloads." *ACI Materials Journal*, 84(3), 224-234.

Stoer, J., and Bulirsch, R. (2002). *Introduction to numerical analysis*, Springer-Verlag, New York.

Sundararajan, P., and Noah, S. T. (1997). "Dynamics of forced nonlinear systems using shooting/arc-length continuation method - application to rotor systems." *Journal of Vibration and Acoustics, Transactions of the ASME*, 119(1), 9-20.

Swartz, S. E., Rosebraugh, V. H., and Berman, M. A. (1974). "Buckling test on rectangular concrete panels." *ACI Journal*, 71(5), 33-39.

Swartz, S. E., and Rosebraugh, V. H. (1974). "Buckling of reinforced concrete plates." *ASCE J Struct Div*, 100(ST1), 195-208.

Tatsa, E. Z. (1989). "Load carrying of eccentrically loaded reinforced concrete panels under sustained load." *ACI Structural Journal*, 86(2), 150-155.

Tazawa, E. (1999). *Autogenous shrinkage of concrete*, Taylor & Francis Books Ltd.

Tvergaard, V. (1979). "Creep buckling of rectangular plates under axial compression." *International Journal of Solids and Structures*, 15, 441-456.

Vecchio, F. J., and Collins, M. P. (1986). "The modified compression-field theory for reinforced concrete elements subjected to shear." *ACI Journal*, 83(2), 219-231.

Vinogradov, A. M. (1985). "Nonlinear effects in creep buckling analysis of columns." *Journal of Engineering Mechanics*, 111(6), 757-767.

Whitney, G. S. (1932). "Plain and reinforced concrete arches." *ACI Journal*, 28(7), 479-519.

Wu, S. T. (1983). "Creep buckling in concrete structures." *Time-Dependent Failure Mechanisms and Assessment Methodologies, Cambridge University Press*, 70-79.

Yun, H. D., Choi, C. S., and Lee, L. H. (2004). "Behavior of high-strength concrete flexural walls." *Proceedings of the Institution of Civil Engineers Structures & Buildings*, 157(SB2), 137-148.

Zielinski, Z. A., Troitsky, M. S., and Christodoulou, H. (1982). "Bearing strength investigation of thin-wall ribbed reinforced concrete panels." *ACI Journal*, 79(4), 313-321.